International Journal of Computational and Engineering

MARCH 2017 VOLUME2 NUMBER1

Publisher: ACADEMIC PUBLISHING HOUSE
Address: Quastisky Building, Road Town, Tortola, British Virgin Islands
UK Postal Code: VG1110

E-mail: editorial@ij-ce.com
www.ij-ce.com

CONTENTS

Current Situation and Significance of Studies on Teacher's Vocational Delay of Gratification

Menglong Li [1,2], Jingsong Nie[1], Yujia Ren[2]
[1] Hunan Provincial Research Institute of Education, Changsha, Hunan Province 410005, China
[2] Physical Education Institute, Hunan First Normal University, Changsha, Hunan Province 410205, China

Abstract: In recent years, vocational delay of gratification has gradually become the focus of psychology, management science and business circles. Researchers have taken preliminary studies on the concept, measurement, positive effect, influencing factors and other aspects of vocational delay of gratification. However, researches on teacher's vocational delay of gratification are still insufficient and it urgently requires us to take in-depth study. This research introduced the origin, development, current studying status and insufficiency of vocational delay of gratification, and discussed the current situation and significance of studies on teacher's vocational delay of gratification, for the purpose of attracting the attention from the academic circle.
Keywords: Delay of gratification; Vocational delay of gratification; Teacher; Management

1. INTRODUCTION

Sigmund Freud, the father of psychoanalytic theory and master of psychoanalysis, found the phenomenon of delay of gratification when conducting experimental studies on children and thought that delay of gratification is a kind of children's ability of self-control, in the way of relieving or eliminating the anxiety and tension brought by delay of gratification so as to regulate and control the present behavior when direct gratification is delayed or impeded but individual object does not exist actually and may produce "fantasy" for the potential reward object. Commenced based on this, the academic circle's enthusiasm for studying "delay of gratification" boomed for a long time and afterwards various interpretations for this concept emerged. Until 1974 when Mischel, the social psychologist from Stanford University, US, proposed the concept of delay of gratification through conducting seminal research on children's delayed gratification – the now-famous "marshmallow experiment", and clearly defined it as a manifestation of psychological maturity, the selective orientation to resist the temptation for an immediate reward and wait for a later reward, and the self-control ability displayed in waiting [1]. It is not only the core element of individual's self-control and the most important skill, significant component of socialization and emotional adjustment, but also the vital target for individual's socialization and self-development, and a fundamental social ability and positive personality variable along with human being's whole life [2]. Mischel defined the concept of delay of gratification and the models in two stages in his works, and systematically summarized and proposed the research paradigm of delay of gratification, elaborated the influencing mechanism of cognition, motivation, environment variable, reward and other factors on delay of gratification, which symbolized that the academic study on delay of gratification entered into a new era. More scholars started studying the application of delay of gratification in different social division of labor and social fields[1].

Since from 1990s, studies on delay of gratification gradually extended to broader objects and domains. Domestic and foreign scholars have conducted beneficial theoretical discussion and empirical researches on the research paradigm, mental mechanism, influencing factors, multicultural comparison, and other aspects of delay of gratification. But this kind of studies mainly focus on developmental psychology field, but the delay of gratification in vocational domain, i.e. studies on vocational delay of gratification just get off the ground. Vocational Delay of Gratification, VDOG, refers to that individual's self-regulation capability for the sake of achieving a series of more valuable long-term results including better completing work tasks, gaining benefit return and obtaining higher vocational target willing to give up rest, entertainment or impulsive behaviors and other chances non-beneficial for current work or instance gratification [3]. In recent years, vocational delay of gratification gradually became the focus attracting psychology, management science and enterprises circles. Researches mainly Researchers have taken preliminary studies on the concept, measurement, positive effect, influencing factors and other aspects of vocational delay of gratification.

2. RESEARCH PROGRESS OF VOCATIONAL DELAY OF GRATIFICATION

(1) Definition of vocational delay of gratification

Some researchers took studies on the concept of vocational delay of gratification. Mischel (1974) considered that delay of gratification can be regarded as a manifestation of psychological maturity and a

part of self-control ability. In the scenario or context of delay of gratification, people are willing to give up the present choice orientation of instant gratification to pursue long-range or more beneficial valuable result in the process of which display their self-control ability [1]. Miller regarded delay of gratification as a value embodiment of work ethics, significantly correlative with other dimensions included by work ethics, as well as an indispensable job attribute for organization and individual [4]. Reynolds and Schiffbauer [5] explained delay of gratification as a selective power from the perspective of vocational development, i.e. "the ability to resist the chances for instant gratification but choose and maintain behaviors beneficial for fulfilling long-term vocational target and achievements". Liu [3] referred to Bembenutty' definition on academic delay of gratification and considered vocational delay of gratification as a self-regulation ability and people's delay of gratification in their career life. People are willing to give up current chances for rest, entertainment and other instant gratification for better completing work tasks and gaining more job returns and achieving higher professional target, and a series of more valuable long-term result. Tobin and Graziano defined delay of gratification from objective perspective and thought individual with high delay of gratification can balance the interest relationship between short-term objective and long-range objective and are more capable of abandoning short-term objective related instant gratification based on long-term target which including a series of motivations and cognitive process. Liu [3], Wang [6], etc. generally defined vocational delay of gratification as individual's self-regulation competence willing to give up current chances for rest, entertainment and other instant gratification for better completing work tasks and gaining more job returns and achieving higher professional target, and a series of more valuable long-term result.

(2) Measurement of vocational delay of gratification

Researchers conducted some studies on the measuring tools of vocational delay of gratification and laid foundation for carrying out further researches. Ray and Najman (1986) compiled the Deferment of Gratification Scale (DGS); Miller, etc. [4] compiled the Multidimensional Work Ethic Profile (MWEP), including vocational delay of gratification as one of dimensions; Liu etc. compiled Enterprise Employee's Vocational Delay of Gratification Questionnaire including two dimensions: work delay dimension and career delay of gratification, totally 8 item[3]. Kang compiled Vocational Delay of Gratification Questionnaire with 12 items including three dimensions: work delay of gratification, vocational delay of gratification and durability[7]. Although these measuring tools are with favorable credibility, the constitutions of employees' vocational delay of gratification are different due to different types of work, positions, and industries. Therefore, measuring tools for specific vocational delay of gratification are still deficient [8].

(3) Positive effect of vocational delay of gratification

The positive effects of vocational delay of gratification are mainly manifested in the impact from two aspects: individual and organization, unanimously showing that both can bring about positive impact on individual development and the fulfillment of organization goals. Miller fund that people choose delay of gratification have higher level of work performance. Liu's research results indicate that vocational delay of gratification plays a mediating role between employee's career planning and occupational satisfaction, and to some extent brings about mediating effect between two factors: employee's vocational training attention value and equal promotion.

(4) Influencing factors of vocational delay of gratification

Researchers studied from two aspects: individual influencing factors (including personality factors, emotions, career stages, and self-career management) and organizational and social influencing factors (including organizational career management, social rejection, and generation gap). This plays a significant enlightening role on discussing staff management countermeasures but there are more fields worthy of in-depth exploration. Researches show that multiple personality factors will influence individual's vocational delay of gratification such as conscientiousness and nervousness; general self-efficacy. Some researches focused on the relationship between negative emotions with delay of gratification but the relationship still requires for systematic studies [6]. It requires for more researches to clarify the relationship between career developmental stages with vocational delay of gratification. Studies on organizational and social influencing factors of vocational delay of gratification were mainly conducted from three aspects: organizational career management, social rejection and generation gap.

3 TEACHER'S VOCATIONAL DELAY OF GRATIFICATION

Teacher's Law regulates that, "teachers are professionals implementing education and teaching obligation, and undertaking the mission of imparking knowledge and educating people, cultivating builders and successor of socialist cause, and improving national quality. Teachers should be loyal to people's education cause." Teacher's work is a special occupation to educate people directly impacting greatly on students' growth with every word and action. Teachers should own high sense of responsibility and strong sense of mission. Teachers are "the basement of education and source of

prosperity". Teachers undertake vital missions to promoting Chinese educational enterprise development and modernization of education. However, currently, there exist general issues among teachers, such as serious occupational burnout, obvious career plateau phenomenon, insufficient job involvement, and huge work pressure, which have brought about negative impact on the development of educational enterprise and the fulfillment of school's educational objectives. Vocational delay of gratification has great significance on individual development and the realization of organizational goals. Under such background, carrying out studies on teacher's vocational delay of gratification is at exactly the right time.

Li and Liu used questionnaire method to hand out 350 questionnaires among 6 colleges and universities to know the current situation of teacher's vocational delay of gratification in universities and colleges. Results showed that, the overall condition of teacher's vocational delay of gratification in universities and colleges is fair (m>16); gender, age, years of working, post, marital status and other demographic variables have remarkable influence on it [9]. The study aroused scholar's attention to the teacher's group vocational delay of gratification. Mohsin and Ayub discussed about the relationship between vocational delay of gratification and job satisfaction among Japanese high school teachers . Huang Tao, etc. used scales to investigate 200 teachers' vocational delay of gratification in secondary vocational schools. Investigation results showed that, the overall condition is good but there exist differences in different dimensions, and birth year and post have remarkable influence on vocational delay of gratification . Liu discussed about the relationship between high school teacher's vocational delay of gratification and career identity. In a word, studies related to teacher's vocational delay of gratification just started and there are only few researches.

4. CONCLUSION

Regarding the contemporary significance, vocational delay of gratification is the core element and most important skill of individual's self-control, as well as the vital target of individual socialization and self-development, and a fundamental social ability and positive personality variable accompanying people's whole life. It has not been a long time since studies on delay of gratification have extended to specific vocational fields and aroused scholars' attention to carry out a series of researching work, but currently a lot of issues remain to be further explored. Particularly studies on teacher's vocational delay of gratification just initiated so that it urgently requires for our in-depth study.

It is of great significance to explore teacher's vocational delay of gratification: 1) it can enrich the empirical analysis on Chinese vocational delay of gratification and promote the indigenous researches on vocational delay of gratification; 2) it can expand the research contents of vocational delay of gratification, broaden the research fields of vocational delay of gratification, and consummate the research system of vocational delay of gratification; 3) it can help deepen the understanding of vocational delay of gratification, assist teachers complete career planning, and facilitate teacher's career development; 4) it can provide basis and support for schools and educational administration sectors to formulate related policies and promote the long-term development of educational business.

ACKNOWLEDGMENT

This work is supported by Hunan Province Philosophy and Social Science Fund [16YBA097] and Hunan Provincial Education Science Twelfth Five Year Plan Project [XJK015BJC006].

REFERENCES

[1]Mischel W., "Process in delay of gratification. In: Berkowitz L. Advances in experimental social psychology," New York: Academic Press, 1974, 7: 249-292.

[2] Menglong Li, Jingsong Nie, Yujia Ren, "Teachers' Individual Career Management and Vocational Delay of Gratification," International Journal of Simulation Systems, Science & Technology, 2016, 17(3): 8.1-8.4.

[3]Liu Xiaoyan, Hao Chundong, Chen Jianzhi, et al., "Influence of organizational career management on occupational commitment and job satisfaction-analysis on the mediating effect of vocational delay of gratification," Acta Psychologica Sinica, 2007, 39(4): 715-722.

[4]Miller M J, Woehr D J, Hudspeth N., "The meaning and measurement of work ethic: const ruction and initial validation of a multidimensional inventory," Journal of Vocational Behavior, 2002, 60(3): 451- 489.

[5]Reynolds B, Schiffbauer R., "Delay of gratification and delay discounting: A unifying feedback model of delay-related impulsive behavior," The Psychological Record, 2005, 55(3): 439-460.

[6]Wang Zhongjun, Liu Yunjuan, Yuan Deyong, "Research review on vocational delay of gratification," Advances in Psychological Science, 2012, 20(5): 705-714.

[7]Kang Yanhong, "Studies on the relationship between vocational delay of gratification and career self-management," Taiyuan: Shanxi University, 2009.

[8]Li Ying, "Content structure of junior civil servant's vocational delay of gratification and related researches," Guangzhou: Jinan University, 2014.

[9]Li Yali, Liu Guixiong, "Studies on the current situation of college and university teacher's vocational delay of gratification," Journal of Hubei University of Economics, 2010, 24(6): 185-186.

.

Research Progress of Solar Photovoltaic / Thermal (PV/T) Water-Cooled Collector

Wang xin
Hebei University of Technology, Tianjin 300000, China

Abstract: Due to the increasing consumption of traditional energy sources, solar energy has been paid more and more attention. In the use of photovoltaic solar thermal, PV/T integration has become a research hotspot because of its high efficiency, as the core part of the collector has attracted a lot of scholars research and innovation. This paper analyses and compares the advantages and disadvantages of different types of structure of the existing water cooled heat exchanger set, summarizes the research results of scholars at home and abroad, and puts forward some suggestions on the future of the water cooling type heat collector research direction.
Keywords: PV/T; water cooling; heat collector;

1. PREFACE

With the increase of population and the rapid development of economy, the traditional energy consumption is increasing, and our demand for energy is increasing. According to the prediction of the current production rate, the global oil can only supported by 2068, and natural gas only to 2075 [1]. According to the International Energy Agency (IEA) predicts that carbon dioxide emissions will be more than doubled by 2050[2]. In this case, clean energy comes into the public view. As one of the most abundant clean energy, solar energy has been paid more and more attention.

For the use of solar energy is currently divided into two aspects of photovoltaic and photothermal. By the end of 2011, the world PV installed capacity reached 65 GW[3]. But because of the low efficiency and high cost of photovoltaic cells, it has not been widely popularized. Then with the silicon solar cell technology continues to mature, the improvement of monocrystalline silicon surface micro structure and partition doping, the photoelectric conversion efficiency is greatly improved and the solar cells whose efficiency reach 10% to 18% have been mass produced[4]. When the solar battery work, only 6% to 15% solar energy which actually project to photovoltaic panels turn into electrical energy and output while the remaining 85% are converted into heat and discharged into the environment because only in a certain range of the solar spectrum can produce photoelectric effect. The temperature rise of 1 degrees per cell will result in a reduction of the output power by 0.4% to 0.5%. The heat released can let the operating temperature of solar cell be more than 50 degrees and the temperature will even reach to 80 degrees if the heat dissiation is poor[5],which seriously affects the working efficiency of the solar cell. If the photovoltaic panel and the collector combine the as the PV/T collector, it not only can be bring the extra heat away produced by medium in time, controlling the working temperature of the solar cell and improving the work efficiency, but also can provide a large number of low grade energy using this part of heat, greatly improving the comprehensive utilization efficiency of solar energy. In the case of the same output, compared with the separate solar panels and ordinary solar collectors, it covers an area of less, very promising. According to the forecast, it will experience a similar growth as the photovoltaic and photothermal[6]. The water collector with its convenient use, no need of two heat transfer, good optical properties, high heat capacity and other advantages of good has been studied theoretical and experimental widely. Many domestic and foreign scholars have conducted a lot of research and the author summarizes the domestic and foreign scholars' studies on the solar photovoltaic / thermal (PV/ T) water-cooled collector in recent years and discusses the existing problem and the future develop direction.

2. RESEARCH PROGRESS OF WATER-COOLED HEAT COLLECTOR

The heat transfer mode and structure of the collector are diverse, and there are heat transfer methods such as the surface of the battery or the unidirectional flow path, the surface or the back double flow channel and the circuit channel type. The main structures including tube plate, fin tube and flat box. The tube plate and the tube fin type own small water capacity, good pressure bearing and convenient processing while the heat transfer effect is not good. The heat transfer performance of flat box is brilliant, but the pressure bearing is not good and it is not easy to process.

Wei Xiao[7] eta.l compared single tube type vertical pipe coiled pipe straight section along the length direction of the plate bending and the bending direction of the plate width of the transverse bending mode and found that the battery temperature is lower, the power generation efficiency is higher and the flow resistance is lower using the vertical bending mode which has a better performance than the transverse bend. Due to the severe aging of the tube type system, Yin[8] proposed double cooling system to maintain a balanced overall component

temperature distribution effectively. In addition, Adnan[9-10] also simulated the other seven forms of circulations. In the experiment, the spiral flow has good performance and the heat efficiency can reach 50.12%, while the serpentine flow is only 32.35%.

Cai Kang[11] eta.l working in University of Shanghai for Science and Technology designed a battery cooler. The water runs through a aluminum box board with fin built-in which is placed on the back surface of solar battery and exchanges heat with the solar cell backboard. This method can make the temperature of background reduced by 15 degrees and the power generation efficiency can raise up 12%. But the high cost of water cooling device and the complex box plate groove bring pressure to the large-scale production.

Li Guangming [12] eta.l combined the Aluminum Alloy backplane type single crystal silicon photovoltaic modules and stainless steel flat box type heat collecting plate to make a new integrated photovoltaic / thermal (PV/T) composite system and tested the system in Kunming area. The results show that when the system with the water tank capacity(m) of 75 kg ran under the condition of fine operation, the average power efficiency, the thermal efficiency, comprehensive efficiency and comprehensive efficiency are respectively in 14%, 37%, 51%, 70.72%.

Erzat Erdil, Mustafa Ilkan and Fuat Egelioglu[13] designed a photovoltaic thermal component which solar panels are 0.6 square meters. The heat transfer is installed on the back of the solar cell to conduct heat transfer and the performance is measured on the building of Cyprus. The electric energy produced by hot water was reduced by 11.5%, The equivalent amount of hot water is about 2.8kWh. When the battery plate reached 10 square meters and the hot water output unchanged, power consumption reduced only 1%, the payback period is about two years. This offers a reference for the large-scale promotion of photovoltaic / thermal integrated in the future.

Earle wilson[14] designed by nature to let the water battery back to take away the heat such as the use of the flow of the river to achieve cooling process,. Stefan Krauter[15] let the water flow on the surface of the solar battery and added a water pumps which provide forced circulation in battery cooling. It not only improves the power efficiency but also replaces the glass layer with "water film" at the same time to solve the problem that common collector's surface area scales after a long-term use. The verification results show that the battery temperature is reduced by 22 degrees and the efficiency increased by 8% ~ 9% after deducting the pump power consumption.

3. CONCLUSION

In the integration of components, the designs of photovoltaic and photothermal combination are quite flexible. Some of the present researches are mainly about the use of heat and pursuit of improving the amount of thermal energy in power generation at the same time; Some designs are based on photovoltaic power generation and mainly used to reduce the photovoltaic battery's working temperature to improve the conversion efficiency of photovoltaic cells. During the production and use, we should choose the most suitable scheme according to the actual needs. At present, the PV/T technology is still in the preliminary stage of development and the technology is not mature enough. The designs has appeared have advantages and disadvantages as well. Only when we research and analysis these defects in further, improve the PV/T collector constantly and increase its practicability, can it be popularized and applied. Our research and extension work must proceed from reality and on the basis of the requirements of China's national conditions and strive to be simple and reliable, low cost, easy to process and maintenance and try to own small footprint, small space data. It is supposed to reduce the operating temperature of solar cell as far as possible and improve the photoelectric conversion efficiency to make the most of the solar energy, which is extremely important because of the traditional energy shortage now and then.

REFERENCES

[1]BP group. BP World Energy Statistics Yearbook (June 2012) [R]. 2012

[2]The International Energy Agency. Energy Outlook: for the 2050 situation and strategy of [M]. Zhang Aling, the original Kun translation. Beijing: Tsinghua University press, 2009

[3]Polaris solar PV. Global PV installed capacity will reach 230GW integration will continue [EB/OL]. 2012-07-09.

[4]Qin Hong, Zhang Renyuan, Shen Hui, et al. Experimental study on power supply and heat supply of cool storage type solar cell module [J]. HVAC, 2009, 39 (10):90-93.

[5]A european guide for the development and market introduction of PVT technology[R]. www.pvtforum.org.

[6]Wei Xiao. Intelligence. PV/T components with different bending direction performance of photovoltaic / thermal integrated coil compared and optimized [J]. 6.2012 (03).

[7]H.M.Yin.DJ.Yang.G.Kelly.et al.Design and performance of a novel building integrated PV thermal system for energy efficiency of buildings[J].Solar Energy.2013.87(1):184-195.

[8]ADNAN.IBRAHIM,M.MY.OTHMAN,M.H.RUSLAN,et al.Performance of Photovoltaic Thermal Collector (PVT) With Different Absorbers Design[J].WSEAS Transactions on Environment and Development,2009,5(3):321-330.

[9]Adnan Ibrahim,Goh Li Jin.Roonak Daghigh.et al.Hybrid Photovoltaic Thermal (PV/T) Air and Water Based Solar Collectors Suitable for Building

Integrated Applications[J].American Journal of Environmental Sciences.2009.5(5):618-624.
[10]Cai Kang, Guan Xin, Liu Peng, et al. Design and research of solar cell cooler [J]. energy research and information, 2009.25 (3): 1655-1660.
[11]Li Guangming, Liu Zuming,, Liao Hua,, et al. Experimental study on a new type of PV/T solar energy utilization system [J]. proceedings of the Chinese society of electrical engineering, 2013, (16): 83-89.
[12]Erzat Erdil、Mustafa Ilkan、Fuat Egelioglu, An experimental study on energy generation with a photovoltaic(PV)solar thermal hybrid system[J].Energy,2008,33:1241-1245.
[13]Earle wilson.Theoretical and optional thermal performance of a ‘wet’ crystalline silicon PV module under Jamaican conditions [J].Renewable Energy 34(2009)：1655-1660
[14]Stefan Krauter. Increased electrical yield via water flow over the front of photovoltaic panels[J].Solar Energy Materials & Solar Cells,2004,82:131-137.

The Design and Calculation of Hgt-200-T Mixed-Flow Drying Tower

Yang Xianliang, Gao Kun
School of Energy and Power Engineering, North China Electric Power University, Baoding 071003, China

Abstract:In this paper, we introduces the process, structure features and design calculation of HGT-200-t mixed-flow corn drying machine.The machine uses four period of drying,two period of tempering and one period of cooling.The result of experiment and actual drying operation shows that the machine has large range of dehydration and good quality of drying.The machine adopts single pylon continuous operation,so the moisture of high moisture corn can drop to safe moisture content one time.The machine has low consumption of energy, high degree of automation and low drying cost.

Keywords：Corn; dryer; low energy consumption

1. INTRODUCTION

Our country is a big agricultural country and Hebei province is a big agricultural province.With the increasing of farmers and food manufacturers,the demand for food constantly increase,the planting area of grain is gradually expanding and the corn yield increases year by year. The corn harvest moisture is about 25% ~ 25% in Hebei province and grain will mildew rot without timely drying. At present, the agricultural drying equipment is relatively deficient,so people dry grain mainly by sun drying in countryside[1].It leads to low efficiency, big labor intensity,and severe waste. We could solve the problems of drying of the harvested grain in time only by mechanized drying.Meanwhile,we can avoid and reduce the loss and keep the quality of the grain, improve the economic benefit of agricultural production[2]. HGT-200-t mixed-flow corn drying machine adopts four period of drying,two period of tempering and one period of cooling.It has high efficiency of drying and save energy obviously.It is suitble for big and small grain production household and food manufacturers.

2. WORKING PRINCIPLE OF MIXED-FLOW DRYING TOWER AND DESIGN OF DRYING PROCESS

The hot air of mixed-flow drying tower is offered by the hot blast stove.After heating by heat exchanger, clean air is blowed into the drying tower by hot-air blower. The internal of drying tower is mainly composed of layers of staggered angular ventilation box.Outside the Angular box is full of grain and grain flow from top to bottom.Hot air enter box from inlet angle and across the grain layer in up and down direction. Exhaust expel from exhaust angular box.The directions of hot air and grain flow are the same and opposite,so we call it mixed flow.When hot air across the grain layer, it transfer heat and moisture with grain:Hot air trainsfer heat to grain and raise its temperature. When grain warm up, moisture is evaporated into air and exhaust gas discharge.Grain after drying flows down to the tempering period.This period makes inside and outside layer temperature and moisture of grain keep balance and reach homogeneous precipitation.Than the grain flows into the cooling period and cool to the storage temperature.The flow chart of whole drying process is showed in figure 1.

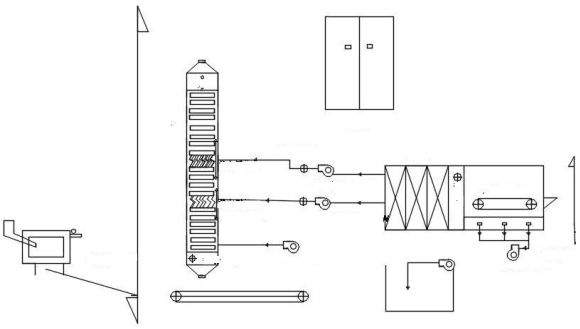

Figure 1 The flow chart of whole drying process

The process has perfect electronic control system and achieves hot blast temperature automatic control,material level control,arrange grain speed automatic operation, etc.The process is mainly composed of hot blast stove, heat exchanger, temperature sensor, blast temperature sensor, blower, fan, cooling fan, induced draft fan, heat drying tower and elevator.And drying tower is mainly composed of tower top,tempering period, grain storage period, drying period, cooling period and grain discharge period(Figure 1).Drying period and cooling period adopt the structure of angular ventilation box.Air intake and exhaust angular box have the different size and the same equal amount.Arrangement is shown in figure 2.

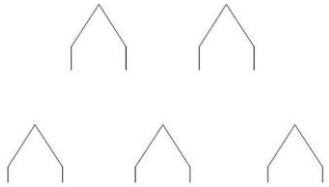

Figure 2 Angular box arrangement

3. MAIN PROPERTIES AND CHARACTERISTICS

(1)Drying period and cooling period adopt the structure of angular ventilation box and cross

distribution arrangement.It can save angle box number and make the grain heated evenly.
(2)We uses hot dip galvanized color plate to package it,so it is not easy to rust.Meanwhile,it has beautiful appearance and long service life.Beside,it covers a small area and it is convenient for outdoor installation.It saves investment.
(3)All institutions are modular assembly. It has strong interchangeability and is easy to install and maintain.
(4)It dry grain continuously , reduce turnover and increase the number of drying.It can realize large-scale continuous production.
(5)It adopts unique four page wheel volume grain discharge machine.It avoid extrusion and plugging of grain.It can adjust the speed of grain discharge in different frequency.It equipped with perfect automatic control system and achieves hot air temperature control and material level control. It has high automation level and is easy to operate.
(6)It has multi-usage.It can dry many kinds of grain, such as corn, rice, wheat, sorghum, soybeans, etc.

4. THE MAIN DESIGN AND CALCULATION

4.1 The calculation of water evaporationwater

(1)water evaporation of drying period W_1 (water yield per hour of drying period)

$$W_1 = G_1 \times \frac{\omega_1 - \omega_2}{100 - \omega_2} = 8333.33 \times (30-14) \div (100-14.5) = 1510.72 kg/h \quad (1)$$

G_1 is the quality of corn dryed by drying machine per hour,8333.33kg. ω_1 is the moisture content of corn before drying, 30%. ω_2 is the water content of corn from drying period,14.5%).

(2)Water evaporation of cooling period W_2 (water yield per hour of cooling period)

$$W_2 = (G_1 - W_1) \times \frac{\omega_2 - \omega_3}{100 - \omega_3} = (14.5-14)/(100-14) \times (8333.33 - 1510.72) = 39.6082 kg/h \quad (2)$$

ω_3 is the water content of corn from cooling period).

(3)Water evaporation of drying tower W (water yield per hour of drying tower)

$$W = W_1 + W_2 = 1550.3282 kg/h \quad (3)$$

4.2 The determination of dry air amount

$$L = \frac{W_1}{d_f - d_1} = 1510.72/(0.036717 - 0.010424) = 57457.12 kg/h \quad (4)$$

d_f is the moisture content of the gas out of the drying tower.d_1 is the moisture content of hot air blowed into drying tower).

We have already known that the the temperature of hot air delivered into drying tower is 120℃.The density is $\rho_{120℃}$ =0.89834147kg/m^3.So the volume flow of drying hot air is

$$Q = L/\rho_{120℃} = 57457.12/0.89834147 = 63959.109 m^3/h \quad (5)$$

4.3 The type selection of main air blower

According to the amount of hot-air blower deployed in drying tower,we can calculate air volume required by a single air blower.Considering the hot work efficiency and the change of the actual work condition, air volume of air blower should have a certain margin.We can select air blower according to (1.05-1.1) times of calculating air volume[3].The pressure of main air blower is determined by the heating furnace heat exchanger, and network total resistance.it is generally greater than 1.5Kpa .

According to the above conditions,we choose Y-73-9-d type boiler induced draft fan as two hot air blower.As shown below are the performance parameters of air blower.Air volume:23003m^3/h-441286m^3/h.Air pressure:1775pa-2668pa.The motor power:37kW.

4.4 The type selection of cooling air blower

According to experience,the ratio of the air volume used to cool grain and the amount of grain dried by drying machine is about 2 to 1.It can guarantee the temperature of grain out of the drying machine reach storage requirement directly, on the basis we can calculate cooling air volume[4].

The mass flow of air cooler is

$$L' = 2 \times G_1 = 2 \times 8333.33 = 16666.66 kg/h \quad (6)$$

We have known that 15 ℃ air density is $\rho_{15℃}$=1.226kg/m^3.Volume flow of air cooler is

$$Q' = L'/\rho_{15℃} = 16666.66/1.266 = 13594.34\ m^3/h \quad (7)$$

According to the above conditions,we choose Y5-47-6 - c type centrifugal fan as a air cooler. As shown below are the performance parameters of the air cooler.Air volume:8370m^3/h-15410m^3/h.Air pressure:1824Pa-2658Pa.The motor power:15kW.

4.5 Type selection of hot air stove

According to the heat quantity of hot air supplied , Boiler heating load can be estimated on the base of the efficiency of heat exchanger.If we choose the heat exchange whose heat exchange efficiency is 86%,the heat exchange of hot air input by boiler is

$$q = \frac{h \times L}{\eta_t} = 149.56 \times 57457.12 \div 0.86 = 9992194.032 kj/h \quad (8)$$

According to drying tower heat consumption , we choose standard series of hot blast stove.As shown below are the performance parameters. Type: 5LM-II-240. Heating load: 240×10^4 kcal/h. heat-supply temperature: ≤250℃. Fuel consumption: 840Kg standard coal. The installed capacity: 50 kW.

5. CONCLUSION

The temperature of hot air used in HGT - 200 - t type drying tower is high.The amount of precipitation one time is large(about 20%-25%).It uses the indirect heating (heat exchanger).It has no pollution to grain and has low coal consumption.It has these advantages: even drying,good drying quanlity,no anxious burnt grain,etc. It is suitable for popularization and application.

REFERENCES

[1]Cheng-zhi wang.Grain drying principle and the design of grain drying[M]．Harbin Publishing House, 1996：3 -13.

[2]Duan Tieqing, Liu Lin, Wang Mingyang.Parameter determination of corn dryer [J].Grain circulation technolog, 1999(6)：24 -25．

[3]Li Yunke, Yan Hanshu.Simple calculation of design parameters for grain dryer[J].process equipmen, 2012：17-18.

[4]Wang Zhijie.Design and calculation of basic parameters of grain dryer[J].Journal of Heilongjiang Bayi Agricultural University.1992(2)59-65.

Analysis of the Air-Gap Coefficient in Magnetic Field of Electromagnetic Harmomic Movable Tooth

Ren Yubo
Mechanical Engineering Institute, Yanshan University, Qinghuangdao, 066004, China

Abstract: The flexible wheel in electromagnetic harmonic movable tooth is deformed under the action of magnetic field force, which causes the air gap length to change at any time, and changes the magnetic field distribution of air gap. The inner bore of stator slot is provided with the tooth groove, so that the air gap flux density produces higher order tooth harmonic components. For the above two cases, the air gap function is introduced in this paper introduce to analyze the magnetic field, to deduce the electromagnetic harmonic movable tooth transmission considering the air gap coefficient of stator slot and flexible wheel deformation, therefore, the total air gap coefficient is obtained, which can describe the magnetic field and the force state of the flexible wheel more accurately.
Keywords: Electromagnetic harmonic; flexible wheel; magnetic field; air gap coefficient

1. INTRODUCTION

When harmonic electromagnetic movable tooth drive system is at work, armature group conduction will produce a rotating magnetic potential and the magnetic induction established by the magnetic potential is a rotating magnetic field of B_δ in the air gap, because the flexible wheel is deformed under the magnetic force, resulting in air gap length changing at any time, the air gap magnetic field distribution has been changed.[1]The inner bore of stator slot is provided with the tooth groove, so that the air gap flux density produces higher order tooth harmonic components.[2] It can be seen that the correct description of the magnetic field is of important influence on analyzing the working state of the electromagnetic harmonic movable tooth drive system.

2. CONSIDERING THE AIR-GAP COEFFICIENT OF STATOR SLOT

First, supposing that the flexible wheel does not deform, so as to determine the air gap coefficient when the stator has slots. When the stator and the flexible wheel are applied with a constant magnetic potential, the magnetic induction is larger because the air gap is smaller at the tooth tip, the distribution of magnetic field lines at the tooth top is denser. The distribution curve of air gap flux density is shown in Fig. 1.

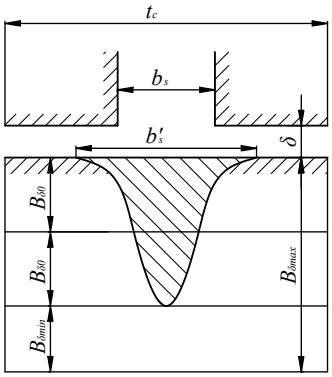

Figure 1 Distribution curve of air gap magnetic field under trough

Because the air gap size is generally smaller compared with the tooth width, the magnetic flux density is actually the same as that of the uniform air gap in most areas of the tooth width to be $B_{\delta\max}$, at the center of the slot, the air gap flux density is minimum to be $B_{\delta\min}$, $B_{\delta\min}$ is related to the gap size and the width of the slot.

The area of the shaded area in Figure 1 indicates the decrease in flux at a tooth pitch due to the presence of the stator slot when the air gap potential is constant. It can be seen that the air gap flux density reduction makes the average flux density in a pitch decrease from the original uniform air gap $B_{\delta\max}$ to $B_{\delta 0}$ ($B_{\delta 0}$ is the average value of air gap flux density). If we want to calculate $B_{\delta 0}$, we can use a smooth stator with an equivalent air gap δ' replace the original slotted stator. The equivalent air gap δ' should be the same as the original $B_{\delta 0}$ air gap flux density. The relationship between equivalent air gap δ' and the real air gap δ is expressed as follows:

$$\delta' = k_{\delta 1}\delta \tag{1}$$

Wherein, $k_{\delta 1}$ ——the air gap coefficient, which is expressed as a multiple of the equivalent air gap increase when the stator has a slot on one side.

Obviously

$$k_{\delta 1} = \frac{\delta'}{\delta} = \frac{B_{\delta\max}}{B_{\delta 0}} > 1 \tag{2}$$

Therefore, when the stator has a slot, the average air gap flux density is as follows

$$B_{\delta 0} = \frac{1}{k_{\delta 1}} B_{\delta \max} \tag{3}$$

The calculation of air gap coefficient is as follows: assuming that the depth of the slot is infinite and the slot pitch is infinite, that is, only one slot is considered. The first assumption is that the depth of the stator slot in the electromagnetic harmonic drive is much larger than the slot width.[3] In this case, assuming that the slot depth is infinite, its influence on the air gap flux density distribution is small. The second assumption is that the ratio of air gap is not wide in the slot width, in the near distance from the notch, the flux density has quickly reached a smooth air gap under the flux density. The results obtained according to the above two assumptions are not different from the results after complex calculations in the actual size in reality. The conformal transformation method[4] is used to calculate the air-gap magnetic field with the tooth pitch of t_c.

$$B = \frac{\rho + u^2}{\sqrt{(\rho+1)(\rho+u^4)}} B_{\delta \max} \tag{4}$$

Wherein, $B_{\delta \max}$ ——the uniform air gap magnetic flux density,

$$B_{\delta \max} = \frac{\mu_0}{\delta} F$$

u ——the real part of calibration magnetic potential analytic function.

$$u = \frac{b_s}{2\delta} + \sqrt{1 + (\frac{b_s}{2\delta})^2} \tag{5}$$

ρ ——the variable parameter associated with the coordinates from the center of the slot.

$$x = \frac{\delta}{\pi}\left[\ln\frac{\left(\sqrt{\rho+u^4}+\sqrt{\rho+1}\right)\left(u^2\sqrt{\rho+1}-\sqrt{\rho+u^4}\right)}{\left(\sqrt{\rho+u^4}-\sqrt{\rho+1}\right)\left(u^2\sqrt{\rho+1}+\sqrt{\rho+u^4}\right)} - 2\frac{b_s}{\delta} arctg\left(\frac{1}{u}\sqrt{\frac{\rho+u^4}{\rho+1}}\right)\right] + \frac{b_s}{2} \tag{6}$$

According to Formulas (4) - (6), the distribution curve on the smooth surface B is shown in Fig. 2.

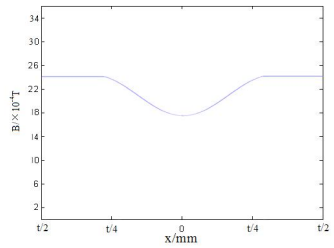

Figure 2 The magnetic flux density in a slot pitch

As can be seen from Figure 2, when x is close to $t_c/2$, B has been basically reached $B_{\max}$. The calculation result can be applied to the case of one slot with one pitch t_c.

According to the calculated results, the amplitude of the flux density drop at the center of the slot to be:

$$B_d = 2\beta B_{\delta \max} \tag{7}$$

β can be determined through the following formula:

$$\beta = \frac{1 + u^2 - 2u}{2(1+u^2)} \tag{8}$$

In the unit core length, the value decrease in the magnetic flux within a tooth pitch can be expressed as

$$\Delta\phi = b_s' \ \beta B_{\delta \max} = \sigma b_s \beta B_{\delta \max} \tag{9}$$

Wherein, $\sigma = b_s'/b_s$, the magnetic flux ϕ_t in a pitch on a unit axial length is:

$$\phi_t = B_{\delta \max} t_c - \Delta\phi = (t_c - \beta\sigma b_s) B_{\delta \max} = (t_c - \gamma\delta) B_{\delta \max} \tag{10}$$

Wherein, $\beta\sigma b_s = \gamma\delta$

Therefore, the average magnetic induction of the air gap is:

$$B_{\delta 0} = \frac{\phi_t}{t_c} = \frac{t_c - \gamma\delta}{t_c} B_{\delta \max} = \frac{1}{k_{\delta 1}} B_{\delta \max} \tag{11}$$

The air gap coefficient is:

$$k_{\delta 1} = \frac{B_{\delta \max}}{B_{\delta 0}} = \frac{t_c}{t_c - \gamma\delta} \tag{12}$$

Wherein,

$$\gamma = \frac{4}{\pi}\left[\frac{b_s}{2\delta}\tan^{-1}\frac{b_s}{2\delta} - \ln\sqrt{1 + (\frac{b_s}{2\delta})^2}\right] \tag{13}$$

Fig. 3 is the relationship curve of γ and b_s/δ ,when $1 < \frac{b_s}{\delta} < \infty$, if considered approximately

$$\gamma \approx \frac{(\frac{b_s}{\delta})^2}{5 + \frac{b_s}{\delta}} \tag{14}$$

As shown by the dotted line in Fig. 3, the error is less than 10%, which has a smaller influence on the air gap coefficient $k_{\delta 1}$. Therefore, the accuracy $k_{\delta 1}$ obtained by Formula (14) is sufficiently accurate.

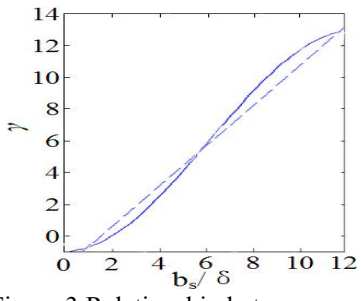

Figure 3 Relationship between γ and b_s/δ

In the electromagnetic harmonic movable tooth transmission, considering the influence of tooth pitch, width and air gap length on the air gap coefficient of stator slot, the author analyzes and calculate the air

gap coefficient of the stator slot in the electromagnetic harmonic tooth movement with the above factors, and parts of the results are shown in Fig.4, Fig.5 and Fig.6.

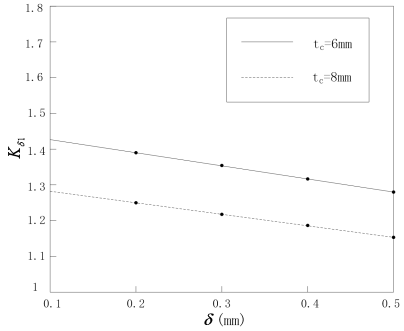

a) $b_s = 2.5\,\text{mm}$

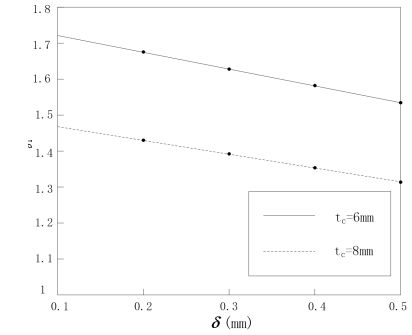

b) $b_s = 3.5\,\text{mm}$

Figure 4 Relation between $k_{\delta 1}$ and δ

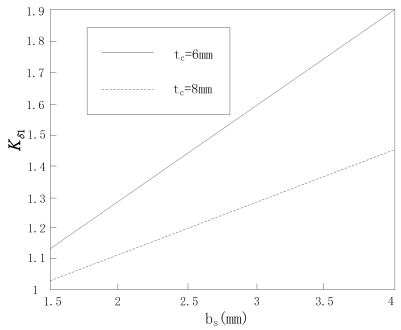

a) $\delta = 0.4\,\text{mm}$

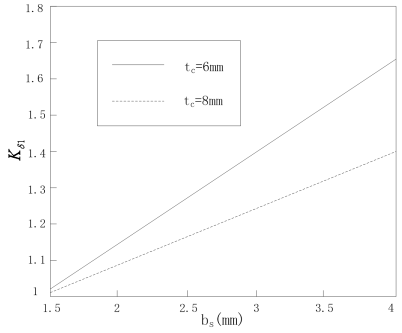

b) $\delta = 0.6\,\text{mm}$

Figure 5 Relation between $k_{\delta 1}$ and b_s

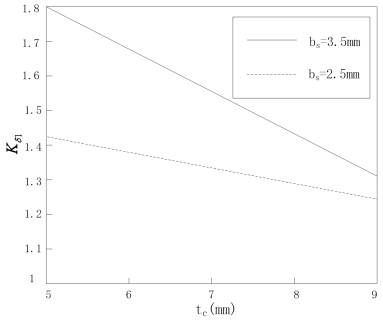

a) $\delta = 0.4$ mm

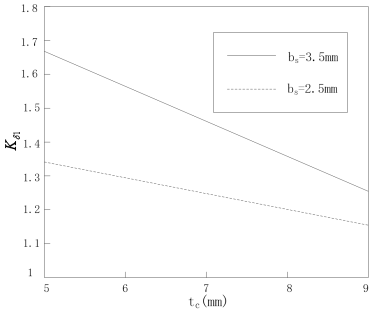

b) $\delta = 0.6$ mm

Figure 6 Relation between $k_{\delta 1}$ and t_c

It can be seen from Fig. 4 – Fig. 6 that the change rule of $k_{\delta 1}$ with the above-mentioned factors is as follows:

(1)With the increase of air gap length δ, $k_{\delta 1}$ decreases. In the case of a wider stator slot and a smaller tooth pitch, the reduction amplitude $k_{\delta 1}$ is larger. On the contrary, the narrower the stator slot is, the larger the tooth pitch is, the reduction amplitude $k_{\delta 1}$ is smaller.

(2)With the increase of slot width, $k_{\delta 1}$ increases. In the case of a smaller tooth pitch, the larger the increase amplitude $k_{\delta 1}$ is, the greater the pitch is, the smaller the increase amplitude $k_{\delta 1}$ is. This is because the pitch is small, the magnetic flux density near the notch is affected by the adjacent teeth, therefore, it cannot reach $B_{\delta \max}$.

(3)With the increase of tooth pitch t_c, $k_{\delta 1}$ decreases. When the smaller the tooth pitch t_c, the larger the slot width b_s, the smaller the air gap δ, the greater the reduction amplitude $k_{\delta 1}$, when the tooth pitch t_c increases to a certain value, the reduction amplitude $k_{\delta 1}$ region is stable.

In short, in order to obtain higher efficiency, so that the stator notch has a small effect on the air gap flux density, it is needed to minimize notches and increase pitch on the basis of guaranteeing transmission performance. In addition, when the air gap length increases, the equivalent air gap changes little, and

the increase of air gap length results in decrease in the electromagnetic force of flexible wheel. Therefore, under the premise of ensuring the deformation space of flexible wheel, the smaller air gap length, the better it will be.

3. CONSIDERING OF AIR-GAP COEFFICIENT OF FLEXIBLE WHEEL DEFORMATION

As for the harmonic electromagnetic oscillating tooth gear transmission, the air gap magnetic field should not only consider the cogging effect, but also consider the deformation of the flexible wheel due to its working principle, then the air gap length is a function changing with armature surface[5] , and is not a constant.

Here, d_m is the maximum deformation of the flexible wheel, δ' is the equivalent uniform air gap length taking into account the flexible wheel is not deformed with the stator slot. Obviously, $\delta_{\min}=\delta'-\delta_m$, $\delta_{\max}=\delta'+\delta_m$. If the average air gap flux density is $B_{\delta 0}$ when Uniform air gap length is δ' , the flux is ϕ_t . When the flexible wheel is deformed, the air gap flux density will change, and the magnetic flux density at the moment is ϕ' , the corresponding average magnetic flux density B . So the air gap coefficient is:

$$k_{\delta 2}=\frac{\phi_t}{\phi'}=\frac{B_{\delta 0}}{B} \tag{15}$$

When the saturation of iron is not considered, the air gap flux density is $B(x')=\dfrac{\mu_0 F_\delta}{\delta(x')}$ and wherein, F_δ is the air gap magnetomotive force. Therefore

$$\phi'=\int_0^\tau B(x')L_g dx'=\mu_0 L_g F_\delta\int_0^\tau\frac{dx'}{\delta(x')} \tag{16}$$

Wherein, L_g ——the axial length of air gap.

τ ——winding polar distance

x' ——Stator perimeter expansion

It is generally assumed that the shape of the flexible wheel is elliptical and its long axis is $a=r+d_m$, and short axis is $b=r-d_m$, the length of the air gap is: .

$$\delta(x')=R-\sqrt{a^2\sin^2\frac{\pi}{\tau}x'+b^2\cos^2\frac{\pi}{\tau}x'} \tag{17}$$

Wherein, R is the stator equivalent radius, $R=r+\delta'$, then the above formula can be rewritten as:

$$\begin{aligned}\delta(x')&=\delta'+R\left[1-\sqrt{(1+\frac{d_m}{R})^2\sin^2\frac{\pi}{\tau}x'+(1-\frac{d_m}{R})^2\cos^2\frac{\pi}{\tau}x'}\right]\\&=\delta'+R\left[1-\sqrt{1+\frac{d_m^{\,2}}{R^2}-2\frac{d_m}{R}\cos\frac{2\pi}{\tau}x'}\right]\end{aligned} \tag{18}$$

Because $\dfrac{d_m}{R}<<1$, then

$$\delta(x')\approx\delta'+d_m\cos\frac{2\pi}{\tau}x' \tag{19}$$

The coefficient of the air gap is $k_{\delta 2}$, it can be obtained from Formulas (15) and (16)

$$\begin{aligned}k_{\delta 2}&=\frac{\int_0^\tau B_{\delta 0}L_g dx'}{\int_0^\tau B(x')L_g dx'}=\frac{\tau}{\delta'\int_0^\tau\frac{dx'}{\delta(x')}}\\&=\frac{\tau}{\int_0^\tau\frac{1}{1+\frac{d_m}{\delta'}\cos\frac{2\pi}{\tau}x'}dx'}\end{aligned} \tag{20}$$

The distribution curve of flux density of the air gap curve without considering saturation is shown in Fig. 7.

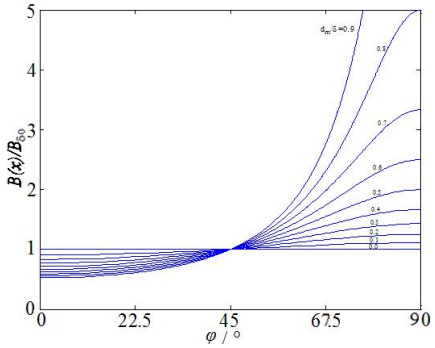

Figure 7 The gap magnetic flux density distribution under different saturation

$k_{\delta 2}$ is given at different values d_m/δ' in Tab. 1.

Table 1 Gap coefficient

d_m/δ'	0.1	0.2	0.3	0.4	0.5	0.6	0.7	0.8	0.9
$k_{\delta 2}$	0.994	0.978	0.952	0.914	0.863	0.797	0.710	0.596	0.431

It can be seen from Fig.7 and Tab.1 that with the increase in d_m/δ' , the absolute value of air gap magnetic density and the ratio of uniform magnetic density increased significantly, and the air gap coefficient decreased gradually.

Considering that the air gap flux density can not grow infinitely, it will be affected by the saturation of magnetic field in the iron core. Usually, magnetic circuit design makes saturation magnetic dense $B_s=(1.6\sim 4.9)B_\delta$,[6]the maximum magnetic density of air gap must satisfy $B_{\max}<B_s$, so, after flexible wheel is deformed, the air gap coefficient will be:

$$k_{\delta 2}=\frac{\tau B_{\delta 0}}{\int_0^\tau B(x')dx'}=\frac{\tau B_{\delta 0}}{\int_{\frac{1-\alpha}{2}}^{\frac{1+\alpha}{2}}B(x')dx'} \tag{21}$$

Wherein, α —the calculation pole arc. The distribution of $B(x')$ should take the effects of saturation into account.

3.1 AIR-GAP COEFFICIENT IN STRAIGHT AXIS

When the peak value of the magnetic potential corresponds to the minimum position of the air gap, i.e., the long axis of the flexible wheel, it belongs to the straight axis magnetic circuit state. Without deformation, the maximum magnetic flux density in the air gap is $B_{\delta 0}$, and magnetic flux is ϕ_t; after the deformation, the air gap flux is $\phi' = \dfrac{\phi_t}{k_{\delta 2}}$, the equivalent magnetic flux density is B, because when the magnetic potential is not changed, so after the deformation, the length of air gap decreases, the magnetic flux density increases. The reduced air gap length δ'' can be calculated from the following formula:

$$F_\delta = H\delta' = \frac{B_{\delta 0}}{\mu_0}\delta' = \frac{B}{\mu_0}\delta'' \tag{22}$$

Thus, the equivalent air gap length δ''

$\delta'' = k_{\delta 2}\delta'$

δ'' is called the calculation of air gap length after the flexible wheel is deformed.

Supposing the air-gap magnetic potential is sinusoidal distribution, then

$$k_{\delta 2} = \frac{\sqrt{2\psi(1-\psi)}}{arctg\sqrt{\dfrac{2\psi}{1-\psi}}} \tag{23}$$

Wherein, $\psi = \dfrac{d_m}{\delta'}$

The air gap flux density distribution is shown in Fig. 8, and the air gap coefficient is shown in Tab. 2.

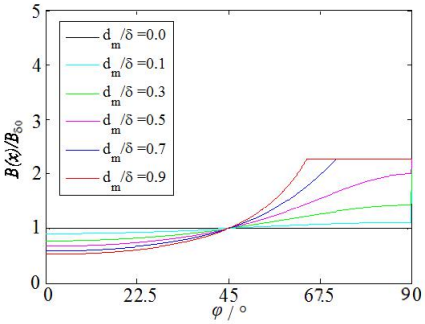

a)flux density distribution when the saturation density is 1.6

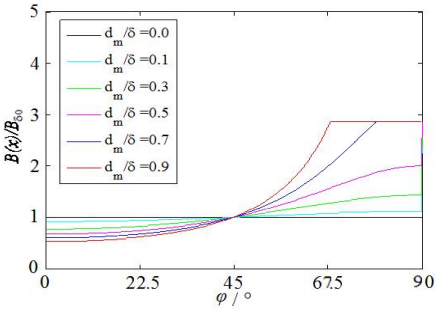

b) flux density distribution when the saturation density is 2.0

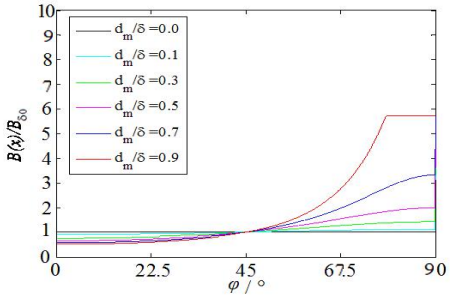

c) flux density distribution when the saturation density is 4.0

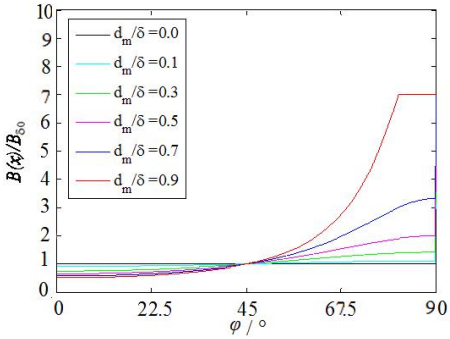

d)flux density distribution when the saturation density is 4.9

Figure 8 The gap magnetic flux density distribution under different saturation coefficient

Table 2 The gap coefficient under different saturation coefficient

ψ / B_s/B_δ	0.1	0.2	0.3	0.4	0.5	0.6	0.7	0.8	0.9
1.6	0.963	0.919	0.868	0.826	0.808	0.797	0.790	0.786	0.783
2.0	0.963	0.919	0.868	0.808	0.740	0.700	0.679	0.666	0.656
4.0	0.963	0.919	0.868	0.808	0.740	0.661	0.569	0.484	0.447
4.9	0.963	0.919	0.868	0.808	0.740	0.661	0.569	0.459	0.401
∞	0.963	0.919	0.868	0.808	0.740	0.661	0.569	0.459	0.317

It can be seen from Fig.5 and Fig.8 that the magnetic flux density increases with the increase of the flexible wheel deformation. And because of the saturation effect, the air gap flux density will no longer increase after a certain value increases. With the increase of the saturation coefficient, the influence of the air gap change on the air gap flux density will also increase. The change trend of the air gap coefficient shown in Tab. 2 also indicates it. This is because the smaller the gap length, the greater the influence of air gap flux on the flexible wheel, so at the minimum length of the air gap has the largest force of the magnetic

field.

3.2 air-gap coefficient in the cross axis STATE

When the magnetic potential peak corresponds to the maximum position of the air gap that is the short axis of the flexible wheel, it is cross-axis magnetic circuit state, then $k_{\delta 2}$ is

$$k_{\delta 2}=\frac{2(\sqrt{2\psi(1+\psi)})}{\ln(\sqrt{1+\psi}+\sqrt{2\psi})-\ln(\sqrt{1+\psi}-\sqrt{2\psi})} \tag{24}$$

When ψ takes different values, the variation of $k_{\delta 2}$ with the different saturation coefficients is shown in Tab.3.

Table 3 The gap coefficient when quadrature-axis magnetic potential sinusoidal distribution

B_s/B_δ \ ψ	0.1	0.2	0.3	0.4	0.5	0.6	0.7	0.8	0.9
1.6	1.029	1.052	1.079	1.073	1.068	1.052	1.019	0.962	0.859
2.0	1.029	1.052	1.075	1.089	1.098	1.112	1.136	1.162	1.170
4.0	1.029	1.052	1.075	1.089	1.098	1.137	1.172	1.201	1.232
4.9	1.029	1.052	1.075	1.089	1.098	1.137	1.172	1.225	1.268

3.3 the air-gap coefficient when the magnetic potential peak at any one position φ

Under normal circumstances, when the amplitude of the air gap sinusoidal magnetic potential in any one position φ_0, then

$$F(x')=F_a\cos(\frac{\pi x'}{\tau}-\varphi_0) \tag{25}$$

The air - gap flux density is obtained

$$B(x')=\frac{\mu_0 F_a}{\delta(x')}=\frac{\mu_0 F_a\cos(\frac{\pi x'}{\tau}-\varphi_0)}{\delta'-d_m\cos(\frac{2\pi x'}{\tau})}=B_{\delta 0}\frac{\cos(\frac{\pi x'}{\tau}-\varphi_0)}{1-\frac{d_m}{\delta'}\cos(\frac{2\pi x'}{\tau})} \tag{26}$$

Wherein, F_a ——the air gap magnetomotive force at φ_0.

$B_{\delta 0}=\frac{\mu_0 F_a}{\delta'}$ is the equivalent air gap magnetic flux density amplitude after considering stator slot.

Then

$$k_{\delta 2}=\left|\frac{\int_{\varphi_0-\frac{\pi}{2}}^{\varphi_0+\frac{\pi}{2}}B_{\delta 0}L_g dx'}{\int_{\varphi_0-\frac{\pi}{2}}^{\varphi_0+\frac{\pi}{2}}B(x')L_g dx'}\right|=\frac{2\tau}{\pi}\int_{\varphi_0-\frac{\pi}{2}}^{\varphi_0+\frac{\pi}{2}}\frac{1-\beta\cos\frac{2\pi x'}{\tau}}{\cos(\frac{\pi x'}{\tau}-\varphi_0)}dx' \tag{27}$$

$$=\frac{2}{\cos\varphi_0\int_{\varphi-\frac{\pi}{2}}^{\varphi+\frac{\pi}{2}}\frac{\cos\frac{\pi x'}{\tau}}{1-\psi\cos\frac{2\pi x'}{\tau}}dx'+\sin\varphi_0\int_{\varphi-\frac{\pi}{2}}^{\varphi+\frac{\pi}{2}}\frac{\sin\frac{\pi x'}{\tau}}{1-\psi\cos\frac{2\pi x'}{\tau}}dx'}$$

$$=\frac{1}{\cos\varphi_0\sqrt{\frac{1}{2\psi(1-\psi)}}arctg\,(\cos\varphi_0\sqrt{\frac{2\psi}{1-\psi}})+\frac{\sin\varphi_0}{2}\sqrt{\frac{1}{2\psi(1+\psi)}}\ln\frac{\sqrt{1+\psi}+\sqrt{2\psi}\sin\varphi_0}{\sqrt{1+\psi}-\sqrt{2\psi}\sin\varphi_0}}$$

Obviously, $\varphi_0=0^\circ,90^\circ$ are respectively corresponding to the straight axis and cross axis state, Tab.4 are the $k_{\delta 2}$ of φ_0 changes from 0° to 90°.

Table 4 $k_{\delta 2}$ value when φ_0 changing from 0° to 90°

φ_0 \ β	0	0.1	0.2	0.3	0.4	0.5	0.6	0.7	0.8	0.9
0	1.000	0.963	0.919	0.868	0.808	0.740	0.662	0.570	0.460	0.317
10	1.000	0.965	0.923	0.872	0.814	0.746	0.667	0.576	0.465	0.321
20	1.000	0.969	0.932	0.885	0.829	0.763	0.685	0.593	0.481	0.333
30	1.000	0.978	0.947	0.906	0.855	0.792	0.716	0.624	0.509	0.356
40	1.000	0.989	0.967	0.934	0.890	0.833	0.761	0.670	0.553	0.392
50	1.000	1.000	0.990	0.968	0.934	0.885	0.820	0.733	0.615	0.445
60	1.000	1.012	1.013	1.003	0.981	0.945	0.890	0.812	0.700	0.524
70	1.000	1.021	1.033	1.035	1.027	1.004	0.965	0.903	0.805	0.637
80	1.000	1.028	1.047	1.058	1.060	1.050	1.028	0.985	0.912	0.777
90	1.000	1.029	1.052	1.079	1.073	1.068	1.052	1.019	0.962	0.859

It can be seen from Tab.3 and Tab.4, when φ_0 changes between 0° and 90°, if the flexible wheel is not deformed, $k_{\delta 2}$ is always 1; when $\varphi_0<60^\circ$, with the increase of deformation, then $k_{\delta 2}$ decreased, and the greater the deformation, the greater the

magnitude of $k_{\delta 2}$ decreases, this is because the greater the region deformation , the smaller the air gap, resulting in an increase in magnetic density; when $\varphi_0 > 60^\circ$, with the increase of deformation, $k_{\delta 2}$ also increases, when the deformation is to a certain extent, $k_{\delta 2}$ no longer increases, but slowly reduced, this is because the greater the region deformation, the air gap increases, magnetic density decreases. Due to the influence of saturation, when deformation reaches to a certain extent, $k_{\delta 2}$ no longer increases but decreases. The smaller the saturation coefficient, the sooner it enters the situation.

3.4 total air-gap coefficient of electromagnetic harmonic drive

In the electromagnetic harmonic drive, when the stator is slotted and the flexible wheel is deformed, the air gap magnetic field distribution pattern is complex, which is related to the relative position of the stator and the flexible wheel deformation. When the stator (tooth) slot is at any relative position after deformation of the long and short axis of flexible wheel, the Laplasse Equation in the air gap magnetic field is very difficult to solve. Therefore, there is no strict formula to obtain the air gap magnetic field in any relative position, the analytic formula of air- gap magnetic field distribution can be given at some special positions (stator teeth to the flexible wheel long axis or the stator slot to the flexible long axis). In order to find out the total air gap coefficient of the electromagnetic harmonic movable tooth drive, in this paper, the stator slot is used to the basis to analyze the position of the long axis of the flexible wheel, then the air gap coefficient k_δ can be approximated by the following methods:

If only the stator has a slot, the air gap coefficient can be determined according to (2), when the flexible wheel is deformed under the action of electromagnetic force, the air gap coefficient can be determined according to (15). In the case with the stator slot and the flexible wheel deformation, k_δ is determined by the following formula

$$k_\delta = \frac{\delta''}{\delta} = k_{\delta 1} k_{\delta 2} \tag{28}$$

4. CONCLUSIONS

As for the deformation of flexible wheel under the action of the harmonic electromagnetic movable teeth drive in the magnetic field, the air gap will change at any time; the concept of air gap function is introduced. Through the analysis of the magnetic field, the air-gap coefficient is given considering the harmonic drive stator slot and the flexible wheel deformation, and thereby, obtaining the total air gap coefficient of electromagnetic harmonic oscillating tooth drive. And the analysis results are helpful to correctly describe the magnetic field state of electromagnetic harmonic oscillating tooth drive.

ACKNOWLEDGMENT

The author is very grateful to the Hebei government by the support of science and technology project (Item No. 15211921).

REFERENCES

[1]Yan Yihua,You Zhuping, Magnetic field in electromagnetic harmonic drive[J], mechanical drive, 1993,17(1): 4-7.

[2]Ren Yubo, Research on electromagnetic harmonic movable tooth drive[D],Yanshan university, 2014: 58-66.

[3]Yan Weili,Yang Qingxin,Wang Youhua, Numerical analysis of electromagnetic field in electrical engineering[M], Machinery Industry Press, 2015.

[4]Vishwanath Hegde,G.S. Maruthi,Experimental investigation on detection of air gap eccentricity in induction motors by current and vibration signature analysis using non-invasive sensors[J],Energy Procedia, 2012, 14: 1047-1052.

[5]Lizhong Xu, Yongli Liang,Torque for an electromagnetic harmonic movable tooth drive system, Mechanism and Machine Theory[J], 2016,98:190-198.

[6]F.R. Cunha, H.L.G. Couto,A new boundary integral formulation to describe three-dimensional motions of interfaces between magnetic fluids[J],Applied Mathematics and Computation,2008, 199 (1): 70-83.

Dissipative Particle Dynamics Simulation Research on the Characteristic of Grinding Fluid Particles

ZHOU Zeng-wei, LI Jun-ye, QIAO Ze-min, ZHANG Xin-ming, XU Ying
College of Mechanical and Electrical Engineering, Changchun University of Science and Technology, Changchun 130022, China

Abstract :On grinding fluid particle properties on the state of the mesoscopic simulation analysis of using dissipative particle dynamics (DPD) features, for simulating a single DPD grinding fluid particles, and get its density, pressure, temperature curve; Comparing different number of DPD particles, calculation results show that the steady state after the differences, and its surface state of workpiece have obvious distinction in research of abrasive flow processing two phase flow is of great significance.
Keywords： Dissipative particle dynamics, grinding fluid particles, two phase flow

1. INTRODUCTION

Grinding fluid (abrasive) is a kind of solid - liquid two-phase mixture what make of viscoelastic, softness and cutting of semisolid carrier and a certain amount of sand mixing. In two-phase flow, there are interaction between solid and the liquid, solid particles have an action with the motion of fluid,due to the driving of the fluid phase,the mutual collision occurred between the grinding particles and grinding particles, grinding particles and the surface of the job, thus the wall is constantly subjected to force and friction and wear [1]. This wear is the grinding effect of abrasive particles on the machined surface, as shown in figure (1). It has practical significance on the study of the dynamic characteristics of the grinding fluid, the control of the viscosity, temperature, pressure, and the accuracy of the surface.

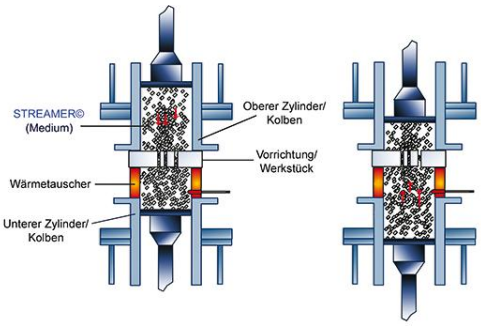

Fig. 1 Schematic diagram of abrasive flow machining

In recent years, study of grinding fluid particle dynamics focuses on macroscopic characteristics of abrasive particles by study on the morphology and aggregated state of particles by the traditional finite difference method, finite element method,method of boundary element and the smooth particle hydrodynamics (smoothed particle viscous, SPH) [2]. We can obtain the grinding state of surface at macroscopic state by analysis on the coupling of multi physics field simulation .but the analysis of job are limited , effective analysis of the microscopic state cannot be got. It is the morphology of the abrasive particles under the microscope as show in Fig. (2). In recent years, the research on the microscopic state of objects is gradually emerging in the microscopic, At the microscopic state, the structure and properties of atoms, electrons and molecules play a significant role, in the mechanical engineering field, the introduction of nanotechnology in micro state brings great changes in precision and ultra precision machining, in the grinding abrasive flow machining process with discrete and an a atom, a plurality of atoms or atomic layer is removed through analysis of atomic states of grinding fluid particles, the most widely used molecular dynamics,Through analysis of atomic states of grinding fluid particles, it is removed by the way of an a atom and a plurality of atoms or atomic layer at the grinding abrasive flow machining process, we acquire micro and detailed analysis in the abrasive flow machining process. The flow behavior of the fluid is simulated by tracing the position and momentum of each particle molecule[3]. Although molecular dynamics in molecular systems with less number of simulation has achieved considerable success, Spatial and temporal that scale molecular dynamics can be calculated at present is limited to nanosecond, nanometer level owe to the limit of the speed of the computer. However, the static and dynamic physical properties grinding fluid directly related to system flow performance are often in milliseconds, micron scale temporal and spatial scales, namely mesoscopic (mesoscopic) scale [4], the extremely demand for computation of the simulation work is not available at present when we molecular dynamics (MD) used to simulate complex fluids. Mesoscopic simulation actually plays a role in the construction of a bridge between the dynamics of the fast molecular scale and the slow macroscopic scale.

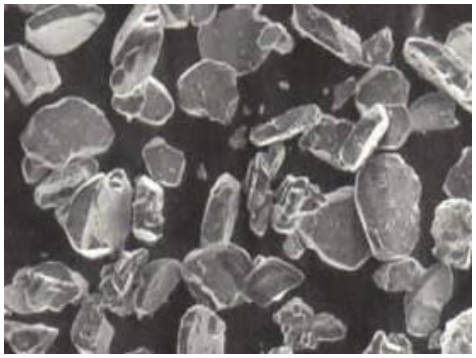

Fig. 2 The earliest mesoscale simulation of fluid simulation

The earliest mesoscale simulation of fluid simulation technology is the gas grid method (gas approach lattice), and then the lattice-Boltzmann method has been greatly improved by adopting to the distribution function. Dissipative particle dynamics (particle dynamics dissipative, abbreviated as DPD) is a new mesoscale numerical simulation technology raised by Hoogerbrugge and Koelman[5],DPD method is to improve defects of the lattice gas automata, is fluid particles require along plaid motion. After introducing the theory of molecular dynamics,the fluid particles are not limited by the lattice, and remove in the role of the interaction ,The DPD method does not adopt to be corresponding to the particles anymore, but also adopt the "Particles" that correspond to a small region of a polymer or fluid, the concept of "particles" in DPD has the concept of coarse-grained (coarse-graining) [6],the movement of each particle represents the collective action of a large number of molecules (so-called fluid particles),its particles move in a continuous space rather than discrete lattices, and follow the Galilean invariance, the DPD method is a bridge of continuous micro molecular dynamics method and macroscopic fluid mechanics method, which is a real mesoscale simulation technology.

2. DPD THEORETICAL MODEL AND METHOD

2.1 theoretical model

In the DPD system, the basic unit is the momentum vector which is called "particle". These particles move in a continuous space and discrete time, The interaction occurred in each particle in a certain range and the surrounding particles, the interaction force between particles includes 3 kinds [7]of which are conservative force, dissipative force and random force,the so-called "particle" in DPD system has the concept of coarse granulation (ocars-egraining), and the movement of each particle represents the collective behavior of a large number of molecules, DPD simulate method is divided into two steps: one is to solve the Newton equation of motion, to determine the position and velocity of the particle free movement; another is to determine the collision between particles, based on the Newtonian equation of motion, the change of the position and velocity of the particles in the DPD system is the formula (1).

Based on the Newtonian equation of motion, the change of the position and velocity of the particles in the DPD system is the formula (1) r_i v_i and f_i represent the position, velocity and the resultant force vector of the particle i and t represent time. The mass of per particle in the DPD system is the mass of each particle, that is1, and the size of the force acting on each particle is equal to the value of the acceleration of the particle.

$$\frac{dr_i}{d_t} = v_i \qquad m_i \frac{dv_i}{dt} = f_i \tag{1}$$

The sum of the symbols in the formula (2) indicates that the force between all the other particles within a certain truncated radius is not included in the particle I, (If the distance between particles $r_{ij} > r_c$, the interaction between the particles is zero.)

$$f_i = \sum_{j \neq i} (F_{ij}^C + F_{ij}^D + F_{ij}^R) \tag{2}$$

In the formula, the conservative force F_{ij}^C is the repulsive force acting on the particle in the direction of the connection between the two particles, which can be expressed as the formula (3).

$$F_{ij}^C = \begin{cases} a_{ij}\left(1 - \frac{r_{ij}}{r_c}\right)\hat{r}_{ij}, r_{ij} < r_c \\ 0, r_{ij} \geq r_c \end{cases} \tag{3}$$

a_{ij} is coefficient of conservative force, represents the maximum repulsive force between the particle I and the J;

$$r_{ij} = r_i - r_j, r_{ij} = \left|r_{ij}\right|, \hat{r}_{ij} = r_{ij} / \left|r_{ij}\right|$$

Like the conservative force, the random force and the dissipative force also act in the direction of the line of the particle's center of mass. The effect of J particles on the I particles in the dissipative force (or resistance) F_{ij}^D can be expressed as(4),random force F_{ij}^R can be expressed as(5).

$$F_{ij}^D = -\gamma \omega^D \left(r_{ij} \cdot v_{ij}\right)\hat{r}_{ij} \tag{4}$$

$$F_{ij}^R = \delta \omega^R (r_{ij}) \theta_{ij} \hat{r}_{ij} \varepsilon_{ij} \Delta t^{-\frac{1}{2}} \hat{r}_{ij} \tag{5}$$

Dissipation factor of a in formula, the negative sign indicates the direction of dissipation force and the relative velocity always in the opposite direction; ω^D and ω^R are the weighting function of the distance r_{ij} between the particles; ω^D and ω^R is 0, ε_{ij} is random number, mean value is 0, varianceis1,when $r_{ij} > r_c$,For each time step, each pair of particles are independent of each other. v_{ij} is relative velocity between particles,

$v_{ij} = v_i - v_j$, θ_{ij} is the Gauss distribution of the random function, When $i \neq j, k \neq l$,

$$\langle \theta_{ij}(t) \rangle = 0$$
$$\langle \theta_{ij}(t)\theta_{kl}(t') \rangle = (\delta_{ik}\delta_{jl} + \delta_{il}\delta_{jk})\delta(t-t') \quad (6)$$

the dissipative force reduces the relative velocity between the two particles, the particle kinetic energy and the cooling system; Random force makes the irregular movement of particles more severe, and the temperature of the system higher. Research of Espanol shows that ω^D and ω^R , γ and δ are related to each other, they can only take one, according to the theory of stochastic dissipation and the law of conservation of energy, the dissipative force and random force need to meet the equilibrium condition. Its expression is type(8)

$$\omega^D(r_{ij}) = [\omega^R(r_{ij})]^2 = \begin{cases} (1-r_{ij})^2, r_{ij} < r_c \\ 0, r_{ij} \geq r_c \end{cases} \quad (7)$$

$$\delta^2 = 2\gamma k_B T , \quad (8)$$

$k_B T$ is the Boltzman temperature for the system, $k_B T$ token as a unit of energy, the truncated radius is used as the unit length,77that is $k_B T = 1, r_c = 1$.

The difference between molecular dynamics and molecular dynamics is that the interaction between particles in the system is realized by the force of some unique phenomena. We choose quality of particles and inter particle interaction effects of truncation distance as a unit, all cases were through divided by the particle mass and radius, with dimensionless units to quantitatively, using the theorem of equipartition of energy with temperature to a velocity of all particles. This is equivalent to the $\sqrt{mr_c^2 / k_B T}$ that the unit to measure time. After this treatment, all the quantities are non dimensional.In DPD simulation, R, V and T are the length, speed, and time of physical units defined as the formula (9).In this way, the results of a DPD simulation can be linked to many kinds of physical systems.

$$\bar{r} = \frac{r}{r_c}, \bar{v} = \frac{v}{\sqrt{k_B T / m}}, \bar{t} = \frac{t}{\sqrt{mr_c^2 / k_B T}} \quad (9)$$

2.2 numerical integration method

At present, the commonly method people used is the modified algorithm velocity-verlet[8]proposed by Groot and Warren. It is relatively simple and reliable, the specific expression of the formula (10), Δt is the relaxation factor and time step, When 入 is 0.5, the formula (10) is reduced to Veolcity-Verlet integral format. Under certain conditions, the temperature stability of 入=0.65 is better.

$$r_i(t+\Delta t) = r_i(t) + \Delta t v_i(t) + \frac{1}{2}(\Delta t)^2 f_i(t)$$
$$\bar{v}_i(t+\Delta t) = v_i(t) + \lambda \Delta t f_i(t)$$
$$f_i(t+\Delta t) = f_i(r_i(t+\Delta t), \bar{v}_i(t+\Delta t)) \quad (10)$$
$$v_i(t+\Delta t) = v_i(t) + \frac{1}{2}\Delta t(f_i(t) + f_i(t+\Delta t))$$

3. PHYSICAL MODELING AND NUMERICAL SIMULATION

3.1Analysis and calculation of DPD particles in a single grinding liquid particle

The silicon carbide (SiC) particles in the grinding fluid were analyzed, and the DPD particle model was established in Figure 1.

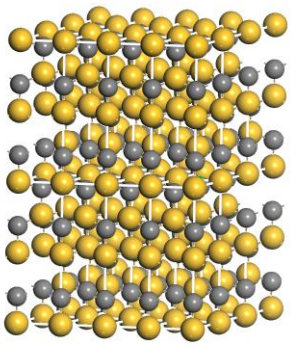

Fig. 3 physical model of SiC particles In the process of modeling of silicon carbide particles, the number of silicon carbide particles to select a certain range, and its boundary conditions need to be redefined, the composition of silicon carbide atoms is composed of a silicon atom and two carbon atoms, the initial state is a certain proportion, and the boundary conditions are selected for the multi atom constitution.

In the computer simulation setting, 100 identical DPD particles are projected onto a 10 x 10 non dimensional computational region, We use traditional DPD method, make the system to achieve the equilibrium state of the traditional DPD method in conservative power function is a purely repulsive, after reaching the equilibrium state, the DPD particles roughly evenly covered with the region as a whole, when the system reaches the equilibrium state, the application of new conservative force potential function and improved time integration algorithm in empirical coefficient 入 = 0.65 to expand DPD simulations.

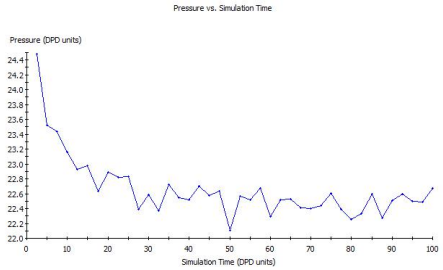

Fig. 4 pressure change during simulation

As shown in figure (4),in the simulation process of SiC particle, the state of stress in the presentation of a decreasing trend when simulate 100 steps, the pressure value from the initial 24.5N gradually decreases , the pressure is the most intense, the acceleration curve is obvious, from the state of 24.5N to 22.8N, DPD particles have a certain compression form in 0--15 step number; 15 step number to 100 the number of steps from the simulation process, the pressure is maintained 22.6N stress at the moment tends to be stable, silicon carbide DPD abrasive is gradually showing stable form.

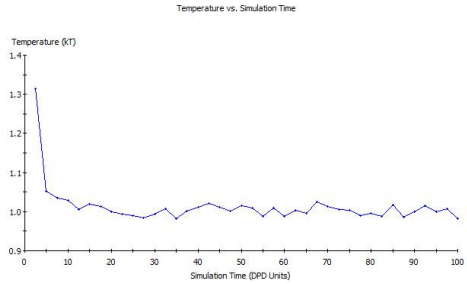

Fig. 5 temperature variation in simulation process

Also in the silicon carbide DPD particle simulation process, the analysis of the temperature change trend, from the image we can select the initial temperature of 1.3KT, In the initial simulation process, from 0 -- 5 steps in the simulation, temperature from 1.3KT greatly reduced to 1.05KT, temperature also appears to the state of severe decline. Then from 5 step number to 100 step simulation, silicon carbide DPD particles gradually stabilized to 1.0KT, DPD particles also gradually tends to be stable.

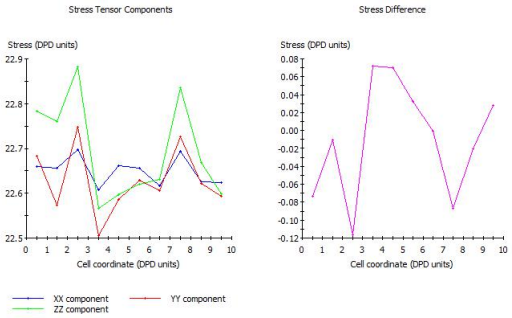

Fig. 6 the difference of pressure and pressure in the atomic coordinate

As shown in figure (6), through the analysis of the pressure tensor, we can know that from the chart, in the X direction, the pressure tensor initially to maintain the 22.65N. Through the changes in the atomic unit, after the atomic unit of change, the state was up and down, the highest 22.70N, the lowest was 22.60Nessentially unchanged, and in the Y direction, the pressure tensor showing vigorous exercise state, in the initial atomic coordinates, by 22.7N plunged to 22.6N, and under the zero - 3.5 atomic coordinates of the state, reached minimum values for 22.5N, maintain and subsequently fluctuations decreases, maintained at around 22.6N.And in the Z direction, with the floating the atomic coordinates, the pressure tensor also showed agglomeration changes of morphology, the peak value 22.9N from the initial 22.8N, under the zero - 3.5 atomic coordinates, the sharp decline to 22.5and ,stay in the subsequent state, showing a sharp rise again without a stable performance form in the whole process.

We can get that DPD particles with the pressure unit growth from the initial -0.08 to state 0, subsequently decline to the lowest value of -0.12, with the increase of the atomic coordinates, reached a peak value of 0.08 and stabilize the two coordinates and began presenting a decreasing trend, and reach the initial state in the whole process of change, showing the unstable state from the pressure difference coefficient in the image.

After simulation of silicon carbide DPD particles, the shape changes and finally reached a stable state, the parameters of the numerical value also gradually stabilized after a series of fluctuations, as shown in figure (7).

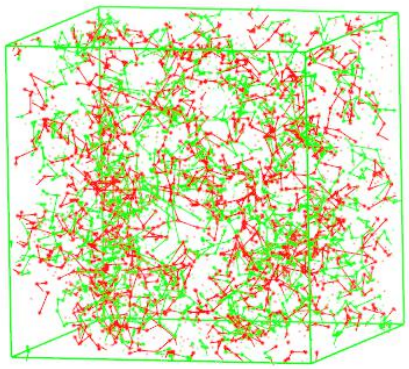

Fig. 7 morphology of silicon carbide particles under steady state

3.2 DPD particle analysis of different number of grinding fluid particles.The dissipative particle dynamics simulation was carried out by establishing the DPD particle model from simulation and comparison of 100, 200, and 300 DPD particles .

After analyzing and calculating, the density curve, the diffusion rate and the radial distribution function curve all have obvious difference, As shown in figure (8), compared to 100, 200 an DPD particles, the simulation results of 300 DPD particles more stable, and its aggregate state is also relatively good, generally showing a uniform distribution of the state.

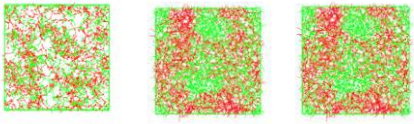

(a) (b) (c)

Fig. 8 simulation of SiC DPD particles with different numbers

As shown in figure (9),the morphology of the particles was observed under the microscope, the results showed that the morphology of SiC particles was similar to the DPD particles in the macroscopic state, the state of uniform distribution is also presented, and the distribution is more uniform, gap phase of smaller, decentralized state is better and decentralized state is also good, with the increase of macro particles. On the other hand, the same results are obtained with the simulation analysis, which provides a theoretical basis for the fusion of DPD particle states and hydraulic oil and other suspensions in the future.

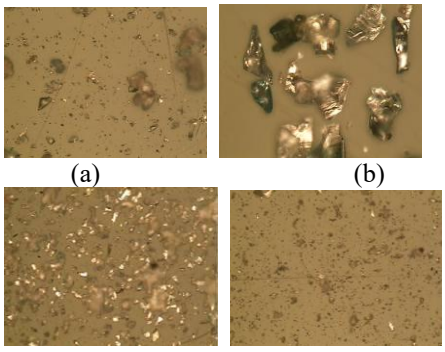

(a) (b)

(c) (d)

Fig. 9 morphology of SiC particles with different numbers under microscope

4. CONCLUSIONS

(1)The density, pressure and temperature of the single particle DPD particles are in good agreement with the theoretical values, which provide a numerical analysis for the mesoscopic state of the abrasive particles through the dissipative particle dynamics analysis of the abrasive particles;

(2)The DPD particles are gradually reduced and stabilized at about 22.4N When the number of simulation steps is increased, and the temperature also increases with the number of steps to reduce the state, reaching 1KT, we can very good control of the DPD particles, and applied tothe mesoscopic analysis through these values;

(3)Compared with the different number of DPD particles, the condensed state of the particles in the mesoscopic state is different, and the stability is different, the density of DPD particles is better, also the two phase flow will have a more significant impact.

ACKNOWLEDGEMENTS

The authers would like to thank the national natural science foundation of china No. NSFC 51206011, Jilin province science and technology development program of Jilin province No. 20130522186JH and No.20160101270JC, project of education department of jilin province NO.2016386.

REFERENCE

[1]Zhan Pinghai. Characteristics and application of abrasive flow processing technology [J]. metal processing.2009 (6): 17-21.

[2]Chang Jianzhong, Liu Moubin, Liu Hantao. Dissipative particle dynamics simulation of droplet dynamics [J]. Journal of physics, 2008, 57 (7): 3954-3961.

[3]Shen Tong, Wu Yongquan, Jiang Guochang.1873K liquid iron molecular dynamics and dissipative particle dynamics [J]. Shanghai metal, 2008, 30 (6): 23-27.

[4]Xu Shaofeng, Wang Jiugen. A new solid wall surface boundary conditions of dissipative particle dynamics [J]. Journal of Zhejiang University, 2013, 47:1-8.

[5]Groot R D. Mesoscopic simulation of polmer-surfactantaggregation[J] .Langmuir,2000,16:7 493-7502.

[6]Chen Shuo, Zhao Jun, Wang Dan et al. Dissipative particle dynamics simulation of drops in the micro channel [J]. Journal of Shanghai Jiao Tong University, 2005, 39 (11): 1833-1837.

[7]Kong Yihua, Zhang Chuhua, Xi Guang. Dissipative particle dynamics in the numerical simulation of the flow in the application [J]. Journal of Xi'an Jiao Tong University, 2006, 40 (9): 1104-1108.Dissipative particle dynamics simulation of

[8]Sun Xiangdong. DNA in micro channel [D]. Jilin: Jilin University, 2007

The Research on Transient Thermal Stress of Coal Mine Ventilation Air Methane Oxidation Bed

Ma Ling[1], Wang Tianyi[2,]*
[1] The Nursing College of Zhengzhou University, Henan, 450001, China
[2] Henan normal University, Henan 453002, China

Abstract: Through the consults and analysis of documents, we screen more than 100 initial indicators and use factor analysis by SPSS software to extract 21 main factors to simplify the evaluation of schools difficulty; then we follow the dictionary in different regions of US will divide schools into 13 classes, and combine clustering analysis to reduce the difficulty of determining the school. After we determine the investment school, we determine 17 schools according to the ratio of each type of school and other factors, then we assume that a return-on-investment(ROI) is related only with the scores and the investment amount and meet the simple linear weighted, so an optimal investment strategy is a simple linear programming model that make this five-year ROI maximize which can determine a simple investment strategy. Model testing and sensitivity, factor analysis model can only give 63.308% of the original index information, and in the test of the ROI we consider selecting a few good indicators of neural network simulation training, but did not get a better result .So we make some creative proposals, which may greatly improve our model for handling large data further.
Keywords: Factor Analysis; Clustering Analysis; Linear Programming; Neural Network

1. INTRODUCTION

The Goodgrant Foundation is a charitable organization that intends to help improve educational performance of undergraduates attending colleges and universities in the United States. To do this, the foundation plans to donate a total of $100,000,000 (US100 million) to an appropriate group of schools per year, for five years, starting July 2016. Besides, they do not want to duplicate the investments and focus of other large grant organizations such as the Gates Foundation and Lumina Foundation. It requires us to develop a model to determine the optimal investment strategy, and meet the following requirements:

- Identifies the schools, investment amount per school, the return on that investment, and the time duration that the organization's money should be provided to have the highest likelihood of producing a strong positive effect on student performance.
- Contain a 1 to N optimized and prioritized candidate list of schools you are recommending for investment based on each candidate school's demonstrated potential for effective use of private funding.
- Include an estimated return on investment (ROI) defined in a manner appropriate for a charitable organization such as the Goodgrant Foundation.
- Model and subsequent strategy must be based on some meaningful and defendable subset of these two data sets that are provided.

2. BACKGROUND

2.1 education

In recent years, charges of American higher education institutions are increasing. With the increasingly competitive pressures greater society, more and more people go to college and tuition fees are more expensive, despite government subsidies and other charities, which makes a lot of low-income families and disadvantaged groups more difficult to obtain higher education. Lumina Foundation study found only 9 percent of students from the lowest income quartile complete bachelor's degrees, compared to 54 percent of students from the highest income quartile. Only about 56 percent of low-income students with test scores in the highest quartile complete bachelor's degrees, compared to 80 percent of their higher-income peers. Therefore, some of the charities want to invest in this area of higher education, to improve the level of education of society, accelerate industrial upgrading and promote social development.

2.2 charitable funds

It is more representative of the Gates Foundation and Lumina Foundation, The former has two charitable projects related to education, It is College-Ready Education program aims to ensure that all students graduate from high school prepared to succeed in college, and our Postsecondary Success program aims to dramatically increase the number of young people who obtain a postsecondary degree or certificate with labor-market value. The latter has a big goal, they plan to make the United States 60 percent of people with higher education qualifications.

2.3 big data background

Big data analysis is currently widely used in all areas of society. Big data gradually gained a certain extent changed the way people think. Viktor

Mayer-Schönberger is one of the first insights into the development trend of the era of big data scientists, In his book Big Data: A Revolution That Will Transform How We Live, Work, and Think in terms of big data era does not need us to understand "why", but only need to know "what is." This is a change of thinking, a profound reflection of our social life. American education system statistics detailed data all aspects of higher education, Information about the data more than seven thousand US higher education institutions from the U.S. National Center on Education Statistics and the College Scorecard data set obtained by the analysis, you can elect to obtain an appraisal for this charity like the Goodgrant Foundation institutions philanthropic investment strategy.

3. ASSUMPTIONS

In the process of analysis and thinking, there are the following difficulties:

- Data containing more NULL, the school may be unpublished or not, and which for us will cause great difficulties in data processing
- The title given indicators are complete enough and whether the data is reliable
- In establishing the estimated return on investment model, there are many indicators need to be considered, but the data and indicators and not complete

To overcome these difficulties, to simplify the problem, we make the following assumptions:

- Replace NULL data processing 0.
- The title of the index to complete and sufficient data is reliable.
- The estimated return on investment with our ratings and investment into a simple linear relationship, and there is a weight, and we set the right weight and score like PCTPELLinvestment in the same university the same year.
- All the statistical data is random, there is no interference of human factors.
- This hypothesis explains the raw data can basically reflect the objective reality.
- The geographic differences in American higher education are not obvious. This assumption meets certain objectivity.

4. SYMBOL DESCRIPTION Tab. 1.

Table 1. Symbol Description

X_p	P-Indicator
F_m	m -th factor
a_{ij}	Load factor
ε	Special factor
W_i	Weight Factors weight
Y_i	i year's forecast of return
X_i	i year's forecast of return
S_i	The i -th university investment
$\bar{\omega}$	Weights
Z_i	Update cluster mean
E	Calculation criterion function
P_i	Input variables
$w1_{ij}$	Input layer to the hidden layer weights
$w2_{ki}$	The hidden layer to the output layer weights
$a1_i$	Hidden layer node
$a2_i$	Output node
$f1$	Training function
$f2$	Passed into the function
$b2_i$	Threshold
$a1_i$	Threshold

5. MODELS

We primarily use the scorecard data of various institutions of higher education, more than seven thousand in all universities according to certain statistical laws for the development of philanthropic investment strategy choice of school, first, we simplify the evaluation, and secondly, to different geographic locations universities grouping, and cluster analysis in each group, after the use of neural networks for intelligent data mining process, and then build the evaluation model.

5.1 data processing

At first Annex among schools scorecard data and preliminary analysis of data cleaning, remove some useless data based on objective factors. Then measure the similarity between each index, and further processes the data, particularly the use of Pearson correlation coefficient that is calculated based on any two indicator vector cosine angle itself normalized. Pearson correlation coefficient:

$$r(x,y)=\frac{\sum XY-\frac{\sum X\sum y}{N}}{\sqrt{\left(\sum X^2-\frac{\left(\sum X\right)^2}{N}\right)\left(\sum Y^2-\frac{\left(\sum Y\right)^2}{N}\right)}} \quad (1)$$

Where X is the x-coordinate of the vector formed by, Y is the y coordinate of the vector formed by, r is related to the strength. The strength of the correlation $r(x,y)$ index of less than 0.8 to remove, so that the number of indicators downsized to 75. Fig. 1 is three-dimensional

schematic diagram of the Correlation Strength.

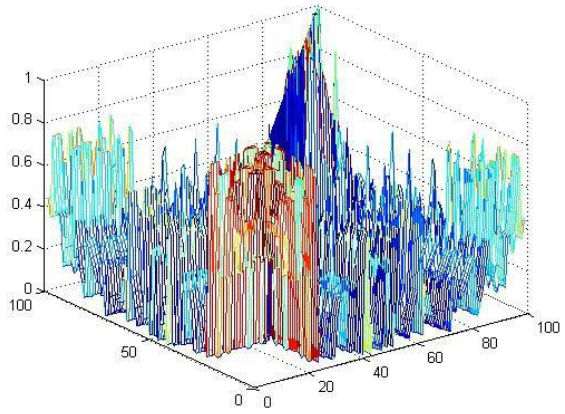

Figure 1 three-dimensional schematic diagram of the Correlation Strength

Since the student SAT scores and ACT scores have increased influence on the performance of students into the school, so these two indicators added to finally obtain 77 indicators.

5.2 factor analysis

factor analysis：

Let $X=\left(X_1,X_2,\cdots X_p\right)^T$ be a random vector factors observable, $F=\left(F_1,F_2,\cdots F_m\right)^T$ indicators vector unobservable. Have:

$$\left\{\begin{array}{c} X_1=a_{11}F_1+a_{12}F_2+\cdots+a_{1m}F_m+\varepsilon_1 \\ X_2=a_{21}F_1+a_{22}F_2+\cdots+a_{2m}F_m+\varepsilon_2 \\ \cdots \\ X_p=a_{p1}F_1+a_{p2}F_2+\cdots+a_{pm}F_m+\varepsilon_p \end{array}\right\} \quad (2)$$

which is: $X=A\times F+\varepsilon$, $\varepsilon=\left(\varepsilon_1,\varepsilon_2\cdots,\varepsilon_p\right)$

Which is a special factor, F_i for the first common factors a_{ij} for the load factor, the larger the a_{ij} absolute value, indicating that the greater the degree of dependency between X_i and F_i .

5.3 cluster analysis

For the purposes of different positions, it contains a different number of university schools, relatively large amount of data, in front of our factor analysis from the perspective of longitudinal indicators extracted, but not very good, effective from the horizontal to each region a comprehensive assessment of the school. So we thought K-introduced clustering to classify data on the transverse process [2]. The sample is assigned to reduce their nearest center distance, and the objective function value.

$$\sum_{\substack{i=1 \\ j\in\{1,2,\cdots,k\}}}^{n} \min\left\|Z_i-H_j\right\|^2 \quad (3)$$

Update cluster mean

$$\overline{Z_i}=\frac{1}{\left|C_i\right|}\sum_{Z\in C_i}Z \quad (4)$$

Calculation criterion function E

$$E=\sum_{i=1}^{k}\sum_{Z\in C_i}\left|Z-\overline{Z_i}\right|^2 \quad (5)$$

K-value of clustering is a big advantage can specify the number of groups, but we can‘t be certain of a district judge. Hence the need for hierarchical clustering methods in their initial classification. Hierarchical clustering of the basic process: start each sample each separate category, and then follow the defined distance between the samples (between-class distance at this time is equivalent to the distance between points) to calculate the distance between the nearest two categories combined into a new category, such as reducing class, the relative capacity of the sample is reduced, so repeat. We use SPSS software operates using pedigree chart can be a good observation of the whole process of clustering and clustering, classification and make choices, one of a case study:(Map and data sheets).

By the hierarchical clustering on, we can make good use of K- value classification [4]. We press scorecard data in LOCALE school division will be in the same location into a school class, received a total of 13 categories. Respectively thirteen regions K- value cluster analysis, cluster analysis by means of SPSS software, mainly in three classes. Map and data table:

By K- value, we can clearly observe the population size of the capacity to lay the foundation for the evaluation of each region.

5.4 neural networks

Back-propagation neural network is a network of the W-H is a generalized learning rule, nonlinear differentiable function weights training multilayer networks, which adjust the weights using the back-propagation learning algorithm [3]. Fig. 2: $K=1,2,3,\cdots s2$ $i=1,2,3,\cdots s1$ $j=1,2,3,\cdots r$

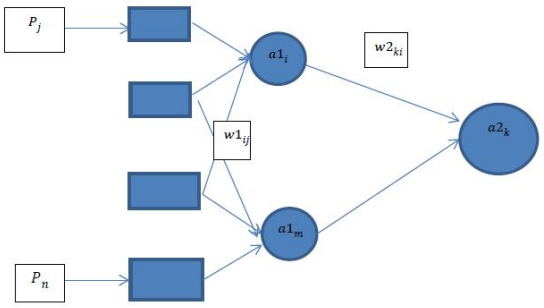

Figure 2 neural network

The main idea of neural networks for Q input learning sample: $P_1, P_2, \cdots P_q$, Sample output corresponding thereto is known: $T_1, T_2, \cdots T_q$. Thus, the square error of the output layer and the network is minimized. Actual output of the network $A_1, A_2, \cdots A_q$ and Target vector $T_1, T_2, \cdots T_q$, discrepancies between the right to modify its value, A_m so that the desired $T_m(1,2,\cdots,q)$ as close as possible. Assuming that the input is P .Input neurons having r , there $s1$ neurons in the hidden layer, the activation function $F1$, there $s2$ neurons in the output layer activation function corresponding to $F2$, the output is A , the target vector T the output of the hidden layer neurons ranked i .

$$a1_i = f1\left(\sum_{j=1}^{r} w1 p_j + b1_i\right), i = 1,2,\cdots,s1 \tag{6}$$

K-th output neuron output layer

$$a2_i = f2\left(\sum_{j=1}^{s1} w2_{ki} a1_i + b2_k\right), k = 1,2,\cdots s2 \tag{7}$$

$$E(W,B) = \frac{1}{2}\sum_{k=1}^{s2}(t_k - a2_k)^2 \tag{8}$$

The use of back-propagation gradient descent evaluated weight changes and errors. Hidden layer weight change:

$$\Delta w1_{ij} = -\eta\frac{\partial E}{\partial w1_{ij}} = -\eta\frac{\partial E}{\partial a2_k} * \frac{\partial a2_k}{\partial a1_i} * \frac{\partial a1_i}{\partial 1_{ij}}$$

=

$$\eta\sum_{k=1}^{s2}(t_k - a2_k) * \dot{f2} * w2_{ki} * \dot{f1} * p_j = \eta * \delta_{ij} * p_j \tag{9}$$

Among them

$$\delta_{ij} = e_i * \dot{f1}\ e_i = \sum_{k=1}^{s2}\delta_{ki} w2_{ki} \tag{11}$$

Similarly available

$$\Delta b1_i = \eta\delta_{ij} \tag{12}$$

Back propagation process is actually calculated by the error output layer , and then is obtained by multiplying the output layer activation function of the first derivative .

Since there are no hidden layer is given directly target vector, the use of the output layer reverse transfer obtains the amount of change hidden layer weights.

Then calculate

$$e_i = \sum_{k=1}^{s2}\delta_{ki} * w2_{ki} \tag{13}$$

Also by the first derivative of the $f1$ ei layer activation function 'multiplying and get δ_{ij} , in order to determine the amount of change $\Delta w1_{ij}$ front layer weights, if there in front of the hidden layer, so follow the same method as above and so on, it has been the output error ek layer by layer to the first layer of anti-projections so far. In each type of school, the use of cluster analysis to pick out the largest proportion of a class to train the neural network, and then all the schools in the region of such data into the neural network analysis and evaluation, the school's results in each region output value, the resulting value and factor analysis combined as a comprehensive index to rank schools, elected by rank list of investment candidates in all regions.

6. MODEL EVALUTION

We are in the process of determining university, for a given data into vertical and horizontal two aspects to consider, for each indicator corresponding longitudinal data have a NULL case, we take with 0 replaced, this calculation is relatively simple, and later we also used to go into the mean, and extract the main factor, the results have not been good (explained variance) of 85%) by factor analysis [5]. In addition, we refer to the 2004 US News and World Report ranking university standards and the right weight (w1), using a neural network to simulate and predict the US University and binding factor analysis scoring situation into account, to determine a candidate school investment and investment and return the amount forecast earnings. For landscape we are simply classified according to the university population in different regions, the university on the basis of classification by cluster analysis, which can greatly reduce the computation.

7. ADVANTAGE AND SHORTCOMING

- Advantage

  Vader down to simplification purposes: for large data vertical and horizontal two dealing in schools, first in a different population size, simple classification, and on this basis to give a more simple clustering situation; on indicators by factor analysis, and strive to extract less comprehensive index from a plurality of indicators and in the original index more representative of the amount of information to simplify the situation of the problem under BP Network Simulation： Artificial network to take some of the indicators of training and

simulation, forecasting University……

- Shortcoming

The factor analysis extracted 21 factors, are still too many, and how difficult it has reasonable binding interpretation of the meaning, in addition to their original data only 63.308% confidence level is not high. Our analysis that the reason may be incomplete and missing data on the value of the data processing is not ideal.

8. ROI

According to our hypothesis 2

- Estimated return on investment with our ratings and investment into a simple linear relationship, and there is a weight[6], but we set this right as scores of heavy and PCTPELL
- Investment for the same university the same year

We can list the forecast return on investment formula

$$Y_i = (1-\varpi) \times X_i + \varpi \times S_i \tag{14}$$

$$\sum_{i=1}^{17} X_i = 100000000 \tag{15}$$

$$R = \max \sum_{i=1}^{17} Y_i \tag{16}$$

$$S_i, X_i, Y_i \geq 0 \tag{17}$$

It is essentially a linear programming model:

Y_i The i-th year return forecast

X_i The i-th investment of the university

S_i University of the i-th score

ϖ Weights

This allows us to determine the amount of investment and return on investment forecast.

9. MODEL EVALUTION

We are in the process of determining university, for a given data into vertical and horizontal two aspects to consider, for each indicator corresponding longitudinal data have a NULL case, we take with 0 replaced, this calculation is relatively simple, and later we also used to go into the mean, and extract the main factor, the results have not been good (explained variance) of 85%) by factor analysis. In addition, we refer to the 2004 US News and World Report ranking university standards and the right weight (w1), using a neural network to simulate and predict the US University and binding factor analysis scoring situation into account, to determine a candidate school investment and investment and return the amount forecast earnings. For landscape we are simply classified according to the university population in different regions, the university on the basis of classification by cluster analysis, which can greatly reduce the computation.

ACKNOWLEDGMENT

This work is supported by Science and technology research projects of Educational Commission of Henan Province(No.15A880033,17A880011), Youth Science Foundation of Henan Normal University(No. 2012QK55)

REFERENCES

[1]Rakesh Agrawal,Johannes Gehrke,Dimitrios Gunopulos,Prabhakar Raghavan. Automatic Subspace Clustering of High Dimensional Data [J]. Data Mining and Knowledge Discovery . 2005 (1)

[2]Simpson T Ian, Armstrong J Douglas, Jarman Andrew. Merged consensus clustering to assess and improve class discovery with microarray data[J]. BMC Bioinformatics, 2010, 11(1).

[3]Van RooO A J F,et al.Neural Network Training Using Genetic Algorithm. World Scientific . 1996

[4]http://www.extremeoptimization.com/Documentation/Statistics/Multivariate_Analysis/K-Means_Cluster_Analysis.aspx

[5]JUAN, J. (1982), “Programme de Classification Hiérarchique par l'Algorithme de la Recherche en Chaîne des Voisins Réciproques,”Les Cahiers de l'Analyse des Données, VII, 219–225.

[6]Zhang Jie, Gong Xinshu.Evaluation on the Urban Agglomeration Capacity of Xinjiang-Based on Factor Analysis and Cluster Analysis,School of Economy&Trade, Shihezi University, Shehezi, Xinjiang 832003.

[7]http://www.njcdgjs.cn/_siteId/127/pageId/218/columnId/1394/articleId/2 469/DisplayInfo.ashx

[8]https://www.luminafoundation.org/files/resources/affordabilitybenchmark-1.pdf

[9]http://www.gatesfoundation.org/What-We-Do/US-Program/College-Ready-Education

Using Data Mining Technologies to Solve the Problem of Space Junk: A Case Study

*Wang Tianyi *, Zhang Jin*
Henan Normal University, Henan 453002, China

Abstract: The human legacy of all kinds of garbage in space is growing. It prevents Space exploration activities and carries out an impact on the future development of our aviation industry stumbling block. In order to solve the problem of space junk, we establish the quality of the space distribution model, using the model to analyze cost that the cost of dealing with space junk by laser technology and large satellite. We compare the costs of the two models and get the use of the time efficiency. Based on the evaluation results, we get the conclusion that laser technology and large satellite technology to deal with space junk has high cost, high risk, so it is not suitable for investment in private company. Finally, we provide an innovative solution to avoid collisions with space junk: Firstly, a space monitoring system is established, and the location of the space debris is analyzed by using radar laser technology. Then using the space garbage collection spacecraft takes different solutions to different sizes of garbage. Large garbage are collected directly based on their location, and transported to a lower or higher earth orbit; For small fragments can achieve garbage sky maneuvers to predetermined orbit by changing laser radiation intensity ,so as to avoid collision.
Keywords: Laser Mass distribution model; Space debris processing project; Risk assessment; Radar laser technology.

1. INTRODUCTION

The International Academy of Astronautics (IAA) in the 2001 "orbital debris situation report" [1] in artificial space debris "(ESA notation) or" orbital debris "(NASA representation) for the following definition: "Orbital debris that is no longer expected to recover any invalid assumptions artificial Earth orbiting objects of its expected function or any other desired specified functions, including fragments and parts."

Space junk, is numerous, both had "died a natural death", but still in all kinds of space orbit satellite circles the abandoned wreckage of rocket propulsion, spacecraft have accidental explosion or collision of fragments, and some screws and washers and the like components. In addition, the astronauts during space operations may be "littering" junk left behind or missed items can also cause space junk. The existence of space debris serious threat to the safety of spacecraft in orbit, while the continuous generation of space debris orbit the limited resources pose a serious threat.

On February 11, 2009, United States in 1997 launched a communications satellite "Iridium" star and a star in 1993 Russia launched the universe -2251 satellites (defunct satellites. It is reported the satellite is now no longer work) collided in space, resulting in a large amount of space junk and may pose a threat to the International Space Station. NASA said that this is the first time in human history satellite collision, the location is located in Siberia over about 805km. Located in Houston's Johnson Space Center of orbital debris expert Mark, Matney said, the Russian satellite lost control. According to reports, the "iridium" satellite weighs about 560kg, the Russian satellite weighs 1t, so it is expected that the collision will produce a lot of space junk, but it is unclear details. The issue has been widely discussed by the news media.

A number of methods to remove the debris have been proposed. These methods include small, space-based water jets and high energy lasers used to target specific pieces of debris and large satellites designed to sweep up the debris, among others. The debris ranges in size and mass from paint flakes to abandoned satellites. The debris' high velocity orbits make capture difficult.

Our team needs to develop a time-dependent model to determine the best alternative or combination of alternatives that a private firm could adopt as a commercial opportunity to address the space debris problem.

The main effects of the model we have established include:

(1)Quantitative and/or qualitative estimates of costs, risks, benefits, as well as other important factors.

(2)Model should be able to assess independent alternatives as well as combinations of alternatives and be able to explore a variety of important "What if?" scenarios.

(3)Identify business opportunities exist. If there is a feasible solution for different kinds of solutions, we compare different removal fragmentation schemes, and if this is not possible, we provide an innovative scheme to eliminate the collision.

2. ASSUMPTIONS

(1) Assuming that the space junk real time monitoring system is available.

(2) Do not consider the influence of track change.

(3) Only track factors.

(4) Without taking into account the two collisions

between the tracks.
(5) Power generated by the laser is large enough.
(6) Laser capable of accurately targeting at a different speed to intercept the rapid ring of objects in space.
(7) Large satellite can work well in space
(8) The cost of large satellite manufacturing can be accepted.

3. MODEL

3.1 laser technology model

The principle of the laser: the heat emitted by the laser will cause a small fraction of each space junk to be evaporated. The laser must be accurate aiming to intercept with thousands of miles per hour in the sky rapid circular small objects. The heat emitted by the laser is so powerful that it forms a small jet of plasma, essentially equivalent to transforming the space junk into a fuel for a small jet that will launch debris into orbit. Smaller pieces will burn out after the track is lost. Other debris will need to be carefully introduced into orbit, so that it will eventually fall into the Pacific Ocean.

From the aspect of the cost of laser research, the use of laser technology for space debris (this technology not only handle large pieces of space junk, small pieces of space junk can handle), we use some of the data collected on the network, establish the cost of debris quality correlation model as follows Fig. 1.

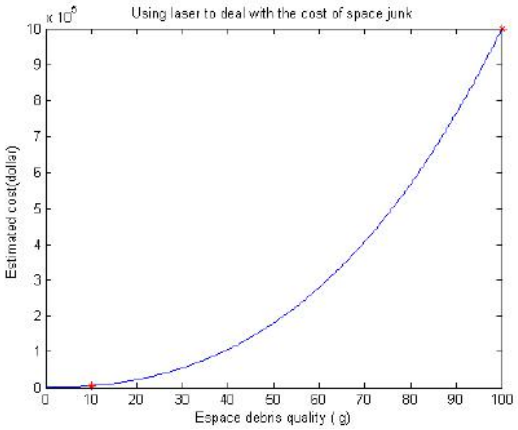

Figure 1 Using laser to deal with the cost of space junk [2]

The image we found that with time, space junk relationship between quality and handling costs show an increasing trend. If the total mass of the space junk exceeds a certain value, the process of increasing the cost of space junk, it will be increasing the risk of earnings getting smaller and smaller.

3.2 large satellite model

Large satellite processing principle of space junk: the large satellites by the carrier and the sub machine can be inferred from around the position of the earth and high-speed running of the space junk, and the use of sub machine special adhesive for recycling. And then gradually slow down to change the running track. After a period of time into the atmosphere, making burned.

Starting from the large satellite, using the network to get some data to establish the cost of large satellite to eliminate space junk and the size of the space junk quality model is as follows Fig. 2.

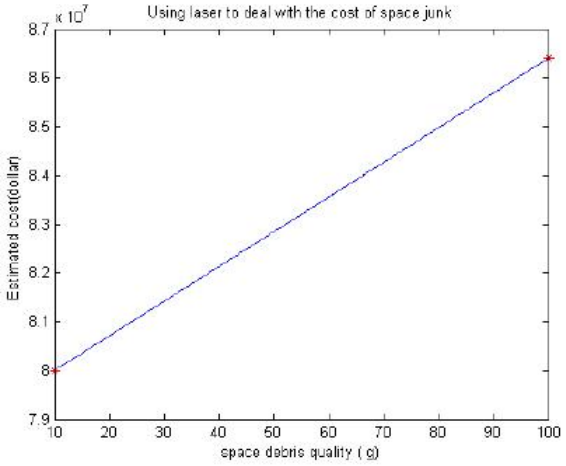

Figure 2 Cost of processing space junk with large satellites [3]

The image we found that with time, if the relationship between the quality of space junk and handling costs between the linearly increasing trends. If the quality of space junk is increasing, the cost of increasing the processing space junk, it will be increasing the risk of earnings getting smaller and smaller.

3.3 discussion on laser technology model and large satellite model

Known: $$m_1 + m_2 = E \tag{1}$$

The average cost of laser technology destroyed debris model:

$$K = \left(X * m_1 + Y * m_2\right)/E \tag{2}$$

The average cost of large pieces of the destroyed satellite model:

$$H = Z * \left(m_1 + m_2\right)/B * E + N \tag{3}$$

So, the two models are compared in terms of cost:

K/H analysis:

If $K/H < 1$, the laser technology costs less.

If $K/H > 1$, then the cost of large satellite costs less.

If $K/H = 1$, then both it costs the same.

Two models are compared in terms of time efficiency:

For different space debris:

If the situation is more urgent, it is recommended to use the laser.

If the situation is more complex, can be two complementary.

3.4 innovative project

3.4.1 Laser radar technology

According to recent international research on the monitoring of space debris and the aerospace industry risks of mainly diameter in 10cm below the space

junk, because the diameter is too large space junk, and from the earth can be easily observed, the ground command center to issue timely instructions and allow the spacecraft to escape.

Radar is one of the most common methods used to detect moving objects. In recent years some automatic control engineering, using the principle of Kalman filter and the gate of a mobile settings to tracking a target motion, so that the search radar with edge searching tracking function. In the use of linear Kalman recursive formula or simple linear extrapolation, assuming that the targets (such as space junk) do rectilinear motion, the equations of motion is linear. Obviously, when the target (such as space junk) do maneuvers, using linear filtering or linear extrapolation to target state estimation, will result in a larger error, easy to cause the loss of the target. Due to the limitation of the wavelength, the precision of radar location cannot be very high. The ranging from a few millimeters of debris, locating radar will not give the accurate position, so the radar detection technology application scope is limited , generally apply only to determine the initial position of space junk

The direction of laser is very good, not easy to divergence, light intensity stability, so we can use the laser detection technology laser detection technology for space garbage positioning.

The error equation can be obtained by using the SLR station to measure the distance to the space junk:

$$V = \frac{d\rho}{da}\Delta a + \frac{d\rho}{de}\Delta e + \frac{d\rho}{di}\Delta i + \frac{d\rho}{d\Omega}\Delta\Omega + \frac{d\rho}{d\omega}\Delta\omega + \frac{d\rho}{dM_0}\Delta M_0 + \rho^c + \rho^m \quad (4)$$

Where:

a Long axis of satellite orbit

e Eccentricity of satellite orbit

i Inclination of satellite orbit

Ω The ascending node of the satellite orbit

ω Satellite perigee distance

M_0 Flat near point angle of satellite in time element t_0

By formula (4), the method can be used to solve the 6 orbital parameters (root number) of space junk, and then to obtain the 6 orbital parameters of space junk. So the space position of the space junk can be determined.

Although the positioning accuracy of laser monitoring technology is much greater than that of the radar, it is difficult to directly find the small target space garbage due to the limitation of laser characteristics.

If the first use of radar to determine the range of space junk, and then use a laser to make precise observations, the monitoring of space debris can be more effective, the development of laser radar technology. The basic principle of laser radar transmitter laser beam with a beam of a certain power, through the dissemination of atmospheric radiation to the target surface, reflected from the surface of the target back to the echo is received by the receiver, by the signal processing to extract useful information from the echo. Laser radar is working in the band of light in a new radar system, compared with microwave and millimeter wave radar and has high working frequency, short wavelength and distance, high speed and angular position measurement accuracy, small size, light weight, flexible, conducive to the unique advantages of airborne and spacecraft, etc. [4].At present, the laser radar can adopt$_{0.53}\ \mu m$, 0.63 μm , 0.8 to 0.9 μm , 1.06 μm , 1.54 μm , 2 μm and10.6 μm , and7bands.

According to the relevant literature [5], the general formula for the single base and biostatics laser radar ranging equation is:

$$P_r = \left(4K_s P_s \eta_t / n\varphi^2 R_1^2\right)\Gamma\left(T_{A2}/4\pi R_2^2\right)\left(\pi D^2 \eta_r/4\right) \quad (5)$$

Where:

P_r Laser transmit power (W)

K Beam distribution function

T_{A1} Transmitter to target atmospheric transmittance

η_t Transmitter optical system efficiency

ϕ Beam width or divergence (rad)

R_1 Transmitter to target distance (m)

Γ Target laser cross section (m)

T_{A2} Target to receiver atmospheric transmittance

R_2 Target to receiver range (m)

D Receive window diameter (m)

η_r Receiver optical system efficiency

P_r Received power (W)

Under the condition of the external atmosphere or the atmospheric attenuation, the single base laser radar ranging, $R_1 = R_2 = R$, $T_{A1} = T_{A2} = T_A$, Simplified formula (6):

$$P_r = KP_s T_A^2 \Gamma D^2 \eta_t \eta_r / 4\pi\varphi^2 R^4 \quad (6)$$

3.4.2 Model

Integrated the above analysis, we designed to avoid the collision of innovative program is as follows:

Manufacturing space garbage collected spacecraft, space junk to locate using the laser radar detection technology, launching space garbage collection spacecraft, the hunk of space debris collection and encapsulated in the location, according to their location, their delivery to the low or high earth orbit. Garbage collection ships like this can be used to collect old rocket debris, such as: the propulsion

system or drag force enhancement device is collected on the spacecraft, so that it can be landed as soon as possible to the ground. In addition, the collection of the spacecraft can also collect old satellite. For small fragments can by laser radiation intensity changes to achieve garbage sky maneuvers to predetermined orbit, so as to avoid collision.

4. STRENGTH AND WEAKNESS

Now we will analyze the strengths and weaknesses of each sub-model in our paper:

Laser technology model:

Strength:

⑴ The implementation of the fast, hazardous debris in the collision warning several hours before and within a few days can be eliminated.

⑵ High flexibility, can handle several pieces of LEO orbit, or even different tracks or heights.

⑶ Low cost, the laser system can be used repeatedly, do not need space to launch.

⑷ There is no impact on the space environment, and will not produce new debris associated with the launch or collision in orbit.

Weakness:

⑴ Equipment requires a higher precision.

⑵ Requires accurate monitoring of space debris.

Large scale satellite model:

Strength:

⑴ Strong pertinence.

Weakness:

⑴ Large satellites cannot be reused.

⑵ Manufacturing satellite cost is higher.

⑷ With a longer time.

Laser radar technology

Strength:

High working frequency, short wavelength, high precision, small size, light weight, flexible, flexible, and other unique advantages of airborne and spacecraft.

Weakness:

Atmospheric transmission environment has a great influence on the performance of lidar system, and meteorological factors such as rain, fog and snow can make the performance of lidar become worse.

5. CONCLUSION

From the above model, we can draw the conclusion that:

We create the quality of space debris distribution model can get space debris basic quality distribution, and analysis of the laser technology and large satellite technology to deal with the cost of space debris, found the need for costly and its accuracy is still to solve the problem of space junk, once the emergence of laser mistakes or satellite launch failure will cause huge losses. So we think business does not exist.

Then we propose innovative schemes to avoid collisions:

We first proposed a perfect space detection system, using lidar technology will space junk positioning processing, then the space garbage collection spacecraft will be large garbage collection package, for small pieces of junk with laser the orbit and the space junk as soon as possible to fall to the ground, a step by step to reduce collision may, thereby eliminating collisions.

6. MODEL IMPROVEMENT

Because of the limited time and data, we can't build the model perfectly. However, if time and data allow, we can set up a number of indicators in the index system, to achieve a more comprehensive effect. In addition, the final prediction curve, time and data permitting, we can use gray prediction model, so perhaps you can better predict the next few years, the number of space junk trend.

In the establishment of the model, we can try a variety of models, each model can be solved, and finally select the best model, this is also the direction of improvement.

ACKNOWLEDGMENT

This work is supported by Science and technology research projects of Educational Commission of Henan Province(No.15A880033,17A880011), Youth Science Foundation of Henan Normal University(No. 2012QK55)

REFERENCES

[1]IAA Space Debris Subcommittee. Position Paper on Orbital Debris. IAA, 2001.

[2]Anselmo L. Space debris mitigation extension of the SDM tool [R]. Pisa European Space Agency, 2000.

[3]Ma Xiao-yu, Cui Ping-yuan. PIB model ship in the space debris environment modeling use. [J]. Flight mechanics, 19 (2): 73-77, 2001.

[4]Anselmo L. Updated results on the long-term evolution of the space debris environment [J]. Advances in Space Research, 1999, 23(1): 201-211.

[2]Clare Di fall. American media: Lasers could cost thousands to millions of dollars in addition to space junk .http://news.qq.com/a/20111101/00112.htm.January 30, 2016

[3]The author is a researcher at the Beijing Institute of space science and technology information. Japanese media: Japanese research and development space garbage cleaning satellite this year listed (Photos).http;//news.163.com/15/0217/11/AILDGUMH00014AEE.html?f=jsearch .January 30, 2016

[4]Wen Ping-chuan, Cai yun. Based on AHP Fuzzy Comprehensive Evaluation Cooperative Project Risk Assessment Model. [A].1002-6487 (2011) 01-0057-04.

[7]Lin Xiao-tao. Design of Adaptive radar positioning system . Computer and Digital Engineering, 21 (2): 32-40, 1994

[6]Tan Xian-yu. Research on laser ranging equation of laser radar . Electro optic and control, 12-1, 2001

Influencing Factors and Countermeasures in Clinical and Biochemical Examination

Yan Xie[1],Ruimin Fu[2]
[1] Clinical Laboratory, Henan province people's hospital, Zhengzhou, 450000
[2] Department of Life science, Henan Institute of Education, Zhengzhou, 450046

Abstract: By analyzing the factors that may affect the test results before, during and after the analysis of clinical biochemical tests, the control strategies was explored to reduce or eliminate the test error and improve the accuracy of the test results, which made the biochemical tests serve the clinic well.
Keywords: biochemical tests; influencing factors; countermeasures

1.INTRODUCTION

Biochemical testing [1] is one of the most widely used clinical examinations, which not only can timely reflect the patient's physical condition, but also provide early warning signals for the detection of some diseases[1-3]. Laboratory physicians often divide the whole process of clinical biochemical tests into three stages: pre-analysis, analysis and post-analysis[4-6]. The pre-analysis phase is the stage which test items are selected by doctors and the samples are sent to laboratories[7-8]. The intermediate stage is the stage which the sample is run, stored and tested in the laboratory. The post-analytical stage is the stage which the test results are reported to the clinical application. The biochemical examination process is complex and prone to errors, which could affect the clinical judgment. Therefore, the factors which could affect the biochemical test results in different stages and their countermeasures are analyzed briefly by combing with my years of work experience.

2.INFLUENCING FACTORS AND CONTERMEASURES IN PRE-ANALYSIS STAGE

The prerequisite to avoid the influence factors in the pre-analysis stage is to ensure the accuracy and reliability of the test results. Some studies reported that approximately 80% of the test results in the unsatisfactory results of clinical feedback were traceable to samples that did not meet the requirements. The main reason is that the influencing factors in the pre-analysis stage ,such as patient factors, specimen collection, preservation and transportation factors, can't be fully controlled by the inspectors, which are need to match the medical staff and patients.

2.1 patient factors

Patients' coordination is the prerequisite for quality assurance in the biochemical test. The test results could be affected by patient status, diet and medication. Therefore, the patients should been told the precautions in details by medical staff before the specimen are collected. In principle, the specimen should been collected when patients are calm and in the rest stage[9-10].

Studies have pointed out some changes in blood electrolytes and other test results, such as liver function, may be caused by patients with strenuous exercise due to energy consumption, loss of body fluids and severe breathing. We should note that fasting blood in the morning should be processed after fasting 12h.Though fasting blood is to prevent the impact of diet, but the fasting time is not as long as possible. If the fasting time is getting too much longer, the patients will be hungry for too long, which their protein will be reduced and bilirubin will be increased.

In addition, the drugs used in patients will have some impacts, such as some of the adverse reaction caused by drug itself will cause damage to liver and kidney function, which will cause some changes in related indicators. To reduce this interference, some drug which may affect the result should be suspended in the detection, otherwise the deviation in the results should be considered [11-12].

2.2 SPECIMEN FACTORS

2.2.1 collection of specimens

Specimen collection is a key step to assure the quality of biochemical tests. Therefore, every aspect of the specimen collection must be valued and avoided. In principle, the acquisition time should be in the morning and the stomach should be empty. For some diseases, such as acute myocardial infarction, the diagnosis of the most valuable time should be mastered, which the sample is generally collected 4-6h after the onset. Both the venous blood position of the patient and the tightness of tourniquet can affect some test results. Therefore, patients usually are taken supine or sitting blood. The tourniquet should be used within 1min, seeing the back of the blood immediately after release[13-15].

Some studies have reported that the blood position of subject can affect the protein-related substances and high relative molecular mass concentrations. For example, total protein, albumin, alkaline phosphatase will increase more than 5% when the subjects are standing. Furthermore, blood should be avoided when the patients are in infusion, which it is better to blood after the infusion for a while. If blood must be done in the fusion, the blood position should be the side of

the arm without blood transfusion [16].

2.2.2 specimen preservation and inspection

Specimens should be treated as soon as possible after the collection, otherwise, if it is placed at room temperature for too long, it will make the blood composition changes. Thus the experimental results could be affected. The most desirable specimens are preventing hemolysis, anti-pollution. One of the most common factors which could affect the accuracy of biochemical tests result is hemolysis.

Some indexes such as cereal third transaminase, aspartate aminotransferase, and alkaline phosphatase in red blood cell are higher than in the plasma. The hemolysis will cause these substance in plasma pseudo-increased. Moreover, the other indexes such as blood sodium and blood calcium in red blood cell are lower than in the plasma. Therefore, the hemolysis will cause these substances in plasma pseudo-decreased. Biochemical anticoagulant tube is a special test tube used in biochemical tests. The anticoagulants commonly used are heparin, oxalic acid, citrate, etc. If the specimens need anticoagulation, they should be collected based on the requirements of the test items, the proportion between anticoagulant dosage and blood must be correct. The test tubes and reagents shouldn't been replaced randomly along with the number of blood samples, otherwise, the test results could be affected.

In addition, to avoid contamination, the specimen is needed pretreatment under a higher temperature. The specimens collected in wards should be received in laboratory by some specially-assigned person. The collected specimen should be checked to make sure whether the information filled in the inspection application form is consistent with the specimen. The specimen should be checked with strict accordance with the sample test method. The number and appearance of samples should be checked and the specimen couldn't reach requirement should be re-taking.

3. THE FACTORS AFFECTING THE ANALYSIS STAGE AND COUNTERMEASURES

Analyses stages must be completed by the laboratory staff which not only is familiar with the standard operating procedures but also have the qualifications. In this stage, the laboratory environmental conditions should be controlled within the scope of requirements and the testing equipment should be in normal working condition[17-18]. Besides, the suitable reagents and consumables should be possessed. These factors must have a standardized management in laboratory, otherwise it will directly affect the quality of the analysis[19-20].

3.1 laboratory environmental factors

The environmental conditions in the laboratory can directly affect the test results. Environmental conditions to meet the standards, which the temperature and humidity should be controlled within the requirements, and regular disinfection must be done to avoid microbial contamination.

3.2 instrument factors

The sample test results could be directly affected by the factors such as instrument performance, proper operation and good maintenance. The early and late maintenance weekly and monthly of the instruments is very important. Every instrument in the laboratory should be maintained by specially assigned person. Thus some technical staff should be cultivated to be responsible for the maintenance of equipment. Automatic biochemical analyzer should be responsible by the specially assigned person in the samples detection. The staff which is responsible for the samples addition should not only upload the samples to instrument but also unload the sample from the instrument and put them away in classification. Meanwhile, the operation of instrument should be observed so as to solve problems in time.

3.3 sample addition factors

Specimen should be loaded firstly after sending to the laboratory. Sample addition should use one-time sample tube to prevent sample cross-contamination[21]. Some automatic analyzer sample cups are without bar code identification, thus they should be manual loaded and the sample rack number note should be noted. The sample must be placed at the sample cup position correctly. Both the sample type and sample size should be noted to avoid inspection error. The sample state should be paid attention when the samples are loaded. The staff should observe whether there is clot or fibrous protein in the serum and plasma, to avoid clogging instrument aspiration needle. Meanwhile, they should ensure whether the amount of serum or plasma is able to do instrument detection.

3.4 reagent factors

Clinical biochemical kits include a wide range of types[22]. In the use of clinical biochemical kits, the quality of reagents should be paid attention to and the same items between the kits should do the appropriate comparison, which choose a suitable kit with stability and wide range. Since then, the high-quality kits, with low blank rate, small difference between bottles, low absorbance of positive-type reagents, high absorbance of reverse-type reagents and fast end-reaction speed, will be chosen. The unqualified product in the quality arbitration should be resolutely resisted. The dosage of reagents should be identified and prepared according to the amount of samples. The remaining reagent will cause waste or lead to the mixture of new and old reagents, which will affect the test results.

3.5 inspection personel factors

The inspection personnel should not only have the qualification of inspection but also be familiar with the operation process of biochemical testing. Moreover, they should have the ability to analyze and control the factors that can avoid the influencing

factors and have strong sense of responsibility, earnest attitude and rich work experience. Some practitioners with low level of knowledge or careless attitude will directly lead to errors[23].

4.THE FACTORS AFFECTING THE POST-ANALYSIS STAGE AND COUNTERMEASURES

The main work of the post-analysis stage is shown as follows: firstly, the results issued laboratory should be checked. Secondly, information feedback should be re-checked. Only pay attention to each link, test results could be timely obtained and accurate, which could be efficient to serve the clinic.

4.1 checking factors

Although the automation of biochemical analysis reduce the error happened in filling test report, the determination of the audit requirements results increased. When check the results, the staff should firstly confirm whether the test items are same with the application items.Meanwhile, the front and back contrast of same applicant should be paid attention to and the analysis of abnormal results should be accepted and rejected, which require the examiner to have certain basic clinical knowledge. For example, when some of the enzymes item increased while other individual enzyme item decreased down to zero, which point out that enzyme activity is too high to lead the substrate depletion. Therefore, the reaction process curve should be checked and determined.

The increasement of alkaline phosphatase, aspartate and total protein and the decreasement of bilirubin often prompt severe hemolysis in specimens. To this problem, the staff should carefully check and analyze the results, which the review system should be established and the inspection report card could be issued. Furthermore, if a critical value is found in the test result confirmation, the concerned doctor should be informed immediately and the record of measure taken at the critical time should be made. In order to prevent the clinician from doubting about the test results, the specimen should be retained at room temperature for at least 48h after the examination.

4.2 feedback factors

In order to improve the accuracy of the test, clinical laboratories should be closely linked to clinical. Focus on clinician's feedback[24], on the one hand, the experimental results in the clinical diagnosis could be understood and mastered. On the other hand, the laboratory work could be improved continuously. After receiving the feedback, the reasons should be immediately found out and corrected. On occasion, sample should be re-blooded for inspection.

5. CONCLUSION

Clinical biochemical tests are an important part of laboratory medicine. Clinicians have paid more and more attention to the reliability and accuracy of test results. Only the various factors that may affect the test results are avoided and relevant factors are controlled and analyzed, the accurate, timely and effective inspection report could be issued. From aspects mentioned above, each test must rely on the cooperation among patients, medical staff and inspection staff. The test result could not rely entirely on the instrument, which the test error could be eliminated and reduced.

REFERENCES

[1]Schackmann M J A, Ofman R, van Geel B M, et al. Pathogenicity of novel ABCD1 variants: The need for biochemical testing in the era of advanced genetics[J]. Molecular genetics and metabolism, 2016, 118(2): 123-127.

[2]van Berkel A, Lenders J W M, Timmers H. Diagnosis of endocrine disease: biochemical diagnosis of phaeochromocytoma and paraganglioma[J]. European Journal of Endocrinology, 2014, 170(3): R109-R119.

[3]Richards D B, Cookson L M, Berges A C, et al. Therapeutic clearance of amyloid by antibodies to serum amyloid P component[J]. New England Journal of Medicine, 2015, 373(12): 1106-1114.

[4]Garrahy A, Casey R, Wall D, et al. A review of the management of positive biochemical screening for phaeochromocytoma and paraganglioma: a salutary tale[J]. International journal of clinical practice, 2015, 69(7): 802-809.

[5]Borntrager C, Lyon A R. Client progress monitoring and feedback in school-based mental health[J]. Cognitive and behavioral practice, 2015, 22(1): 74-86.

[6]Couper K, Kimani P K, Abella B S, et al. The system-wide effect of real-time audiovisual feedback and postevent debriefing for in-hospital cardiac arrest: the cardiopulmonary resuscitation quality improvement initiative[J]. Critical care medicine, 2015, 43(11): 2321.

[7]Chetwynd A J, Abdul-Sada A, Holt S G, et al. Use of a pre-analysis osmolality normalisation method to correct for variable urine concentrations and for improved metabolomic analyses[J]. Journal of Chromatography A, 2016, 1431: 103-110.

[8]Lee T H, Lee E, Park T, et al. Procedure of Seismic Performance Evaluation of LNG Receiving Terminal Facilities[J]. Journal of the Korean Society of Safety, 2014, 29(4): 110-115.

[9]Hartgerink J M, Cramm J M, Bakker T, et al. The importance of multidisciplinary teamwork and team climate for relational coordination among teams delivering care to older patients[J]. Journal of Advanced Nursing, 2014, 70(4): 791-799.

[10]Capdevielle D, Salesse R, Varlet M, et al. Social Motor Coordination in Schizophrenia Patients: From Impairment to Rehabilitation[J]. European Psychiatry, 2015, 30: 285.

[11]Deng J, Yu P, Yang L, et al. Competitive coordination of Cu2+ between cysteine and pyrophosphate ion: toward sensitive and selective sensing of pyrophosphate ion in synovial fluid of

arthritis patients[J]. Analytical chemistry, 2013, 85(4): 2516-2522.
[12]Girault A, Ferrua M, Lalloué B, et al. Internet-based technologies to improve cancer care coordination: current use and attitudes among cancer patients[J]. European Journal of Cancer, 2015, 51(4): 551-557.
[13]Nilsson K, Brulin C, Grankvist K, et al. Factors Associated with Nursing Students' Adherence to Venous Blood Specimen Collection Practice Guidelines: a Cross Sectional Study[J]. Nurse Education in Practice, 2016.
[14]Pakzad-Vaezi K, Levasseur S D, Schendel S, et al. The corneal ulcer one-touch study: a simplified microbiological specimen collection method[J]. American journal of ophthalmology, 2015, 159(1): 37-43.
[15]Frazee B, Enriquez K, Ng V, et al. Abnormal Urinalysis Results Are Common, Regardless of Specimen Collection Technique, in Women Without Urinary Tract Infections[J]. Academic Emergency Medicine, 2014, 21: 54.
[16]O'brien E, Parati G, Stergiou G, et al. European Society of Hypertension position paper on ambulatory blood pressure monitoring[J]. Journal of hypertension, 2013, 31(9): 1731-1768.
[17]Craig H. Isotopic variations in meteoric waters[J]. Science, 1961, 133(3465): 1702-1703.
[18]Audia P G, Locke E A, Smith K G. The paradox of success: An archival and a laboratory study of strategic persistence following radical environmental change[J]. Academy of Management Journal, 2000, 43(5): 837-853.
[19]Karapetrovic S, Casadesús M. Implementing environmental with other standardized management systems: Scope, sequence, time and integration[J]. Journal of cleaner production, 2009, 17(5): 533-540.
[20]Simon A, Bernardo M, Karapetrovic S, et al. Integration of standardized environmental and quality management systems audits[J]. Journal of Cleaner Production, 2011, 19(17): 2057-2065.
[21]Didion J P, Buus R J, Naghashfar Z, et al. SNP array profiling of mouse cell lines identifies their strains of origin and reveals cross-contamination and widespread aneuploidy[J]. BMC genomics, 2014, 15(1): 847.
[22]Santocchi E, Guiducci L, Fulceri F, et al. Gut to brain interaction in Autism Spectrum Disorders: a randomized controlled trial on the role of probiotics on clinical, biochemical and neurophysiological parameters[J]. BMC psychiatry, 2016, 16(1): 183.
[23]Li Y, Zhao Z, Zhang J, et al. Retrieving system, retrieving method, and security inspection device based on contents of fluoroscopic images: U.S. Patent Application 14/580,571[P]. 2014-12-23.
[24]O'hagan S, Manias E, Elder C, et al. What counts as effective communication in nursing? Evidence from nurse educators' and clinicians' feedback on nurse interactions with simulated patients[J]. Journal of advanced nursing, 2014, 70(6): 1344-1355.

Apreliminary Study on the Combination of Gps Technology and Orienteering Electronic Timing System in Orienteering Teaching

Xiaoqing Chen
Institute of Information Technology of Guilin University of Electronic Technology, Guilin, 541004, China

Abstract:The orienteering in schools have been carried out like a raging fire across the whole country. But, in the orienteering teaching and training process, there are some urgent problems we should solve: difficult organization, security check, placement of time and the map production cycle is long, the teachers can not be the leading part in the analysis and summary after the competition. In resent years, the GPS has been widely used in the field of the map making, event tracking, training analysis etc, and it has been solved some problems that need to be solved in the practice teaching and training of the orienteering. In this article, through the study of the GPS technology application, and prospect its application, we find a bold idea about combining the GPS technology and directional electronic timing system.
Keywords: GPS; Orienteering; teaching and training

1.THE ORIENTEERING TEACHING AND TRAINING PROBLEMS

1.1 the management of the class

International Orienteering Federation define the orienteering as “Orienteering athletes with map and compass, according to the provisions of the order, then complete seek for several plotted in figure and ground check point independently and finish the exercise as short as possible ”. [1] The orienteering is a sports event which combine the rich mass, fun, knowledge, competitive and military significance, and set the wisdom and physical strength in one sport event. The orienteering generally hold in the schools、gardens and the forest. The athletes will on the basic of their own technology and ability, and choose some different running routes. There are many problems in the process of teaching and training, such as cross-country running which have no fixed site, no fixed running route, large range of motion and soon.

The orienteering generally hold in the schools 、gardens and the forest. Because there is no fixed venue, and in the running process, the athletes have no fixed line. So, after the start, the athletes will scattered in every corner of the venue which will let the classroom teaching in a state of not monitoring. Therefore, when we get into the check point, we do not know whether it is a wrong point, whether we are running, whether to run out of the scope of the map or not, the teachers can not observe, but also can not grasp. In contrast, the directional movement of the classroom organization will be more difficult.

1.2 the problem of the security

Comparing with the use of the other fixed sports venues, the orienteering is carried on in the field which expand the range of the motion, and the site diversity, complex landform and physiognomy that makes the teachers can not effectively monitor, so the security problem is a key problem in the process of teaching and training. Because of the snake, vehicle, dangerous terrain and other factors which have a great threat to the athletes personal safety. When the athletes training in the field and being lost in it, the communication equipment is in a state of no use, so the security problem is the most important thing that the teachers should care about.

1.3 the storage time of checkpoints

When we in the progress of teaching and training of other sports, the sports equipment can be easily transported to their sports venues so that we do not need too much time to arrange it. However, the arrangement of the orienteering checkpoint need to be prepared for the venue before the starts. Due to the location of the orienteering is not fixed, the scope is large, and some places are nearby, but some places are very far which makes the checkpoints are in the uneven distribute, thus that will need more time and manpower in it.

1.4 the making of the map

As for a teacher who does not know how to make a orienteering map, both teaching and training, they all in a passive aspect. The characteristics of the map can not be used repeatedly, which determines the importance and necessity of the teachers' draw learning. Therefore, for the teacher, to participate a training or study by themselves, these are very important way to learn how to draw a map well. But, in order to make a map, it will spend much time on seeking the base map, measuring the field, drawing the computer and so on. In particularly, it will takes more time and energy to produce a high precision map.

1.5 the analysis and summary of the technical after the game

Because of the characteristics of the project itself, such as teaching, training and competing, the athletes do all the things by themselves, so the couch can not observe the whole process of the athletes. Thus the

summary and analysis of orienteering sports usually complete by the description and painting trajectory etc, then they will know the problems and find their teachers to help them to solve these problems. Furthermore there is no way for the teachers to guide and correct the athletes in time, and the leading role of teachers can not come out in the orienteering.

2. THE APPLICATION OF GPS TECHNOLOGY IN ORIENTEERING

The global positioning system,which we called GPS in English. The GPS consists of space satellite, ground control and subscribe equipment. And the subscribe equipment combine with the receiver hardware and the software in the computer, and the GPS data post-processing package. The handset of the orienteering GPS is one of the subscribe equipment. The main function is to capture the satellite according to a certain angle of the selected satellite to be measured, and track the operation of these satellites. When the satellites signal are captured by the receiver, the change rate of the pseudo distance and the distance between the receiving antenna and the satellite can be measured, and also can demodulate the date of the satellite orbit parameters etc. According to these date, the microprocessor in the receiver can be calculated on the basic of the positioning calculation method, and then get the location of the user's latitude and longitude, height, speed, time and other information [2] . After the appearance of the GPS technology, especially for the Selective Availability after the the United States military relieve it, the accuracy of the GPS civil signal has been greatly improved, so that the use of GPS with orienteering athletes in training and competing places can be monitored in a feasible lever [3] . Based on the review of the comrade Xie Hao, the use of the GPS in the orienteering, mainly reflected in the following aspects: 1.GPS orientation; 2.the application of GPS technology in orienteering; 3.real time tracking ; 4.training analysis.

2.1 gps orientation

With the popularity of GPS receivers, the GPS orientation arises at the historic moment which is a new form orienteering. The form is similar to the foot orienteering that we use the time to decide whether we win or not. But the different part is that GPS receiver replaced the compass, and we only mark the starting point and end point position in the map. At present, the GPS orientation does not have the clear and unified definition and rule, mainly a number of clubs in the exploration of various models in the United States, the United Kingdom and Estonia. [4] In primary and secondary schools and even universities, there are less GPS orientation developed in our country. However, the wear of the GPS can not need the checkpoints, which greatly reduces the training time, the preparation time of the classroom and the burden on the teachers.

2.2 the application of gps technology in orienteering

The orienteering map production, mainly use the OCAD software. Above the OCAD8 version , we launched a new function that we can transform the date from the GPS receiver. For the moment, there are two types we use the GPS to make the orienteering map: 1、 using the GPS receiver aided geographic information to collect orienteering map base map; 2、 using GPS receiver and PC edge to measure the field in the whole process. Through the research and practical application of GPS equipment, it is found that the application of GPS equipment in auxiliary map making which have a good impact on it. GPS has the advantages of high speed, high precision and reliability of the data information, which makes the work efficiency. Therefore, the method of GPS aided surveying and mapping has played a positive and effective role in solving the problem of map making in teaching and training.

2.3 the real-time tracking in orienteering

Because the orienteering is holding in the outdoor jungle, so that the audience can not know the specific performance of athletes in the competition process which makes the competition not so attractive. Thanks to the development of GPS technology, the Danish TracTrac company provides real-time tracking service that allowing the audience to watch the specific performance of athletes in orienteering. This product is based on a technique that the athletes carry the GPS receiver, record the player's real-time trajectory, and record it, through the GPRS and then the signal will be transmitted to the server. Thus, to achieve the real-time tracking of the players in the game, and then the audience can see the game from live broadcast of the TV and the Internet. In the 2016 national student orienteering championship, the Organizing Committee take the safety factor into consideration, and equipped with the GPS for the athletes for their first time to participate in orienteering. Therefore, in the use of this product, the classroom organization and security issues of the orienteering will be solved.

2.4 the training analysis

GPS can records the trajectory, which is of great value to orienteering teaching, training and competition. It can automatically obtain the actual trajectory of athletes, with the help of special analysis software, you can detailed analyze the pros and cons of the game. In the process of general orienteering teaching course, the students can understand the situation in the orienteering by the data of GPS receiver. The practice has proved that the GPS trajectory can accurate mastery to the whole process of athletes in training, and from the technical data, it can statistics and analysis the different training stage athlete , it also can help to improve the leading role of coaches in the training process.

3. THE ORIENTEERING ELECTRONIC TIMING SYSTEM

There are three common ways in timing: 1、 the

traditional manual timing, with the use of check card and needle punch; 2、the professional electronic timing system; 3、the large capacity fingerprint electronic timing system and registration system. Because the traditional manual timing needs a lot of manpower and material resources, and it is also easy for athletes to cheat, so it has been eliminated in the official competition. In 2011, the Hua Ruijian company launched a large capacity fingerprint electronic timing system. But, at present, the use of this system is very few. On the contrary, the units often use the ordinary professional electronic timing system. The athletes wear the contactless smart card (refers to the card) and get to the checkpoints, and through the read and write process of the contactless smart card reader and contactless smart card (point sign device) to record the time and number that the athletes through the sites. After the competition, we can use the operational software to solve the information in the card, which will get the athlete's segment score, total score, visited checkpoints and whether the score are valid or not, as well as competition rankings. The electronic timing system not only reduces the labor cost of manpower and material resources, but also improves the fairness and impartiality of the competition.

4. THE OUTLOOK AND VISION

Now, although the professional electronic timing system also has some problems, there are no choice to avoid it: 1、registered in others name ; 2、and exchange refers to the card to running. However, before the system is upgraded, and a simple, convenient and practical new product is developed, it is still has a great impact on the orienteering.

Furthermore, the GPS technology also has some problems: 1.the signal is not stable, when we in the dense forest, valleys, or tall buildings, etc, the accuracy of the GPS will decline. 2.the GPS can not get the date of the altitude or the date are in low accuracy. But, the GPS technology has solved several problems in the orienteering teaching and training process. Moreover, the European Union, Russia and China are developing more accurate satellite navigation systems. EU's "Galileo" system which let the accuracy of civil development will be raised to the 1M level. The application prospect of GPS in orienteering has a good effect.

If we can aid the GPS technology into the orienteering electronic timing system, and can combine the two things in one product, especially for some useful functions that will not only can use for timing, but also can trace and record the trajectory, since several problems in orienteering teaching and training can be solved,which will makes the enthusiasts and coaches fall in love with it. Moreover,the accept price of the electronic timing system and GPS are very expensive, if the combination of the two products, the cost will be reduced, and it will become a popular product.

REFERENCES

[1]IOF Foot- O Competition Rules.2007.

[2] Zhen Gao, Guifu Feng. Global Positioning System (GPS) and its application. Space Electronic Technology, 1997 (1): 11-15.

[3]Hao Xie. Effects of vegetation environment on the training effect of Orienteering Athletes using GPS. The ports sciences of Zhejiang .2011.5 (3): 63-65.

[4]Satellite, in my hands GPS Orienteering.The digital world, 2007 (7): 138-141.

[5]Jian Sun, Ling Li. The research on the improvement of the analysis of the GPS track in the directional sports training.The proceedings of the third National School Orienteering Conference.2013.9

[6]Hao Xie , Jian Wang. Research on the application of GPS technology in orienteering.The sports science of Zhejiang .2009 (1): 61-64.

[7]Yujiang Liu,Shichun Liu. Preliminary study on electronic drilling and timing system of Orienteering.The sports science and technology of Liaoning .2001.12 (6): 38-39.

Study on the Influence of the Policy of Replacing Business with VAT on Project Cost

Dongyang Geng[1,], Lijun Cao[1], Weiwei Wang[2]*
[1.] School of Management Science and Engineering Hebei GEO University, Shijiazhuang, China
[2.] School of Economics and Management, College of Si Fang of Shijiazhuang Tiedao University, Shijiazhuang, China

Abstract: China's tax system has been gradually perfect Replacing Business with VAT system, which will also affect the construction industry. Through an in-depth understanding of the Replacing Business with VAT system, with Replacing Business with VAT, through the Replacing Business with VAT impact of the construction industry project cost, through the impact of the general contracting and construction industry tax impact analysis, need to Through the coordination of the development of the construction industry to complete the construction of internal tax management force optimization, strengthen the construction industry tax planning.
Keywords: Replacing Business with VAT; Construction; Construction cost

1. INTRODUCTION

The current tax system has been unable to meet the economic development needs, need to give the current tax system reform. Replacing Business with VAT refers to the business tax into value-added tax, will be repeated in the past to change the status of levy. For the business tax into value-added tax, although the tertiary industry services industry, but also on the construction industry has an impact.

2. REPLACING BUSINESS WITH VAT ON THE CONSTRUCTION COST

2.1 Replacing Business with VAT on the construction industry organization and mode of operation of the impact

China's current large-scale construction industries, mostly through multi-level legal form, usually have many subsidiaries and subsidiaries, and the project contract to create the project department of the construction and management of the responsible. For example, in China Railway Construction, constitute a layer by layer within the enterprise approach. For the business tax model, the project department on behalf of all turnover of the company to pay sales tax. While the value-added tax is the way through the vote with the tax, the characteristics of the chain deductible, that is, all aspects of tax payment must be strictly in accordance with the proceeds and deductions for the way the output tax, if the chain is longer, The risk of large taxation, and signed subcontracting contracts will also increase the stamp duty, so, with the corporate level and the management level of the increase, the Replacing Business with VAT management more unfavorable.

2.2Replacing Business with VAT in the project cost management

The project cost management will affect the bid price of the project, so it is of great significance in the project contracting. Because the business tax is the price within the tax, the project cost with taxes, and comprehensive tax rate is relatively fixed, the tender offer is relatively simple. But the value-added tax for the price of foreign tax, Replacing Business with VAT after the tender offer through the VAT output tax, the project cost separately, which completely changed the original cost of construction products and pricing rules, and in the construction, Input tax and cannot be correctly estimated, and Replacing Business with VAT after the urban construction tax and education base is required to pay the VAT tax, so all the more difficult to correctly assess the process of project tax status, which will tend to tender offer Greater impact, which will project the contract to cause a greater impact.

2.3 Impact of Contract Business with VAT on general contracting

In accordance with the general contracting characteristics of the project, the general contracting of the project in the construction enterprise project, including the mountain to the procurement of the final design to the construction of all the process, Replacing Business with VAT will have two effects on the project: (1) Based on the change. Construction tax levied in accordance with the Interim Regulations on business tax and value-added tax on the construction business tax levied on self-produced goods for value-added tax collection, regulations limit the construction of self-produced goods is mixed sales, and tax based on more vague, more difficult Exempt from repeated taxation status. After the implementation of Replacing Business with VAT, the project's general contracting will not have multiple taxation situation, (2) increase the burden of tax burden. The current construction industry has been increasing the number of projects in the construction industry. Although it can be deducted from the input VAT, it will also increase the burden of taxation. As a result, the construction cost is increased in terms of utilities, cement, concrete and construction workers. Replacing Business with VAT It is more difficult to obtain VAT-specific invoices. Therefore, after the Replacing Business with VAT, the overall tax burden of the general contracting for

construction works has been raised.

2.4 Replacing Business with VAT on the accounting and cost management

The project cost includes the labor cost, the material fee, the mechanical use fee, the indirect expense as well as other direct expenses to constitute. Business tax status, the project cost includes VAT. After the Replacing Business with VAT, the project in the income, cost accounting should be in accordance with the price-tax separation policy. Because the accounting model changes, it will make all the standards have changed.

(1) The impact on the key indicators. In the case of no change in the current total amount of the business tax, the implementation of the separation of the value - added tax will directly reduce the income. Because the amount of input tax is not sufficient, the separation of costs and costs is much lower than the amount of income separation, so that the total amount of profits will be reduced. The increase in tax burden and even make all the advance tax time, but also makes the net cash flow from operating activities will be reduced, so that the payment of funds to increase the pressure, the asset-load ratio

Standards have also increased.

(2) The impact of accounting. Construction companies have long turned over to the business tax; the staff accounting for the concept of deep business tax, the establishment of the accounting project is relatively simple business tax accounting covers only to the provision, pay two aspects of business. The business tax and additional debit, the corresponding tax payable for business tax payable in the process of payment, the corresponding tax payable for business tax to be debited, and bank deposits After VAT, the construction industry to pay VAT, cross-level accounts in the major changes, and more cumbersome, for the construction industry, causing the greater the troubled staff.

2.5 Replacing Business with VAT on the impact of corporate tax management

In the way of business tax, construction enterprises do not attach importance to tax management, loosening in management, staffing is not perfect, job responsibilities planning is vague, tax planning scope is narrow. With the implementation of Replacing Business with VAT, tax management has become a more systematic project, tax planning area has expanded, but also increased the difficulty of management, improve the professional standards of the staff.

Value-added tax deductible by way of not only get the corresponding deduction vouchers, and taxpayers need to VAT invoices and even customs import value-added tax special payment book for the day of calculation, until 180 days should be to In charge of the Inland Revenue Department for certification or deduction. If the taxpayers get irregular invoices and beyond the time limit cannot be deducted, it will increase the corporate tax burden, increased risk.

3. CONSTRUCTION COSTS FOR REPLACING BUSINESS WITH VAT

3.1 Change business philosophy, to create and improve the internal bidding system

With the Replacing Business with VAT tax system changes, so that the management of affairs and business management personnel have changed, the project planning and decision-making should be preceded by the plan. Compared with the original payment of business tax, engineering pricing from the tax price is not included in the price, which in turn has changed the construction industry for a long time the project pricing plan, and the bidding of enterprises has a direct impact. For participating in the offer, the enterprise should keep abreast of the contents of Replacing Business with VAT, to create in line with the enterprise in the VAT system in the tender offer system and management system. In terms of the bid price of the construction project, the cost of VAT should be effectively assessed. The bid-winning rate of the project and the source of the input tax shall be taken into consideration. The invoice of the maximum input tax shall be obtained as far as possible so as to give the quotation of the enterprise more competitive conditions.

3.2 Focus on the training of relevant personnel

Replacing Business with VAT is the only way for executives to be aware of the impact of Replacing Business with VAT and to strengthen management and analyze the issues of Replacing Business with VAT before they can focus on Replacing Business with VAT. You can take the work of Replacing Business with VAT seriously. Construction companies need to increase the training scope of Replacing Business with VAT. All staff should be involved in the training of Replacing Business with VAT, control the impact of Replacing Business with VAT on all the layers, let people understand the change of content, organization. The staff need to increase the number of training to understand the relevant knowledge of value-added tax in order to facilitate the guidance of other departments to work.

3.3 The Supplier shall select carefully

In terms of construction cost, the cost of materials and equipment accounts for a large part of the cost. Since the purchase of building materials has a large tax burden on enterprises after the Replacing Business with VAT, the supplier Procurement of building materials discount situation has a greater impact, which also has a greater impact on the development of enterprises. Suppliers should have the general taxpayer qualification, and also need to have the ability to issue value-added tax invoices. These aspects should be reflected in the contract. Moreover, if the supplier is only small-scale taxpayers, construction companies and suppliers should be in the purchase and sale before the negotiations to negotiate the price of the transaction,

and suppliers can not issue VAT invoices and the formation of the price discount and VAT invoice output tax Degrees, to maximize the benefits.

3.4 to reduce the timely collection of value-added tax on the construction industry

Through the development of the construction industry in recent years can be found, especially for the implementation of Replacing Business with VAT policy, the development of construction enterprises will be due to the increase in value-added tax rate to reduce the tax burden balance, if this has long been developed, If the balance point is beyond the value-added tax, the situation of value-added tax burden exceeds the tax burden of business tax, thus affecting the economic development of construction enterprises. According to the development of the construction industry point of view, this situation will not be able to effectively stimulate the development of the construction industry. In order to stimulate the development of the construction industry, exempt from the Replacing Business with VAT policy to increase the tax situation, the need for Replacing Business with VAT rate coordination, by reducing the construction industry, the value-added tax, reduce Replacing Business with VAT the Role of Tax Burden in Construction Industry.

4. CONCLUSION

All in all, under the development of social economy, the country's tax policy has also been a great innovation and reform, not only need to ensure the rationality of the tax, but also need to protect the fairness of taxation, integration of local management of regional tax differences. The policy of Replacing Business with VAT has some advantages and disadvantages. How to maximize the benefits and maximize the reduction of the disadvantages is the aspect of the current construction project cost needs to be discussed. And, in the future work, the corresponding accounting personnel also need to constantly analyze Replacing Business with VAT, to maximize the economic benefits of building enterprises, so that construction companies get a better hair

ACKNOWLEDGMENTS

The authors acknowledge the Teaching reform project of Hebei GEO Unibersity: 2016J02

REFERENCES

[1] The value added tax: Its causes and consequences . Michael Keen, Ben Lockwood. Journal of Development Economics. 2009 (2)

[2] Tax policy and reform in Asian countries: Thailand’s perspective. Somchai Sujjapongse. Journal of Asian Economics. 2005 (6)

[3] On selective indirect tax reform in developing countries. M. Shahe Emran, Joseph E. Stiglitz. Journal of Public Economics. 2004 (4)

[4] Direct or indirect tax instruments for redistribution: short-run versus long-run. Emmanuel Saez. Journal of Public Economics. 2003 (3)

[5] The Distributional Effects of Indirect Tax Changes in Italy. Paolo Liberati. International Tax and Public Finance. 2001 (1)

An Experimental Research of Gathering Powder into the Ball in The Place of Miaogou Yanshan and Sijiaying

Yu Tang, Yanghuan Xu, Xiaocan Wen and Xiaoqiang Guo
North China University of Science and Technology,Tangshan,063210,Hebei,China

Abstract: This paper shows that a higher pelletizing ratio can be achieved when the bentonite content is 1.2% through the way of adaptive polynomial fitting .Under the condition above ,this paper analysis two kinds of iron ore powder mixture ratio in a condition of getting an optimal pelletizing ratio through building the neural network model. Beyond that, this paper also finds out the main compounds in the iron ore powder through principal component analysis model and then return to nature factors and at the same time, it promotes the method to a condition of seeking the optimal solution when there are variety of iron ore powder involved.

Keywords: BP neural network; adaptive polynomial fitting; principal component analysis; fine powder pelletizing

1. INTRODUCTION

With the rapid development of Chinese green economy, iron and steel industries are facing a huge reform, and the position of pellets in the steel industry is more and more advanced and its usage is extending rapidly, at the same time the quality requirements are increasingly strict.This paper analysis the influencing factors of making pellets based on experimental research of gathering powder into the ball in the place of Miaogou,Yanshan and Sijiaying.

2.ANALYSIS OF BENTONITE CONTENT'S INFLUENCE ON PELLETIZING RATIO OF IRON ORE POWDER.

2.1 The building of adaptive polynomial fitting model

Suppose that N pairs of data points have been known which is $(\tilde{x}_i, \tilde{y}_i, i = 1,...,N)$ .The m – 1 least-square fitting polynomial of the data column is

$$\mathrm{F}_m(\mathrm{m}) = a_1 + a_2 x + ... + a_m x^{m-1}$$

Among which, $m \le n$ and m is no more than 20. In the actual calculation, in order to prevent arithmetic overflow, generally x_i is replaced by the following formula: $\tilde{x}_i = x_i - \overline{x}$

$$\overline{x} = \sum_{i=1}^{N} x_i / N$$

Among which,

The form of the fitting polynomial is as follows,

$$\mathrm{F}_m(\mathrm{m}) = a_1 + a_2(x - \overline{x}) + ... + a_m(x - \overline{x})^{m-1}$$

At this time, this formula is the standard form for polynomial fitting. Among which m - 1is the biggest number for polynomial fitting. a_i is the fitting coefficient waiting to be calculated.

2.2 The solve of the model of influence on iron ore powder pelletizing ratio.

According to the national standards of pelletizing grain diameter, this article selects 10-12.5 mm grain size pelletizing rate's percentage plus 12.5-16 mm grain size pelletizing rate's percentage as variable factors. And using the adaptive polynomial fitting model to analysis the impact of the bentonite's changes.

(1) According to the information mentioned above, through analyzing bentonite content's influence on Sijiaying iron ore powder pelletizing ratio and then getting the function equation which involved the and bentonite ratio.

Table 1 The influence of bentonite content on the Sijiaying iron ore powder pelletizing and moisture

Serial number	The distribution percentage of pellet grain size(%)				moisture(%)
	<10mm	10-12.5mm	12.5-16mm	>16mm	
0.6	14.21	50.00	21.58	14.21	8.3
0.9	41.83	34.66	14.34	9.16	8.4
1.2	4.07	21.11	59.26	15.56	8.5
1.5	3.75	23.75	51.25	21.25	8.5
1.8	17.67	20.14	55.48	6.71	8.6

$$y_1 = 686.32x^4 - 3442.3x^3 + 6196.8x^2 - 4688.5x + 1308.4 \quad (1)$$

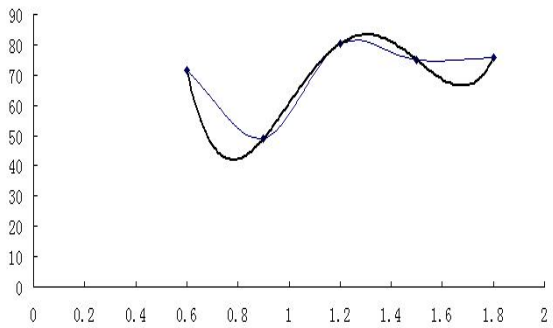

Figure 1 The fitting curve of bentonite content fit Sijiaying iron ore powder palletizing

(2) The analysis of bentonite ratio's influence on the Yanshan iron ore powder pelletizing

$$y_2 = 411.11x^4 - 1923.1x^3 + 3194.9x^2 - 2224.3x + 619.74 \quad (2)$$

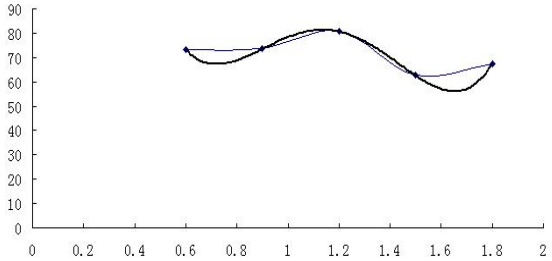

Figure 2 The fitting curve of bentonite content fit Yanshan iron ore powder pelletizing

The analysis of bentonite ratio's influence on the Miaogou iron ore powder pelletizing .

Table 2 The influence of bentonite content on the Yanshan iron ore powder pelletizing and moisture

Serial number	The distribution percentage of pellet grain size(%)				moisture(%)
	<10mm	10-12.5mm	12.5-16mm	>16mm	
0.6	12.68	43.66	29.58	14.08	7.5
0.9	5.75	17.24	56.32	20.69	7.9
1.2	15.50	43.80	36.82	3.88	8.0
1.5	34.07	42.96	19.63	3.33	8.3
1.8	29.39	41.22	26.34	3.05	8.6

Table 3 The influence of bentonite content on the Miaogou iron ore powder pelletizing and moisture

Serial number	The distribution percentage of pellet grain size(%)				moisture (%)
	<10mm	10-12.5mm	12.5-16mm	>16mm	
0.6	23.66	38.93	27.48	9.92	8.5
0.9	18.42	37.28	39.91	4.39	8.1
1.2	42.72	38.83	17.48	0.97	8.9
1.5	44.25	36.28	16.81	2.65	9.3
1.8	55.45	31.82	8.18	4.55	10.3

$$y_3 = -395.32x^4 + 1964.8x^3 - 3524x^2 + 2655.9x - 631.66 \quad (3)$$

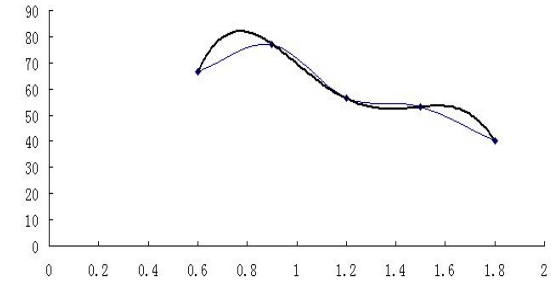

Figure 3 The fitting curve of bentonite content fit Miaogou iron ore powder pelletizing

2.3 The analysis of the result

The equation above and the curve results shows that within the rage of actual ratio, Sijiaying iron ore powder pelletizing is higher when bentonite ratio is 1.2.So the ideal bentonite ratio is 1.2 for Sijiaying iron ore powder pelletizing.And Yanshan iron ore powder pelletizing is higher when bentonite ratio is 1.8.So the ideal bentonite ratio is 1.8 for Yanshan iron ore powder pelletizing.Besides Miaogou iron ore powder pelletizing is higher when bentonite ratio is 1.6.So the ideal bentonite ratio is 1.6 for Miaogou iron ore powder pelletizing.

3.THE ANALYSIS OF THE INFLUENCE OF DIFFERENT RATIO OF IRON ORE POWDER ON PELLETIZING

3.1 The building of BP neural network model

3.1.1 The structure and principle of BP neural network

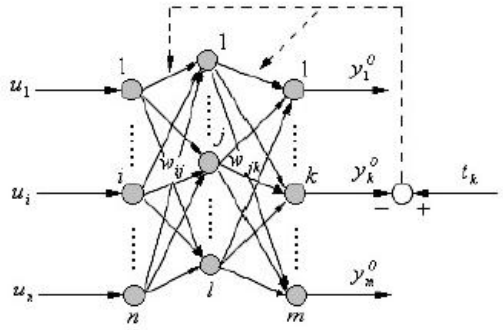

Figure 4 Multi-layer neural network structure

In the figure 4, there are n neurons in the multilayer neural network input layer, and l neurons in hidden layer and m neurons in output layer. Among them ,

w_{ij} is the connection weights between the first i neurons and the first j neurons in hidden layer ,and w_{jk} is the connection weights between the first j neurons in hidden layer and the first k neurons in output layer. For input layer neurons, the role function takes linear function, which is to say the output neurons is equal to the input neurons. The input of the hidden layer and output layer neurons is respectively the weighted sum of the previous layer, and the output of each neurons depends on the degree of the motivation and the corresponding role function. The study of multilayer neural network belongs to supervised learning, and the learning process is consisted by positive information dissemination and error back propagation. First is the positive transmission of the signal, through inputting, the signal is treated step by step through the hidden layer ,and then transmitted to output layer, and in the process, the state of each layer is concerned with the previous layer. If the output of the output layer can not achieve the desired accuracy requirement, and it will enter the back propagation process of the error, and correct the link weight of each layer step by step through error values , so as to reduce the error.

3.1.2 The design of BP neural network

The design of the neurons network involves structure of the neural network, the number of neurons and layers, and neuron's activation function, the initial value and learning algorithms, etc.For BP network, the number of neurons in input and output layer can be determined according to the problem that needed to be solved. Therefore, the design of BP network should based the above several aspects, and as much as possible to reduce the size of the network, shorten the training time of network.

1) The sample data

First of all, there are many factors that can affect the seat comfort, can't all seen as neural network input, otherwise will increase the complexity of system, affecting the precision of the neural network, this article selects the temperature and humidity as influence factors of chair also as input of neural network, the subjective comfort as the output of the neural circuits.

2) The network layer

In theory it has proved that: the BP network neurons with three layers neurons can approximate any nonlinear function. In general, the more the layer number ,the higher precision, but the layer number's increase would lead to the dramatic increase in amount of calculation, in addition, the precision of the network can also be implemented by increasing the number of hidden layer neurons, and this way is more easy to implement. Therefore, gives priority to increase the number of neurons in hidden layer.

3) Number of hidden layer neurons

With less number of neurons, if it can't meet the precision request then can increase properly.

4) The selection of initial weights

Usually choose very small non-zero random number, so that we can ensure the weights of each neuron is able to adjust in their Sigmoid activation function's biggest change place.

5) Learning rate

Learning rate too much will cause the system unstable, too small the network will convergence slowly, so usually choose small learning rate in order to guarantee the stability of the system and it is generally between 0.01 ~ 1.

3.2 The influence analysis of iron ore powder mixture ratio

3.2.1 The pelletizing influence analysis of iron ore powder mixture ratio

When bentonite ratio is 1.2%, this paper studies the influence law of two kinds of iron ore powder's different ratio on the pelletizing and moisture based on neural network model.

Table 4 The influence of the different ratio of Sijiaying and Yanshan's iron ore powder on mixed powder pelletizing and moisture

Serial number	The distribution percentage of pellet grain size(%)				moisture(%)
	<10mm	10-12.5mm	12.5-16mm	>16mm	
Si10%+Yan90%	22.22	52.53	24.24	1.01	7.85
Si20%+Yan80%	22.55	44.12	29.41	3.92	7.88
Si30%+Yan70%	9.09	51.82	25.45	13.64	7.80
Si40%+Yan60%	17.86	47.32	31.25	3.57	7.80
Si50%+Yan50%	6.19	17.53	62.89	13.40	8.24
Si60%+Yan40%	24.66	26.80	38.83	9.71	8.09
Si70%+Yan30%	4.08	17.35	64.29	14.29	8.08
Si80%+Yan20%	4.00	9.00	60.00	27.00	8.46
Si90%+Yan10%	30.94	39.46	19.73	9.87	8.94

This paper randomly selected eight sets data from experimental data table and remained a set of date as the testing data so as to establish the BP neural network.Then through the way of debugging and training,the neural network fitting prediction system about Sijiaying and Yanshan iron ore powder mixed pelletizing can be achieved at the condition of the error is 0.0079.

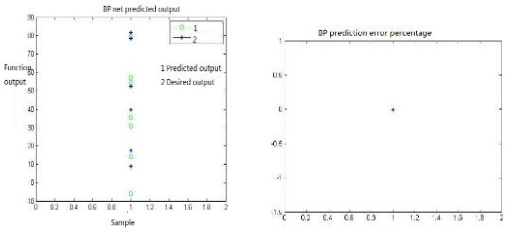

Figure 5 The neural network of iron ore powder

mixed pelletizing in the place of Sijiaying and Yanshan.

Reselect the content at the condition the mixing proportion interval is 5%, then according to the trained Sijiaying and Yanshan's neural network fitting model so as to predict pellet grain distribution percentage corresponding to various content ratio. Just as shown in table 5

Table 5 Iron ore powder mixed ratio pelletizing in the place of Sijiaying and Yanshan

Serial number	The distribution percentage of pellet grain size(%)
	10-16mm
Si10%+Yan90%	76.77
Si15%+Yan85%	74.70
Si20%+Yan80%	73.53
Si25%+Yan75%	75.00
Si30%+Yan70%	77.27
Si35%+Yan65%	77.76
Si40%+Yan60%	78.57
Si45%+Yan55%	77.25
Si50%+Yan50%	80.42
Si55%+Yan45%	62.17
Si60%+Yan40%	65.63
Si65%+Yan35%	66.30
Si70%+Yan30%	81.64
Si75%+Yan25%	65.17
Si80%+Yan20%	69.00
Si85%+Yan15%	71.63
Si90%+Yan10%	59.19
Si95%+Yan5%	54.58

According to the neural network predicted pelletizing, the pelletizing efficiency is highest when the content of Sijiaying is 70% and Yanshan is 30%.

This article selects a ratio interval of 5% to predict pelletizing. To improve the prediction accuracy you can choose a ratio interval at 1%. The prediction accuracy is higher with the interval shorter and can get the best mixing proportion at last through continue search.

3. CONCLUSION

This paper finds that pelletizing efficiency is higher when bentonite content is 1.2% by using the way of adaptive polynomial fitting and under that condition ,this paper analysis two kinds of iron ore powder mixture ratio in a condition of getting an optimal pelletizing ratio through building the neural network model. At last return to chemical composition to find nature factors which affects pelletizing. At the same time promote the way to the condition when seeking for three kinds of iron ore powder optimal mixture ratio. And complete the problem research about pelletizing influence factors analysis.

REFERENCES

[1] Juying Fu, Tao Jiang, Deqing Zhu. Sintered pellets learning [M]. Changsha: Press of Central South University, 1996.

[2] Xiaohui Fan, Lishun Yuan, Liang Cao. Blast furnace concentrate and science matching ore [J],Sintering pellets, 2004, 29 (4) : 2.

[3] Qi Xiao. Theory and practice of briquetting [M]. Changsha: Press of Central South University, 1989.

[4] Juying Fu,Deqing Zhu. Iron oxide pellets basic principle, process and equipment [M]. Changsha: Press of Central South University , 2005.

[5] Xinbing Zhang, Mengwei Zhu. The influence of Bentonite on the pelletizing production in China [J]. Journal of sintered pellets. 2003 (6).

[6] Tong Hou. The basic research of iron concentrate pelletizing performance [D]. Press of Central South University, 2010.

[7] Changhong Dong. Neural network and application [M]. The press of National defense industry , 2005.

[8] Yimin Zhang. Production technology of Pellets [M].The press of Metallurgical industry , 2005.

[9] Hanquan Zhang. The application of Bentonite in iron oxide pellets [J]. Journal of China mining. 2009 (8).

[10]Deqing Zhu,Huimin Li,Wei Yu,Bin Wang,Jian Pan.The reinforcement mechanism of organic composite bentonite in iron ore pellets[J]. Journal of Chongqing University, 2009 (05).

Research on Cross-Border E-commerce Logistics Mode of Agricultural Products under the Background of “One Belt and One Road”

Miao Tian
School of Economic and Management,Zhaoqing University,526000, China

Abstract: In the rapid development of cross-border electronic commerce today, logistics becomes the key issue in the direct impact on cross-border electricity efficiency highly attention from all walks of life.Aiming at the problem of agricultural products appeared in the process of cross-border e-commerce, logistics system reconstruction is an important countermeasure.Each region should seize the strategic background of the "region", actively integrated into the national "area" development planning, through cross-border electronic commerce logistics channel of agricultural products, promote the development of local agricultural products cross-border e-c.Combining with the current situation of the development of cross-border e-commerce, surrounding cross-border e-commerce for agricultural products and cross-border logistics analysis, study the collaborative relationships, the development countermeasures are put forward.
Keywords: One Belt and One Road; Agricultural product; Cross-border e-commerce;Logistics

1. INTRODUCTION

The strategy of “the Belt and Road”in our country is the highest national strategy currently, it is put forward for the provinces and cities of cross-border e-commerce development provides a great historic opportunity.In the process of the construction of "the Belt and Road" all the way through, China will give full play to the regional comparative advantage, to implement a more proactive opening-up strategy, strengthen the interactive cooperation east central and western regions, improve the level of the open economy.Similarly, cross-border e-commerce as a business model based on technology, in promoting the economic integration and globalization of trade has very important strategic significance.Whether for a corporate client or for the client, have greatly strengthened the mutual benefit and win-win results between the participants.Cross-border electricity analysis of agricultural products and cross-border logistics coordination problems, is in the cross-border electricity under the background of rapid development of important issues.

2. CROSS-BORDER E-COMMERCE LOGISTICS DEVELOPMENT PRESENT SITUATION

At present, our country cross-border e-commerce includes mainly use parcel post logistics mode.Domestic express mode is mainly along abundant, EMS, "cross"."Cross" of shentong and yuantong development earlier, and zhongtong, huitong, YunDa is just beginning to start cross-border logistics business, suitable abundant early globalization business layout, to launch "global business", "global" for electrical contractor businesses provide price delivery of services in the economy, low requirements for aging.The internationalization of the EMS business in domestic express the most perfect.In addition, international express mode refers to the four big commercial Courier giant, TNT, DHL, UPS, Fedex.Proprietary storage refers to the seller in the destination countries to establish overseas warehouses, when customer order, through the local distribution to consumers directly.Cross-border railway logistics mode is to point to by air package transportation tank way abroad, again through the cooperation company destination delivery.Third party logistics is refers to provide specialized logistics services company, it is independent of the buyer and the seller's market main body, through business contracts for MaiMaiFang provide logistics services.

(1) The fresh agricultural-product logistics is in focus

Foreign fruit, vegetable, fresh products favored by consumers like, involved in the process of long, however, the product easy to bad, transportation cost is big, the freight may exceed the value of the product itself, etc.How to do it efficiently send fresh products into the hands of customers, to let foreign customers for domestic vegetables, fruits, supply chain optimization approach, promote the development of the domestic agricultural now is an urgent need to solve the problem.

(2) Cross-border e-commerce has a long cycle distribution

Cross-border e-commerce logistics distribution compared with traditional domestic distribution, distribution link is very much involved, customs clearance is not clear, the efficiency is not high, buy goods from overseas websites, goods delivery time is 10 days, less than months above, will be hard to ensure the quality of the goods not only, return money exchange problem is very complicated, combined with block, customs clearance and commodity inspection and other issues, greatly reduce the efficiency of distribution.

(3) The fourth party logistics development rapidly

Traditional third-party Logistics model is common in Chinese e-commerce Logistics mode, but in recent years in order to cater to the fast development of cross-border electricity business in our country, the Fourth Party Logistics mode develop rapidly. The 4PL is mainly aiming at the shortcomings of the third party logistics is put forward to improve strategy, has become the new form of outsourcing of logistics supply chain.Objectively speaking,The 4PL is based on common information provided by businesses and government support, it really will be the government, cross-border electricity companies, Banks and so on domain resource integration planning, formed a complete set of supply chain solutions.Not only can offer business collaborative support for cross-border electricity business enterprise, also can realize the management of value-added services and consulting, for logistics enterprises to build based on smooth business operation of the fourth party logistics platform system.

3.THE PROBLEMS THAT EXIST IN CROSS-BORDER E-COMMERCE LOGISTICS

(1) Lack of the cross-border e-commerce logistics professionals

Cross-border e-commerce construction is one of the important forms of overseas logistics warehouse, belongs to technology-intensive industry, the professional technical personnel and the supply chain management talent demand is higher.Cross-border e-commerce development overseas warehouse in China, the need to employ knowledge of international law, culture and international payments and trade knowledge.Present cross-border electricity logistics talent deficiency is a major problem.

(2) Inventory risk and inventory costs

Overseas warehouse construction need to stock up in advance, and warehousing of goods has particularity.How much inventory of risks: large inventories, can take up liquidity.Less inventory, to bring customers rapid delivery of high quality experience.

(3) Different national environmental constraints

Cross-boundary electricity is different from domestic electricity, electricity is geared to the needs of consumers in different countries, consumption habits and policy has very big difference.In terms of product safety, intellectual property protection is faced with many complicated factors, need to learn intercultural communication and the environment.

(4) Buying cost and high technical requirement

Overseas warehouse construction covers an area of broad, long time needed for the warehouse construction, big money.For information technology put forward higher request, mobile, information technology directly affect overseas warehousing shortcut corresponding ability and operation ability.

4. OVERSEAS WAREHOUSE CONSTRUCTION COVERS AN AREA OF BROAD

Long time needed for the warehouse construction, big money. For information technology put forward higher request, mobile, information technology directly affect overseas warehousing shortcut corresponding ability and operation ability.

According to the characteristics of the various cross-border logistics mode, variety of goods and factors such as comprehensive consideration, the size and the requirements of our customers can choose the appropriate logistics mode and integration of different logistics mode.Because the parcel post logistics cost is low.And large in value, high profit products suitable to adopt the international express logistics mode.Goods sell to the buyer before clear the characteristic of different logistics mode, provide the buyer with diversified logistics choice, let the buyer according to the actual demand to choose the logistics mode, or a variety of cross-border logistics mode share.Such as logistics line + overseas warehouse, in order to improve the logistics efficiency, improve customer satisfaction.

(1) To speed up the cross-border e-commerce logistics professional talent training

In terms of cross-border electronic business logistics professional talent training, industry association to integration of institutions of higher learning and social resources, improve the cross-border electricity logistics talent training scheme.Through the international joint ventures, cultivating international high-end comprehensive talent.

(2) Improve the relevant policies and regulations on cross-border e-logistics

The government can provide low-interest loans and other ways to provide financial support for enterprises to establish overseas storehouse.Introduced by supervision and punishment of fakes, promote the domestic and overseas consumers trust in cross-border electricity enterprise.

(3) Pay attention to personalized and localized service

By providing high quality personalized and localized service, innovating the mode of overseas warehouse, enhance the competitiveness of the enterprises overseas warehouse in overseas markets.Help sellers to solve the problem of inventory goods show retail functionality and implementation, to provide local service and the consumer experience.

ACKNOWLEDGMENT

The paper is supported by the following project funding:1. Institutions of higher learning education teaching reform project of Guangdong province:Under the background of “Internet+”cross-border e-commerce applied talents cultivation mode innovation research---To form a team of “Amazon sellers” as the breakthrough point(Project Number:2016236)2.Philosophy and social science project of Zhaoqing: Promote the development of zhaoqing city commercial Internet + strategy pattern research - to build a virtual industry

cluster as the breakthrough point(Project Number:16QN-04).3. Project of quality engineer and teaching reform of Zhaoqing University(Project Number:201663)

REFERENCES

[1]DENG Xiaoyi. China's cross-border electricity overseas warehouse storage construction in logistics research[J]. Logistics technology,2017(3).

[2]GUO Jianfang. Research on cross-border e-commerce logistics industry development of Hangzhou under the strategy of the “one Belt and one Road”.

[3]Zhang Xiuzhen. Research on status quo of cross-border e-commerce logistics distribution mode[J], Comprehensive forums, 2017(1).

Research on Joint Dispatching of Class Reservoirs with Multi - objective Programming Model

Deyi Liu[1], Cheng Yuan[1], Zhixue Wang[2], Nan Ji[3,],Xaojun Men[3]*
Jun Lin[1,2], Yu Li[1,]*
[1]College of Information Engineering, North China University of Science and Technology, Tangshan,063299, China
[2]College of Electrical Engineering, North China University of Science and Technology, Tangshan,063299, China
[3]College of Science, North China University of Science and Technology ,Tangshan,063299, China

Abstract: Aiming at the water regulation problem of the Kaliba dam on the Zambezi River, this paper establishes a multi - objective programming model for gradient reservoir joint scheduling. Based on the consideration of reservoir safety and benefit, the two objective functions of optimal flood control capacity and maximum power generation capacity are established by combining these constraints, water capacity, reservoir capacity, hydraulic and discharge capacity. Using genetic algorithm to solve the dam flood control capacity of 120 billion cubic meters, the annual generating capacity of 640 billion kilowatts per hour. Finally,the ARIMA model was established based on the monthly flow rate of the Zambezi River in the past six years, and the maximum water flow was obtained from January to March, the maximum water flow was 2.4 cubic meters per second, the lowest water flow from July to October and the lowest water flow of 0.45 cubic Meters per second.
Keywords: Multi - objective programming; Genetic algorithm; ARIMA model

1. INTRODUCTION

Cascade reservoir joint dispatching is a typical large system multi - objective problem. It is different from the single reservoir to only pursue its own comprehensive benefit. The multi-objective optimization of the cascade reservoir requires the multi-objective and multi-objective co-ordination between the multi-objective function of the reservoir and the reservoir. It is necessary to coordinate the interests between the reservoir functions and Coordination of the interests of the reservoir, in order to achieve the most comprehensive benefit of the reservoir. There is a strong hydrological link between the cascade reservoirs. The flood control and power generation schemes of the upper reservoir will affect the dispatching operation of the next-level reservoir or the next-level reservoir, which essentially changes the water supply conditions of the downstream reservoir.

2. MULTI-OBJECTIVE PROGRAMMING MODEL

2.1 Establishment of multi - objective programming model for cascade reservoir joint dispatching

Based on the consideration of safety and reservoir efficiency, this paper selects two objective functions of flood control and power generation. The general principle of the cascade reservoir joint flood control operation is that the reservoirs at the most upstream level should play the role of cutting the peak and the peak, and reduce the flood pressure of the downstream reservoir as much as possible under the premise of ensuring the safety of the reservoir itself. When the cascade reservoirs bear several scheduling functions, power generation, shipping other scheduling to comply with the flood control scheduling, when the number of flood control objects in the cascade reservoirs is large, the protection degree of the protected objects is given according to the importance of the flood protection and the flood control system of the whole river basin. Figure 1 for the cascade reservoir system joint flood control operation diagram.

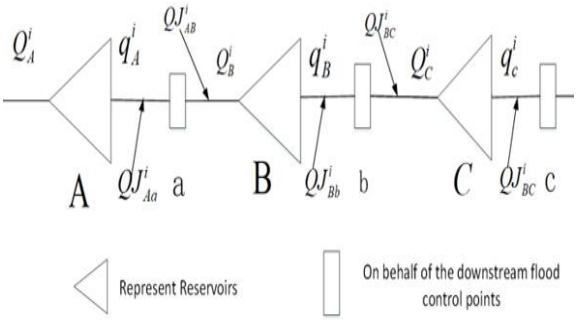

Figure 1 Sketch of the joint flood control operation of cascade reservoirs

Cascade reservoir flood control points encounter flood risk R minimum, then

$$\min R = \min\left[\max\left(R_1, R_2 \cdots R_j \cdots R_N\right)\right] = f_1(x)$$

(1)Water balance constraint:

$$V_j^{i+1} = V_j^i + (Q_j^i - q_j^i)dt$$

(2)Storage capacity constraints

$$V_{max_j} \geq V_j^{i+1} \geq V_{min_j}$$

(3)Water relations between upstream and downstream reservoirs:

$$Q_{j+1}^i = q_j^i + QJ_{j,j+1}^i$$

(4)Discharge capacity constraints

$$q_j^i \le Q_{max_j^i}$$

$j = (A, B, C \cdots)$ in each of the above constraints represents the reservoir number, dt is the amount of water corresponding to the unit flow, V_j^i for the i time of the j reservoir capacity, V_{max_j} and V_{min_j} are the maximum and minimum storage capacity of reservoir flood control.

2.2 For the reservoirs in cascade cascade hydropower stations located on the same river and downstream, as shown in Fig. 2, there is strong runoff connection and hydraulic connection between reservoir groups. Runoff connection is shown in the upper reaches of the hydropower station discharge is the next level of hydropower station reservoir inflow part. The hydraulic connection is mainly manifested in the utilization of the cascade head and the influence of the water level of the lower reservoir of the cascade hydropower station on the working head of the higher hydropower station.

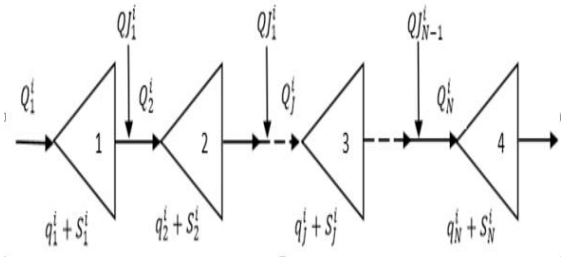

Figure 2 Sketch of cascade reservoirs

The total generating capacity of the cascade during the dispatching period:

$$F = \sum_{j=1}^{N} E_j = \sum_{j=1}^{N} \sum_{i=1}^{T} K_j q_j^i H_{jC}^i \Delta T$$

In this mathematical formula, j indicates the reservoir number, i indicates the time period number, N represents the number of reservoirs, T represents the total number of hours, S represents the reservoir water discharge.

Restrictions:

(1)Water balance and runoff

$$\begin{cases} V_j^{i+1} - V_j^i = (Q_j^i - q_j^i - S_j^i)\Delta T \times 3600 \\ Q_{j+1}^i = q_j^i + S_j^i + Q_j^i \end{cases}$$

(2) Reservoir water storage

$$V_{min_j^i} \le V_j^i \le V_{max_j^i}$$

(3) Hydropower station output

$$N_{min_j^i} \le N_j^i \le N_{max_j^i}$$

(4) Reservoir discharge

$$q_{min_j^i} \le q_j^i + S_j^i \le q_{max_j^i}$$

Among them, the constraints (3) and (4) in the minimum output and minimum flow constraints contradictory, to prevail to meet the output constraints prevail, which reflects the power generation is slightly more important than the shipping.

3.GENETIC ALGORRITHM FOR MULTI - OBJECTJIVE PROGRAMMING MODEL OF JOINT SCHEDULING

In this paper, the use of genetic algorithm for the new reservoir optimization scheduling calculation, and the new power stations were encoded, then simultaneously solve the overall optimal.

3.1 Genetic algorithm solving process

According to the principle of genetic algorithm, set the number of its population, gene bundle discharge Q (chromosome) using 12-bit binary coding, and introduces the constraint. The fitness of the population with the constraint condition was selected, and the cross parent was selected by the method of uniform distribution randomly. The parent was generated by linear cross, getting the formula as follows after the cross operation.

$$\begin{cases} v_{1l}' = v_{1l}\eta + v_{2l}(1-\eta) \\ v_{2l}' = v_{2l}\eta + v_{1l}(1-\eta) \end{cases}$$

The use of non uniform mutation means that the variation of chromosome variation in each generation is different. The variance $d(v_l)$ is a function of the parameters such as the chromosome v_l, the left and right borders b_l and b_r, the current evolutionary g_c, the maximum evolutionary algebra g_m, and the shape coefficient b.

The formula of the individual after mutation：

$$y = \begin{cases} v_l + d(v_l) & sign = 0 \\ v_l - d(v_l) & sign = 1 \end{cases}$$

The evolutionary termination is determined by the judgment of the degree of convergence of the final control and power generation function. The water result of the pessry evolution, and the evolution result error is set at 10%. At the same time, it is impossible to converge for a long time. Therefore, the calculation process can be considered to specify the maximum number of evolution, so that if the limit can not be reached after the convergence, then take the evolution of the final results have been completed as the final result output.

The overall flow of the genetic algorithm is shown in the following figure

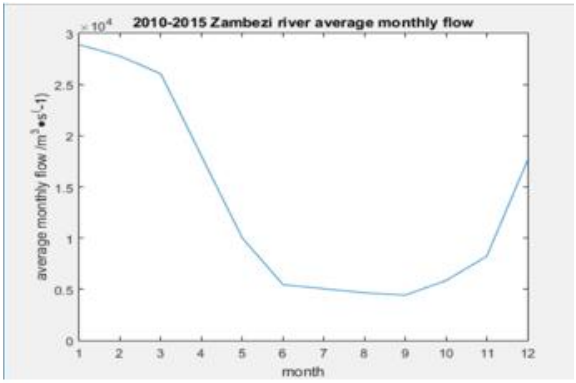

Figure 3 Water flow value curve

The figure shows that 1 - 3 months the largest water flow, belonging to the flood season, dam flood flow in the Zambezi River declined rapidly from March to June. During this period, the dam returned to the impoundment stage, providing sufficient spare water for the upcoming drought period for people to drink and farmland irrigation. 6-9 months water flow is also declining. 9 - 11 months, the water flow to a relatively small rate of recovery. The area of drought is slightly better. 9 - 1 months, the water flow in the Zambezi River is relatively rapid. Drought significantly weakened, River water gradually return to normal, dam also gradually return to the water storage function.

4. CONCLUSIONS

From the perspective of economic efficiency and security, to deal with the Zambi Xi River reservoir class scheduling problem. According to the above analysis, the dam flood control capacity of 120 billion cubic meters, the annual generating capacity of 6.4kw · h to meet the requirements. According to the Zambezi River in the past 6 years, the ARIMA model was established, and the maximum water flow was obtained from January to March, the maximum water flow was 2.4 cubic meters per second, the lowest water flow in July and October, and the lowest water flow of 0.45 m Meters per second. Combined with the ARIMA forecasting model, it is possible to accurately predict the water flow in the rainy season and dry season in the region and to reduce the unnecessary losses in advance for the drought and flood disaster to be faced.

REFERENCES

[1]Shaw, K., Shankar, R., Yadav, S. S., & Thakur, L.S. (2012). Supplier selection using fuzzy AHP and fuzzy multi-objective linear programming for developing low carbon supply chain. Expert Systems with Applications, 39(9), 8182–8192.

[2]Parviz Rezaei, Kamran Rezaie. Application of Fuzzy Multi-Criteria Decision Making Analysis for Evaluating and Selecting the Best Location for Construction of Underground Dam, Tehran, Iran, University of Tehran2013.

[3]Jiwei Li, Research on Multi-objective Optimal Operation and Decision Methods for Cascaded Reserviors, Beijing: North China Electric Power University.2014

[4]Liu Fang, Study on Optimization Method and Application of Reservoir Water and Sediment Dispatching, Beijing: North China Electric Power University.2013

[5]Yuzhen Liu, Yang Kai, Study on the Overall Improvement Strategy of Genetic Algorithm for Optimal Operation of Reservoir, Jiangsu: Hohai University

Optimization Model of "Toll Square" Based on Particle Swarm Optimization and Genetic Algorithm

Tianlong Li[1] ,Hengheng Qu[2] ,Yajuan Qiao[3] ,Xiaojun Men[4] ,Yan Yan[4]*
[1]Yisheng College,North China University of Science and Technology,Tangshan,063210,China
[2] College of Electrical Engineering, North China University of Science and Technology,Tangshan,063210,China
[3]College of Information Engineering, North China University of Science and Technology,Tangshan,063210, China
[4]College of Science,North China University of Science and Technology,Tangshan Hebei,063210,China

Abstract: By comparing the different traffic flow under the block rate and utilization rate,we can conclude that with the increase of the vehicle, the blocking rate increases and the utilization rate decreases. When more unmanned vehicles join the traffic flow, the full coverage simulation strategy is used to calculate the proportion of the three kinds of charging methods under the different proportion of automatic driving vehicles by simulated annealing genetic algorithm (SAGA). In New Jersey, for example, the ETC vehicles on the road accounted for 80% of the total. At this point, the three charges are allocated as follows: one for the artificial toll lanes, two automated lanes, four ETC toll lanes, one non-toll lanes.

Keywords: Toll plaza Frank-Wolfe algorithm Open Shortest Path First(OSPF) Simulated Annealing Genetic Algorithm (SAGA)

1. THE BI-LEVEL PROGRAMMING PROBLEM OF THE OPTIMUM LANE UNDER DIFFFERENT WAYS OF CHARGING

Assumptions: toll plaza's vehicles are divided into automatic and non-automatic driving, autonomous vehicles are cars. Assuming at this time that autonomous vehicles' autonomous driving level is 5, that is, the car can be fully automatic driven. Through the previous research, we can see that the choice of toll station meet the OSPF routing rules. Therefore, autonomous vehicles should strictly comply with OSPF rules. More autonomous (self-driving) vehicles are added to the traffic mix, the proportion of autopilot vehicles is increasing[1].

Each location, whether the toll station is set, is a 0-1 mathematical programming problem (0 said the location does not set up toll stations, 1 that set). As shown in Fig. 1, supposing there are nine interchanges in a certain freeway. Therefore, there are eight toll stations, each of which represents a gene, whose value can be expressed as 0 or 1. Therefore, the feasible solution of the setting location of this highway's toll stations, that is, 8 0 or 1 string, that is, a location chromosome individual1 (10110010).

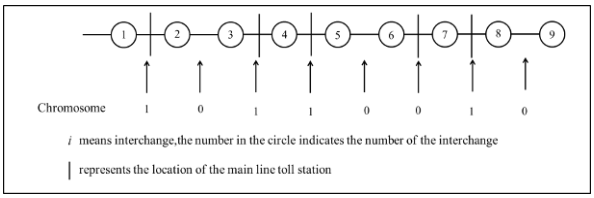

Figure 1 Toll booth location and the corresponding chromosome morphology example

In order to simplify the complexity of the model, this paper assumes that the payment technology at different toll stations is only relevant to the situation on this site. C is the number of lanes, and K is the number of charging methods. Assuming that the feasible charging method has J kinds, $2^{K-1} \le J \le 2^{K}$, the codes with 0 and 1 code length can be used to represent different charging methods, namely a chromosome. For example, a toll station, the feasible toll lane has three types, encoding 01 expresses manual toll lanes, 10 expresses exact-change (automated) lanes, n expresses ETC toll lanes, 00 expresses not toll lanes, if all toll stations use manual toll lanes, needing 8 lanes, then using this toll station to charge different ways to optimize the number of lanes chromosome length is 16.

Fig.2 shows the number of different combinations of lane numbers and the corresponding chromosome (1011011111100100) form2 for individual tolls. The total number of lanes available to decode individual2 is 7, there are 3 ETC lanes, 2 manual toll lanes and 2 mixed toll lanes[2].

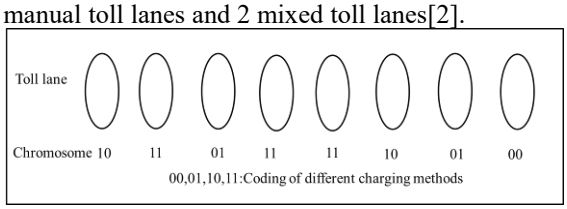

Figure 2 toll stations with different ways of charging the number of
lane combinations and corresponding forms of chromosomes

The relationship between the chromosome individual1 of the toll station and the chromosome individual2 corresponding to the number of lanes of

different charging ways corresponding to each station is shown in Fig.3. For example, a highway with 9 interchanges of a toll station location chromosome individual1 is 01001001. Individual2 corresponds to the locus chromosome individual1 generated by the station into the direction of different charging ways lane combination chromosome.

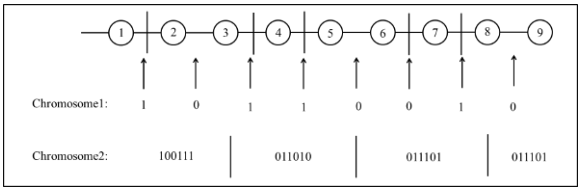

Figure 3 corresponds to the location of 0101001 randomly generated number of toll lane number of chromosomes

2. SOLVING ALGORITHM-SIMULATED ANNEALING GENETIC ALGORITHM(SAGA)

Genetic algorithm is a kind of random search algorithm which is based on natural selection and natural genetic mechanism of biology[3]. The main steps are as follows:

Step.1 Initialization: Set the evolutionary algebraic counter $t = 0$ Sets the maximum evolution algebra T . M individuals were randomly generated as initial population $P(0)$

Step.2 Individual evaluation: The fitness of each individual in population $P(t)$ is calculated.

Step.3 Select operation: The selection operator acts on the population. The purpose of the selection is to optimize the individual directly to the next generation or through the generation of new pairs of cross-genetic re-transmission to the next generation. The selection operation is based on the fitness assessment of the individuals in the population.

Step.4 Crossover: The crossover operator is applied to the population.

Step.5 Variation: The mutation operator is applied to the population. That is, a change in the gene value at certain loci of individual strings in the population. The population $P(t)$ is selected, crossed, and mutated to obtain the next generation $P(t+1)$

Step.6 Termination Judgment:If $t = T$ Then the individual with the greatest fitness in the process of evolution is taken as the optimal solution output and the calculation is terminated.

As the genetic algorithm in the operation of the early individuals are very different, when using the classic roulette mode selection, progeny generation number is proportional to the size of the parent individual fitness. So it is easy to make the offspring of the individual good individual full of the entire population, resulting in premature (Premature) at early stages. In the later stage of genetic algorithm, the fitness is consistent, and the superiority is not obvious when the outstanding individuals produce the offspring, so that the evolution of the whole population stagnates[4]. It is necessary to properly stretch the fitness. In this paper, a simulated annealing genetic algorithm (SAGA) is proposed to solve the optimization model of system resource allocation of tolling system. The algorithm uses the following fitness:

$$F_l = \frac{\exp[f(x)/\mathrm{T}]}{\sum_{l=1}^{M} \exp[f(x)/\mathrm{T}]} \tag{1}$$

Among them, $T = \alpha T_0$

F_l is the fitness of the l -th individual, $f(x)$ as the objective function, M is population size, g is number of iterations, T is the temperature, T_0 is the initial temperature. α is temperature reduction parameter. So that when the temperature is high, the progeny fitness of the genetic algorithm is similar. And when the temperature is declining, the fitness function of the tensile effect of strengthening, so that fitness similar to the individual differences in fitness to enlarge. So that the advantages of outstanding individual is more obvious, significantly improved the performance of GA.

3. MODEL SOLVING AND RESULT

Assuming that autopilot vehicles account for 80% of the total number of vehicles traveling,and a total of 5,000 vehicles. First, determine the parameters of the genetic algorithm, see Table 1. Simultaneously use K to calculate the number of simulated annealing.

Table 1 Parameters of Genetic Algorithm

Parameter	Value	Parameter	Value	Parameter	Value
Number of iterations	1000	Population size	20	Crossover probability	0.7
Mutation probability	0.1	Initial temperature	100	Temperature reduction parameter	0.98

Secondly, the optimal combination of the number of charging and discharging methods for each locus chromosome was obtained by genetic algorithm[5]. The number of manual toll lanes is 1, the number of exact-change (automated) lanes is 2, the number of ETC toll lanes is 4, and the toll lane is 1.

Finally, the degree of fitness of the individual evolutionary process is determined, that is, the fitness of the optimal combination of the number of different charging methods. See Appendix 2 for the procedure.

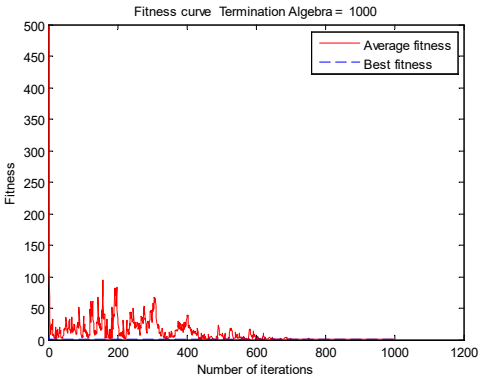

Figure 4 The fitness of individual evolutionary process

When more autonomous (self-driving) vehicles are added to the traffic mix, artificial charge lane number is 1, the number of lanes for exact-change (automated) lanes is 2, the number of ETC toll lanes is 4, and the lane for non-toll lanes is 1. While increasing the proportion of ETC, it will increase the cost of construction, but compared to the efficiency and reduce the income of artificial leakage, it will be more beneficial.

REFERENCES

[1]Deb K, Pratap A, Agarwal S, et al. A fast and elitist multiobjective genetic algorithm:NSGA-II[J]. IEEE transactions on evolutionary computation, 2002, 6(2): 182-197.

[2]High-Throughput Screening in Chemical Catalysis: Technologies, Strategies and Applications[M]. John Wiley & Sons, 2006.

[3]Fortz B, Thorup M. Internet traffic engineering by optimizing OSPFweights[C]//INFOCOM 2000. Nineteenth annual joint conference of the IEEE computer and communications societies. Proceedings. IEEE. IEEE, 2000, 2:519-528.

[4]Ashton W D. The theory of road traffic flow[J]. 1900.

[5]Deb K, Pratap A, Agarwal S, et al. A fast and elitist multiobjective genetic algorithm: NSGA-II[J]. IEEE transactions on evolutionary computation, 2002, 6(2):182-197.

Monthly Runoff Forecasting Model Based on Support Vector Machine and Grey Prediction Agorithm

Fanbei Kong[1],Bo Zhao[1] ,Xiangyu Xu[1],Xiaojun Men[2],Bin Bai[2]*
[1]Yi Sheng College,North China University of Science and Technology,Tangshan Hebei,063210,China
[2]College of Science,North China University of Science and Technology,Tangshan Hebei,063210,China

Abstract: In the context of the urgent need to repair Kariba dam,the Zambezi River Basin has Africa's most valuable and diverse natural resources. The establishment of a multi-dam system management mechanism for the basin is of great significance for sustaining regional economic sustainable development and accelerating the pace of poverty alleviation.Based on the prediction model of runoff of Zambezi River Basin, a prediction model of monthly runoff based on support vector machine and gray forecasting algorithm was established. The results show that the error is within 11%,providing the basal data for establishing the multi- dam system.
Keywords: Kariba dam; SVM; gray prediction; water forecast

1. INTRODUTION

Under the condition that flood discharge is considered when all dams are flooded, the flood peak in flood season is forecasted in the next year. After the forecasting result is obtained, genetic-simulated annealing algorithm is used to optimize the distribution based on minimum cost. [1-2] Because of the low amount of data, the error of single prediction is too large. Therefore, this paper uses the gray prediction as the input and SVM as the input, and establishes the monthly forecasting of the support vector machine-gray prediction algorithm. model. [3-4]In this way, during the process of "diluting" the error, the sharing of the advantages of the two prediction methods and the enrichment of the prediction inner relation are realized.

2. EXPERIMENTAL

2.1 FLOW ANALYSIS

The specific process shown in Fig.1 Prediction model：

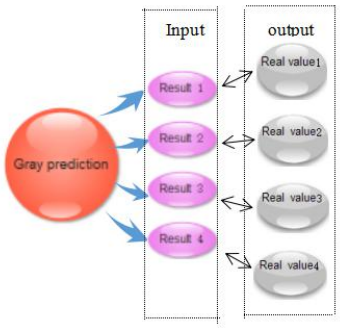

Figure 1 Prediction model

In the process of flood control, the dam needs to deal with the amount of water beyond its own carrying capacity, so as to complete the function of dam flood control and flood discharge. Here, the paper would call the amount of water beyond the carrying capacity as the "surplus water", and the dam flood control function is reflected in the treatment of the “surplus water”.

2.2 GRAY PREDICTION

Gray prediction is a prediction method different from that of regression analysis. The advantage of gray prediction is that it can achieve the effect of forecasting with less data.[5]

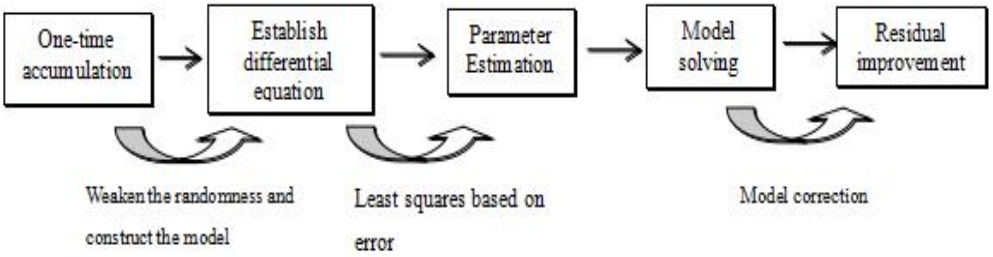

Figure 2 Prediction icon

Taking Mibizi dam as an example, the paper has the gray-radial kernel function SVM prediction-genetic algorithm.

The predicted results for 2016 and 2017 are shown in the following Tab. 1.

Table 1 Prediction results of 2016、2017

2016.1	2016.2	2016.3	2016.4	2016.5	2016.6

3.75E+02	3.57E+02	3.60E+02	5.90E+02	1.11E+03	2.01E+03
2016.7	2016.8	2016.9	2016.10	2016.11	2016.12
3.37E+03	3.39E+03	3.30E+03	1.47E+03	0.665E+02	0.444E+03
2017.1	2017.2	2017.3	2017.4	2017.5	2017.6
3.55E+02	3.55E+02	3.40E+02	5.95E+02	1.41E+03	2.03E+03
2017.7	2017.8	2017.9	2017.10	2017.11	2017.12
3.28E+03	3.46E+03	3.50E+03	1.50E+03	0.670E+02	0.48E+03

The paper made the error image of each month, which are as shown in the following Fig.5. It can be seen that the accuracy is relatively good.

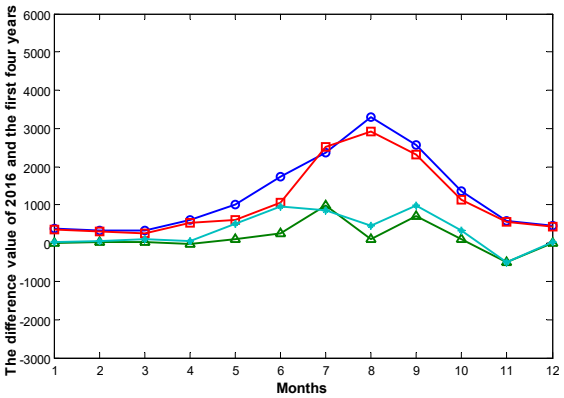

Figure 3 Monthly error image

2.3 SUPP0RT VECTOR MACHINE

In the case of linear regression, finding the corresponding transformation of optimal w is the convex optimization problem:

$$\min \ \frac{1}{2}\|w\|^2 \tag{1}$$

The conditions are:

$$\begin{cases} y_i - w \bullet x_i - b \le \varepsilon \\ w \bullet x_i + b - y_i \le \varepsilon \end{cases} \tag{2}$$

In the above formula, ε is the precision threshold.

By introducing the Lagrangian function and the dual variable to solve the programming problem, the function is:

$$L = \frac{1}{2}\|w\|^2 + c\sum_{i=1}^{t}\left(\xi_i + \xi_i^*\right) - \sum_{i=1}^{t}\alpha_i\left(\xi_i + \varepsilon - y_i + w \bullet x_i + b\right) \tag{3}$$

The final regression function is:

$$f(x) = \sum_{i=1}^{t}\left(\alpha_i - \alpha_i^*\right)\left(x_i \bullet x\right) + b \tag{4}$$

Under nonlinear conditions, the optimization problem becomes optimizing the following formula under KKT constraints :

$$w\left(\alpha, \alpha^*\right) = -\frac{1}{2}\sum_{i,j=1}^{l}\left(\alpha_i - \alpha_i^*\right)\left(\alpha_j - \alpha_j^*\right)k\left(x_i, x_j\right) \tag{5}$$

Estimate the relevant parameters and the regression function will be established.

The following annual trend is based on the actual runoff for 2012-2016 and the predicted runoff from 2017 as shown in the following Fig.4 Predicting runoff.

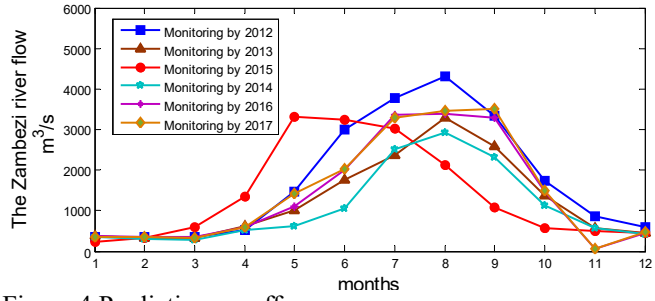

Figure 4 Predicting runoff

It can be found that, except for a few months of drought and flood season, most of the water is partial to normal, and the trend of annual water flow to a certain extent, based on the same trend, so the total water through the water logging period The amount of water and the difference between the normal amount of water can measure the amount of surplus.

From May to June and from September to October, the water flow is in the middle, which belongs to the stage of flow balance. It can be seen from June to September that the water flow is high. The three segments are integrated by this function, which can be used as the total flow for three seconds and the total flow for one second respectively:

$$\begin{cases} \int_6^9 f(x) = 1.029 \times 10^4 \\ \int_5^6 f(x) = 2.07 \times 10^3 \\ \int_9^{10} f(x) = 1.387 \times 10^3 \end{cases} \tag{6}$$

Each section will be converted into the total number of seconds as a unit of time, you can calculate the total peak flow and balance the difference between the flow, that is, the remaining water:

$$11.02 \times 10^{10} - 5.59 \times 10^{10} - 3.61 \times 10^{10} = 1.82 \times 10^{10} \tag{7}$$

3. RESULTS AND DISCUSSION

The Zambezi River upstream water level gap, so the power generation, irrigation and other areas have significant advantages, so the higher income, but at the same time, Low-cost, low-income, and therefore the middle is not only a high-cost high-yield; downstream is low, but the cost is also low, A certain degree of water level advantage, the terrain is relatively moderate, relatively favorable conditions, it

is entirely reasonable to think that it has a negative cost, which combines the geographical position, to build the objective function.

4. CONCLUSIONS

In the context of the Kariba dam to repair, to establish prediction model of support vector machine algorithm of grey prediction of runoff based on the prediction of the basin water, provides the foundation for the establishment of water content data management system of multiple dams.

REFERENCES

[1]Su Huaizhi, Wen Zhiping, Wu Zhongru. Study on dam safety early warning model based on [J]. Theory Journal of Applied Science and Engineering Science, 2009, 17 (SVM): 40-48.

[2]Du Chuanyang, Zheng Dongjian. An improved method for dam deformation monitoring based on [J]. Theory Journal of China Three Gorges University (NATURAL SCIENCE EDITION), 2015, 37 (SVM): 10-14.

[3]Tang Qi, Bao Fei, Li Yuejiao, et al. Dam deformation prediction model based on SAPSO-RVM and its application [J]. hydroelectric energy science, 2015 (4)

[4]Sun Xiaoran, Su Huaizhi,, et al. Application of RS-SVM model in dam safety monitoring [J]. people the Yellow River, 2016, 38 (130-133.): (in Chinese)

[5]Zhou C, Yin K, Cao Y, et al. Application of time series analysis and PSO–SVM model in predicting the Bazimen landslide in the Three Gorges Reservoir, China[J]. Engineering Geology, 2016, 204:108-120.

Influence law Model between Deformed Steel Bar Properties and Chemical Elements

Siwen Li[1] ,Shiyu He[1], Yan Sun[1] ,Shujuan Yuan[2],Bin Bai[2]*
[1]North China University of Science and Technology, Tangshan City, Hebei Province 063210,China
[2]College of Science,North China University of Science and Technology,Tangshan Hebei,063210,China

Abstract：The path coefficients of single element and three performance indexes are determined by structural equation model. According to the principle that the bigger of path coefficient, the greater of influence of the element to the screw thread steel, the influence regular pattern of each element on the properties of the thread steel was obtained, where element C has the following regular pattern: with the increasing of C content, the yield strength and tensile strength is increased while the elongation at break decreased. And then the multiple regression equation is constructed to study the effect of element combination on the properties of thread steel by letting the close degree as dependent variable, each elements as independent variables. Finally, the model is tested by residual analysis. The residual value of 0.7636<1 is obtained, which verifies the correctness of the multiple regression equation.
Keywords: hot-rolled ribbed bar; structural equation model; multiple regression model

1. INTRODUCTION

Hot-rolled ribbed bar is commonly known as deformed steel bar, it's mainly used for skeleton of reinforced concrete component and it requires certain mechanical strength, bending and deformation properties, fabrication weldability in use. The chemical composition [1]in steel is the basic element that influences the final structure property of hot rolled steel. Most deformed steel bar adopts microalloying method, that is to add expensive microelement (such as Mn alloy material, V alloy material, etc.) into steel, adjust the composition proportion and to improve structure property.

At present, most thread steel adopts micro-alloying method that is, adding expensive microelement into steel to adjust the composition proportion and improve structure property. This article has modeled the influence rule between deformed steel bar properties that are the yield strength, tensile strength and elongation at break after breaking and chemical elements like C, Mn, Cr, V, N.by setting up a reasonable mathematical model. In the first study, different chemical elements have been found to have different effects on the properties of deformed steel bar, So we select the elements which have great influence on the analysis of the problem. Firstly, the structural equation model is used to analyze the potential variation rules of many factors. Then through the multiple regression analysis, the relation between the chemical element and the properties of deformed steel bar is obtained.

2. STRUCTURAL EQUATION MODEL

The structural equation model[2] can be used to consider and deal with multiple independent variables. In regression analysis or path analysis, In the calculation of the regression coefficient or the path coefficient of each dependent variable is calculated one by one. It is possible to ignore the existence and influence of other independent variables. So the structural equation analysis can be used to study the potential influence of many kinds of chemical elements.

In the study of the influence of the elements on the performance of deformed steel bar, we find that there are three properties of deformed steel bar such as yield strength, tensile strength and elongation at break after breaking. In order to study the impact of a single element on the three indicators better, we need to build the potential impact of variables, to explore whether there is a synergistic or inhibition effect between the elements or inhibition.

2.1structural equation model

2.1.1selection of independent variables and dependent variables

According to the research results of the first problem, we select the main chemical elements affecting deformed steel bar as independent variables[3]. The yield strength, tensile strength and elongation at break of the screw are used as the dependent variable. And then construct the structural equation model. And then through the amos21.0 software to draw the structure model diagram, the effect of the element on the properties of the steel is given as Fig.1. And then estimate Path coefficients of the model is given the result as Fig.2.

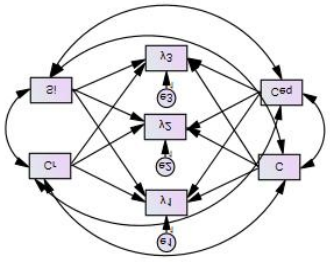

Figure 1 Influence model diagram

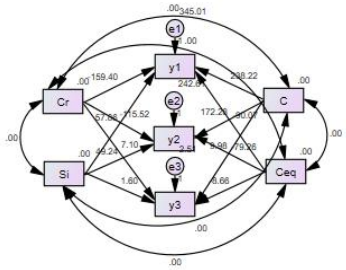

Figure 2 Path coefficient diagram

2.1.2 result analysis

We have known that the path coefficients of C and these three performance indexes are 298.22, 172.28 and 9.98 respectively. It is showed that the yield strength and tensile strength of deformed steel bar will be improved obviously when the C content increases[4], but the elongation rate will not change obviously. In the same way we can know that the increase of Cr content will increase the yield strength and tensile strength, the elongation at break decreases, so that the hardness of the steel bar becomes higher, and the lower the stiffness. According to this method, the influence rules of other elements on the properties of deformed steel bar are summarized.

2.2 establishment of multiple regression model

Multiple regression is a linear regression model with multiple independent variables, which can be used to reveal the linear relationship between the dependent variable and the other multiple independent variables. The mathematical expression of multiple linear regression is as follows:

$$y = b_0 + b_1 x_1 + b_2 x_2 + \ldots + b_n x_n \quad (1)$$

In order to further study the effect of the properties of deformed steel bar and C, Mn, Cr, V, N and other chemical elements, we choose comprehensive index which are measured the performance of deformed steel bar as the dependent variable, various chemical elements as the independent variable, and then establish the multiple regression equation between the properties of deformed steel bar and chemical elements[5].

Because chemical elements and the comprehensive influence index have different dimensions, before the multiple regression analysis, the data should be standardized. Let The data into the equation after standardization in, using SPSS software to carry on multiple linear regression, the regression equation is:

$$y = 0.142x_1 - 0.04x_2 - 0.064x_3 + 0.063x_4 + 0.122x_5 - 0.08x_6 - 0.055x_7 - 0.058x_8 + 0.065x_9 - 0.027x_{10} + 0.028x_{11} + 0.084x_{12} \quad (2)$$

3. REGRESSION EQUATION TEST

In order to prove that the obtained regression equation is correct or not, we put the 2 specification of deformed steel bar data as test data into the equation, and then compare the calculated results with actual data. The comparison chart is Fig.3:

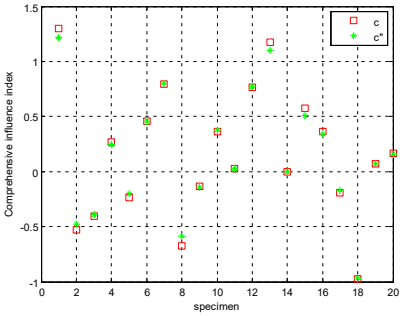

Figure 3 Comparison of the calculated results with the actual data

It can be seen from the figure that the error between the data and the actual data is not very large, and the degree of agreement is high. In order to further explain[6], we carry out the residual test of the data, and its expression is as follows:

$$r^2 = \frac{\sum (y_r - y)^2}{\sum (y - \overline{y})^2} \quad (3)$$

By using the above equation, the results obtained for 0.7636<1, the results calculated by the equation and the error of the actual data are small. It is proved that the multiple regression equation is correct and reliable. In order to further verify the multivariate linear regression equation[7], we have carried on the error analysis to it and draw the scatter diagram as follows:

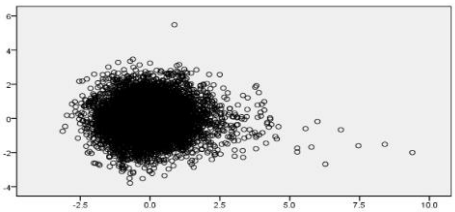

Figure 4 scatter diagram

It can be seen from the Fig. 4 that most of the scattered points are randomly distributed in the cluster with e=0 as the center. It is proved that the model is suitable and the multivariate linear equation is correct.

5. CONCLUSIONS

The conclusion can be got: with the increasing of C content, the yield strength and tensile strength is increased while the elongation at break decreased

ACKNOWLEDGMENT

We want to express our heartfelt thanks to Mr. Yang Aimin. Thanks for helping us.

REFERENCES

[1]ZHANG X L,LI X F,LI J. Correlation analysis and performance evaluation of fusion image quality evaluation index [J]. Acta Automatic Sinica,2014,02:306-315.

[2]Ridho Rahmadi,Perry Groot,Marianne Heins,Hans Knoop,Tom Heskes. Causality on cross-sectional data: Stable specification search in constrained structural equation modeling[J].

Applied Soft Computing,2016,:.
[3]Kok Chooi Tan,Hwee San Lim,Mohd Zubir Mat Jafri. Prediction of column ozone concentrations using multiple regression analysis and principal component analysis techniques: A case study in peninsular Malaysia[J]. Atmospheric Pollution Research,2016,:.
[4]Hubert Anysz,Artur Zbiciak,Nabi Ibadov. The Influence of Input Data Standardization Method on Prediction Accuracy of Artificial Neural Networks[J]. Procedia Engineering,2016,153:.
[5]Wenjing Zhao, Xiaojie Bai , JixiangZhang , Lailiang ou. Test for optimization of ultrasound assisted extraction of melanin from black [J]. food science orthogonal 2010,04:39-41.
[6]Shihao Liu , Wenhua Ye, Yufang Chen , Dunbing Tang, lili Xiao. Optimization design of [J]. vibration and shock machine tool spindle box and orthogonal experiment method based on gray correlation, 2011,07:127-132.
[7]Xiuli Lv. Study on heat treatment process of WL Cast Iron Crankshaft Based on orthogonal test method [D]. Shandong University, 2014

The Surface Modeling Based on Energy Optimization Method

Xiaojun Men, Aimin Yang, Jincai Chang*
College of Science, North China University of Science and Technology, 063210, China

Abstract: Spline has be understood as a certain smoothness segment (slice) polynomial, and it is the fundamental tool for curve and surface modeling.Based on the mechanical properties of the spline, the bending energy of the curved surface is determined according to the elastic deformation equation of the thin plate in the elastic mechanics. Then, the optimization theory is used to make the surface possessed by various geometric condition constraints or external load of the bending energy to obtain the optimal value (usually take the minimum), so as to achieve the shape of the shape of the control effect. This paper introduces the basic principle and implementation method of energy optimization method, and uses this method to give four curved surface constraints and parametric surface constraints.

Keywords: spline function; bending energy; energy optimization; surface modeling

1. INTRODUCTION

With the gradual expansion of computer aided design technology applications, the requirements of curved surface modeling technology also increased. The traditional modeling method[1,2] based on pure geometry model has been difficult to meet the needs of the actual object shape modification, resulting in a physical model[3-5] based curve surface modeling technology.

Since the eighties, surface modeling technology which is relatively mature now has been developed continuously, while B-spline function also gradually occupy the dominant position, and become the basis of research. However, people on the CAD/CAM technology applications continue to expand innovation, modeling technology requirements with the corresponding increasing. It is difficult to achieve the expected effect of the traditional surface modeling technology, which is difficult to achieve the expected effect, especially in the automotive design, such as car cover, home appliances and other artistic design of the creative performance is particularly evident, so seek more flexible and practical modeling method become the key problem, then the energy method [6-9]surface modeling resulting.

In 1987, the Canadian scholar Terzopoulos made a macroscopic description of the Lagrangian dynamics equation, and used the equation to construct the physical energy model, how to establish various external loads on the object and deal with various constraints, and introduce the numerical method to solve the problem of partial differential equation and get the energy surface, which lays the foundation for energy optimization modeling. Since then, many scholars have further developed the idea of energy optimization, and the domestic research on the surface modeling of energy optimization method is beginning to take shape. This paper introduces the basic principle and realization method of energy optimization method.

2. PRINCIPLE

The energy optimization method is a method to study the physical deformation energy by combining the optimization theory[9], that is, using the optimization to solve problem (mathematical programming model), the bending energy of the surface under the condition of various geometric condition constraints or external load to obtain the optimal value (usually take the minimum), thus achieve the shape of the shape of the control effect. In other words, this modeling method is to meet the geometric or non-geometric constraints in the case, to find the surface with the smallest bending energy.

It can be seen that the primary goal of the energy optimization method is to determine the objective function, that is, to determine the bending energy of the curved surface. Energy model can be from two aspects, one is from the physical deformation of the starting, drawing on the elasticity of the thin plate elastic deformation equation, you can get the following model:

$$\Pi = \iint (\alpha_{11} w_x^2 + 2\alpha_{12} w_x w_y + \alpha_{22} w_y^2 + \beta_{11} w_{xx}^2 + 2\beta_{12} w_{xy}^2 + \beta_{22} w_{yy}^2 - 2 f \cdot w) dxdy \quad (1)$$

In the formula:w is the desired surface which has parameters x and y, f is the given external load.

The other is starting from the geometric nature, such as area, length, curvature and curvature of the rate of change and other aspects of the constraints, then get the energy model.

1) Moreton and Sequin express the energy function by the rate of change of curvature:

$$U = \int [(\frac{\partial k_1}{\partial x})^2 + (\frac{\partial k_2}{\partial y})^2] dA$$

2) Kallay uses the square of curvature to represent the energy functional:

$$U = \int (k_1^2 + k_2^2) dA$$

However, the effect of these two different energy models on the shape of the surface is obvious and

difficult to deal with, and the model (1) is easier to handle and includes the physical deformation energy of the two parts of the bending and tensile resistance, which make the surface has a good smoothness, this physical energy model is the most widely used.

Euler equation using energy function:

$$(\beta_{11}\frac{\partial^4 w}{\partial x^4}+\beta_{12}\frac{\partial^4 w}{\partial x^2\partial y^2}+\beta_{22}\frac{\partial^4 w}{\partial y^4})-$$
$$(\alpha_{11}\frac{\partial^2 w}{\partial x^2}+2\alpha_{12}\frac{\partial^2 w}{\partial x\partial y}+\alpha_{22}\frac{\partial^2 w}{\partial y^2})=f$$

Combined with the theory of elastic mechanics, you can know: α,β are the given material characteristic parameters, f is the external load of the deformable object. For ease of calculation, we can ignore their effects, that is α,β are1, f is 0.

3. PROCESSING

Known given B-spline surfaces:

$$w(x,y)=\sum_{i=0}^{p}\sum_{j=0}^{q}P_{i,j}N_{i,p}(x)N_{j,q}(y)$$

In the absence of external energy when the energy model of the treatment, using the energy optimization method to new surface modeling, the objective function of finishing, there are:

$$\Pi=\sum_{i,j}^{p,q}\left[P_{i,j}\sum_{k,l}^{p,q}\left(P_{k,l}\times S_{i,j,k,l}\right)\right]$$

$$S_{i,j,k,l}=\int_0^1\int_0^1\begin{bmatrix}\alpha_{11}N_{i,p}'(x)N_{j,q}(y)N_{k,p}'(x)N_{l,q}(y)+\\2\alpha_{12}N_{i,p}'(x)N_{j,q}(y)N_{k,p}(x)N_{l,q}'(y)+\\\alpha_{22}N_{i,p}(x)N_{j,q}'(y)N_{k,p}(x)N_{l,q}'(y)+\\\beta_{11}N_{i,p}''(x)N_{j,q}(y)N_{k,p}''(x)N_{l,q}(y)+\\2\beta_{12}N_{i,p}'(x)N_{j,q}'(y)N_{k,p}'(x)N_{l,q}'(y)+\\\beta_{22}N_{i,p}(x)N_{j,q}''(y)N_{k,p}(x)N_{l,q}''(y)\end{bmatrix}dxdy$$

In the optimization theory, shaped like:

$$\begin{aligned}\min\quad & f(x)\\ s.t.\quad & h_i(x)=0,1\le i\le m\\ & g_j(x)\ge 0,1\le j\le n\end{aligned}$$

is the mathematical programming or optimization problem, which $f(x)$ is the objective function of the problem, $h_i(x),g_j(x)$ are constraint.

The multidimensional grid spline surface can be regarded as a thin plate from the mechanical point of view. The bending of the spline surface is essentially a small deflection of the elastic thin plate. It is obvious that the deformation problem of the thin plate spline is an optimization problem under certain constraints, that is, the objective function is minimized under the constraint condition of the corresponding energy of the thin plate. Thus, the energy model can be transformed into a mathematical quadratic programming problem:

$$\begin{aligned}\min\quad & \Pi\\ s.t.\quad & h_i(x)=0,1\le i\le m\end{aligned}$$

In the current energy optimization method, the constraint condition is mainly applied to the constraint condition, so the model can be transformed into unconstrained quadratic programming problem:

$$\min\quad \Pi$$

4. SURFACE MODELING

Energy-based curved surface modeling technology as a modeling method, there is no uniform concept, but its design is very clear: the curve or surface as a flexible deformation of the beam or shell, given the quality, damping, deformation, etc. Physical properties, the introduction of energy functional formula, through some mechanical principles to establish the deformation curve surface control equation, and then use a certain numerical method to solve a certain constraint to meet the numerical solution. In other words, the energy optimization method is to find geometric and non-geometric constraints and external load conditions to find the case with the smallest physical deformation of the curve of the surface.

(1)Feasibility analysis of energy optimization method

From the definition of the spline function, the spline surface is the extensional product of the monosampl spline function. Therefore, the energy optimization method can be applied to the cubic cubic spline function, and then applied to the tensor product Cubic spline surface.

Given node $u_1,u_2,u_3\in[0,1]$,any set of constants y_1,y_2,y_3 .In the mechanical sense, the cubic spline function can be regarded as a simplified cubic polynomial formed by the elastic thin beam after small deflection deformation. Suppose given two polynomial functions:

$$w_1(u)=a_1u^3+a_2u^2+a_3u+a_4$$
$$w_2(u)=b_1u^3+b_2u^2+b_3u+b_4$$

Thus, the definition of interpolation can be obtained:

$$\begin{cases}w_1(u_1)=a_1{u_1}^3+a_2{u_1}^2+a_3u_1+a_4=y_1\\ w_1(u_2)=a_1{u_2}^3+a_2{u_2}^2+a_3u_2+a_4=y_2\\ w_2(u_2)=b_1{u_2}^3+b_2{u_2}^2+b_3u_2+b_4=y_2\\ w_2(u_3)=b_1{u_3}^3+b_2{u_3}^2+b_3u_3+b_4=y_3\end{cases}$$

In addition, as a spline function, from the definition point of view, to meet the boundary conditions:

$$\begin{cases}w_1(0)=0\\ w_2(1)=0\end{cases}$$

Combined with the energy functional analysis of the unary spline curve, the bending energy of the curve is:

$$U=\int_0^1 w_{uu}^2du=\int_{u_1}^{u_2}w_{1uu}^2du+\int_{u_2}^{u_3}w_{2uu}^2du$$
$$=\int_{u_1}^{u_2}(6a_1u+2a_2)^2du+\int_{u_2}^{u_3}(6b_1u+2b_2)^2du$$

Applying the integral mean theorem,

$$\xi \in [u_1, u_2], \eta \in [u_2, u_3]$$

$$U = (6a_1\xi + 2a_2)^2(u_2 - u_1) + (6b_1\eta + 2b_2)^2(u_3 - u_2)$$

When the bending energy is minimized, the first derivative of the energy functional is 0,that is:

$$U' = (\int_{u_1}^{u_2} w_{1uu}^2 du + \int_{u_2}^{u_3} w_{2uu}^2 du)' = 0$$

Which can be transformed into indefinite integral problem:

$$U' = w_{1uu}^2 + w_{2uu}^2 = 0$$

Finishing available:

$$\begin{cases} w_{1uu}^2 = 0 \\ w_{2uu}^2 = 0 \end{cases} \Rightarrow \begin{cases} w_{1uu} = 0 \\ w_{2uu} = 0 \end{cases}$$

Based on the above eight conditions, the relationship between the unknown quantity can be obtained, the whole spline curve satisfies the second order smoothness, which proves that the spline function is a natural spline function, which also shows the feasibility of the energy optimization method.

From the perspective of the spline basis function, given the cubic B-spline curve:

$$w(u) = \sum_{i=0}^{3} P_i N_{i,3}(u)$$

In the formula:

$$\begin{cases} N_{0,3}(u) = \frac{1}{6}(1-u)^3 \\ N_{1,3}(u) = \frac{3u^3 - 6u^2 + 4}{6} \end{cases} \quad \begin{cases} N_{2,3}(u) = \frac{1 - 3u^3 + 3u^2 + 3u}{6} \\ N_{3,3}(u) = \frac{1}{6}u^3 \end{cases}$$

Thus, the potential energy of the cubic spline curve is:

$$\Pi = \int_0^l (\partial w_u^2 + \beta w_{uu}^2 - 2fw) du$$

According to the principle of energy optimization, the potential energy of the curve at a certain point to obtain a minimum, the point of the first derivative is zero, that is, the minimum potential energy principle:

$$\delta\Pi = 0$$

Use the points to get:

$$EI\frac{d^4 w}{dx^4} = f$$

The finishing energy model is:

$$\Pi = \sum_{i=0}^{3} [\sum_{j=0}^{3} (P_i * P_j \cdot S_{i,j})]$$

In the formula:

$$S_{i,j} = \int_0^1 [\alpha N_{i,3}'(u) N_{j,3}'(u) + \beta N_{i,3}''(u) N_{j,3}''(u)] du$$

$$= \int_0^1 [\alpha(2u^4 - \frac{13}{2}u^3 + 5u^2 + \frac{1}{2}u + 1) + \beta(4u^2 - 24u + 8)] du$$

$$= \frac{203}{120}\alpha + \frac{10}{3}\beta$$

In addition, the spline curve satisfies the boundary condition:

$$\begin{cases} w(0) = \frac{1}{6}(P_0 + 4P_1 + P_2) \\ w(1) = \frac{1}{6}(P_1 + 4P_2 + P_3) \end{cases}$$

$$\begin{cases} w'(0) = \frac{1}{2}(P_2 - P_0) \\ w''(0) = P_0 - 2P_1 + P_2 \end{cases} \quad \begin{cases} w'(1) = \frac{1}{2}(P_3 - P_1) \\ w''(1) = P_1 - 2P_2 + P_3 \end{cases}$$

By combining all the conditions, the smoothness of the spline function is verified, and the feasibility of the energy optimization method is explained.

(2) Curve modeling of boundary curve constraints

Through the analysis of the principle of energy optimization and the method of model processing, the energy optimization method is used to solve the surface vertices. In other words, if given by the B-spline curve to control the constraints expressed by the vertex, you can use the mathematical programming method to solve the energy surface. The following four examples of the boundary curve as an example, illustrates the energy optimization method of surface modeling method.

The four curves of the four B-splines are connected in turn, and the two curves $C_0, C_1(C_2, C_3)$ in the $x(y)$ direction have the same node vector and power. As shown in Figure 1, the energy optimization method is used to construct the four B-spline curves as the boundary Surface.

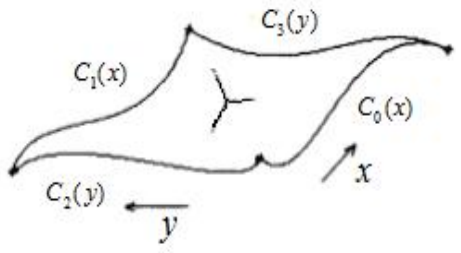

Figure1 Curves boundary constraint

Let the given four B-spline curves be:

$$C_0(x) = \sum_{i=0}^{mx} P_{0,i} N_{i,sx}(y), C_1(x) = \sum_{i=0}^{mx} P_{1,i} N_{i,sx}(y)$$

$$C_2(x) = \sum_{j=0}^{my} P_{2,j} N_{j,sy}(y), C_3(x) = \sum_{j=0}^{my} P_{3,j} N_{j,sy}(y)$$

Then, the power and surface vectors of the energy surface in the x, y direction can be consistent with the power and node vectors of the boundary curves in the corresponding directions, so the objective function can be determined according to the energy model.

The known boundary and the boundary curve have the same power and the node vector, then the boundary control vertex of the required surface coincides with the control vertex of the boundary curve, so the solution of the surface can be transformed into the solution optimization model:

$$\min \quad \Pi = \sum_{i,j=0}^{mx,my} [V_{i,j} \sum_{k,l=0}^{mx,my} (V_{k,l} * S_{i,j,k,l})]$$

$$s.t. \quad \begin{array}{l} V_{i,0} = P_{0,i}, V_{0,j} = P_{2,i} \\ V_{i,mx} = P_{1,i}, V_{my,j} = P_{3,i} \end{array}$$

Combined with the optimization theory, the model is a quadratic programming of linear equality constraints, which can be transformed into unconstrained quadratic programming using the reduced order method,that is:

$$\min \quad \Pi = \sum_{i,j=0}^{mx,my} [V_{i,j} \sum_{k,l=0}^{mx,my} (V_{k,l} * S_{i,j,k,l})] \qquad (2)$$

And all the first subscripts in the model contain 0,*mx* or the second subscript contains 0 and *my*,the control vertices are the control vertices of the boundary curve, and the rest of the control vertices are the unknowns required. Thus, the use of unconstrained quadratic programming theory, only need to get the surface of the internal control of the vertex can be, there are:

$$\frac{\partial \Pi}{\partial V_{i,j}} = 0 \quad \begin{matrix} i = 1,2,\cdots,mx-1 \\ j = 1,2,\cdots,my-1 \end{matrix} \qquad (3)$$

Using the iterative method to solve the equation, we can get the inner vertices of the surface (unknown control vertices), where the iterative formula is:

$$V_{i,j} = -\frac{\sum_{k\neq i,l\neq j}^{mx,my} V_{k,l}(S_{i,j,k,l} + S_{k,l,i,j})}{2S_{i,j,i,j}} \quad \begin{matrix} i = 1,2,\cdots,mx-1 \\ j = 1,2,\cdots,my-1 \end{matrix}$$

Based on the above analysis, we can get the algorithm of solving energy surface:

Step1 Determining the value of the boundary vertex $V_{i,0}$, $V_{i,mx}$, $V_{0,j}$, $V_{my,j}$ of the energy surface according to the power and nodal vectors of the B-spline curve in the parameter *x,y* direction, and initializing the inner vertex;

Step2 Using the Simpson numerical integration formula to determine $S_{i,j,k,l}$, and give the maximum number of iterations which is referred to as Max;

Step3 Loop statement for *t*=0;*t*<*Max*;*t*++

for *i*=1;*i*<*mx*;*i*++

for *j*=1;*j*<*my*;*j*++

Calculate $V_{i,j}$;

Step4 Determine the surface according to the control vertices.

Finally, the boundary is generated by four B-spline curves has the energy surface $w(x,y)$, as shown in Figure2:

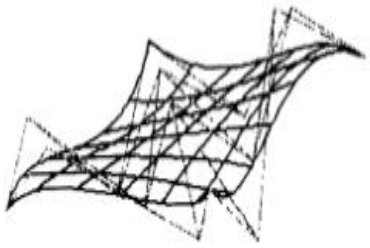

Figure2 Curve constraint generated energy surface

(3) Parametric surface - constrained surface modeling

In the case of surface modeling, parametric surface patches are used as constraints in many cases, resulting in energy surfaces that meet the design requirements and achieve the desired effect, which plays an important role in surface splicing, transition and extension [10].

Suppose that the curved patch is a B-spline slice:

$$w(s,t) = \sum_{i=0}^{p1}\sum_{j=0}^{q1} P_{i,j} N_{i,p1}(s) N_{j,q1}(t)$$

and the resulting energy surface is:

$$s(x,y) = \sum_{i=0}^{p2}\sum_{j=0}^{q2} P_{i,j} N_{i,p2}(x) N_{j,q2}(y)$$

Thus, the patch is:

$$\iint_{p2,q2} [\sum_{i,j}^{p1,q1} P_{i,j} B_{i,p1}(s) B_{j,q1}(t) - \sum_{i,j} P_{i,j} B_{i,p2}(x) B_{j,q2}(y)]^2 \, dsdt = 0$$

Combine the energy model of the treatment method can be obtained energy surface, as shown in Figure 3 which is the B-spline surface constraints generated by the energy surface.

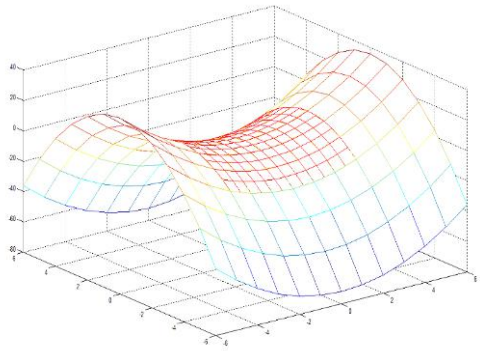

Figure 3 Surface constraints generated energy surface

5. CONCLUSION

Through the energy functional analysis of the unary spline function and the multivariate spline function and the optimization theory method, the method of energy optimization method is introduced, namely: the solution of the optimization problem (mathematical programming model) geometric condition constraints or the application of external load conditions make the curved surface of the bending energy to obtain the optimal value (usually take the minimum), so as to achieve the shape of the shape of the control effect. Finally, this method is applied to the four surface curve constraints and parametric surface constraints of the surface modeling. However, it is still necessary to establish a new method of geometric modeling based on mechanical load information and compound energy constraints and to construct new energy functional.

ACKNOWLEDGMENT

The surface modeling method based on energy optimization,funded by the Scientific Research Fund of North China University of Science and Technology. (Z201620).

REFERENCES

[1]ID.TERZOPOULOS, J.PLATT, A.BARR.

Elastically deformable models[J]. Computer Graphics, 1987, 21(4):205-214.
[2]H.QIN, D.TERZOPOULOS. Dynamic NURBS swung surface for Physics-based shape design[J]. Computer Aided Design, 1995, 27(2):111-127.
[3]H.QIN, D.TERZOPOULOS. Triangular NURBS and their dynamic generalizations[J]. Computer Aided Geometric Design, 1997, 14(4):325-347.
[4]Wang Renhong. The numerical approximation [M]. Beijing: Higher Education Press, 2012.
[5]Guo Huaitian. B-spline curve and curved surface research [D]. Anhui: Hefei University of Technology, 2012,4.
[6]Xiong Yunyang. The study of the spline curve surface of the CAD/CAE [D]. Zhejiang: Zhejiang University, 2014, 1.
[7]Li Zhilong. Based on the elastic deformation of surface reconstruction and smooth [D]. Dalian: Dalian University of Technology, 2010, 6.
[8]BIAN K, YINGLIN K. Global continuity adjustment and local shape optimization technique for complex trimmed surface model[J]. Chinese Journal of Mechanical Engineering, 2010, 3(2):225-232.
[9]Wang Yanjun, Qiao Zhian. Optimization theory and method [M]. Shanghai: Fudan University Press, 2011.
[10]Chen Youlan. Surface smoothing and surface construction method research and application [D]. Xi'an: Xi'an University of Science and Technology, 2012, 6.

A Simulation Model of Road Lane Based on Cellular Automata

Yan Long[1], Yanhong Kang[1], Yuhang Pan1 ,Yan Yan[2,], Xiaojun Men[2]*
[1]Yi Sheng College, North China University of Science and Technology, Tangshan 063210, Hebei, China
[2]College of Science, North China University of Science and Technology, Tangshan Hebei,063210,China

Abstract: Highway section is the most basic urban road system components; this paper analyzes the behavior of mixed traffic flow in urban road sections, and constructs the cellular automaton model of traffic flow in ordinary road section and dedicated lane sections. And two strategies are simulated and analyzed: There is no dedicated lane of self-driving car, and all vehicles share all the road resources; Setting up the dedicated lane of self-driving car, but only allowing the self-driving car to use, then traffic effect of each strategy is evaluated.
Keywords: cellular automaton; Lane space-time map; Lane access mode

1. INTRODUTION

Traffic congestion has long been a problem which demands prompt solution in many countries, and the self-driving car, as an emerging transportation, has gained more and more attention. The key issues in the research of self-driving car [1] include environmental perception, behavior decision and motion control; as well as the conditions for the establishment of special lanes is also the focus of the study.

At present, many domestic and foreign scholars have proposed a variety of intelligent evaluation methods for self-driving cars, such as cost function method, fuzzy comprehensive evaluation method, expansion analytic hierarchy process based on the chaos and so on, as well as lanes set of the city bus. However, there are few methods to set up special lanes for self-driving cars, so the domestic and foreign scholars have mostly used the method of setting the bus lanes in the study of the special lanes of self-driving cars. According to the bus lower frequency, Viegas and Lu [2], Eichler and Daganzo and Zhu [3] discussed the intermittent bus lanes, and analyzed the road without bus lanes, intermittent bus lanes and bus lanes three cases.Shi Chunhua [4] discussed the setting way, form, size of bus lane and the design of the station and the way to handle the intersection. According to the actual survey data, Huang Yanjun [5] established the speed model of public cars and social vehicles under the condition of no bus lanes and bus lanes, and through comparative analysis, the vehicle running state and speed variation characteristics are obtained. These methods provide a certain theoretical basis for the setting of bus lanes, but there are some differences in the special lanes of unmanned vehicles.

Based on the study of bus lanes on the basis of the study, Thurston, Washington, Pierce, King, and, Snohomish four regions are used as the background, and to explore the unmanned vehicle lane setting conditions. Lane that only allow unmanned vehicles traveling is suitable for traffic problems, In order to verify the feasibility, effectiveness and superiority of the conclusion, the author uses cellular automata to simulate the actual traffic flow of the common road section and the special lane, and the specific conditions of four areas to set up special lanes for unmanned vehicles are obtained.

2. THE CELLULAR AUTOMATON MODEL AND SIMULATION OF SPECIAL LANES FOR ROAD

2.1 Traffic flow simulation of four car section

In order to study the condition of Thurston, Pierce, King, and Snohomish four zones to set up the dedicated lane for self-driving cars, first of all, we get the route code and route range of the four areas, and calculate the daily traffic volume of each region according to the data given, as shown in table 1.

Table 1 Daily traffic volume of each area

	The including route	Route range	Daily traffic volume (*1000)
Thurston	Interstates 5	100.93-114.93	165.8
Pierce	Interstates 5	114.93-139.5	5064
King	Interstates 5	139.5-177.76	13104
	Interstates90	1.94-25.37	
	State Route 520	0-12.83	
	Interstates 405	0-25.02	
Snohomish	Interstates 5	177.76-212.67	5325
	Interstates 405	25.02-30.32	

In this paper, taking the Piece area as an example, we simulate the traffic flow of the 123.28-131.35 mileposts on line five. Through the simulation, this paper explores the traffic conditions. According to the conditions, the dedicated lane can be set up for self-driving cars in Piece area.

In the model, the open boundary is used to simulate the traffic flow under two kinds of strategies. Space time diagram of the two lanes is obtained, as shown in Figure 2.

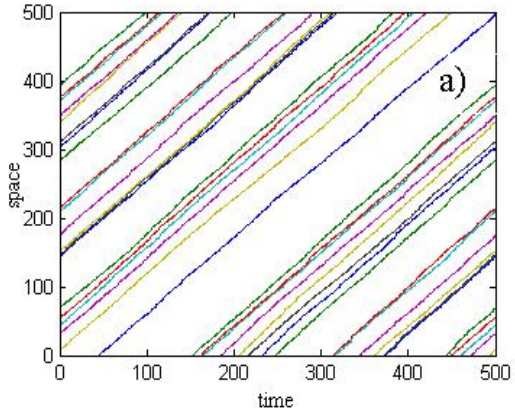

a) The first lane using strategy 1

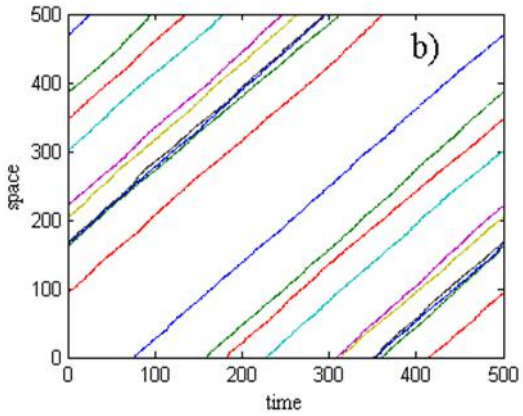

b) The first lane using strategy 2

Fig. 1 Spatial and temporal distribution of the inner lane of the two lanes under the three lane access modes

It can be obtained from figure1 that there are great differences in the spatial and temporal distribution of the first lane which under the three access modes, there are more short-term congestion in a, there is almost no congestion in b, the slope of the vehicle trajectory is almost the same, and the color of the track line is the deepest, there aren't dedicated lanes in a, and traffic lane is not restricted [6].

In the first lane of b only allow private sharing vehicles traveling in the lane, it is a single private sharing of traffic, traffic density is low, the vehicle is basically at maximum speed, the difference of the spatial and temporal distribution is small, although the change of road rules are different, but reflected in the second lane, only the first and second lane's change is limited, it does not affect the lane changing behavior of second and third lane vehicles.

In order to clearly compare the traffic flow of each lane under the two strategies, in this paper, use random distribution as the initial state [7], the upstream generates the vehicle with a fixed probability of 0.2, the traffic flow is simulated under two conditions: no special lanes, dedicated lanes and only allowed self-driving cars to drive, the first 200 time steps are removed by the initial state, and the changing trend of the number of vehicles in the following 800 time steps is obtained, as shown in Figure 3:

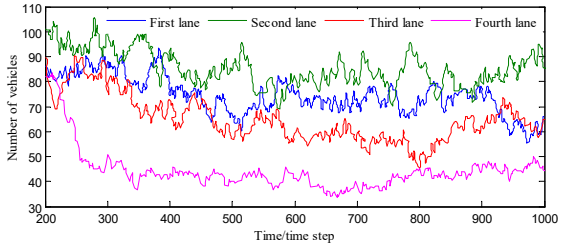

a) No dedicated lanes

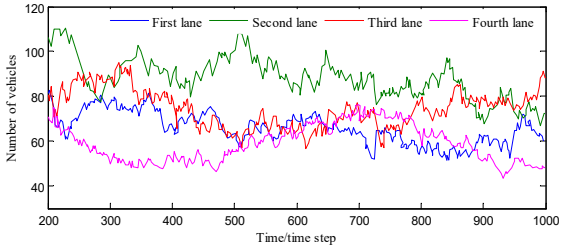

b) There is a dedicated lane and only allow self-driving cars to drive

Fig. 2 The changing trend of the number of vehicles in each lane under two strategies

It can be seen from Figure 2 (a) that the number of vehicles with four lanes is stable, and it fluctuate little with time, and the number of vehicles is satisfied with: $N_2 > N_1 > N_3 > N_4$. It can be seen from Figure 2 (b) that there is a dedicated lane and only allow self-driving cars to drive, the number of vehicles is satisfied with: $N_3 > N_2 > N_4 > N_1$. The first lane is a dedicated lane for unmanned self-driving cars, so the number of vehicles in the first lane is less when the proportion of the self-driving vehicles in the upstream mixed traffic flow is low. The other three lanes are mixed traffic, so the density is higher than the first lane, comparing with (a), the traffic volume of (b) increased significantly, which shows that under some conditions, the use of strategy 2 is more conducive to the simulation of road traffic flow. In order to further explore the conditions of setting up the lane of the self-driving car, a model for determining the condition of the special lane is established.

3. Determination model of special lane condition

In this paper, a four-lane section with dedicated lanes only allowing unmanned vehicles to enter is studied, and the proportion of unmanned vehicles in the upstream vehicle is changed[8], the proportion of self-driving is changed from 0 to 0.8, and the simulation of each model is carried out by a total of three times, and a total of 240 sets of traffic flow simulation data are obtained, according to this, draw the change trend of road traffic flow and average speed of single lane under different self-driving car ratio, as shown in Figure 3-4:

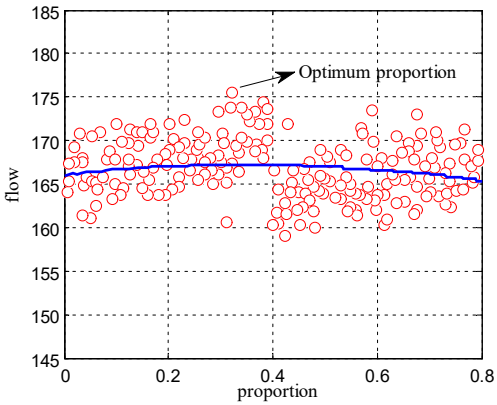

Fig.3 The ratio of self-driving car- flow diagram

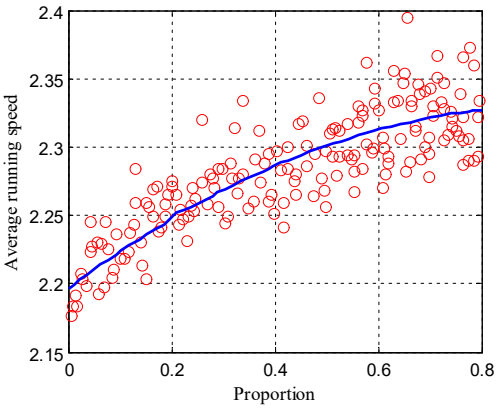

Fig.4 The ratio of self-driving car- average speed of traffic diagram

It can be seen from Figure 4, with the increase in the proportion of self-driving cars, the average speed of self-driving cars driving in the dedicated lane initially showed an upward trend, after a period of time, the growth trend slowed down, and eventually stabilized. This is because when the ratio of self-driving car is zero, there are only non-self-driving vehicles in the upstream mixed traffic flow, because the unmanned vehicle lane does not allow non-self-driving cars, so the road is not fully utilized; When the proportion of unmanned vehicles increased, more and more self-driving cars have improved the space utilization rate of private roads, the traffic pressure of non-dedicated lanes has been reduced, the vehicle lane change is more free and the average running speed of vehicles has been increased. Due to the nominal speed limited in the United States in these areas is 60 mile/h, so the average speed of traffic can't be unlimited increase; when the proportion of self-driving cars reaches to the upper limit of 90%, it is equivalent to the absence of a dedicated lane traffic flow. According to figure 3, set the lanes and only allow self-driving cars driving mode, when the proportion of vehicles in the upstream of the self-driving car reached 32.3%, it is helpful to improve the road traffic operation of Pierce to set up a dedicated self-driving lane.

4. Conclusion

In this paper, two solutions to the problem of whether to set up a dedicated lane are put forward. (1)There is no dedicated lane of self-driving car, and all vehicles share all the road resources; (2)Setting up the dedicated lane of self-driving car, but only allowing the self-driving car to use, In order to clearly compare the traffic flow of each lane under the two strategies, in this paper, use random distribution as the initial state, the upstream generates the vehicle with a fixed probability of 0.2, the traffic flow is simulated under two conditions, a comparison between the two proposals shows that, since a dedicated lane is only restricted to self-driving vehicles, it is not necessary to designate a dedicated lane for self-driving vehicles when the proportions of self-driving vehicles are 32.3%, 41.2%, 26.8% and 36.9% in Thurston, Pierce, King, and Snohomish respectively.

REFERENCES

[1]Xu Wei, Gong Jianwei, Jiang Yan. Model predictive control of self-driving cars[M]. Beijing: Beijing Institute of Technology press, 2014.

[2]Viegas, J., Lu, B. The intermittent bus lane signals setting within an area [J]. Transportation Research Part C, 2004, 12(6):453-469.

[3]Zhu, H.B. Numerical study of urban traffic flow with dedicated bus lane and intermittent bus lane [J]. Physical A, 2010, 389(16):3134-3139.

[4]Shi Chunhua, Yang Xiaoguang, Zeng Song. The set and design of urban public traffic lane[J]. Urban Rail Transit Study, 2000, (2):49-52.

[5]Huang Yanjun, Chen Xuewu, Zhang Weihua. Comparison of traffic flow model in front and rear sections of bus lane [J]. Journal of Huazhong University of Science and Technology (Urban Science Edition), 2003, 20(4): 68-70.

[6]Zhang N X, Zhu H B, Lin H, et al. One-dimensional cellular automaton model of traffic flow considering dynamic headway[J]. Acta Physica Sinica -Chinese Edition-, 2015, 64(2):24501-024501.

[7]Zhao H T, Nie C, Li J R, et al. A two-lane cellular automaton traffic flow model with the influence of driver, vehicle and road[J]. International Journal of Modern Physics C, 2015, 27(2):1650018.

[8]Nemec P, Cullinane B, Clement M C. Determining and displaying auto drive lanes in an autonomous vehicle:, 2015.

Simulation Study on Traffic Effect of Unmanned Vehicles Based on Cellular Automata

HaoMen[1],Shichao Yu[1],Yuhan Li[2],Xiaojun Men[3]*
[1]*College Of Electrical Engineering, North China University Of Science And Technology, Tangshan 063210,Heibei,China*;
[2]*College Of Metallurgy And Energy, North China University Of Science And Technology, Tangshan 063210,Heibei,China*;
[3]*College Of Science , North China University Of Science And Technology, Tangshan 063210,Heibei,China;*

Abstract :Based on the simulation study on the traffic effect of unmanned vehicles, several roads of King, Snohomish, Thurston and Pierce are selected as the research objects. First, this paper proposes a multi-speed mixing of cellular automata under open boundary conditions Vehicle lane and multi-lane traffic flow model, the cellular automata (Cellular Automaton) model was established. Secondly, the cellular automata was used to simulate the single lane and multi-lane driving, and the vehicle density About 0.04, the traffic flow peak; Finally, the multi-lane driving line numerical simulation analysis, obtained multi-lane unmanned co-operative car (Self-driving, cooperating cars) accounted for 50% of the time will significantly ease the traffic Pressure, that is, the higher the proportion of traffic, the better the traffic effect.
Keywords: Cellular automaton; Self-driving; cooperating cars; Numerical Simulation.

1. INTRODUCTION

Nowadays, the volume of traffic has exceeded over the full design capacity in many districts of USA. For considering to relieve the pressure by pulling in driverless automobile , Yuan Yifan et al built the dynamic model of driverless automobile that bases on nerve network and put forward the optimized PID control method of vertical and horizontal vehicle dynamic model that both aim at the deficiency of the driverless system acting slowly, overloading or vibrating. Tian Geng, in studying the field of driverless automobile, built the city roadway model and the vehicle dynamic model and the drive emulation platform under the typical city roadway circumstance. That provides theoretical support for driverless automobile driven on real circumstance of city roadway.

This article uses the theory of cellular automata to put forward the single line and multiline traffic stream model of cellular automata multi speed hybrid vehicle and build the theoretical model of cellular automata that both are for the simulant study of traffic effect about driverless automobile.

2. ALGORITHM MODEL

From the above evaluation model analysis, we can see from the road capacity of the first analysis. In the case of actual traffic, the number of vehicles on the lane is constantly changing, the open boundary conditions to study the traffic flow can better reflect the real traffic characteristics, in order to better reflect the reality of mixed traffic phenomenon, this paper proposed in the open Under the boundary conditions, the cellular automata multi-speed hybrid vehicle single-lane traffic flow model should consider and open in consideration of the probability of occurrence of vanishing probability, probability of occurrence, random deceleration probability, lane length and the effect of different types of vehicles on mixed traffic. New phenomena arising from the study of boundary conditions.

2.1 cellular automaton theoretical model

The road is regarded as a one-dimensional discrete lattice chain of length, and each lattice point may be vacant at every moment, or it may be a vehicle .There are two vehicles with the highest speed being mixed on the road, wherein the state of the vehicle is expressed by the speed, and the distance between the first vehicle time and the immediately preceding vehicle is represented by the position indicating the time of the first vehicle: Time to change, the change process is in accordance with the NS model evolution rules for speed and location of real-time updates, NS model update rules are:

●Acceleration process : $V_i(t+1) \to Min(V_i(t)+1, V_{Max})$;

●The deterministic acceleration process is : $V_i(t+1) \to Min(V_i(t), gap_i(t))$;

●The probability of random deceleration process : $V_i(t+1) \to Max(V_i(t)-1,0)$;

●The vehicle position is updated to : $x_i(t+1) \to x_i(t)+V_i(t+1)$.

The condition of the open boundary is defined as: a grid point in the lane, at the beginning of time, the lane in the lane outside the probability of generating a

car, so that the maximum speed of the car, the equivalent of 60mile / h the car in accordance with the above evolution The speed of the car at the beginning of time has been maintained at 0, then close to the right side of the lane to the probability of deceleration of the vehicle, the lane can also be considered within the lane of the right side of the road, Of the vehicles at the right boundary disappears with probability. At that time, the boundary is in a partially open state; then the full open boundary conditions.

2.2 numerical simulation analysis of single

Here we define the following macroscopic quantities: The total number of vehicles on the lane at time t is the average density, mean velocity, average flow. In the numerical simulation, the initial time lane full space, and then at the beginning of the lane to a certain probability of constantly adding to the vehicle, which joined the speed of the vehicle is the probability of occurrence, while driving in the lane according to the above rules update the location of the vehicle , Velocity distribution.

2.3 numerical simulation analysis of multi lane driving

Take 520 lanes as an example, the NS model is used to simulate the vehicle on the road. The simulation parameters are as follows :the maximum speed of the vehicle is $V_{\max} = 4.1136$, equivalent to 60mile/h and road length $L = 2000$, each cell has a length of 6, so the actual length of the road is 12.83 mile; The proportion of manned, cooperating cars is S_{dyn} =1, stochastic slowing down probability $P = 0.15$, self-driving, cooperating cars ratio is $p_{fc} = \{0.1, 0.2, 0.3, 0.4, 0.5, 0.6, 0.7, 0.8, 0.9\}$.

The initial condition of the road is empty and the vehicle is randomly added at the first 100 moments, from the beginning of the 101st moment, manned, cooperating cars according to the feedback information to choose the road.

Froming the beginning of the 20000 moment ,the simulation data of the continuous 10000 moments are used to analyze the data ,Comparison of the performance parameters for the traffic F and the number of vehicles in which the definition of flow N:

$$F = V_{mean} \times N / L$$

In the formula, N is the number of vehicles on the road, and the average density of V mean on the road. L for road length. Among them, the flow of F reflects the capacity of the road, the vehicle N reflects the capacity of the road capacity.

3. SOLUTION OF THE MODEL

Now we use the MATLAB software to simulate the numerical simulation, select the 520 National Road (State Route 520) as the reference road, the simulation results shown in Fig.1, Fig.2.

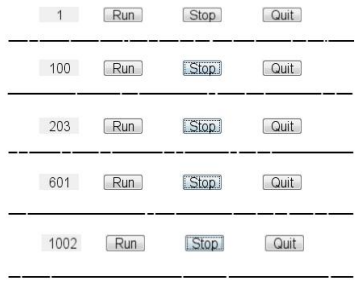

Figure 1 road situation simulation diagram

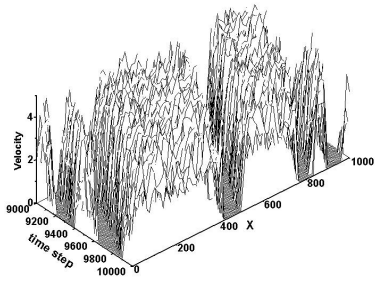

Figure 2 Road and space simulation map

Run simulation of vehicle driving conditions, the number of vehicles in the number of steps with the passage of time, the number of vehicles in the road distribution of the road to produce space-time simulation.

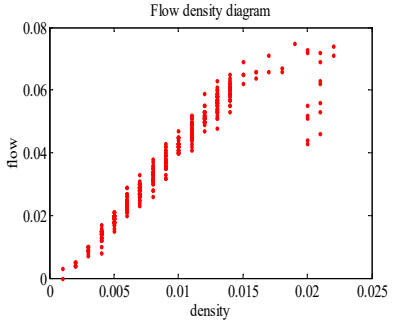

Figure 3 Low-step vehicle flow density map

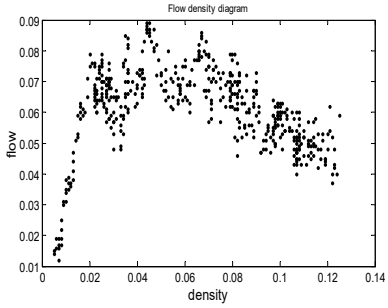

Figure 4 High-step vehicle flow density map

As can be seen from Fig. 10, it can be seen that the traffic volume of the road increases with the increase of the vehicle density during the initial period of time. As shown in Fig. 11, it can be seen clearly that, as time passes, Of the density increases, but the traffic volume decreases, this time there is a traffic jam situation. It can be seen from the figure that the maximum value of traffic flow reflects the road capacity, the maximum density of vehicles is about 0.04.

This paper analyzes the 5, No. 90, No. 405 and No.

520 highways, With 10% as a file, in the road to join self-driving, cooperating cars ,Has been increased from 10% to 90%, through the simulation of the above model data, The average flow standard self-driving, cooperating cars in each percentage is obtained, As shown in Fig.5,Fig.6.

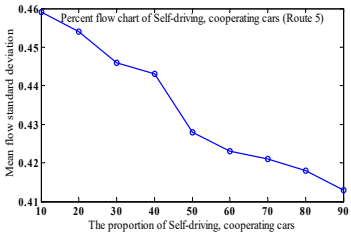

Figure 5 Standard deviation of average flow rate of No. 4 road

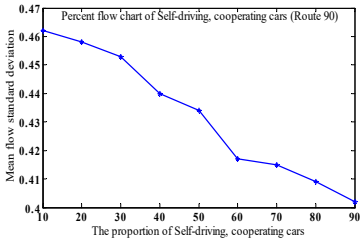

Figure 6 Standard deviation of average flow rate of No. 90 road

Through the above figure can be seen in the number of self-driving, cooperating cars in the road 5 in the ratio of 10% to 90% of the average flow standard deviation coefficient. It can be seen at this time there is a critical point in 40%, between 30% to 40% and the balance between 60% and 70%.The standard deviation coefficient of the average flow rate of 10% to 90% in Road No. 90.It can be seen at this time there is a critical point in 50%, there is a balance between 60% and 70%.

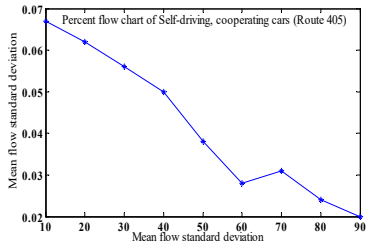

Figure 7 Standard deviation of average flow rate of No. 405 road

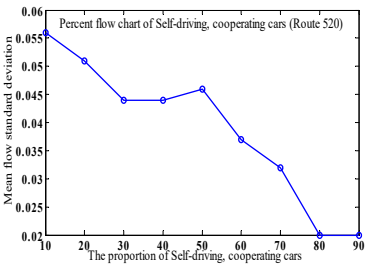

Figure 8 Standard deviation of average flow rate of No. 520 road

Through the above figure can be seen in the number of self-driving, cooperating cars in the road 405 in the ratio of 10% to 90% of the average flow standard deviation coefficient. It can be seen at this time there is a critical point in the 60% and 70%, there is no equilibrium. The standard deviation coefficient of the average flow rate of 520 to No. 90% on Road No. 10%.It can be seen that there is a critical point between 30% and 50%, and there is a balance between 30% and 40%.

Through the above four in each percentage of the average flow of unmanned vehicles can be clearly seen in the standard deviation map, the standard deviation of the average flow decreases with the increase of the proportion of the self-driving, cooperating cars. Therefore, we can draw a conclusion that when the proportion of self-driving, cooperating cars is 50%, the traffic pressure is obviously reduced, that is, the higher the proportion of traffic, the more obvious the effect.

REFERENCES

[1]Yuan Yifan ,Liang Jun,Liu Changning, Chen Lei,Wu Longwei,Chen Long,Jiang Haobin. Simulation and Realization of Neural Network Integrated PID Control Based Unmanned Driving Vehicle Dynamic Model[A]. Society of Automotive Engineers of China.Annual Proceedings of China Automotive Engineering Society(2014)[C]. Society of Automotive Engineers of China:,2014:7.

[2]Tian Geng. Research on Bionic Lane-changing Decision Decision-making Model for Autonomous Vehicle under Dynamic Urban Environment[D].Beijing Institute of Technology,2016.

[3]Nowogrodzki A. Self-driving cars alone won't ease gridlock[J]. New Scientist, 2016, 229(3057):21-21.

[4]Marzoug R, Ezzahraouy H, Benyoussef A. Cellular automata traffic flow behavior at the intersection of two roads[J]. Physica Scripta, 2014, 89(6).

[5]Lárraga M E, Alvarez-Icaza L. Cellular automata model for traffic flow with safe driving conditions[J]. Chinese Physics B, 2014, 23(5):216-226.

[6]Weyer J, Fink R D, Adelt F. Human–machine cooperation in smart cars. An empirical investigation of the loss-of-control thesis[J]. Safety Science, 2015, 72:199-208.

[7]Caracciolo D, Noto L V, Istanbulluoglu E, et al. Climate change and Ecotone boundaries: Insights from a cellular automata ecohydrology model in a Mediterranean catchment with topography controlled vegetation patterns[J]. Advances in Water Resources, 2014, 73:159–175.

Feature Extraction of Optical Information

*Chengran Ren[1], Shihao Zhao[2], Huiqi Zhang[1], Xiaojun Men[3]**
[1]College of metallurgy and energy of North China University of Science and Technology ,Tangshan,Hebei 063210,China.
[2]College of Information Engineering of North China University of Science and Technology, Tangshan Hebei,063210,China.
[3]College of Science of North China University of Science and Technology, Tangshan Hebei,063210,China

Abstract: For the problem 1, this paper gives the Excel data in the table using MATLAB for image processing, three tables corresponding to the curve (see Figure 1, Figure 2, Figure 3), and then find the various graphs of the Peak points: 690,947,1042,1214,1627,1715,to ensure the existence of special points, and take the two points of the midpoint of the peak value: 345,818,994,1128,1420,1671, to ensure that the trend of graphics, the value of these 13 is Optical information characteristics.
Keywords: Partial Least Squares Regression Analysis Cross-validation Eigenvalue

1. INTRODUCTION

In order to find out the characteristics of the optical information data in the question ,we consider to use the MATLAB software to draw the multiple sets of data in the Excel table, and then find the optical information data according to the characteristics of the observation graphs, such as the trend, peak value feature[1].

2. EXPERIMENTAL

2.1 the establishment of the model

First, the data in the Excel table is processed by MATLAB, and the curves of frequency and light intensity are obtained. Since the peak of the image has a clear to the performance of the unique features of the point, so the first selection of peak points to reflect the special values of the entire image[2][3]. Then, in the peak point selection so as to further reflect the choice, the trend of image. And finally to select the peak and midpoint to replace the Excel group of data.

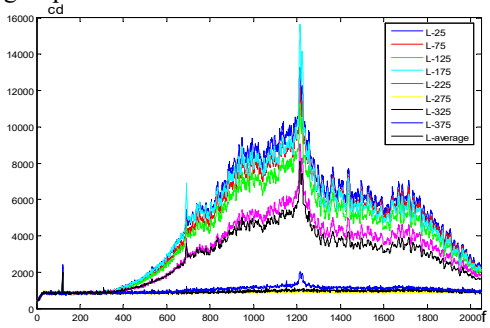

Figure 1 The data plot in Table 1

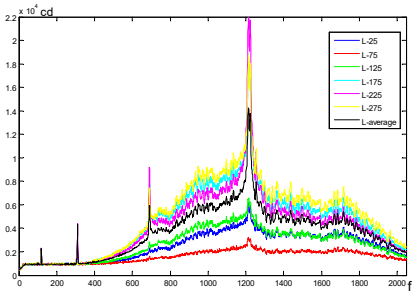

Figure 2 The data plot in Table

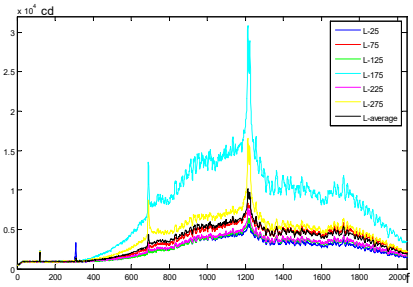

Figure 3 The data plot in Table III

2.2.solution of the model

Under the three-curve model of the Problem , we find the peak point on the graph, as shown in figure 4：

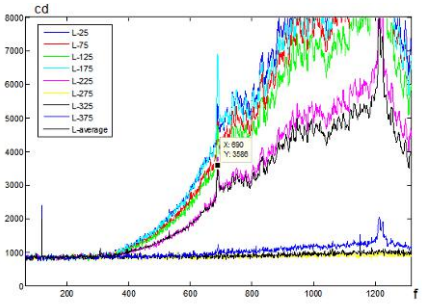

Figure 4 The first peak point

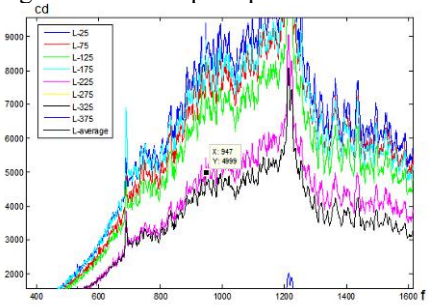

Figure 5 The second peak point

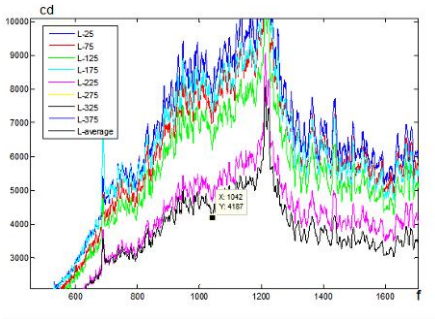

Figure 6 The third peak point

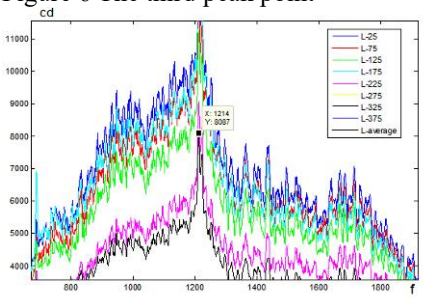

Figure 7 The fourth peak point

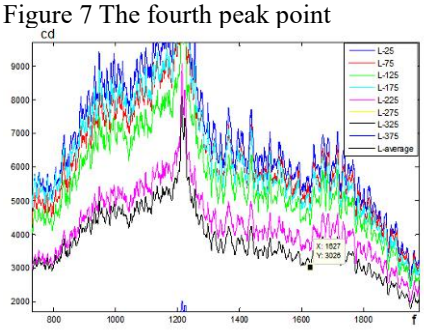

Figure 8 The fifth peak point

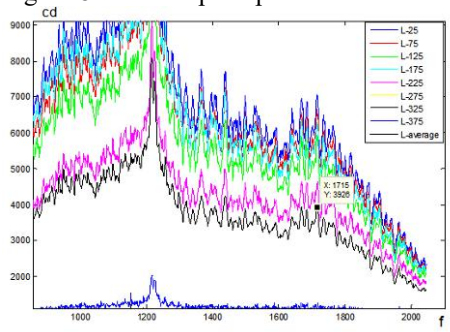

Figure 9 The sixth peak point

From figure 4, we can see that in Tab1, the first peak point corresponds to the order, and the corresponding frequency of each peak point is 947,1042,1214,1627,1715. In the same way, the order of peak points in table 2 is 690,1014,1041,1214,1630,1716; the order of peak points in table 3 is 690,1014,1041,1213,1613,1716.And then to reflect the trend of the curve, so take the midpoint of each peak value, and finally find the characteristics of optical information data[4][5] in table 1:

Table 1 The values found in each table λ

Excel	1	2	3
f	345	345	345
	690	690	690
	818	852	852
	947	1014	1014
	994	1027	1027
	1042	1041	1041
	1128	1127	1127
	1214	1214	1213
	1420	1422	1413
	1627	1630	1613
	1671	1673	1664
	1715	1716	1716
	1881	1882	1882

REFERENCES

[1] Lifan Mao, Jun Jiang, Ruihua Long, Ni Li, Hui Huang, Shan Huang. Medium and long term electric load forecasting based on partial least squares regression analysis [J]. power system technology, 2008,19:71-77.

[2]Fenghua Xu. Research on some problems in partial least squares regression [D]. Shandong University of Science and Technology, 2006.

[3]Bing Chen, Shan Li, Bao-Hai Wu, Ming-Wei Wang.Multi-process quality analysis and prediction based on size correlation and partial least-squares regression [J].

[4]Bingxiang Tang. Research on boiler flame temperature detection based on digital image processing [D]. Hunan University, 2006.

[5]Xiaoling Cui. Wavelet neural network inversion flame temperature assisted Steelmaking Endpoint judgment research based on [D]. of Nanjing University of Science and Technology, 2006.

The Study Based on Newton's Law-regression Analysis About the Safety of Transportation in Washington State

*Hao Men[1], Shichao Yu[1] ,Yuhan Li[2],Liya Wang[3]**
[1]College Of Electrical Engineering, North China University Of Science And Technology, Tangshan 063210, Heibei, China;
[2]College Of Metallurgy And Energy, North China University Of Science And Technology, Tangshan 063210, Heibei, China;
[3]College Of Science , North China University Of Science And Technology , Tangshan 063210,Heibei,China;

Abstract: This paper chooses the traffic in Washington, DC as the main research object, and establishes the safety analysis model. First of all, First of all, it uses the literature method and notices the traffic safety which is meanly threatened by the driving distance which is lower than the safety distance Based on this, the traffic line spacing is regarded as the safety of the standard; Followed by Newton's second law of motion and regression analysis the ,we establishes the Single - lane driving distance model. The conclusion is that the maximum distance of the vehicle is 5m and 70m when the speed is 20mile / h and 60mile / h respectively. Finally, combined with the friction power of the vehicle, we establishes the driveway spacing model based on the the friction dynamic. The distance between 20mile / h and 60mile / h is 6m and 80m, respectively. while the driving distance of the lane is 20mile / h and 60mile / h.

Keywords: Newton's law-regression analysis; Friction dynamics theory; Traffic safety

1. INTRODUCTION

In today's world, with the rapid development of traffic levels, car ownership has increased year by year, followed by a lot of traffic safety issues. In the study of road traffic safety, Zhao Xinyong carried out a research on highway traffic safety performance evaluation based on multi-source heterogeneous data, and put forward the evaluation index system of regional expressway network traffic safety performance. Sun Lu and some other people used the micro-traffic simulation software to simulate the traffic flow condition under certain road traffic conditions, identify and analyze the traffic conflict in the process of traffic simulation, and evaluate the traffic safety situation of the interweaving area. It is of great significance to carry out the safety study of road traffic for the development of safe road traffic mode and to prevent traffic accidents.

This article takes the traffic of Washington state as the research object, and establishes the safety analysis model. First, through the literature method, the traffic line spacing is taken as the standard of safety, and then combined with Newton's second law and regression analysis, the single-lane driving distance model is established to analyze and study the traffic safety.

2. AlGORITHM MODEL

To state the influence of Self-driving and cooperating cars on traffic, based on the analysis of the traffic capacity, the safety performance analysis is increased in this paper.

2.1 based on newton’s law-regression analysis of single-lane travel distance model

Newton 's second law of motion states that the acceleration of one object is proportional to the force, and to the reciprocal of the mass of the object. The direction of the acceleration is the same as the direction of the force. It is expressed by the formula:

$$a \propto \frac{F}{m} or F \propto ma \tag{1}$$

The relationship of displacement and velocity is

$$v^2 = 2ax \tag{2}$$

We can get form the above two formulas:

$$(\frac{v}{3.6})^2 = 2\mu\beta l \tag{3}$$

$$fW = \beta\frac{W}{g} \tag{4}$$

Among them: β —the acceleration of brake deceleration, m/s^2;

μ —the efficiency of braking, which is in the range of the actual velocity, taken 1;

g —gravitational acceleration, taken $9.8m/s^2$;

f —longitudinal sliding friction coefficient of tire and road surface;

W —the mass of the car, kg;

l —Minimum vehicle spacing, m.

from (3) and (4):

$$l = \frac{v^2}{2\mu g f \times 3.6^2} \tag{5}$$

The longitudinal sliding friction coefficient varying with the vehicle speed as is shown in the following table.

Tab. 2 The relation between longitudinal frictional coefficient and speed

v(mile/h)	20	25	30	35	40	45	50	55	60
f	0.40	0.35	0.35	0.30	0.30	0.30	0.25	0.25	0.20

Learn from regression analysis of relationship between velocity and longitudinal frictional coefficient:

$$f = 2.2719 \times v^{-0.487} \tag{6}$$

2.2 vehicle-running distance model based on friction dynamics

The time interval between consecutive one lane of traffic operation of the vehicle is called gap. It means: (1) This particular gap is acceptable for the driver. (2) When the driver tried to change lanes, it found that the size of a certain gap.

In this paper, the method of calculating the ideal gap and the gap of traffic flow in the method of ideal safety clearance estimation. Assume that when the vehicle speed is less than the speed of the main line or the weaving vehicle, it must accelerate to complete the behavior of changing lanes. The average acceleration of the vehicle is the velocity linear equation of the merging vehicle. The use of dynamic equations to accelerate the confluence of the ideal safety gap is based on the required time: due to acceleration caused by time loss and safe parking time.

(1) Safe stop time:

$$(T_R + T_F) = \left(\frac{L_f}{v} + RT\right) + \left(\frac{L_r}{v} + RT\right) = \frac{L_f + L_r}{v} + 2 \cdot RT \tag{7}$$

among them, T_R represents the safety time between the ramp vehicle and the following vehicle; T_F represents the safety time between the ramp vehicle and the leading vehicle; L_f and L_r represents the length of the main and ramp vehicles; v represents the combined flow speed; RT indicates the reaction time of the driver.

(2) Due to acceleration caused by the loss of time:

$$T_L = \frac{u + v}{b \cdot v} + \frac{(a/b) - v \cdot \ln\left(\frac{a - b \cdot v}{a - b \cdot u}\right)}{b \cdot v} \tag{8}$$

Due to acceleration caused by the loss of time:

among them, u represents the traffic flow speed of the process; v represents the traffic flow speed after merging; a , b represents a constant.

The equation for calculating the ideal safety clearance of confluence is:

$$T = T_R + T_F + T_L = \frac{L_f + L_r}{v} + 2 \cdot RT + \frac{u + v}{b \cdot v} + \frac{(a/b) - v \cdot \ln\left(\frac{a - b \cdot v}{a - b \cdot u}\right)}{b \cdot v} (u < v) \tag{9}$$

among them, T_F represents the safety time between the ramp vehicle and the leading vehicle; T_R denotes the safety headway between the ramp vehicle and the following vehicle; T_L represents the time loss due to acceleration.

After determining the values of a and b ,in order to use the ideal safety clearance equation, the values of a and a/b are 4.8mph/sec and 80mph,The reaction time was 1 second.

When the vehicle is changing lanes, it is necessary to make some corrections to the equation due to the fact that the merging vehicle must accelerate. Assume that the vehicle decelerates in the following relationship:

$$\frac{dv}{dt} = f \cdot g \tag{10}$$

Where f is the friction coefficient of the car tire and the road surface: g is the acceleration of gravity; Similarly, in accelerating or merging, the ideal safety gap consists of two factors: (1) The time required for safe parking is the same as above;

(2) Loss of time due to deceleration.

the normal driving time is:

$$\frac{u \cdot t + \frac{1}{2}(f \cdot g) \cdot t^2}{u} = t + \frac{1}{2} \cdot \frac{f \cdot g}{u} \cdot t^2 \tag{11}$$

(2) The time required for deceleration is

$$t = \frac{u - v}{f \cdot g} \tag{12}$$

From (4.3.9) and (4.3.10), the loss time can be obtained as follows:

$$T_L = \left(\frac{u - v}{f \cdot g} + \frac{1}{2} \cdot \frac{f \cdot g}{u} \cdot \left(\frac{u - v}{f \cdot g}\right)^2\right) - \left(\frac{u - v}{f \cdot g}\right) = \frac{1}{2} \frac{(u - v)^2}{2u \cdot f \cdot g} \tag{13}$$

Therefore, when the merging vehicle is larger than the speed of the main road traffic, the ideal equation for calculating the safety clearance is:

$$T = T_R + T_F + T_L = \frac{L_f + L_r}{v} + 2 \cdot RT + \frac{1}{2}\frac{(u-v)^2}{u \cdot f \cdot g}(u \geq v) \quad (14)$$

Due to the presence of self-driving, cooperating cars and manned, cooperating cars in the road, So the introduction of correction factor δ to amend the safety clearance, the equation is:

$$T = T_R + T_F + T_L = \frac{L_f + L_r}{v} + 2 \cdot RT + \frac{1}{2}\frac{(u-v)^2}{u \cdot f \cdot g} + C\delta(u \geq v) \quad (15)$$

3. SOLUTION OF THE MODEL

Through the above model, get the relationship between the vehicle speed and the minimum vehicle distance in the normal running of single lane as shown in Fig.1:

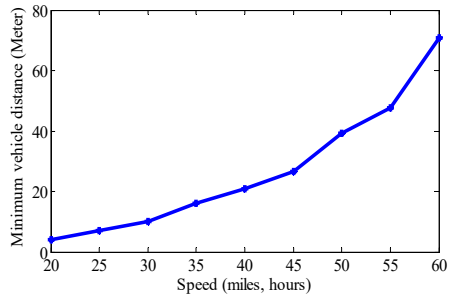

Figure 1 The relationship between the speed of a single lane and the minimum vehicle distance

From the above figure, it can be clearly seen that the greater the vehicle speed is, the greater the minimum vehicle distance is. In order to ensure the safety of vehicles the minimum distance of is 5m, when the speed is 20mile / h, and the minimum distance is 70 m when the maximum speed of is 60mile / h.

By solving the model, the relationship between the speed of the vehicle and the minimum vehicle distance at which the vehicle travels on the lane changing can be obtained. As shown in Fig.2.

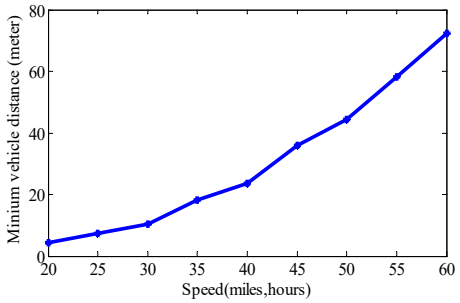

Figure 2 The relationship between vehicle speed and minimum headway

From the figure it can be clearly seen that the faster speed of the vehicle, the further safety distance. When the speed is 20mile / h, the minimum distance is 6m; When the maximum speed is 60mile / h, the minimum distance is 80m. Ensure the safety of vehicles.

REFERENCES

[1]Zhao Xinyong. Freeway Traffic Safety Evaluation Method Based on Multi-Source Heterogeneous Data[D].Harbin Institute of Technology,2013.

[2]Sun Lu,Li Yanping,Qian Jun,Yu Ye. Evaluation of Weaving Sections with Respect to Traffic Safety Based on Traffic Conflict Technique[J]. China Safey Science Journal,2013,(01):55-60.

[3]Sordyl J. Application of the AHP method to analyze the significance of the factors affecting road traffic safety[J]. Transport Problems An International Scientific Journal, 2015, 10(2):57-68.

[4]Lárraga M E, Alvarez-Icaza L. Cellular automata model for traffic flow with safe driving conditions[J]. Chinese Physics B, 2014, 23(5):216-226.

[5]Mohan D, Tiwari G, Mukherjee S. Urban traffic safety assessment: A case study of six Indian cities[J]. Iatss Research, 2016, 39(2):95-101.

[6]Goniewicz K, Goniewicz M, Pawwski W, et al. Road accident rates: strategies and programmes for improving road traffic safety[J]. European Journal of Trauma and Emergency Surgery, 2016, 42(4):433-438.

The Optimization Design of Accommodation Lane Based on Simulated Annealing Algorithm

Hao Men[1], Shichao Yu[1],Yuhan Li[2], Bin Bai[3]*
[1]College Of Electrical Engineering, North China University Of Science And Technology, Tangshan 063210, Heibei, China;
[2]College Of Metallurgy And Energy, North China University Of Science And Technology, Tangshan 063210, Heibei, China;
[3]College Of Science , North China University Of Science And Technology , Tangshan 063210,Heibei,China;

Abstract: The foundation is based on the best way of study of the improved simulated annealing algorithm. Firstly, it improving the simulated annealing algorithm, optimizes the objective function .Secondly, it using the method of traffic capacity and road safety combined optimization, establish the optimization model. Thirdly, it carries on the analysis of data processing. It is concluded that safety and traffic capacity index proportion were 0.5953 and 0.4047 when the traffic effect is best. The lanes setting model is set up based on cellular automata. First of all, this paper chooses King, Snohomish, Thurston and Pierce the four city as the main research object. Then the main traffic routes around the state is looked up according to map. Finally by using cellular automaton analyzing it, it is concluded that King and Snohomish (Thurston and Pierce) in the self - driving accounted for less than 45% (50%), set up a special lanes for the best, more than 45% (50%), do not set the lanes to best.
Keywords: Simulated annealing algorithm; accommodation lane; optimization design; traffic result;

1. INTRODUCTION

Nowadays self-driving car technology becoming mature, it has become a lot of road management idea that introducing a self-driving car to road traffic. So the driverless cars, after the introduction of road lanes of the optimization design is of great significance.

In 2014, Tong Wencong studied bus lanes before and after the set of traffic parameters change, assessed bus lanes set of total capacity, time and cost of energy consumption before and after the change. In 2015, Wang Yatao studied electric vehicle lanes , and using the method of statistical analysis deduced the width of the electric bicycle lanes and formula of the number of lanes, and using the deduced the formula of Jiao Zuo Ying Bin road for the design of the electric vehicle lanes.

In this paper, the design of unmanned lanes were studied. In this paper, the design of unmanned lanes were studied. Using improved simulated annealing algorithm, the objective function was determined. Through the two index on the safety of road traffic capacity the optimization model was established. These aim to establish the lanes setting model based on cellular automata. As a result, the optimized design of lanes can be optimized.

2. THEORY OF CELLULAR AUTOMATA

2.1 the theoretical basis of the improved simulated anneealing algorithm

As a heuristic algorithm, the simulated annealing one includes the functions of state generation, state acception, temperature update, and internal circulation update, and the criteria of internal circulation termination and external circulation termination, the design of whose segments will decide the optimal performance of SA algorithm. The inferior solution can be accepted in a limited way and the tip-out superior solution is made possible to be used in a flexible way, but with a long time in problem-solution, the loss of the superior solution in the exploration, and the relative difficulty in defining the initial value and decreased step length of temperature T. In order for a superior solution, this paper focuses on the improvement of the traditional simulated annealing algorithm.

In the search process of algorithm, the intermediate superior solution will be in memorized and updated in a real-time way, making it an intellectualized algorithm, with the design of a new updated function of temperature. Its times of being accepted can be used to adjust the scale of temperature reduction, i.e., the self-adaptation. The establishment of dual threshold will simplify the process of computation in a state of superior solution. The improved SA algorithm involves the two phases as follows.

1) The improvement of the annealing process

Step1: The initial temperature is set to be t_0 ,with initial solution acquired in a random way. The superior solution is made to be B=S, with the current state of $s(0) = S, p = 0, i = 0;$

Step2: In the case of $t = t_i$,t, B, $s(i)$ is a sampling process of calling and improving parameters, with the

resumption of the acquired superior solution B_0 and the current s' and $s(i+1)=S'$

Step3: if f(B)≤f(B0),then P=P+1,else B=B0,P=0

Step4: In the process of temperature reduction,

$\beta = acceptnum/(\max step + acceptnum)$;

$t_{i+1} = e^{-\beta}$;i=i+1;

Step5: if $p \geq \max step1$ then goto step5 ; else gotostep2

Step6: B serves as the ultimate solution output, with the termination of the algorithm.

2.2 the establishment of the model of annealing algorithm

1) Solution space

Discritization treatment is conducted on the five simulated data groups of security (A), traffic capability (T), percentage in the rush hours (G), effect in the intersection (J), and road management (D) in a respective way, with the establishment of solution space.

In the case of the solution space of $s=\{s_1, s_2, s_3 \ldots s_n\}, s$ is a combination of what is possible.

2) The definition of conditions

The initial condition T_0 and the termination temperature T_f are defined,with the random choice of the initial state of $S=S(0)$.

3) The new function is defined.

Max:

$$f(t,v)=\frac{1}{N_t}\sum_{i=1}^{N_t} V_i(t)\cdot\rho_t+\frac{L_f+L_r}{v}+2\cdot RT+\frac{1}{2}\frac{(u-v)^2}{u\cdot f\cdot g}+C\delta$$

4)The choice process

Under temperature T and according to the state V of the current solution, the adjacent sub-aggregate of N(S) is produced, where a new state S' is acquired in a random way to become the candidate solution to the present one, with the computation formula of $f=f(S')-f(S_0)$.

5) The annealing process

A new temperature T is acquired according to a given method of temperature reduction, with T checked to see whether it is lower than the designated threshold value of temperature termination. The slower designated threshold value will mean the termination of the annealing process, with B as the ultimate output solution of the algorithm. The bigger threshold value will make it necessary to be transferred to the sampling process of Metropolis, a search state under the new temperature.

3. SOLUTION OF THE MODEL

3.1 the superion solution

We can get from the simulated annealing process as follows.

Performance	Metric correlation path
A	0.5953
T	0.4047

From the outcome of the annealing, we can see the best communication with the security index of 0.5953and the traffic capacity index of 0.4047 respectively, from which we can see the peak value of road traffic volume and the average one when self-driving cars make up a different percentage as is shown in the following table.

The percentage of self-driving cars(p_{fc})	Peak value	Average traffic flow
≥ 50%	53217.13	24150.94
≈ 50%	43100.19	17569.29
30% ≤ p_{fc} ≤ 50%	20503.221	16627.91
≤ 30%	17241.38	9862.67

3.2 the design of specialized lanes based on cellular automation

With the employment of the principle of cellular automation, we can assume that specialized lanes are intended for self-driving cooperating cars while the ordinary lanes intended for both what is mentioned before and manned cooperating cars. The four lanes under this research are divided according to the four zones. In the case of 2 lanes, and the designation of specialized lanes, both kinds of lanes will be given a simulated analysis of one-lane wheel value, otherwise the simulation will be conducted according to multi-lane wheel value. In the case of over 2 lanes, the ordinary lanes will be given the analysis in accordance with the multi-lane model and the specialized ones according to one-lane wheel value.

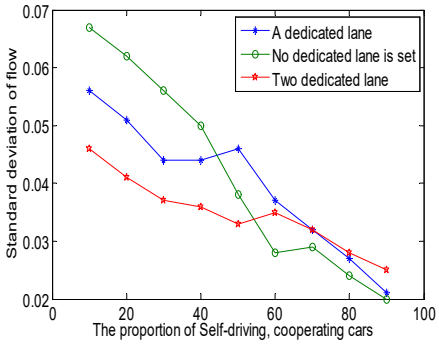

Figure 1 The situation Map of Road Traffic in the City of King

Let's conduct an analysis of the road traffic in the city of Snohomisch as is shown in Fig.2 With their percentage of less than 55%, the designation of two specialized lanes is the preferred one. In the case of the percentage of over 55%, it is advisable not to designate specialized lanes.

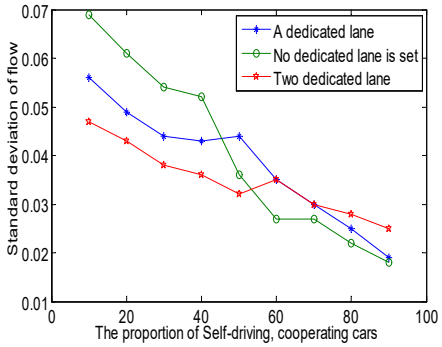

Figure 2 The situation Map of Road Traffic in the City of Snohomisch

Let's conduct an analysis of the road traffic in the city of Thurston as is shown in Figure 20. In the case of no specialized lanes for self-driving cooperating cars, the designation of a specialized lane will render us a decrease of the standard deviation of average traffic volume with the increase of the percentage of self-driving cooperating cars. With their percentage of less than 45%, the designation of one specialized lane is the preferred one. In the case of the percentage of over 45%, it is advisable not to designate specialized lanes.

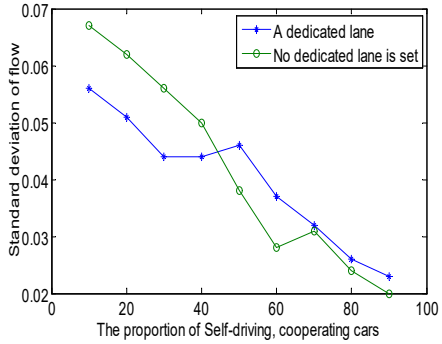

Figure 3 The situation Map of Road Traffic in the City of Thurston

Conduct an analysis of the road traffic in the city of Pierceas as shown in Fig.4. In comparison with Thurston, Pierce indicates a similar emulational result. With their percentage of less than 45%, the designation of one specialized lane is the preferred one. In the case of the percentage of over 45%, it is advisable not to designate specialized lanes.

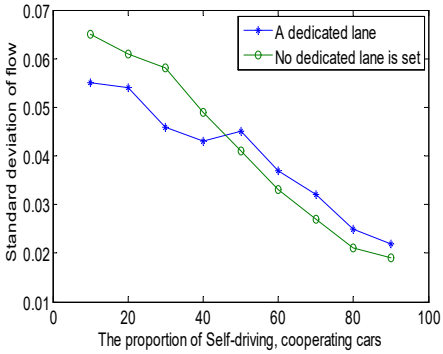

Figure 4 The situation Map of Road Traffic in the City of Pierce

REFERENCES

[1]Tong Wencong, Liao Fang. Evaluation on Comprehensive Benefits of Exdusive Bus Lane Setting:Taking Jingtong Expressway as an Example[J]. Urban Transport of China,2014,(06):63-69.

[2]Wang Yatao,Li Xianghong,Song Huiying. A Preliminary Study of Electric Bicycle Lanes Design Methods[J]. Highway Engineering,2015,(01):270-274.

[3]Portal G M, Ritt M, Borba L M, et al. Simulated annealing for the machine reassignment problem[J]. Annals of Operations Research, 2016, 242(1):1-22.

[4]Lanza M, Gutierrez A L, Perez J R, et al. Coverage Optimization and Power Reduction in SFN Using Simulated Annealing[J]. IEEE Transactions on Broadcasting, 2014, 60(3):474-485.

[5]Atiqullah M M, Rao S. Parallel processing in optimal structural design using simulated annealing[J]. Aiaa Journal, 2015, 33(12):2386-2392.

[6]Los J H, Gabardi S, Bernasconi M, et al. Inverse simulated annealing: Improvements and application to amorphous InSb[J]. Computational Materials Science, 2016, 117:7–14.

Modeling and Simulation of Robot Spraying

Ping Huo[1], Lai Wei[1], Aimin Yang[2]*
[1]College of Mechanical Engineering, North China University of Science and Technology, Tangshan 063210, China
[2]College of Science,North China University of Science and Technology,Tangshan Hebei,063210,China

Abstract: The spray model is the basis for spray trajectory optimization, which reflects the accumulation of paint on the surface to be sprayed. In this paper, a modeling method of torch model and its application in plane spraying trajectory optimization are studied. According to the physical model, a simplified mathematical model is used to describe the flow distribution function of the paint flow in the torch flow field. And from the above function, further obtained the spray coating deposition equation. According to the simulation experiment and the actual spraying of the data were compared to prove the correctness of the model.
Keywords: spray-painting; off-line programming; simulation

1. INTRODUCTION

In the sanitary ceramics production process, glazing technology is the key.China's ceramic industry is now widely used in the way of artificial glazing, hand glaze and the operator's proficiency, operating habits, and even emotional factors are directly related to product quality is difficult to guarantee, Workers labor intensity, but also on human health damage [1-2]. In other countries, the robot glaze has become a more mature technology, but also the ceramic production process easier to achieve automation links [3]. As of the end of 1998, the world's active spraying robot 25122 units, in general, the robot spray has a more extensive application abroad, and has a good effect[4].

One of the problems that must be solved with the use of robots is how to teach the glazed robots. The existing spray production lines, robots generally use manual teaching, this method is a lot of defects, the use of less flexible [5-6]. Therefore, it is necessary to carry out effective guidance on teaching and mapping, that is, it is necessary to carry out spray trajectory planning. The important problem to be solved by spray trajectory planning is that when the robot moves in a certain trajectory in its working space, Glaze accumulation, which requires studying the spatial distribution model of the spray moments and determining the glaze action of the robot according to this model.

In this paper, through the study of the physical characteristics of the torch, a mathematical model is established to describe the physical characteristics of the spray gun, the glaze and the influence of the various changes in the spraying process on the spray.To study the distribution of the surface flow at any point on the torch The establishment of the model will make it possible to describe the spraying process mathematically, which can lay an important foundation for the development of the offline teaching system.

2. THE SPATIAL DISTRIBUTION MODEL OF GLAZE

In order to design an optimal spray trajectory for each specified surface, it is first necessary to know the coating growth rate (um / s) at any point on the work piece, that is, the gun model, since the gun model determines the thickness of the coating on the surface Distribution, therefore, the first step in the study of the spraying process is to establish a corresponding surface of the gun mathematical model. In the broad sense, the gun model is relative to the plane. To establish the coating growth rate model on the plane, we must first consider the influence of spraying characteristics, spraying equipment and the spatial distribution of the coating. On this basis, To create a simple and practical spray model.

2.1 spraying characteristics and the impact of spraying equipment

The characteristics of the torch directly affect the distribution of the coating, because the spraying effect by a number of factors: such as the complexity of the workpiece surface, the gun position and the distance from the workpiece surface. By studying the characteristics of the torch to find a more accurate model of the spatial distribution of the coating, we can study the distribution of the coating surface of the complex free surface, so as to further optimize the gun trajectory. Here the plane spray characteristics for the study. Spraying equipment has a great influence on the characteristics of the torch. The main influencing factors are spray gun and nozzle. The cross section of the torch formed from the nozzle is generally circular and has the same coverage in all respects. The current spray gun angle is generally less than 600, and high efficiency, good operating performance, can be sprayed with sticky and quick-drying paint, both can achieve uniform and beautiful results. This torch is generally isotropic, that is, the torch in the cross-section in all directions are the same nature, where the isotropic torch as the object of study.

2.2 the influence of the spatial distribution of coatings

The process of spraying is a very complicated process. In order to analyze it scientifically, a series of hypotheses are established according to the need of

research, and a mathematical model is established to describe the spraying process.

(1) Jet continuity hypothesis

According to the test, most of the nebulizer generated droplets are in microns, that is, their diameter is relatively small. Experimental and theoretical data show that the spray gun produces an average droplet diameter of less than 100 μm . For such dense and small particles, we can think that the jet is continuously distributed on a macro scale. The concentration of the coating depends on the spatial distribution function of the torch. This assumption is consistent with the actual situation, but also can simplify the establishment of mathematical model.

(2) Influence factor hypothesis

The establishment of the spatial distribution model of paint is the first problem to be solved in the mathematical modeling of spraying. The influence factors of the space distribution model are: gun, air, nozzle and nozzle. Changing any of the factors will affect the spatial distribution of the coating, this paper assumes that its influencing factors remain unchanged.

At present, some scholars have carried out a series of studies on the spatial distribution of coatings, for instance： β distribution model, double β elliptic distribution model and finite range model. In this paper, the spray pattern of spray glaze from the spray pattern, combined with the diffusion characteristics of the coating particles to simulate. According to the results of the existing tests, the thickness of the torch sprayed within the θ range is uniform. The presence of this spray pattern is premised on the moderate pressure, the smaller the opening angle of the spray and the good atomization. As shown in Figure 1.

The nonuniform part of the spray pattern is determined by a number of factors, which are generally considered to be due to the diffusion of particles, that is, the result of free movement. In the process of free movement and diffusion, the uniform and nonuniform parts of the spray pattern and the contours of the surface of the workpiece should be continuous, where we simulate with a function as shown in Figure 2.

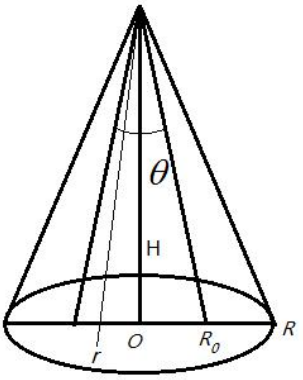

Figure 1 Spatial distribution model for coatings

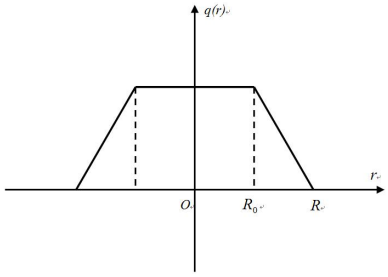

Figure 2 Coating growth rate model

Thus, the following equation is obtained：

$$q(r)\begin{cases} A & 0 \le r \le R_0 \\ A \cdot \dfrac{R-x}{R-R_0} & R_0 < r < R \end{cases} \tag{1}$$

$q(r)$ indicates the ratio of the thickness of the coating to the A at the point r from the torch axis, and R_0 represents the radius of the coating to a uniform range, and R represents the radius of the coating coverage

In Figure2.1, $R_0 = H\tan(\theta/2)$.The weight of the coating is measured according to the different gun test, which indicates that the coating thickness is uniform within the range of the spray angle θ and the thickness of the coating outside R is 0.

In the actual spraying process, it is necessary to obtain the thickness of the coating required for the surface of the workpiece, using mathematical formulas to describe it more intuitive. Taking into account isotropic, the flow Q on the entire cross section is:

$$Q = \frac{1}{3}\pi A(R_0 + R)^2 \tag{2}$$

So

$$A = \frac{3Q}{\pi(R_0 + R)} \tag{3}$$

The formula for calculating the coating thickness per unit time is:

$$q(r)\begin{cases} \dfrac{3Q}{\pi(R_0+R)} & 0 \le r \le R_0 \\ \dfrac{3Q}{\pi(R_0+R)} \cdot \dfrac{R-r}{R-R_0} & R_0 < r < R \end{cases} \tag{4}$$

The above coating thickness equation is calculated by the spatial distribution model of the primary function. Therefore, the thickness unevenness is continuous from thick to thin, which fully reflects the process of diffusion of paint molecules in the actual spraying process.

3. SPRAY SIMULATION EXPERIMENT

Based on the modeling of the plane spray gun model in the previous section, the rationality and validity of the model of the gun model are verified by the simulation of the coating distribution at any point on

the plane.

Assume that the gun moves at a constant speed along the straight line and remains at a constant distance from the work plane. According to the right hand theorem, the direction perpendicular to the x-axis on the plane is the y-axis. If the amount of spray on the plane is set to z-axis, the three-dimensional Displayed as a bottom radius of R_o, the bottom of the radius of R, high A cone of Figure3 (3.1).

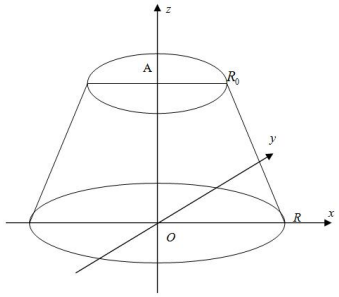

Figure 3 Schematic diagram of spraying

Figure 4 in the gun moving process, the spray range from the torch center *r* is equivalent to the point from the *a* into the spray area, from the *b* point away from the spray area.

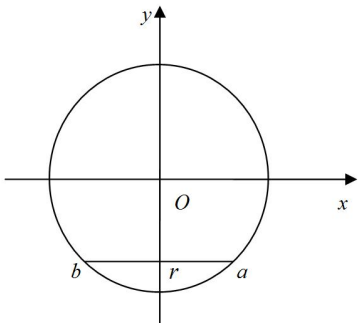

Figure 4 overlooking the diagram

The cumulative thickness of the point is the cumulative thickness of all points on the straight line ab, that is

$$Q_r = \int_s^e q(r)dt \tag{5}$$

Q_r for the cumulative thickness of r points, s into the spray range of time, e to leave the spray range of time. The value of which corresponds to the cross-sectional area cut in the vertical direction at a distance r from the center of the cone in Figure 3. According to the definition of the parabola, the cross-sectional shape is a parabolic and a line segment consisting of:

$$S = \frac{2}{3}lh \tag{6}$$

l for the length of the line, h is the parabola vertex to the line distance. Set the gun to move the speed of v, by the formula 4,5,6 get

$$Q = \begin{cases} \frac{8}{3}A\sqrt{R^2-r^2}\cdot\frac{R-r}{R-R_0}\cdot\frac{\sqrt{R^2-r^2}}{v} & R_0 \le r \le R \\ \frac{8}{3}A\cdot\left(\frac{R-r}{R-R_0}\sqrt{R^2-r^2}-\frac{R_0-r}{R-R_0}\sqrt{R_0^2-r^2}\right)\cdot\frac{\sqrt{R^2-r^2}}{v} & 0 \le r < R_0 \end{cases} \tag{7}$$

When $R=5, R_0=2, A=1, v=1$, by using Matlab, get simulated spray effect shown in Figure 5.

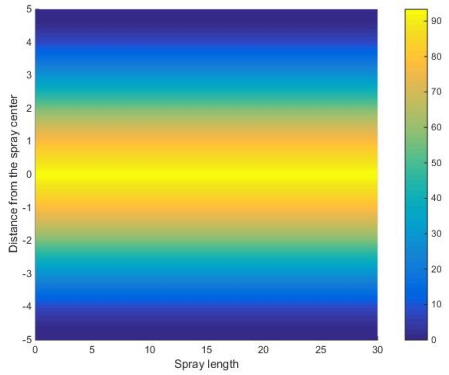

Figure 5 Simulation of the spray effect when $v=1$

When $v=2$, other conditions remain unchanged

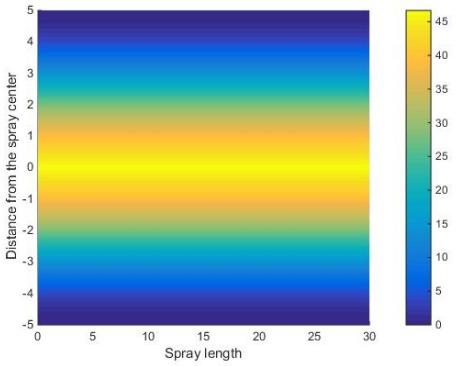

Figure6 Simulation of the spray effect when $v=2$

In this paper, the gun model can describe the actual spray pattern of the gun to a certain extent, which verifies the feasibility of the model modeling method.

REFERENCES

[1]Sun Zengqi, Robot intelligent control, Shanxi education press: 1995.

[2]Wang Xichun, Jiang Yingtao, Painting Technology (First Book General),Chemical Industry Press,1986.

[3]Jackie Neider, Tom Davis, Mason Woo, OpenGL Programming Guide, Silicon Graphics, Addis on-Wesley Publishing Company. 1993.

[4]Wang Zhenbin , Zhao Dean, Wang Yan, A Discussion on the Off-Line Prog ramming System for Painting Robots, Journal of Jiangsu University of Science and Technology(Natural Science),2000, 21(5):78-82.

[5]Lefebver H, Atomization and Sprays, Hemisphere Publishing Corporation, 1989.

[6]Klein A, CAD-based of f-line programming of painting robots, Robotica, 1987, 5(4): 267- 271.

Research on Temperature Control of Zinc Plating Technology Based on Fractional PID System

Leijie Shen[1],Jianhui Wu[2],Hao Men[3],Shichao Yu[3]*
[1]Yisheng College, North China University of Science and Technology, Tangshan,063210, China
[2]School of public health, North China University of Science and Technology, Tangshan,063210, China
[3]School of Electrical Engineering, North China University of Science and Technology, Tangshan, 063210, China

Abstract: The construction and solution of the calculus equation model of the PID controller are of great significance to improve the temperature and field response speed of the combustion chamber of the cold-rolled galvanizing line. Based on the classical integer-order PID control system, a fractional-order PID control system model suitable for temperature control is constructed by studying the combustion process and combustion mechanism of the passivation process of cold-rolled galvanizing line. The adaptive quantum Genetic algorithm is used to analyze and calculate the parameters of the fractional PID controller. The verification results show that the parameters after the setting can improve the accuracy of the combustion chamber temperature and the speed of the field response, which is of great significance to improve the finished product rate of cold rolled galvanized sheet.
Keywords: temperature control; classical PID control system; fractional-order PID controller; adaptive quantum genetic algorithm

1. INTRODUCTION

Cold-rolled galvanizing line passivation process Combustion chamber temperature control process, strip temperature control is cold rolling galvanized production line in the passivation of the key. With the development of control theory, there are various branches, such as fuzzy control [1], neural network [2] and so on, which are combined with [3] the classical PID control and derived a variety of new PID controller. He Yiwen et al. [4] applied the ideal transfer function to the design of the fractional order controller and the parameter setting of the fractional order controller. The experiment proved that the model is not only suitable for fractional order objects but also for integer order objects. Zhang Yanzhu et al. [5] studied the parameter optimization of fractional order controller by fractional order system, and they selected the absolute error integral model as the performance index. Based on the genetic algorithm, the adaptive crossover probability and the mutation probability order controller parameters are optimized, the optimized parameters greatly improve the performance of the system.

Based on the previous researches, this paper studies the integer-order PID control model and establishes the fractional-order PID control model, and the adaptive quantum genetic algorithm is used to solve the model, so as to provide technical support for improving the yield of cold rolled galvanized sheet.

2. CLASSIC PID CONTROL SYSTEM

2.1Structure and Principle of Classical PID Control System

PID controller is an effective and simple control algorithm based on information deviation estimation. The routine control system schematic diagram is shown in the following Fig1.

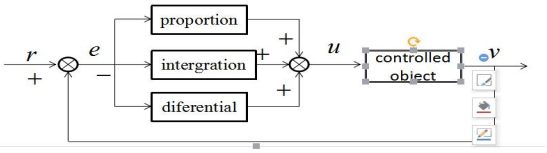

Figure 1 Schematic diagram of the classic PID control system

The PID controller composes the control deviation according to the given value SV and the actual output value PV, and then controls the controlled object by adjusting the deviation proportionally, the integral and the derivative through the linear combination to form the control quantity. The ideal algorithm for obtaining the PID controller from Fig. 1 is:

$$u(t)=K_p\left[e(t)+\frac{1}{T_i}\int_0^i e(t)dt+T_d\frac{dr(t)}{dt}\right] \quad (1)$$

Among them, Kp..Ti ,Td, respectively, said PID controller proportional gain, integration time constant and differential time constant.

2.2 PID controller parameter analysis

(1)The effect of proportional effect on control performance

The proportional gain Kp is introduced in order to reflect the deviation of the control system in a timely manner.

With the increase of the proportional coefficient Kp, the overshoot increases, the system response speed is accelerated, and the steady-state error is reduced, but

the steady-state error can not be eliminated. If Kp≥ 19, the system step response curve becomes divergent, closed-loop system is unstable. That is, the infinite increase in the scale factor Kp causes the system to become unstable.

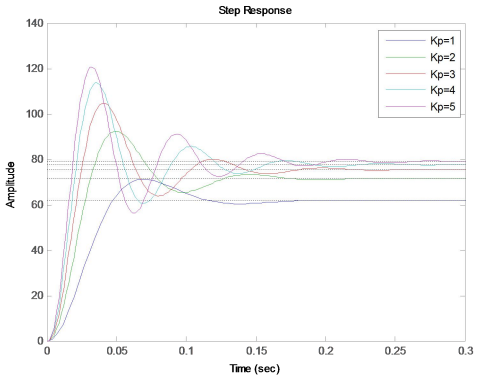

Figure 2 Effect of proportional coefficient Kp on control performance

(2)Effect of integral effect on control performance

The introduction of the integral effect is to make the system eliminate the steady-state error, improve the system's no difference, to ensure that there is no static tracking of the set value.

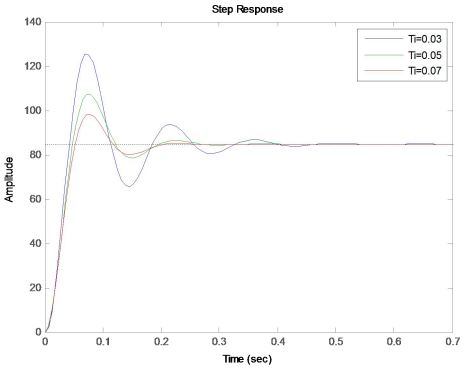

Figure 3 Effect of integral time constant T_i on control performance

The smaller the integral effect of the stronger, otherwise the big points of the role of weak. However, the decrease in Ti value may result in an increase in the overshoot of the system and may slow the system response to steady-state values.

(3)Effect of Differential Function on Control Performance

The introduction of differential effects is mainly to improve the response speed and stability of the control system. The differential action can reflect the change law of the system deviation, predict the trend of deviation change, so it can work for advanced control effect.

With the increase of the differential time constant Td, the response speed of the closed-loop system response is accelerated and the adjustment time is reduced. However, since the link is a derivative of the error (that is, the error rate of change takes effect), excessive Kd values can cause problems due to system delays or long delays in the controlled object. In addition, the differential link does not work for systems where the signal does not change or slows down.

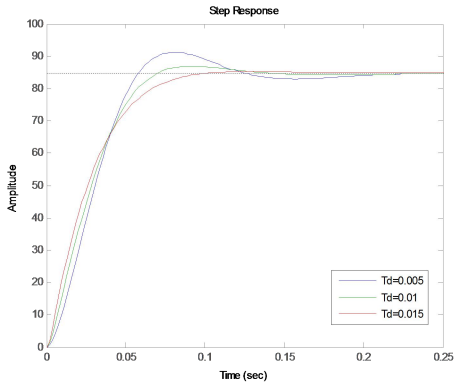

Figure 4 Effect of differential time constant Td on control performance

3.FRACTIONAL ORDER SYSTEM AND FRACTIONAL ORDER $PI^{\lambda}D^{\mu}$ CONTROLLER

3.1Introduction to Fractional Control System

Fractional-order control system refers to the controller using fractional order differential or integral characteristics to describe the dynamic characteristics of the system model. In this paper, we study the linear continuous fractional order system. The general form of the differential equation is:

$$a_n D^{\beta_n} y(t)+a_{n-1} D^{\beta_{n-1}} y(t)+\cdots+a_1 D^{\beta_1} y(t)+a_0 D^{\beta_0} y(t)$$
$$=b_n D^{\alpha_n} u(t)+b_{n-1} D^{\alpha_{n-1}} u(t)+\cdots+b_1 D^{\alpha_1} u(t)+b_0 D^{\alpha_0} u(t) \quad (2)$$

First of all, we need to assume that equation (3) can meet the initial conditions of zero, with Laplace to change it, the transfer function described in the system can be obtained as follows:

$$G(s)=\frac{b_m s^{\beta_m}+b_{m-1} s^{\beta_{m-1}}+\cdots+b_0 s^{\beta_o}}{a_n s^{a_n}+a_{n-1} s^{a_{n-1}}+\cdots+a_0 s^{a_0}} \quad (3)$$

Also $G(s)$ is described as fractional transfer function

3.2 Description of Transfer Function of Fractional Order Controller

Professor Podlubny first proposed the concept of fractional-order PID controller, λ is the differential order, μ is the integral order. Because of these two adjustable parameters, so the controller parameter tuning area to the previous "point" into the current " surface", so that the controller can be more flexible to control the controlled object. Similar to the integer order PID control structure, Fig.5 describes the structure of the fractional PID controller block diagram.

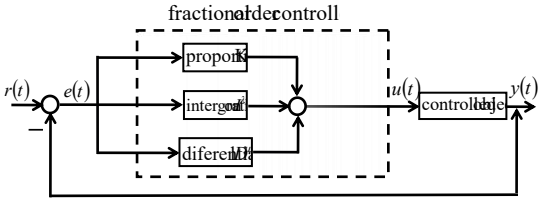

Figure 5 Structure of the fractional order $PI^{\lambda}D^{\mu}$ controller

In the Fig5, the PID controller is represented by $C(s)$, and the controlled object model is represented by $G(s)$, and its transfer function is as shown in equation (3)

$$C(s)=K_P+\frac{K_1}{s^{\lambda}}+K_D s^{\mu},\ (\lambda,\ \mu\in N^*) \tag{4}$$

4. FRACTIONAL - ORDER PID PARAMETER TUNING BASED ON PARALLEL QUANTUM GENETIC ALGORITHM

The parameter tuning of a fractional-order PID controller can be viewed as a multi-objective optimization problem, which is intended to compromise between the speed and stability of system control.

On the basis of the basic quantum genetic algorithm, the parallelism thought is added, and all the individuals are divided into several independent subpopulations according to certain topological structure. The multi-state gene quantum bit coding method is used to express the individuals in the subpopulation. Best immigration and quantum cross-operation to exchange information between sub-populations [4], by designing a reasonable objective function to set the parameters. Parameter tuning method steps are as follows [5]:

Step 1: Initialize the randomly generated population $Q(t)=\{q_1^t,q_2^t,\cdots,q_n^t\}$. q_j^t is the j-th quantum chromosome in the t-th population, and the quantum number of q_j^t is in the form

$$q_j^t=\begin{bmatrix}\alpha_{j1}^t & \alpha_{j2}^t & \cdots & \alpha_{jm}^t\\ \beta_{ji}^t & \beta_{j2}^t & \cdots & \beta_{jm}^t\end{bmatrix},\ (j=1,2,\cdots,n) \tag{5}$$

n is the number of quantum chromosomes in the population; m is the number of quantum bits that make up the quantum chromosome.

Step 2: The corresponding binary solution $P(t)=\{x_1^t,x_2^t,\cdots,x_n^t,\}$ (quantum collapse) is obtained by the state of the individual in $Q(t)$, where $x_j^t=\{x_{j1}^t,x_{j2}^t,\cdots,x_{jn}^t,\}$ is a binary string of length m (representing three optimization parameters), which is generated by generating a random number between 0 and 1 R, if $|\alpha_{jk}^t|>r$, then take $x_{jk}^t=1$, otherwise take $x_{jk}^t=0$.

Step 3: Each of x_j^t in $P(t)$ is converted into a real value of within the range of[5] the corresponding variable, and the individual fitness evaluation function is defined to calculate the fitness for each chromosome.

$$f(q_j^t)=\frac{1}{w_{1\sigma}+w_2 t_r+w_3\sum_{k=1}^{n_s}\frac{|e_k|}{n_s}} \tag{6}$$

Where $\sigma=|y_p-y_{ref}|/y_{ref}\times 100\%$ is the overshoot of the system, yp is the output peak, yref is the input reference value; tr is the rise time; $e_k=y_k-y_{ref}$ is the output error of the sampling time k, ns is the number of sampling points. For the actual PID design problem, the weighting coefficient wi of each of the denominator of the fitness function can be adjusted to obtain a PID controller with different control performance according to the specific requirements of the system.

According to Eq. (6), the fitness value of each chromosome in the current population is calculated. After comparison, the best individual is found, and the corresponding binary of the best individual is stored in $B(t)=\{b_1^t,b_2^t,\cdots,b_n^t,\}$. If the termination condition is satisfied, the algorithm will be terminated, otherwise continues.

Step 4: Q(t) is updated by the quantum revolving door $U(\Delta\theta_i)$, according to the $\begin{bmatrix}\alpha_i'\\ \beta_i'\end{bmatrix}=U(\Delta\theta_i)\begin{bmatrix}\alpha_i\\ \beta_i\end{bmatrix}$ and rotation angle method [5].

x_{jk}^t and b_{jk}^t are the k-th positions of the solution x_j^t and the current optimal solution b_j^t, respectively, $f(x_j^t)$ and $f(b_j^t)$ are their fitness function, $\Delta\theta_k$ is the rotation angle, and the convergence rate of the control algorithm. $s(\alpha_{jk}^t\beta_{jk}^t)$ is the direction function of the rotation angle. Fig.6 is a schematic representation of a quantum revolving door acting on a qubit.

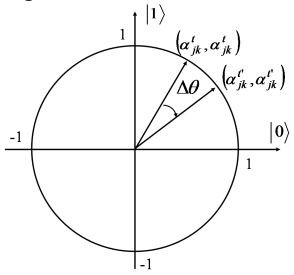

Figure 6 Quantum revolving door

Step 5: Let t = t + 1 and return to step 2.

5. CONCLUSIONS

The theory of fractional calculus is introduced into the design of PID controller to extend and amplify the control flexibility, robustness and anti-jamming of PID controller. The idea of applying adaptive quantum genetic algorithm to controller parameters is proposed. By defining the fitness function including the system output overshoot, rising time and steady-state error index, the above-mentioned index terms are weighted according to the actual performance requirements of the control system, and we can obtain the approximate optimal PID parameters satisfying different performance requirements , to achieve automatic PID controller parameters set.

REFERENCES

[1]Zhang Yanzhu, Ge Zheng, Wang Yanmei. Parameter Optimization of Fractional Order System Based on Adaptive PID Controller[J]. Journal of Shenyang University of Technology. 2015.34(2):6-12.

[2]Chen Xinglin, Chen Zhenyu. Design of long - range linear motor control system based on fractional - order PID and internal model[J]. Journal of Tianjin Polytechnic University, 2016,01:59-64.

[3]Li Shanshan, Zhao Chunna, Guan Yong, Shi ZhiPing, Wang Rui, Li Xiaojuan, Ye Shiwei. The Verification of the Consistency of Fractional Calculus Definitions in HOL4[J] .computer science, 2016,03:23-26+53.

[4]HAN K H,PARK K H,LEE C H,et al.Parallel quantum-inspired ge-netic algorithm for combinatorial optimization problem[C]Proc of IEEE Congress on Evolutionary Computation.2001: 1422-1429

[5]Zhang Xinghua, Zhu Xiaorong, Lin Jinguo. Parameter Self - tuning of PID Controller Based on Quantum Genetic Algorithm[J] Computer Engineering and Applications, 2007,(21):218-220+241.

Research on Optimization of Iron and Steel Sales Logistics Network based on Genetic Algorithm

Wenrui Wu[1],Xingjun Luo[1] ,Di Zhang[1],Yunhua Qu[2],Liya Wang[3]*
[1]College of Mining Engineering,North China University of Science and Technology,Tangshan Hebei,063210,China
[2]Qian'An College,North China University of Science and Technology,Tangshan Hebei,063210,China
[3]College of Science,North China University of Science and Technology,Tangshan Hebei,063210,China

Abstract: the iron and steel industry is the basic industry of our country's economic development, and also is an important symbol of the level of industrialization of a country. But at present, China's steel industry has entered a high cost, low profit status. Therefore, in order to build an effective steel sales logistics network to reduce the cost of steel sales logistics, improve customer satisfaction. This paper has primary finished steel sales logistics network node based on constructed with a lowest cost goal programming, is solved by genetic algorithm, finally selects the most appropriate logistics nodes, and factory to transport path between logistics nodes and the corresponding transportation volume, logistics transportation paths between nodes to customer with the corresponding traffic.
Keywords: Iron and steel logistics; network node; genetic algorithm

1. INTRODUCTION

Steel is the pillar industry of a country, is also a comment on a country's comprehensive national strength is strong or not important standard, is the foundation of a country.Modern steel supply chain upstream of the iron and steel enterprises in China due to reduced production reduction of living space and the compression steel circulation enterprises step by step. Market surplus and steel price transparency, making a large number of steel trade logistics enterprises due to decline can not bear high inventory caused by market losses frequently. The existence and development of the iron and steel trade logistics enterprises are facing many problems. Today, in order to save the cost of steel enterprises in the labor and production costs, it is only in the sales of logistics, there are still many places can be compressed. According to the data show that China's iron and steel industry logistics rate is 11%, and Japan iron and steel logistics cost only 6.2%. Compared with Japan, China's iron and steel enterprises is still higher than 5 percentage points, if China's iron and steel industry can reach the level of Japan, will lower the cost of three, China's iron and steel cost and great compression space. At the same time, according to some steel logistics cost accounting to found that the iron and steel enterprise logistics costs more than 70 one hundred million yuan[1], accounting for 18% of the steel finished goods sales, it can save logistics cost of nearly 300 million a year by improving the enterprise logistics management and logistics distribution ,it is feasible to reduce the cost and make use of this method.

At present, the competitiveness of iron and steel enterprises to improve service and sales innovation , sales logistics can not only provide services to the downstream industry chain, but also can make the sales model of success. By constructing a perfect and reasonable sales network, to improve the iron and steel company service, contribute to fewer sales in the process of logistics cost, but also help to iron and steel enterprises develop value-added services, so that the logistics center into a profit center.To narrow the distance between customers and understand the needs of customers., from a single mode of production to the consumer to guide the production model, improve the service level of enterprises, enhance the core competitiveness of enterprises.

In the sales logistics network, the logistics node plays an important role, logistics network can play the maximum value, the logistics node is the basic. Therefor correct construction of iron and steel sales logistics network nodes location is a decisive factor.The development of iron and steel logistics direction has a lot of.,sales logistics is a good entry point ,at the same time, the improvement of sales logistics network is the key to make sales logistics change from cost center to profit center, and sales logistics network can be low-cost, efficient operation and reasonable node location.Therefore, to achieve the purpose of steel enterprises to get rid of the difficult situation, it is necessary to conduct in-depth research on the steel distribution logistics network node location, which is the core of this paper. Therefore, to achieve the goal of iron and steel enterprises out of trouble ,need to steel logistics network node location for in-depth study .These are also the core of this paper.

At present, the domestic and international research on the iron and steel logistics are mainly based on the production logistics.About the logistics network

problems, Liu He, Wang Jian, study on the ideas and methods of regional logistics hub and spoke network construction, from the level of social and economic development, logistics market supply and demand and infrastructure construction three aspects to build the hub node selection index system [1];Wang Xinlei analysis evaluation of comprehensive strength of the research unit of the index and determine the different levels of the city center through the establishment of evaluation index system of logistics network,according to the weighted average travel time and estimate the time cost of node to the logistics center, choose urban radiation scope of axis of potential model partitioning, build the central regions "axis - spider" logistics network system[2]; Li Tong and Wang Zhongtuo established[3] tree underground logistics network layout model China large city expanding this characteristic by Steiner 's minimum tree (SMT) as the theoretical model

On the node layout problem,Wang Lingdeng using enumeration method and greedy optimization algorithm combined method solves the preset position set in the relay node can act as a relay node in the set position,a reasonable choice of relay node location and storage network for relay nodes to add new sensor nodes caused by the additional problem[4].Wang Qi Zhu king in view of the present layout algorithm overlooked relay relay node communication capacity and network problem such as the overall energy consumption, the communication path irreversible and the relay node communication capacity and other constraints into existing relay node layout model, and proposed evaluation based communications network layout algorithm minimum distance factor of the new standard[5]; GeXiJun adopt qualitative analysis and quantitative evaluation method of combining the research of urban logistics node layout[6].

At present the study of iron and steel sales logistics mainly focus on steel sales logistics supply chain, iron and steel sales logistics mode such as qualitative, iron and steel sales logistics information management research,and the quantitative research on steel sales logistics is less

2.OPTIMAL LOCATION DECISION MODEL BASED ON GENETIC ALGORITHMS

Of iron and steel sales logistics network node location in addition to consider by choosing whether to conform to the long-term development of the iron and steel logistics nodes, while also considering the build the node does not reduce the cost of the sales logistics network, is not able to meet customer service. In actual steel logistics network can usually selected in advance in some locations as the initial network node, through certain conditions and algorithm between the nodes establish logistics network, in order to achieve the required for the actual operation.

2.1 Site selection model construction

Figure 1 is the iron and steel sales logistics network simplified, the figure shows the level of a single logistics network. The supply point in the diagram indicates that the iron and steel enterprise's production base, the demand point is the downstream customer of the iron and steel enterprise. Iron and steel enterprises downstream customers that demand and more dispersed, and away from the production base from, so the points contained in the region as a demand, the demand within the region all the scattered the sum of the demand.

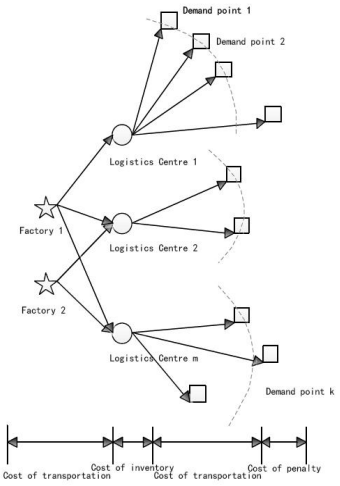

Fig.1 Logistic network schematic diagram

Aiming at the actual situation of the iron and steel enterprises, iron and steel enterprises will generally have a production base, production base of each will produce different kinds of products, and for iron and steel enterprises downstream customers, the quantity of different kinds of different customer needs are not the same, and different stock of finished products into the not the same, so for the iron and steel enterprises of the actual situation in this paper for computing the total cost of iron and steel sales logistics network give full consideration to the iron and steel production product kinds of factors. The main considerations in the total cost of the iron and steel sales logistics network such as shown in Figure 4, the transportation cost, inventory cost, operation cost and penalty cost, which cost penalty is that when the distance between the demand for logistics service node points more than optimal service radius outside, logistics node will because of distance and the existence of the loss of all kinds of hidden beyond the, paper is to punish cost to represent.

The construction of iron and steel sales logistics network node is to timely meet the needs of customers, so customer satisfaction as steel sales logistics network considering the target node location. While customer satisfaction reflects the way mainly has two kinds, one is the time factor, the response time is the steel sales logistics node to customer needs. Another is the coverage factor, in order to reflect within steel sales logistics node optimal service radius steel output coverage. Because the

response time is needed to test the calculation related to a variety of factors, and each time related factors to simplify, this will lead to response time results is not accurate, so papers in this paper to cover the amount of to reflect the level of customer service.

The analysis can determine the problems needed to be solved at this stage is the selection of the final location of the iron and steel sales logistics nodes, determine the number and different product supply, logistics nodes and demand between transportation route and traffic.

2.2 model assumptions

In order to facilitate the establishment of the model, make certain assumptions, assuming the system to meet the following conditions:

● The inventory of the steel distribution logistics node can meet all the requirements of the service area.

● The demand for a finished product is only provided by an iron and steel logistics node

● The production and demand of the finished product plant is constant and the value is known.

● The factory production of different types of each product, the yield is known and the variety of finished goods

● It has many types of each demand point to the demand for finished goods, finished goods and a variety of known demand

● The unit cost of transportation product value, the different modes of transport unit transportation cost difference

● The products of different types, the unit inventory for each product cost is different

● The finished goods transport costs and transport distance and volume is proportional

● A transport demand products to complete the demand point

● The calculation of the logistics cost, without considering the cost of loading and unloading cost

2.3 Mathematical Modeling

Objective function:

$$\max Z_2 = \sum_{r=1}^{p}\sum_{j=1}^{n}\sum_{k=1}^{q} p_{rjk} V_{jk} \tag{1.4}$$

$$\begin{aligned} \min Z_1 = & \sum_{r=1}^{p}\sum_{i=1}^{m}\sum_{j=1}^{n} c_{ro}\cdot d_{rij}\cdot p_{rij} \\ & + \sum_{r=1}^{p}\sum_{i=1}^{m}\sum_{j=1}^{n} r_{rj}\cdot p_{rij} \\ & + \sum_{r=1}^{p}\sum_{j=1}^{n}\sum_{k=1}^{q} c_{ro}\cdot d_{rjk}\cdot p_{rjk} \\ & + \sum_{i=1}^{n} C_j\cdot\theta_j \\ & + \sum_{r=1}^{p}\sum_{j=1}^{n}\sum_{k=1}^{q} \max\left\{d_{rjk}-D_j,0\right\}\cdot u_{jk}\cdot p_{rjk} \end{aligned} \tag{1.3}$$

2.4 Model Interpretation

Goal 1 equation (1.3) represents the lowest total cost of logistics system operation. There are an integral part of transportation costs, inventory costs, operating costs and the cost of punishment.

transportation cost : $\sum_{r=1}^{p}\sum_{i=1}^{m}\sum_{j=1}^{n} c_{ro}\cdot d_{rij}\cdot p_{rij} + \sum_{r=1}^{p}\sum_{j=1}^{n}\sum_{k=1}^{q} c_{ro}\cdot d_{rjk}\cdot p_{rjk}$ show the total transport cost of r kinds of products from the factory i to the logistics center j, and then from the logistics center j to the total transport cost of demand point k.

Inventory cost: $\sum_{r=1}^{p}\sum_{i=1}^{m}\sum_{j=1}^{n} r_{rj}\cdot p_{rij}$ represents the total cost of r products in the logistics center j.

Logistics node operation cost: $\sum_{i=1}^{n} C_j\cdot\theta_j$

Penalty cost: $\sum_{r=1}^{p}\sum_{j=1}^{n}\sum_{k=1}^{q} \max\left\{d_{rjk}-D_j,0\right\}\cdot u_{jk}\cdot p_{rjk}$ logistics center j means that when one needs to provide distribution point k, if the distance between them is more than the radius of the best, then they would have given a penalty cost.

Goal 2 equation (1.4) logistics node that is the highest level of logistics services to maximize cover all logistics center in the best service radius distribution amount. According to the constraint condition of constraint, when the distance between the logistics center and needs points more than the best service radius, then the demand will not be covered logistics center point. When the steel distribution logistics network node layout best service within a radius of coverage bigger the better.

3. STEPS OF GENETIC ALGORITHM

Genetic algorithm GA said solution of the problem into "chromosomes", In the algorithm which is based on the string of binary code. Is presented in this paper, before performing genetic algorithm (ga), and a group of "chromosome", that assumption. Then put these assumptions solution in the problem of "environment", and according to the principle of survival of the fittest, choose a suitable environment of "chromosome" replicate, again by cross, mutation process produces more adapt to the environment of a new generation of "chromosome" group. In this way, the generation to evolve, finally will converge to one of the most to adapt to the environment "chromosome" on, it is the problem of the optimal solution.

The main operation process of genetic algorithm has the following steps:

3.1 Chromosome encoding

The so-called coding, is from phenotype to gene mapping, the data in the solution space is its form of expression.Before you search the solution space solution according to the table; Into the genetic space genotype data string structure, these string structure data by different combination constitutes a different

chromosome. Each chromosome must through some code said to show certain aspects of chromosome characteristics. Chromosome usually used to represent by optimization of the parameters and initial individual said initial solution problem. Commonly used encoding genetic algorithm with binary code and real number coding, natural number coding, gray code coding and multi-parameter coding, etc. Encoding directly affect the search ability of the algorithm and the final result.

3.2 Generating initial population

Random selection on the initial data structure, known as a data structure on each chromosome, chromosome constitute group, genetic algorithm with the string structure as the initial point for iteration. Is the population size, solving the different stresses the best population size should be different in theory. Population is too small, genetic algorithm will be limited by the search space; however, if the population is too large, then search and optimize the need to spend too long. Therefore, in general, if the solution of the problem of nonlinear, the larger the value.

3.3 Test evaluation of fitness function

Genetic algorithm based on fitness function evolution search, basic does not use external information, using the fitness value of each individual in a population. Its decision to groups of each individual genetic how much risk to the next generation group is proportional to the individual fitness. In order to accurately estimate the probability that all individual fitness should be as a negative, for different kinds of problems good predetermined by the conversion rule between the objective function to individual fitness, especially good to determine when the objective function value is negative.

3.4 Choose operation

Choose the excellent individual from the current population, the excellent individuals directly inherited to the next generation or by individual genetic crossover matched to the new process of the next generation is called selection operation.

Selection operation is in accordance with certain selection strategy, according to individual fitness value from the previous generation groups choose excellent individual genetic to the next generation. The purpose is to enable strong adaptability of the individual increases the probability of the next generation with.

There are now commonly used to select operator: Geometric ranking selection and roulette wheel selection and retain the best selection and random competition selection, type selection, no playback, random selection, optimal preservation strategy, no playback remainder randomly selected, stochastic tournament selection.

3.5 Crossover operation

Crossover operator, also known as gene recombination, is the father of the individual randomly paired, some of the structure to replace the operation of the reorganization of the new individual, the new individual combined with the characteristics of their parents. Cross operation to improve the search ability of the algorithm, genetic algorithm is the most important means to obtain a good individual.

The real coded crossover is in the form of intermediate recombination, discrete recombination and linear recombination, and so on. The crossover operator ensures the diversity of the population and avoids the phenomenon of non mature convergence.

3.6 Mutation operation

Mutation operation are randomly change the individual genetic information of an operation, it is in the process of cross missing genes for repair and replacement, as soon as possible to prevent genetic algorithm convergence to local optimal solution.

Its operating process is given in advance of the group a probability of each individual, will be one or a few genes on value change for other allele. Mutation provides the new individual opportunity. Mutation operation to increase the ability of genetic algorithm to find the optimal solution.

Mutation operator of genetic algorithm because of its local search ability and used as auxiliary operator, mutation operator commonly used with uniform variation, basic variation, non-uniform mutation, boundary mutation, the scope of variation in 0.001-0.1 range, usually shoulds not be too big.

3.7 Algorithm termination

Algorithm can be terminated by the following two ways:

Set the fixed m The genetic aximum iteration, this algorithm to achieve the default number of iterations that terminate, but not good grasp the number of settings, it is not conducive to the optimal solution.

The optimal value criterion, not a fixed number of iterations, the algorithm iteratively, until you find the optimal solution to meet the preset conditions.

3.8 Deceptive analysis

In genetic algorithm, the problem of the individual generation with high value of the high value of the genetic algorithm is called the fraud problem. The cheating problem affects the normal operation of the genetic algorithm, which makes the result easily fall into the local optimal solution, which affects the accuracy and efficiency of the algorithm. Its production and gene encoding, fitness function, etc..

The improved genetic algorithm can solve the deceptive, mainly has the simple multi population genetic algorithm, hierarchical genetic algorithm, parallel genetic algorithm and adaptive genetic algorithm and other improved methods.

The principle of simple multi population genetic algorithm is to make the migration and gene transfer of the population of each group is not exchange, the independent evolution of each sub population, multi group co evolution, the group does not interfere with

each other. It is proved that the simple multi population genetic algorithm is beneficial to maintain the diversity of the population, improve the evolutionary effect of the population, and overcome the deceptive.

4.IRON AND STEEL SALES LOGISTICS NETWORK NODES LOCATION APPLICATION

4.1 B steel company profile

B steel company has three major production bases.Now at about 20 million tons of iron and steel production scale, product structure is given priority to with plate steel tubes, rods wire is complementary, stainless steel products are under development.B steel company car plate, shipbuilding plate, home appliance plate, pipeline steel, tubing and other high-end products in the domestic market share is located in the forefront, as well as work die steel with high quality, high performance bearing steel, spring steel, cord with the major suppliers of steel and steel used in aerospace.B steel company has a fully functional e-commerce platform, at the same time across the country set up a modern steel processing center, can quickly respond to user needs, to provide users with a full range of value-added services.With the development of a new round of development strategy, B steel company is accelerating the pace of integration operation, concentrated to develop large impact on the market and strategic investment is needed in China's steel industry structure adjustment, can compete with the international top steel products of steel products, enhance the comprehensive competitiveness of steel industry in an all-round way.

4.2 Data sources

B steel group sales range is wide, but in different parts of the sales volume has a large gap, so the thesis choose sales in more than 100000 tons of sites as possible, alternative points of evaluation index system of data derived from the 12 alternative points of the indexes in statistical yearbook statistical yearbook 2013, 2013 and the related literature.Genetic algorithm model is involved in all kinds of data from field study team of B steel, at the same time some data in the model is not involved in the process of investigation and research, by empirical judgment or literature.

4.3 The optimal location decisions

Assume that B steel plan from six cities of N as the processing and distribution center, the overall cost minimum, the six cities, use the following collection said:

$$P = \{p_1, p_2, p_3, p_4, p_6\}$$

Paper USES the above optimal location decision model based on genetic algorithm, and use matlab2013a software programming using genetic algorithm to solve the model, the specific design is as follows:

(1) Encoding and decoding

In this case, the node has three factories, processing center has six alternative address, demand center to 14, so the number of decision variables include for 3 * 6 = 18, number of decision variables contain is 6 * 14 = 84 The decision variables can only take 1 s and 0 s, variable number is 6.Caused by the decision variables, said how much is the amount of transportation and delivery of goods for, belong to the numeric types, and the number is more, if USES the binary coding scheme, will cause the rapid expansion of algorithm search space, therefore appropriate to adopt floating-point coding, coding string not too long, so convenient and decoding, can significantly improve the efficiency of the operation, so the paper select floating-point coding.

Due to a distribution center is not selected, there is no supplier to supply it to the user does not exist in the distribution of the situation, only a distribution center is selected, the supplier may supply the distribution center, the distribution center is likely to deliver goods to the users, so although the decision variables and decision variables, is not independent of each other, value determines, changes.When not, and contains variables are 0, only at the time, and contains all the variables are not zero.This algorithm the chromosome is mainly composed of three parts: the chromosome of the top 30 said shipments from the factory to the processing and distribution center, the center of the chromosome, 84 from the processing and distribution center to the volume of each demand point whether or not the end of the chromosome 6 on behalf of the six cities selected variables;namely:

$$x_{ij} = [x(1,1:6); x(1,7:12); x(1,13:18)]$$

$$x_{jk} = [x(1,19:32); x(1,33:46); x(1,47:60); x(1,61:74); x(1,75:88); x(1,89:102)]$$

$$thita = [x(1,102:107)]$$

(2) The population initialization

Randomly generated a length of 107 individual coding, initial population.Population size table contains the number of individuals, it directly affects the convergence of genetic algorithm and computation efficiency.When population is small, can improve the operation speed, but reduces the diversity of population, easy convergence to the local optimal solution;Population is large, and increase the amount of calculation, the lower the efficiency of genetic algorithm.Group size can be selected according to the length of the chromosome.In this paper, group size for 300.

(3) Fitness function

In this case the objective function for minimum, according to the analysis of the section 4.4.1 desirable fitness function as(1.3).

(4)GENETIC OPERATIONS

In this case the genetic operation, the choice of operation the roulette wheel selection method is adopted; To adopt the crossover operation with single-point crossover, take 0.65 crossover probability, mutation in the form of random mutations, take 0.008 mutation probability.

(5) RESULT ANALYSIS

Regional logistics center location results

According to the result of regional logistics center location matlab running, select the "1, 3, 4, 5" the four cities.

Factory supply scheme to regional logistics center

With the regional logistics center in the factory on the basis of traffic between the results get supply scheme in table 1.

Table 1 The transport volume between factories and regional logistics center

	1	3	4	5
A	22	116	100	11
B	159	1	12	3
C	13	2	134	101

(Unit: million tons)

To distribution center for regional logistics center

In the regional logistics center to the distribution center for traffic running results on the sorting table 2.

Table 2 The transport volume between regional logistics center and demand point

	D	E	F	G	H	I	G
1	92	27	25	35	1	1	3
3	3	3	19	3	75	1	1
4	1	0	0	0	0	259	5
5	0	5	2	0	0	1	173
	K	L	M	N	O	P	Q
1	0	25	0	0	0	1	1
3	8	34	0	2	0	7	0
4	11	23	0	1	0	0	0
5	4	35	11	2	2	2	4

(Unit: million tons)

Network logistics cost

The network logistics cost is 3 billion 220 million 500 thousand yuan from the result of operation.

6. SUMMARY AND PROSPECT

6.1 conclusion

In recent years, due to the excess capacity of the steel industry and irrational structure and other reasons, China's steel industry has entered a high cost, low profit status. In this state, more and more steel enterprises in the steel sales logistics industry scene. Distribution logistics link face to face with the customer and the market, to the enterprise to improve profitability, modernize operations, strengthen market competitiveness effect is outstanding, in order to through optimizing steel logistics network, reduce logistics cost way to increase sales margin of steel. It is in this background, the thesis study of iron and steel sales logistics node location.

The main work and research results of this paper are as follows:

Paper systematically analyzes the situation of iron and steel industry, iron and steel enterprise sales and logistics development present situation, thought the distribution logistics network is constructed to iron and steel enterprise development for direct product sales, is the enterprise out of the small profit, in the future market competition is an important means to gain a foothold.

According to the decision of the optional points of steel sales logistics network node, this paper construct the logistics network cost minimum, can meet the demand of steel demand of genetic algorithm optimization model and design the corresponding calculation process, model solution is realized by using MATLAB genetic toolbox, finally selects the most appropriate logistics nodes, and factory to transport path between logistics nodes and the corresponding transportation volume, logistics node to the customer of the transport path and corresponding traffic.

6.2 Expectation

Due to limitations of the study period, the research work of this paper there are still many shortcomings to be further supplemented and improved, mainly in the following aspects:

This paper involves a number of variables, some numerical variables is the actual survey data, some data is based on literature or empirical estimates, so there are some deviations from the actual situation.

The research is under the assumption of single steel products sales, but in this paper based on the study, change and steel of the type that the inventory cost, the demand variables, transportation of different types of steel products can be optimization problem is solved.

REFERENCES

[1]Wang Jian, Liu He. Construction and Empirical Study of regional logistics network based on the theory of axial radial [J].Economic geography, 2014 second

[2]Wang Shengyun, Wang Xinlei. The construction of the "hub and spoke" logistics network in the central region -- Based on the 3 points of view of the cost of highway and railway transportation, the progress of [J]. geographical science, the twelfth phase of 2012.

[3]Li Tong, Wang Zhong. Simulation of plant growth algorithm based on optimal distribution of large urban underground logistics network [J].Systems engineering theory and practice, 2013 fourth.

[4]Wang Ling . Research on the relay node placement algorithm for wireless sensor networks [J]. Journal of physics, 2012 twelfth.

[5]Wang Zhu, Wang Qi. Research on WSN relay node placement algorithm with multi constraint fault tolerance [J].Electronic journal, 2011 third.C

[6]Ge Xijun, Liu Kai, Qin Lu.Urban logistics node layout method research and empirical analysis [J]. Logistics technology, 2006 third.

Road Merging Problem after Toll Collection

Jingshuo Yang[1], Minghui Zhang[2], Ziting Yuan[3]*
[1]Mechanical College, North China University of science and technology, Tangshan 063210, Hebei, China
[2]Collage of Information Engineering, North China University of science and technology, Tangshan 063210, Hebei, China
[3]Collage of Mining Engineering, North China University of science and technology, Tangshan 063210, Hebei, China

Abstract: To solve the problem of road merging. We applied analytic hierarchy process (AHP), combined with the main features of the toll area, we select six toll area indexes, including size of the toll booth, radius of curvature, lane width, throughput, vehicle size and lane length. The optimal solution of the toll area is calculated, so that we know the charging area is an arc-shaped area with a radius of curvature of 48.8m and its size is 11.57km2. At the same time, an improved zipper model is proposed, and the road merging problem is studied. The results show that the road capacity is increased by 12.1% while the traffic capacity is saturated.
Keywords: Improved Zipper Model; Road Merging; AHP

1. INTRODUCTION

On high way, the charge window is set up more than the number of lanes. After the car parking payment, the traffic must be taken from the wider toll station to form the fan quickly into the conventional lane with fewer lanes, which seriously affect the expressway design flow. In this paper, a mathematical model is established to determine the shape and size of the toll plaza after the toll collection. The road merging scheme after the tolling of the car is given, and the road traffic performance of the toll area is evaluated. After the increase of the autopilot and the lane merger optimization program.

According to the main characteristics of the charging zone, select six related indexes of charge, look for charging zone optimal solution through applying particle swarm optimization algorithm, determining the charge area shape and size. Study in road consolidation issues through an improved model of zippered road consolidation. Have corresponding conclusion through comparing traffic capacity.

2. ROAD MERGING PROBLEM AFTER TOLL COLLECTION

2.1 the determination of charge area index

According to the analytic hierarchy process and combining with the main characteristics of the charging zone, we select six charge area indexes that toll booths size, radius of curve, traffic lane width, handling capacity, car size, lane length to solve in charge area shape and size and road consolidation. Among them, the calculation method of each index as shown below:

1) Toll booths size

According to the actual situation, the size of the toll booths we adopt fixed size, the concrete size: 1.5*2.5*2.5.

2) Radius of curve

The limit of the parallel calculating formula for minimum radius:

$$R = \frac{V^2}{127(\mu + i)} \tag{1}$$

Among them, R is radius of curve; V is vehicle speed; μ is side-way force coefficient; limit value is between pavement and tire lateral friction coefficient; i is the road transverse slope.

3) Traffic lane width

In the empirical formula, speed is the main factors influencing the lane width. Traffic lane width can be got based on following formula.

$$D = F + N_1 + N_2 + S + a_1 + a_2 + a_3 \tag{2}$$

Among them, F is the rear wheel security clearance between the outside and the inside lane; N_1, N_2 is security clearance between the adjacent two cars; a_1, a_2, a_3 is the car width.

If only a single lane in the model:

$$D = F + S + a_1 \tag{3}$$

4) Handling capacity

a) The formula of peak hour traffic:

$$Q_g = Q * Ag \tag{4}$$

In the formula: Ag —peak hour coefficient, according to the engineering design data values: 0.09

Q —the predictions in the 24 hours of traffic flow

b) The formula of average daily traffic

$$Q_r = Q * A_r / R \tag{5}$$

In the formula: A_r —coefficient of traffic during the day, according to the results of the traffic volume forecast in the engineering report, the coefficient of the whole network day is about A_r value is 0.80;

R —hours in the day, according to the engineering design, value is 16;

Q —the predictions in the 24 hours of traffic flow

5) Car size

Car length and width are important index which affects cars across toll station. This index takes web survey in the research. Inquire 35 common cars within Different displacement, different brands, different models through the internet (see appendix A), gather car length and width, draw car length and

width frequency distribution histogram and it summation curve. From Fig.1-Fig.4.

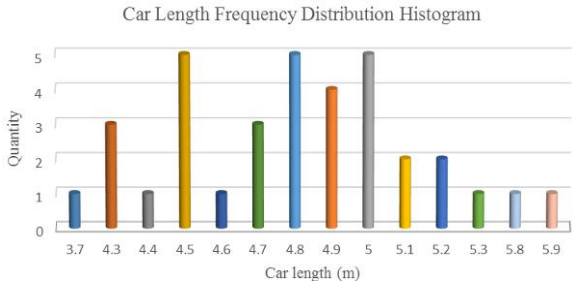

Fig.1 Car length frequency distribution histogra

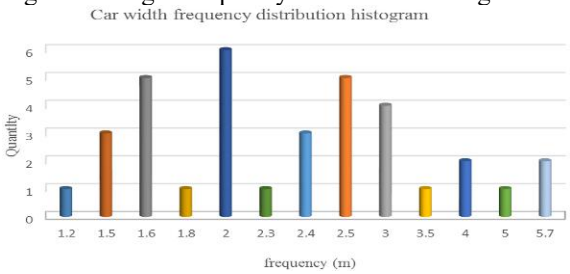

Fig.2 Car width frequency distribution histogram

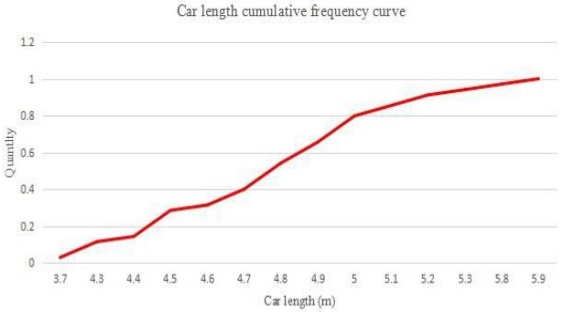

Fig.3 Car length frequency cumulative curve

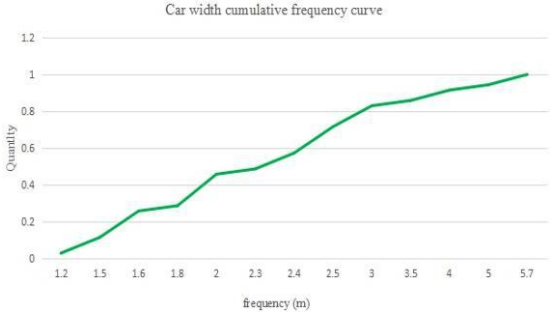

Fig.4 car width frequency cumulative curve

6) Lane length

The design of the lane length is the most important part in geometric parameters of lane. In the modular charge system, the length of the ETC driveway setting is the distance to the driveway automatic railing ETC identification equipment. To determine ETC inward and outward, ETC lane length is affected the following factors:

(1)The highest allowing speed when the vehicle through a toll booth $V_{\max}$;

(2)ECT communications antenna area size.

(3)The time that the illegal driver makes judgment to the roadside lights signal and the braking effect time after judgment T.

(4)Driving distance in the time that illegal vehicle cuts speed from 36km/h to 5km/h S_1.

(5)The automatic railing action time.

(6)The length of the adjacent lane MTC

According to the car features, automotive braking distance calculated by the following formula:

$$S_1 = \frac{V_1^2 - V_2^2}{254(\alpha + \chi)} \tag{6}$$

In the formula: S_1— Braking distance

V_1 —Braking original speed

V_2 —Final braking speed

α —Adhesion coefficient relates to such conditions as the tires and the road and brake, table look-up and dry adhesion coefficient of asphalt concrete pavement is 0.6

χ —Road longitudinal slope, in the general case it is selected -0.2~0.2% , in this research, selecting 0.

2.2 solving in highway toll station shape and size based on particle swarm optimization algorithm

1) Particle swarm optimization algorithm

Particle swarm optimization algorithm has following advantages: convergence speed faster and realize more easily, simple and efficient algorithm structure without large parameter adjustment. [1]Among them, particles by tracking individual extreme value point and the global optimal point adjust the position and own speed. Each generation of speed and position of the individual is improved through the following formula 1 and formula 2:

$$v_{id}^{t+1} = wv_{id}^{t} + c_1 r_1 \left(P_{id}^{t} - x_{id}^{t}\right) + c_2 r_2 \left(P_{gd}^{t} - x_{id}^{t}\right) \tag{7}$$

$$x_{id}^{t+1} = x_{id}^{t} + v_{id}^{t} \tag{8}$$

In the formula, t represents the number of the current particle evolution, w represents inertia weight coefficient v_{id}^{t} represents the speed of iteration of the i particle in the d dimension, x_{id}^{t} represents the position of iteration of i particle in the d dimension, P_{id}^{t} represents the searching individual itself best position of iteration of i particle in the d dimension, P_{gd}^{t} represents the searching global best position of iteration of i particle in the d dimension, r_1 and r_2 are independent random numbers distributed in $[0,1]$, c_1 and c_2 are learning factors, also named accelerated constant, usually taken $[0,2]$, c_1 adjusts the step length of the particle flying towards its own best position, c_2 adjusts the step length of the particle flying towards the global best position. Searching capability of the particle swarm algorithm is to adjust each other between the particle positions, by the speed of the particles affect its position. [2]For example in two-dimensional space, the principle of shifting the next moment location X_i^{t+1} from the current location X_i^{i} is shown on Fig.5:

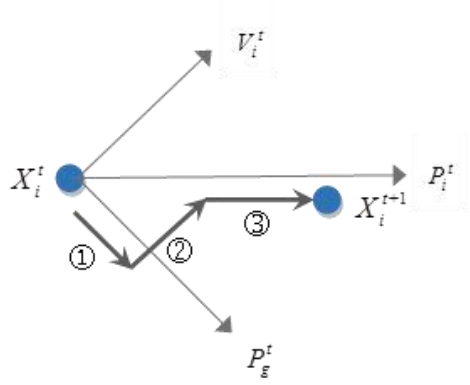

Fig. 5 The theory of particle shifting

In conclusion, the space search ability of particle is composed of three parts working together, only three parts to achieve an appropriate balance, can quickly and efficiently to search the best position, to find out the optimal solution.

2) Particle swarm optimization algorithm steps of the algorithm

Step1: Initialize the population, position and velocity of the particle swarm randomly assigned

Step2: Select the objective function

Step3: Compared with adaptive value of each particle X_i^t and of the best position P_i^t that particle traveled

Step4: Compared with adaptive value of the best position P_i^t that each particle X_i^t traveled and the best position P_g^t that each particle X_i^t traveled in whole situation

Step5: For the global optimal particle, calculate predictive ability in the corresponding ESN with predicted data.

Step6: Improve the particle speed and position according to the formula (7) and (8)

Step7: If not meet the end condition, then return to step (2).

3) Determine the charge area shape and size based on particle swarm optimization algorithm

We put six selected charge area as six dimensional models, according to iterative formula of particle swarm optimization algorithm,[3] with MATLAB calculating (systemin appendix II) get the following result:

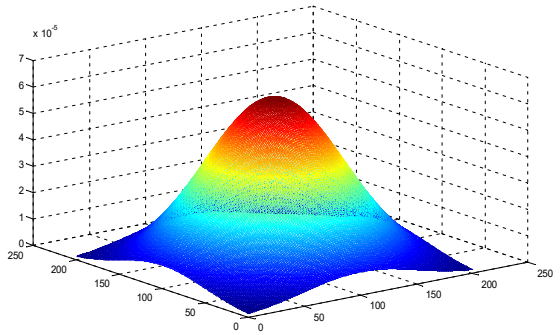

Fig.6 The particle swarm optimal solution

With MATLAB calculating, get the results of multiple iterations as Table 1:

Table 1 Particle swarm optimization algorithm to get the optimal solution

index	The volume of toll boothsV(m)	Radius of the curve R(m)	Lane width D(m)	Average throughput(Vehicle/h)	ETC antenna and guide light distanceLE1(m)	ETC antenna and guide the front distance LE2(m)
result	9.375	48.8	3.6	2130	12	20.3

According to the above results, get the shape of the charge area as the Fig.7:

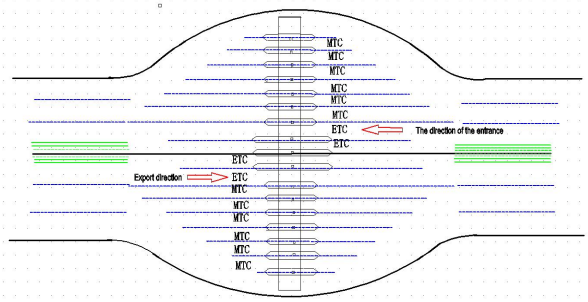

Fig.7 Charging zone figure shape

According to the design of the shape of the charging area and every part distance, calculate the charge area is 11.57km2

2.3 solving on road consolidation issue based on an improved model of zippered road consolidation

Zippered road consolidation (the actual figure as Fig.8) as international traffic rules, it can make some two-lane into one lane, its basic principle is shown on Fig.9. Under this principle, even without traffic lights and traffic police, it also can make people pass the road quickly and efficiently. The basic principle is: after a car passing, the second car does not pass the road until waiting the opposite car pass away. On this basis, we put forward a improved zipper model as Fig. 10. Vehicles are driven in order shown in the figure number and always adhere to the principle of left - in – right.

Fig.8 Zipper actual figure

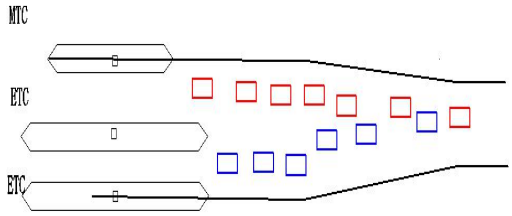

Fig.9 Classic zippered road consolidation

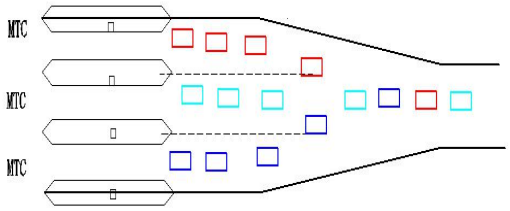

Fig.10 Improved zippered road consolidation

There are 16 toll booths in the charge area. Because our principle is making the road closest to the road fastest, so the way of road consolidation: the inside of the two toll booths according to the classic zipper model, the remaining six toll booths according to the improved zipper model, solve crowed phenomenon caused by selecting road randomly and get a good road passage effect through this road consolidation way. Among them, contrast figure using zippered road consolidation as Fig.11:

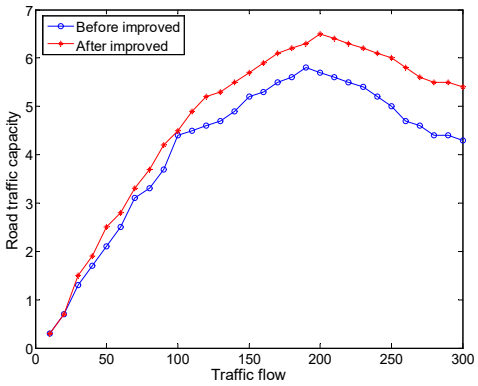

Fig.11 Contrast figure that change traffic capacity before and after

3. RESULTS AND DISCUSSION

See from the model that we proposed, and the road merging problem is studied. The results show that the road capacity is increased by 12.1% while the traffic capacity is saturated.

4. CONCLUSIONS

With the development of technology, more and more people have their cars. So the problem of road merging is coming. To solve the problem of road merging. We proposed an improved zipper model, and we can see easily, the new model is effective for solving the problem.

REFERENCES

[1]Margarita Reyes Sierra, Carlos A. Coello Coello. Improving PSO-Based Multi-objective Optimization Using Crowding, Mutation and ∈-Dominance[C]// Evolutionary Multi-Criterion Optimization. Third International Conference, Emo. 2005:505-519.

[2]Da Y, Xiurun G. An improved PSO-based ANN with simulated annealing technique[J]. Neurocomputing, 2005, 63:527-533.

[3]Bashir Z A, El-Hawary M E. Applying Wavelets to Short-Term Load Forecasting Using PSO-Based Neural Networks[J]. IEEE Transactions on Power Systems, 2009, 24(1):20-27

.

Research On the Node Location of Steel Distribution Logistics Network Based on Rough Set

Di Zhang[1],Xingjun Luo[1], Wenrui Wu [1],Yunhua Qu[2],Liya Wang[3]*
[1]College of Mining Engineering,North China University of Science and Technology,Tangshan Hebei,063210,China
[2]Qian'An College,North China University of Science and Technology,Tangshan Hebei,063210,China
[3]College of Science,North China University of Science and Technology,Tangshan Hebei,063210,China

Abstract: At present, China's iron and steel industry has entered a high cost, low profit status, irrational layout, etc.. In this regard, the siting of steel sales logistic network nodal points of principle and influence factors analysis, provides the basis for the following logistics node location, detailed description of the related theory of logistics of iron and steel and iron and steel sales logistics nodes, laid the theoretical foundation for the later steel sales logistic network nodal points of the research. At the same time, the paper puts forward the method of steel distribution logistics network node location method based on rough set and rough set.
Keywords: Iron and steel logistics; network node; rough set

1. INTRODUCTION

Steel is a national pillar industry, is also an important standard of review of a country's comprehensive national strength and not strong[1]. Produced with the iron and steel industry increased overcapacity and environmental pollution problem is facing the following problems of China's iron and steel industry:
(1) the unreasonable industrial structure, excess capacity is the main problem to the development of China's iron and steel industry in the solution. By the end of 2013, China's crude steel production reached 7.79 tons, excess iron and steel production, steel prices, steel has been part of the company benefits decline. [2]
(2) the industry concentration is too low, the procurement of raw materials of international discourse is not heavy. [3]
(3) internal disorderly competition between Steel Corp, often in a price war. At present, China's steel industry is still the main distribution, supplemented by direct, which leads to the dealer to grasp the initiative. [4]

2. IRON AND STEEL SALES LOGISTICS NETWORK NODE LOCATION ANALYSIS

According to the different levels of logistics nodes, the iron and steel logistics network can be divided into single layer, double layer and multi-layer steel distribution logistics network. Iron and steel sales logistics network schematic diagram was shown in Fig.1.

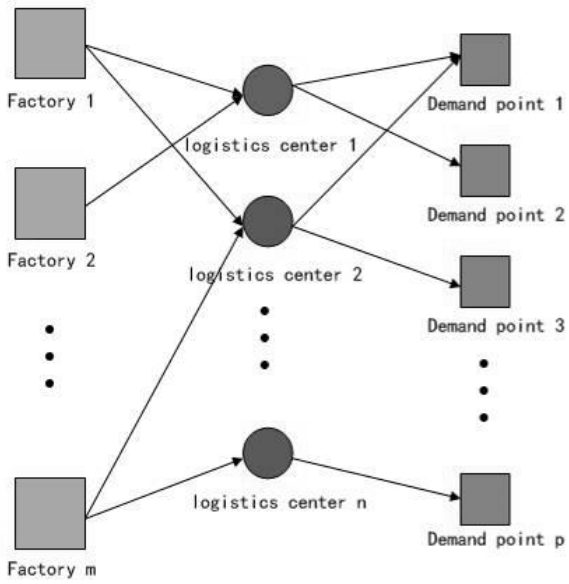

Fig.1 logistics network schematic diagram

The point of this paper is to study the distribution of the single layer network node in the steel distribution logistics of multi product and multi product. That is to choose the right network nodes and location to decide a reasonable distribution, optimize the network system, reduce logistics costs, speed up the cycling of customer demand, improve service quality.

2.1 Factors influencing the Iron and steel logistics node location

On locating the steel sales logistics network nodes, the alternative urban traffic environment, business environment, the competition environment should be considered about whether it is conducive to the construction of the steel logistics center, the factors of iron and steel logistics node location mainly consider the following factors: one is the external factors, one is cost factors, one is iron and steel enterprise customers.

1) External influencing factors

External influence factors are the factors that can reflect the comprehensive strength of the city. [5]

● The natural environment factor

● Transportation factors
● Operating environment factors
● Competitive factors

2) Cost influencing factors

The construction of a logistics node will produce a variety of logistics cost, such as transportation cost, storage cost, loading and unloading costs, operating costs, construction costs, and so on, and the level of these costs directly affect the cost of the logistics networ[6]k, logistics cost constraints directly affect the logistics nodes and position determination.

3) Iron and steel enterprise customer influence factors

Through the analysis of the steel logistics network, it is found that the iron and steel enterprise is far from the demand of steel, and the establishment of logistics node is to quickly respond to customer demand.

2.2 The step of locating Iron and steel logistics network node

The according to the characteristics of steel sales logistics network node location factors and steel sales logistics, combined with the current location of the status quo, the iron and steel sales logistics network node location step is divided into two steps. The first step to the alternative locations for construction of iron and steel logistics node comprehensive ability and the prospects for development were evaluated, for the evaluation value, and eliminate the evaluation value smaller alternative points, [7] then to the rest of the place as the second phase of the alternative points. The second stage selection using genetic algorithm to automatically search the best path, and ultimately determine the steel sales logistics network node location, quantity, transportation and distribution mode and corresponding distribution amount.

3.IRON AND STEEL SALES LOGISTICS NETWORK NODE LOCATION SELECTION PROCESS

In this paper, the comprehensive strength of the alternative site evaluation, first combined with the actual situation of steel sales, to extract the appropriate evaluation indicators for the selection of points, and then build the site selection evaluation system. In the actual evaluation, there is often overlap between each evaluation index, so it is needed to use rough set to reduce the evaluation index. Using the reduction index system was to make evaluation, by calculating the weight of each index, using linear weighted method to calculate the value at the end of each alternative points of evaluation, the evaluation value represents the comprehensive strength of the node, and serve as alternative site basis, selected by selecting as a logistics node to the final decision of the candidate sites.

3.1 Construction of initial index system for comprehensive strength evaluation of alternative points

Alternative points of the comprehensive strength indicates the potential of alternative points for building steel logistics nodes. The evaluation of comprehensive strength is considered by choosing whether there is enough good environment to support the construction and development of the iron and steel logistics nodes. [8] The after consulting related literature foundation considering from the regional logistics industry scale, infrastructure level, macro policy and the level of iron and steel demand four aspects to selecting comprehensive ability evaluation.

To study the issue more comprehensively, from the different aspects of the selection and related indicators, but with the index of inevitable increase caused some evaluation indicators of meaning overlap the possibility and degree of overlap increases and make some less important factors are added in, true to the object of evaluation index set down, affecting synthesis of selecting the evaluation of the comprehensive strength of the accuracy. Therefore, it is necessary to simplify the initial index system.

3.2 Construction of evaluation information system of comprehensive strength of alternative points

construction of the comprehensive evaluation information system is the transformation of the evaluation index system into the representation of the information system. Rough set is mainly used to represent the knowledge information in the two-dimensional information table, and the two-dimensional information table in the rough set is evaluated by Ding Yicheng's comprehensive evaluation information system. General use the following shorthand $S = \langle U, R, V, f \rangle$ or $S = \langle U, R \rangle$ representation of the comprehensive evaluation of information system. In the knowledge representation system, the representation of the domain U, which represents the set of attributes, represents the set of attribute values, which is called the information function. An attribute corresponds to an equivalent relation, and an information table can be regarded as a set of equivalence relations defined.

And evaluation system, the comprehensive evaluation of the information system is the evaluation of the object of the collection (optional point), which means that the attribute set is the index set of evaluation system.[9]Represents a set of index values corresponding to each evaluation index. Then through the interpretation of the corresponding relationship can be built on the comprehensive evaluation of the comprehensive evaluation of alternative information system, specific can be expressed in table 2.

Table 2 Evaluation information table of comprehensive strength

	u_1	u_2	…	u_j
r_1	V_{11}	V_{12}	…	V_{1j}
r_2	V_{21}	V_{22}	…	V_{2j}

…	…	…	…	…
r_{14}	V_{141}	V_{142}	…	V_{14j}

Table 2 evaluation system index both quantitative indicators, as well as qualitative indexes, quantitative indexes corresponding to the attribute value can be obtained by referring to the statistical yearbook, statistical report or query the government's official website, and qualitative indicators need obtained by using expert scoring method.

3.3 Normalization and Discretization of Index Value

● Index value discretization

At present, the discretization method of data is based on the information entropy, the information such as the amount of information, and so on. It also has the IND of Holte and so on. Among them, the two methods of equal interval and equal amount of information may be the most simple method. Interval is the continuous attribute range is divided into $k(k \in N)$,and k is generally decided by the researchers themselves, and method of information content is the first measurement values are sorted, and then the attribute value range into intervals. In each interval package containing an equal number of measurements. The above two methods are static, global and unsupervised methods. From the space and time complexity analysis, these two methods are the most effective. [11] Therefore, this paper chooses the interval method to deal with each index. Use mathematical expressions, such as the formula (2.1), in which k indicates the corresponding value of each index.

$$k = \begin{cases} 1 & 0 \le k < a \\ 2 & a \le k < b \\ 3 & b \le k \le c \end{cases} \tag{2.1}$$

Through the above steps have been aware of the weight of each index and the corresponding value of each index, using the linear weighted method to get the evaluation value of each alternative point.

3.4 Constructing index screening model based on equivalence relation

This step is based on rough set of candidates' evaluation of the comprehensive strength of the core steps, in the optional information system for comprehensive evaluation of according to any index can assessment object collection is divided into a plurality of equivalence classes and the set of equivalence classes is an equivalence relation.

3.5 Calculation of index weight and evaluation value

Corresponding to the objective weight of every index in the evaluation index system in the comprehensive evaluation of information system is the information system of each index of the information system importance, each index in the evaluation system by information entropy to carry out. For the information system in the paper $S = \langle U, R, V, f \rangle$,there is $U / R = (X_1, X_2, X_3, ..., X_{14})$, Then the information entropy of the system $\mathrm{U/R}$ is:

$$H(R) = -\sum_{i=1}^{m} p(\mathrm{X_i}) \ln p(\mathrm{X_i}) \tag{2.3}$$

$$p(\mathrm{X}) = \frac{|\mathrm{X}|}{|\mathrm{U}|}, X \in U / R$$

In the form of , Then the index system of the importance of each index is:

$$S(R) = \left| H(R - \{r\}) - H(R) \right| \tag{2.4}$$

That can be used $\mathrm{S(r)}$ for a value of the indicators weight, the weight is the objective weight, that is, through the known data processing and not artificial experience and get the value of.

Although a variety of theoretical methods based on rough set to solve the weight of each index, but the prior experience is also important, so in the final determination of the weight of the index, the subjective weight is considered.

The weight of the weight calculated by rough set weights and expert to using linear weighted method to get the final index value.

$$\omega^* = \alpha \cdot \omega_1 + (1 - \alpha) \cdot \omega_2 \tag{2.5}$$

Through the above steps already know each index and the weight of each index value corresponding to the linear weighted method to get the evaluation value of each alternative.

3.6 Determination of site selection results

Based on rough set model for the evaluation of the evaluation system are solved, the evaluation on the comprehensive strength of each candidate point value, then to evaluate these values are sorted and rejects does not conform to the performance of alternative, remaining under the place as the next chapter steel sales logistics node location of multi-objective decision alternative.

4. IRON AND STEEL SALES LOGISTICS NETWORK NODE LOCATION APPLICATION

4.1 Steel Corp profile

J Steel Group is China's "Five Year Plan" period, one of the key construction projects, J steel has three major production bases, factories a, wire and bar as a supplement form based on high quality plate and strip, stainless steel material, in the high-end line of bar products structure.

4.2 Data source description

J Steel Group sales of a wide range, but sales of different regions have a big gap, so the choice sales in more than 10 million tons of place as optional and alternative evaluation index system in the target data source in the 12 by selecting 2013 statistical

yearbook, 2013 statistics annual report and related literature. Genetic algorithm model involved in all kinds of data sources in the project group of J steel investigation report, also some data in the model is not addressed in the research process by experience judgment or access to literature to solve.

4.3 J Steel Group sales logistics network logistics node location

● Construction of evaluation index system

The evaluation index system of the second chapter is the initial evaluation system for the comprehensive strength evaluation of the alternative points. The evaluation index system is detailed in table 1.

● Determination of evaluation index system data

Alternative point set $U = \{u_1, u_2, \cdots, u_{12}\}$, table 1 shows the evaluation index system, quantitative indicators can be obtained through access to relevant literature, qualitative indicators are obtained by the expert scoring method. In all indicators and indicators are qualitative indicators, while indicators are quantitative indicators, but because the data is not easy to query, or the use of qualitative methods to its assignment. Qualitative indexes quantitative numerical table as shown in table 3.

Table 3 Value corresponding table of qualitative index

qualitative description	data
1	Poor / few
2	commonly
3	Better / more

The data of quantitative indicators obtained through access to relevant literature, fuzzy qualitative and quantitative information.

The majority of each index table relates to a specific dimension, because of the different evaluation index, economic significance, if there are dimensionless forms, so they are not comparable. It is necessary for each index, only after eliminating the dimension influence each other can be compared, r_8 and r_9 which is discrete, so do not have to be standardized. The specific index dimensionless method is given in chapter two.

industrial production value, social freight volume are in accordance with the discretization of the formula (4.1) standard for discretization of the index data and index of logistics policies and logistics enterprise number (due to limitations of data collection and expert scoring method is used to determine) is in the form of discretization, and therefore do not have to then data discretization.

$$k = \begin{cases} 1 & 0 \le k \le 0.333 \\ 2 & 0.333 \le k \le 0.666 \\ 3 & 0.666 \le k \le 1 \end{cases} \tag{3.1}$$

According to the method of general reduction, the index of the information table is reduced:

$IND(R) = IND(r_1, r_2, r_3, ..., r_n) = \{\{r_1\}, \{r_2\}, \{r_3\}, ..., \{r_n\}\}$

The information table can be obtained after reduction, as shown in table 5:

Table 5 Index reduction form

	r1	r3	r4	r5	r6	r9
u1	2	2	1	2	3	1
u2	3	1	1	1	1	2
u3	1	1	1	1	1	1
u4	2	2	0	1	2	1
u5	2	1	0	2	0	1
u6	2	0	0	1	1	0
u7	1	1	0	2	1	2
u8	3	3	1	1	2	1
u9	2	2	1	0	2	2
u10	2	1	2	1	3	1
u11	3	3	2	1	2	1
u12	2	2	1	2	2	2

● Determine the index weight

The weights of the indexes include two aspects, the index is evaluation model to calculate the index weight based on rough set, on the other hand is decision-making index for the reduction of the given weights, comprehensive consideration, the comprehensive weight of each index value. According to rough set index weight calculation formula to calculate the weight reduction after each index corresponding, according to formula (2.4) and formula (2.5), so as to solve the reduction after each index of the objective weights of evaluation information table are calculated according to the value.

$w_1 = 0.210$, $w_2 = 0.178$, $w_3 = 0.121$, $w_4 = 0.157$, $w_5 = 0.184$, $w_6 = 0.150$

At the same time, according to the decision maker's willingness to give the weight value of the 6 indexes after the reduction.

Determine the evaluation values of each alternative address

$$\partial_j = \sum_{i=1}^{6} V_{ij} \times w_i^* \tag{3.2}$$

Where w_i^* is the comprehensive weight of each index, will be brought into the numerical formula (3.2), you can get the evaluation value of each alternative address comprehensive strength.To sort the preparation of selecting comprehensive evaluation values, compare 1,4,8,9,10,12. Evaluation value is low, will be in the optional excluded, the rest of the place as the second stage decision alternative points. And a new alternative to the new standard, by:

$$P = \{p_1, p_2, p_3, p_4, p_6\}$$

5. SUMMARY

The main research results of this paper are as follows:

The system analysis of the situation of iron and steel industry, iron and steel enterprise sales and logistics development status that iron and steel enterprises through sales logistics network construction to develop direct supply products direct sales model, enterprises out of the predicament of the profit and get a place in the future competition in the market the important way.

The ability for alternative points is the construction of iron and steel sales logistics node, establishes the evaluation system for the evaluation of the comprehensive strength of alternative locations, building the evaluation index system of comprehensive evaluation model based on rough set theory.

REFERENCES

[1]Zhang Rui. Steel zero profit trap [J]. China review, 2013, (6) : 74-76

[2]Yin Ruiniu. Multi dimensional logistics control system of iron and steel manufacturing process [J]. Journal of metals, 1997

[3]Yang Mei, Yao Ming. Research on Construction of Modern Steel Logistics Park[J]. Logistics Engineering and Management,Vol.31,No.3,2009.

[4]Zhao Mingfeng, a party. China Jun steel logistics park operating mode innovation of [J]. logistics technology, 2014 12.

[5]Yang Jing-ping, Liu Xiao-bing. Order-grouping quality design method for steel product based on multi-constrain clustering[J]. Computer Integrated Manufacturing Systems, Vol.15,No.11, Nov. 2009.

[6]Mei Shurong, Huang Xiaochen. Computer engineering and scientific research and development of [J]. logistics management system of iron and steel enterprises, 2011,33 (1): 176-180.

[7]Han succinate, Shan Shiguang what Gawain. A using facial symmetry light illumination normalization method. Journal of computer research and development, 2013,04:767-775.

[8]Ning Jicai, Liu Gaohuan, Liu Qingsheng, Xie Chuanjie. Hydrological response unit spatial discretization and SWAT model improved. Advances in water science, 2012,01:14-20.

Multiple Dam Scheduling System Based on Genetic Simulated Annealing Agorithm

Bo Zhao[1] ,Xiangyu Xu[1],Fanbei Kong[1],Xiaoqiang Guo[2]*
[1]Yi Sheng College,North China University of Science and Technology,Tangshan Hebei,063210,China
[2]College of Science,North China University of Science and Technology,Tangshan Hebei,063210,China

Abstract : In the context of the urgent need to repair Kariba dam, the Zambezi River Basin has Africa's most valuable and diverse natural resources. The establishment of a multi-dam system management mechanism for the basin is of great significance for sustaining regional economic sustainable development and accelerating the pace of poverty alleviation. A multi-dam scheduling system based on genetic-simulated annealing algorithm which combined with the factors affected the cost such as monthly runoff and regional topography were set up. ZRA managers were provided with Extreme water flow under the guidance.
Keywords: genetic algorithm; simulated annealing algorithm; multiple dam system.

1. INTRODUCTION

Zambezi River which has the most precious and diverse natural resources is one of the four major rivers in Africa. Managing the water resources of this basin is very important for sustaining regional economic development and accelerating the pace of poverty alleviation. But in the basin, there is a lack of communication and coordination among the countries in water resources management. The construction of dams in the river basin and the economic benefits of hydropower development have posed hidden dangers to the safety of watershed ecosystems. In the context of the need for rehabilitation of the Kariba Dam, the basin needs to establish a common management mechanism to maximize the economic, social and environmental benefits of the entire basin.

2. EXPERIMENTAL

2.1 model theory

The idea of Genetic Algothms is derived from the objective laws of "survival of the fittest" and "survival of the fittest" in biological evolution, as shown in Figure 4-1. After the initial population of the cycle, the population is partially eliminated and the other part becomes Reproduction. 12 dams were randomly assigned to the flood allocation quota. The low storage capacity was eliminated and the high storage capacity was formed. , The choice of the genetic algorithm is used to change the water allocation quota of the dam, so as to reassign the individuals who make the overall target cost better after the change. In this process, Probability and mutation probability, will further enrich the distribution of the program, so as to further evaluate the program under the multi-selection, continue to be optimized.Genetic algorithm is a highly parallel, random and adaptive optimization algorithm.

The specific process is as follows:

Table 1 The lower bound of capacity limit of each dam

Dam	Lower limit	Dam	Lower limit
Sesheke	1.82×10^{10}	New Kariba	3.86×10^{10}
Cartoon Bora	2.33×10^{10}	Chirundu	3.75×10^{10}
Msuna	3.22×10^{10}	Kanyemba	4.32×10^{10}
Mibizi	4.12×10^{10}	Luangwa	4.25×10^{10}
Massanangoe	3.56×10^{10}	Alfaiate	2.57×10^{10}
Tete	3.23×10^{10}	Marromeu	2.79×10^{10}

An encoding of the problem is chosen to give an initial population of N chromosomes $pop(1), t=1$

The fitness function is calculated for each chromosome in the population $f_1 = fitness(pop(t))$

If the stop rule is satisfied, the algorithm stops; otherwise, the probability is calculated

$$p_i = \frac{f_i}{\sum_{i=1}^{N} f_i}, i = 1,2,...,N, \quad (1)$$

And randomly selected some chromosomes from pop (t) to form a population with this probability distribution.

$$newpop(t+1) = \left\{ pop_j(t) \middle| j = 1,2,...,N \right\} \quad (2)$$

By mating, the probability of mating is that one gets N chromosomes

With a smaller probability p, making a chromosome

of a gene mutation, the formation;

From the above steps found that the genetic algorithm is a fairly formalized algorithm, through the programming algorithm can achieve the calculation function, through matlab2014a optimization.In section 1, the constraints and objective functions are constructed with # dam as an example. Through the corresponding flow, the lower bound of each dam can be determined in turn, as shown in the following Tab.1:

Combined with the objective function constructed , we can get the model problem that the genetic algorithm needs to be optimized:

$$\begin{cases} 1.81\times10^{10} \le x_1 \le \dfrac{Q_k}{3} \\ 2.33\times10^{10} \le x_2 \le \dfrac{Q_k}{3} \\ 3.22\times10^{10} \le x_3 \le \dfrac{Q_k}{3} \\ 4.12\times10^{10} \le x_4 \le \dfrac{Q_k}{3} \\ 3.86\times10^{10} \le x_5 \le \dfrac{Q_k}{3} \\ 3.75\times10^{10} \le x_6 \le \dfrac{Q_k}{3} \end{cases} \& \begin{cases} 4.32\times10^{10} \le x_7 \le \dfrac{Q_k}{3} \\ 4.25\times10^{10} \le x_8 \le \dfrac{Q_k}{3} \\ 3.56\times10^{10} \le x_9 \le \dfrac{Q_k}{3} \\ 3.23\times10^{10} \le x_{10} \le \dfrac{Q_k}{3} \\ 2.57\times10^{10} \le x_{11} \le \dfrac{Q_k}{3} \\ 2.79\times10^{10} \le x_{12} \le \dfrac{Q_k}{3} \end{cases} \quad (3)$$

2.2 technological process

Genetic algorithm method has its own premature convergence, local search ability is not strong and so on, so the quality of the bank capacity can be further improved theoretically. Simulated annealing algorithm can overcome the shortcomings of local optimization ability to a certain extent, The improved idea can not only enhance the global convergence of genetic algorithm, but also accelerate the speed of evolution. Therefore, the two models are combined to establish a composite model of genetic algorithm and simulated annealing algorithm, and the optimization result is further strengthened.

The process of genetic-simulated annealing algorithm is shown as Fig.1 follows:

3. RESULTS AND DISCUSSION

In order to further illustrate the superiority of the algorithm, we use the typical x [sinx] + ycosy function to verify the two-dimensional visualization. Given the range of X and Y as the limiting condition, Respectively, using a single genetic algorithm and genetic - simulated annealing algorithm for optimal solution as shown below:

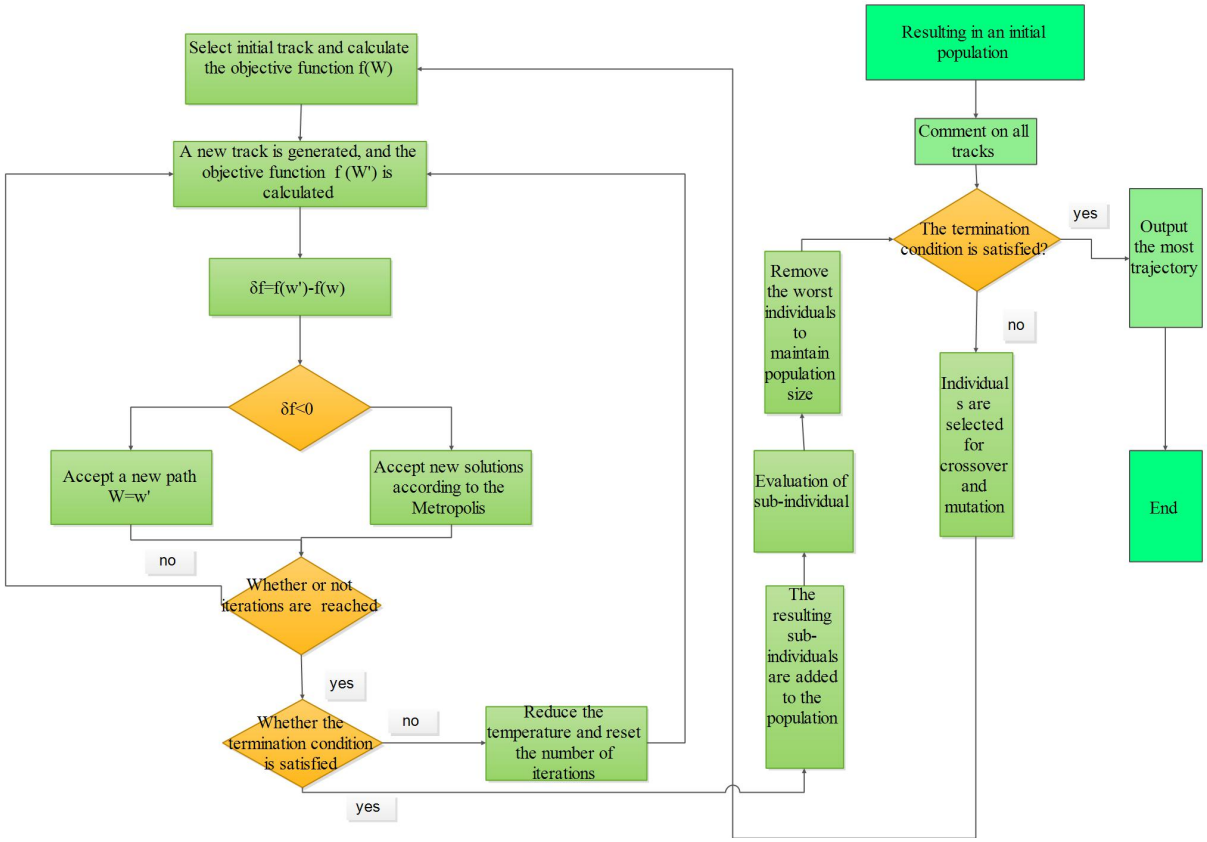

Figure 1 Flow chart of genetic-simulated annealing algorithm

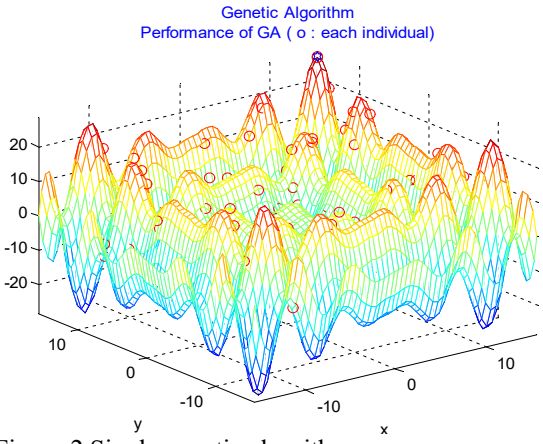

Figure 2 Single genetic algorithm

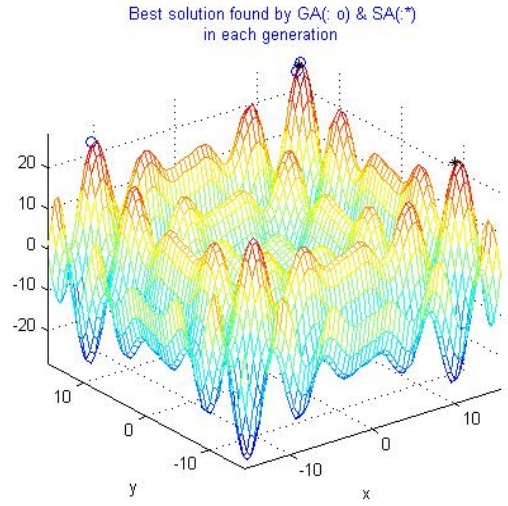

Figure 3 Genetic simulated annealing algorithm

It is found that genetic algorithm "multiple" optimal solution distribution is scattered, which is also the optimization of genetic algorithm. This local optimization will cause some errors, while genetic-simulated annealing has greatly improved the error.

4. CONCLUSIONS

In the context of the Kariba dam to repair, adjustment mechanism through the research of multiple dam water, combined with the influence the cost of the monthly runoff and terrain factors, establish multiple dam scheduling system based on genetic simulated annealing algorithms, to realize the reasonable adjustment to the water Festival, and provide guidance for extreme water ZRA management personnel.

REFERENCES

[1]Jiang Liang. Optimization of BP neural network and its application [D]. Nanchang University, 2014

[2]Wu Shiyong. Research on Optimization of BP neural network and genetic algorithm based on numerical method [D]. Yunnan Normal University, 2006

[3]Zhao Shouling. Research and application of BP neural network structure optimization method [D]. Soochow University, 2010

[4]Wang Jinlong, Ma Guangwen,, et al. Application of BP artificial neural network model to the optimal dispatching rules of two reservoirs in Xiluodu and Xiangjiaba [J]. hydropower and energy science, 2012 (12): 48-51.

[5]Wu Baijie. Research on cascade reservoir scheduling based on improved BP neural network [D]. Huazhong University of Science and Technology, 2010

[6]Li Yong, Wang Jianjun, Cao Lihua. Optimal load distribution of thermal power plant based on BP neural network [J]. power system protection and control, 2011, 39 (): 87-92.

[7]Wu Changwei. Research on load balancing technology based on BP neural network [D]. South China University of Technology, 2012

Designing of Toll Station

Shihao Zhao[1],Chengran Ren[2], Huiqi Zhang[2],Jingguo Qu[3,]*
[1]College of Information Engineering of North China University of Science and Technology, Tangshan Hebei,063210,China.
[2]College of metallurgy and energy of North China University of Science and Technology ,Tangshan, Hebei 063210,China.
[3]College of Science,North China University of Science and Technology,Tangshan Hebei,063210,China

Abstract: According to the complexity of the influencing factors, the weight of each influence index is determined based on the judgment matrix, and the arrangement of the tollbooths with the largest weight is selected. Based on the analysis of the advantages and disadvantages of single-entrance single-exit single-stop toll station and single-entrance single-exit double-stop toll station, a single-entrance. double-exit double-stop charging scheme is designed. By comparison, the throughput of the double-stop toll station is 65.2% higher than that of single-entrance single-exit single-stop toll station, 15.8% higher than that of single-entrance single-exit double-stop toll station.

Keywords:single-entrancedouble-exitdouble-stop model; Fuzzy Comprehensive Evaluation; pass rate

1. INTRODUCTION

According to the background of the toll station, if you want to design a reasonable toll station construction scheme to ensure the smooth flow of vehicles under the premise while reducing construction costs and the congestion of the road junction, you need to solve the problem:Design the shape and size of the charge zone and how to solve the problem of vehicle passing toll station after confluence.

In order to solve the above problems, firstly, the text uses the index selection model based on Analytic Hierarchy Process (AHP) to get the main index in toll station construction process. And then calculate the size of the toll plaza according to the construction scale of the toll station.

2. EXPERIMENTAL

2.1`Index Selection Model Based on Analytic Hierarchy Process

While designing the toll station, the test assume that a lot of elements will affect the construction of it, but in fact, not all the elements can be the best, so the test uses the analytic hierarchy process to weight the factors that affect the toll plaza, and select the factors that have the greatest impact on the toll plaza.

Step1. The Establishment of Analytic Hierarchy Process about Toll Station.

Through the exploration of the construction of the toll plaza[1], six influencing factors are found in this paper, and the hierarchical analysis structure as shown in Figure1 is establishe,

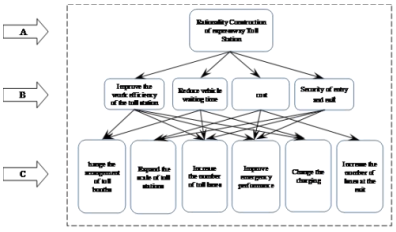

Figure 1 The Rationality construction of structure diagram about expressway toll station

Step 2. Construct the judgment matrix

According to the hierarchical structure diagram, this test compares each element of each layer to get the judgment matrix:

Table.1 Judgment matrix

A	B_1	B_2	B_3	B_4
B_1	1	1/2	5	2
B_2	2	1	9	5
B_3	1/5	1/9	1	1/2
B_4	1/2	1/5	2	1

Judgment matrix A is shown :

$$A=\begin{bmatrix}1 & \frac{1}{2} & 5 & 2\\ 2 & 1 & 9 & 5\\ \frac{1}{5} & \frac{1}{9} & 1 & \frac{1}{2}\\ \frac{1}{2} & \frac{1}{5} & 2 & 1\end{bmatrix} B_1=\begin{bmatrix}1 & 3 & 5 & 7\\ \frac{1}{3} & 1 & 3 & 5\\ \frac{1}{5} & \frac{1}{3} & 1 & 2\\ \frac{1}{7} & \frac{1}{5} & \frac{1}{2} & 1\end{bmatrix} B_2=\begin{bmatrix}1 & 3 & 5\\ \frac{1}{3} & 1 & 3\\ \frac{1}{5} & \frac{1}{3} & 1\end{bmatrix}$$

While the others are as followings:

$$B_3=\begin{bmatrix}1 & 2 & \frac{1}{5}\\ \frac{1}{2} & 1 & \frac{1}{7}\\ 5 & 7 & 1\end{bmatrix} B_4=\begin{bmatrix}1 & \frac{1}{3} & 2\\ 3 & 1 & 5\\ \frac{1}{2} & \frac{1}{5} & 1\end{bmatrix}$$

Step 3. The Consistency Check of Judgment Matrix

During the consistency check of judgment matrix, when the consistence of the judgment matrix is unsured, the corresponding root of the corresponding judgment matrix will also change. So the test uses the change of Eigenvalue of Judgment Matrix to do the consistency check of judgment matrix. In the end, the negative average of the remaining eigenvalues except the largest eigenvalue is used as the index of the consistency of the judgment matrix,

$$CI=\frac{\lambda_{\max}-n}{n-1} \quad (1)$$

When CI is equal to zero, the judgment matrix is consistent, and vice versa.

To measure whether different order judgment matrixes are consistent, the paper introduces the average random consistency value RI to judge matrixes. RI value of judgment matrixes 1-9 is showed in table 2

Table 2 the number of the judgment matrix from 1st to 9th order

1	2	3	4	5	6	7	8	9
0.00	0.00	0.58	0.90	1.12	1.24	1.32	1.41	1.45

The ratio of the consistency index of the judgment matrix CI to the mean random consistency index of the same order RI is called the random consistency ratio, recited as CR. When

$$CR = \frac{CI}{RI} < 0.10 \tag{2}$$

It can be regarded that the judgment matrix is consistent, or it has to adjust the judgment matrix until it is consistent.

Step 4. The hierarchical single sort

(1)Calculate the product of the elements of each row of the judgment matrix

(2)Calculate the n-th root of Mi

$$\overline{W_i} = \sqrt[n]{M_i} \tag{3}$$

(3)Do the normalized treatment to the vector.

$$W_i = \frac{\overline{W_i}}{\sum_{j=1}^{n} \overline{W_j}} \tag{4}$$

So the feature vector we would like to get is

$$W = \left[\overline{W_1}, \overline{W_2}, \cdots, \overline{W_n}\right]^T \tag{5}$$

Calculate the maximum eigenvalue of the judgment matrix $\lambda_{\max}$

$$\lambda_{\max} = n\sum_{i=1} \frac{(AW)_i}{nW_i} \tag{6}$$

Through the calculation of the single rank ofthe judgment matrix, the final result of the judgment matrix is got(Procedures see Appendix 1). The result of Judgment matrix A is

$$W = \begin{bmatrix} 0.2717 \\ 0.3231 \\ 0.1846 \\ 0.2207 \end{bmatrix}$$

$\lambda_{\max} = 4.0076$, $CI = 0.0025$, $RI = 0.9$, $CR = 0.0028$

Similar, we can know B_1, B_2, B_3, B_4

From the result above, it can be seen that the value of CR is less than 0.10, so the judgment matrix has reached satisfactory consistency.

From the table above, the arrangement of toll booths has the greatest impact on the construction of toll stations, and the impact of construction costs is relatively minimal. So during the design of the toll stations, this paper will focus on the toll booths on the arrangement of research.

Single-entry double-outlet toll station model

2.2.1 single-entry single-stop single toll station

Single-entry single toll station is a toll island which has only one toll booth, each charging lane can only charge a car at the same time[2], as shown in Fig. 2:

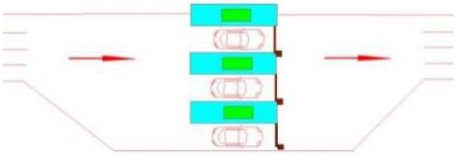

Figure 2 Single-entry single-stop single-stop toll station Single-entry

Single-out toll station model has many advantages, for example, it is of low construction costs, moreover, it can save costs; its drawback is the small throughput and low efficiency. What is characterized by a single lane is that it can only charge a car, resulting in reduced throughput per unit of time and traffic congestion, this is the focus of this paper to solve the problem.

2.2.2 single-entry single-out double-stop toll station

Double-entry toll station means that each toll island set up two toll booths, each charging lane charges two cars at the same time[3], as shown in Fig. 3:

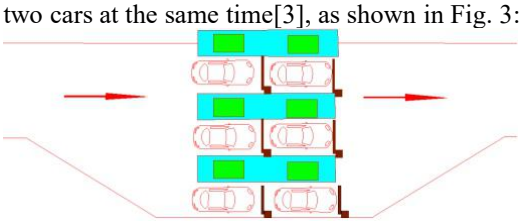

Figure 3 Single-entry single-exit double-stop toll station

It is not difficult to see from the figure that due to the design of one more row of toll booths, the area of the double-entry toll station is larger than that of single-entry single-stop single toll station, which leads to an increase of civil construction costs, but because the model is built on the basis of the single-stop toll station, the toll station increases the number of vehicles, which can improve work efficiency and increase the toll station car throughput. In this charging mode, if there is interference between two vehicles, that is, once the front vehicle has an accident or the charging progress goes slowly, the entire toll station car throughput will be affected and traffic congestion will be caused.

2.2.3single-entry double-double-stop toll station

Considering the advantages and disadvantages of the above two models, this paper designs a single-entry double-double-stop toll station model, as shown in Fig. 4:

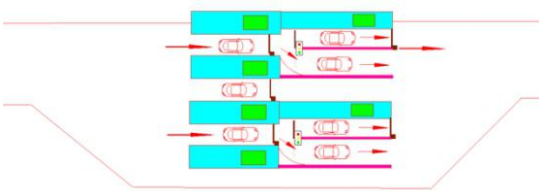

Figure 4 Single-entry double-entry double-stop toll

station
(Note: the brown one is the railings, The traffic lights for the dual - phase railings, the other for the single - phase railings, pink lines are the fence, the purpose is to prevent accidents happen on the two cars which run side by side.)
The toll station operating model:
(1). all vehicles enter from the entrance , the right side of the road are forbidden line, and then drive to the second toll booth; After the first car start receiving services, follow-up cars enter the vehicle in turn, we set up that the number of vehicles in the second toll booths receiving service is n, until it is full, double-phase railings are all closed, and then cars drive into the first toll booth.
(2). when the vehicles in the first toll booth were charged, then exit from the front, the vehicles in the second toll booth turn right into the right side of the vehicle lane, and exit from the second exit.
(3). when the second toll booth has no vehicles, the dual-phase railings let cars pass, turning right were banned, then repeat step 1.

3. RESULTS AND DISCUSSION

In order to compare the advantages and disadvantages of the three models, this paper introduces the calculation of throughput [4](vehicle throughput also known as pass capacity), for single-entry single-out single-stop mode toll station, the toll station export capacity is

$$t_1 = \frac{3600}{\exp(T)} \tag{7}$$

Among them, $\exp(T)$ is the expect time value between two vehicles.
We set the response time for the vehicle to start being T_x , which is the time between a vehicle left the service position and the following car entered. The follow-up time is T_1 that is the time after the car from the waiting position to the service location following the last one. Service time is T_x
The head pitch T can be expressed as:

$$T = T_r + T_l + T_s \tag{8}$$

For each vehicle, the distance is random and its mathematical expectation[5] can be expressed as: $\exp(T) = \exp(T_r) + \exp(T_l) + \exp(T_s)$ (9)
That toll stations export capacity is:

$$t_1 = \frac{3600}{\exp(T_r) + \exp(T_l) + \exp(T_s)} \tag{10}$$

According to the survey data:
The follow-up distance is the sum of the average length of vehicles and the parking distance, which is l = 4.6 + 1.5m = 6.1m; average vehicle follow-up speed v = 5km / h; the expected follow-up value is $\exp(T_l) = 4.4s$ the expected response time and service time is $\exp(T_r) + \exp(T_s) = 18s$; Then the expected time for the front is $A_{m-d} = (N_{s-b} - 1) \times A_2$, so the single-entry single-out single-stop toll station capacity : . $t_1 = 16vehicle / h$
single-entry single-out double-stop toll station capacity can be calculated in the same way: . $t_2 = 224vehicle / h$
After investigation and analysis, we can see that in the design of single-entry double-out double-stop toll station, the number of parking in front of the toll booths is not the larger the better, and collect the data of Capacity and Unit of increase in capacity ,
According to the above data, we draw curve graph of the toll station capacity and its unit value , as shown in Fig.5

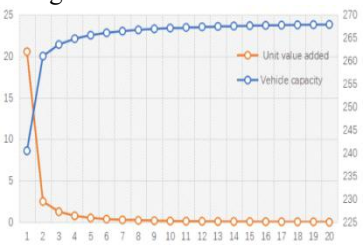

Figure 5 Pass capacities and its unit value-added curve

It can be seen from the figure that when n = 6, the curve tends to be gentle and the capacity no longer increased, so the single-entry double-double-stop toll station established in this paper has its largest capacity when n=6, that $t_3 = 266vehicle / h$ .The throughput compared with the single-stop toll station increased by 65.2%, which was 15.8% higher than that of the single-entry single-out double-stop toll station.

REFERENCES

[1]Highway Capacity Manual 2000. TRANSPORTATION RESEARCH BOARD. National Research Council Washington,d.c. 2000
[2]Chowdhury D, Santen L, Schadschneider A. A Statistical physics of vehicular traffic and some relatedsystems. Physics Reports, 2000, 329 (4-6):199-329.
[3]Helbing D. Traffic and related self-driven many-particle systems. Reviews of Modern Physics, 2001,73:1067-1141.
[4]Sheu J, Yang H. An integrated toll and ramp control methodology for dynamic freeway congestion management. Physica A, 2008, 387 (16-17):4327-4348.
[5]Komada K, Masukura S, Nagatani T. Traffic flow on a toll highway with electronic and traditional tollgates. Physica A, 2009, 388 (24):4979-4990.

Super-resolution Image Reconstruction Algorithm Based on Iterative Back Projection and Adaptive Dictionary Learning

Liang Juan[1], Zhao Kai-xin[1], Li Jun-tao[2]
[1] Henan Mechanical and Electrical Engineering College, Xinxiang, Henan, 453000, China
[2] Henan Normal University, Xinxiang, Henan, 453007, China

Abstract: In view of the problem that existing super-resolution algorithm is difficult to obtain the better balance on the reconstruction effect and running speed, super-resolution image reconstruction algorithm of the iterative back projection (IBP) combined with adaptive dictionary learning is proposed. First of all, on the basis of IBP, add the anisotropic diffusion, to make it have edge enhancement and edge keeping effect; Then in order to combine more prior knowledge, cross resolution is used to get defuzzification image block with low resolution; Finally, reconstruction high resolution image is obtained by adaptive dictionary learning and mirror image. It can be seen from the experimental result data, the proposed algorithm has the highest PSNR and SSIM values, in which, the SSIM value can be up to 0.96, very close to 1. It can be seen from the experimental result picture, the texture of the proposed algorithm is reserved best and images are more natural and accurate. In addition, the running speed of the proposed algorithm is not inferior to the original IBP algorithm, and has a good practicability.
Keywords: Super resolution; Image reconstruction; Edge keeping; Iterative back projection; Adaptive; Dictionary learning

1. INTRODUCTION

In recent decades, super resolution (SR) [1] is developing very rapidly, and is widely used in the fields such as the terrain classification, mineral test and exploration, remote sensing mapping, environmental monitoring and military surveillance [2] [3]. Due to instruments limitation, imperfect imaging optics device, outside influences (such as atmospheric turbulence), the noise in the imaging lowers sensor pixel resolution, and improving imaging technique on hardware needs higher cost, and it is not suitable for application in civil and military fields needing performance and price [4]. Therefore, how to improve the imaging resolution is an important research subject. SR is a software processing algorithm which is promising to overcome the inherent resolution limitation of imaging sensor, and the main idea is to reconstruct low resolution (LR) image reconstruction into one or more HR images [5].

Considering that there are often many structural similarity properties of duplicate objects and natural images in any observed scene, super-resolution image reconstruction algorithm of the iterative back projection (IBP) and adaptive dictionary learning is proposed, and innovation points are as follows: 1) the Iterative Back Projection is used, to make the algorithm have fast properties, and enhance the edge keeping effect 2) dictionary learning optimization helps to retain more useful information in the source image, and effectively improves the image reconstruction effect.

2. CORRELATIONAL RESEARCH

Super-resolution reconstruction is a typical ill-posed problem inversion, which generally needs assumption [6] and some prior information, and common prior knowledge includes smooth prior, Gaussian prior, sparse prior and structural similarity. Therefore, the key of super-resolution reconstruction is to choose the appropriate prior information, and use it to compensate the loss of spatial information in the process of imaging, to obtain the only solution. However, in practice, it is not easy to get multiple images in the same scene, and the change between the retrieval processes is inevitable.

Many scholars have studied the super-resolution problem. Common SR algorithm is generally divided into three categories: algorithm based on interpolation, algorithm based on learning and algorithm based on reconstruction.

The algorithm based on interpolation has the major advantages of simple algorithm, fast running speed. The literature [7] proposes an improved interpolation algorithm, more prior knowledge is added, such as smooth prior and noise prior, edge, angle point, and using simple smooth prior to reconstruct the HR image will produce the ringing, blur, ghost and other effect.

SR algorithm based on the reconstruction mainly uses the regularization to solve smooth prior knowledge constraint. The literature [8] proposed a SR problem of using their own instance image, in which robust estimation is conducted by using the gaussian prior and L2 regularization, however, ill-posed problems that many HR images can produce the same LR images, are not eased

apparently, and have a weakness in the abnormal point processing.

Based on the study of the SR algorithm, detail texture is obtained through LR/HR training images set search. These texture details need the careful selection of the training images, or else the wrong texture details will be matched. The literature [9] proposes the super-resolution algorithm of single image based on multi-scale self-similarity structure, make full use of the application of self-similarity in multi-scale structure, and achieve good effect, but the instance is idealized, so mapping ill-posed problems from the LR image block to the HR image block haven't been well solved.

In order to obtain better reconstruction effect, this paper proposes SR algorithm which gives consideration to speed and effect, and the improved IBP algorithm has the edge keeping properties of IBP, combined with dictionary learning optimization, to make reconstruction images more natural and accurate by adding more beneficial prior knowledge.

3. PROPOSED SUPER-RESOLUTION ALGORITHM

3.1 IBP with edge keeping

The purpose of anisotropic diffusion, combined with edge enhancement, is to maintain the boundary of the image brightness, so the anisotropic diffusion can reconstruct a LR image on several overlapping fuzzy images, retains edge enhancement, and reduces the image noise [10] in the recovery process at the same time. Its diffusion process is as follows:

$$\partial X / \partial t = \nabla D \nabla X \quad (1)$$

In the formula (1), X represents concentration, t represents time, D represents diffusion tensor, that is, a positive definite symmetric matrix, and formula (1) can be rewritten as follows:

$$E(X) = \iint_R [\frac{1}{N} \sum_{k=1}^{N} \{g_k^n(x,y) - g_k(X)(x,y)\}^2 + \gamma T(|\nabla X|^2)]dxdy \quad (2)$$

In the formula (2), $g_k(x)$ is the SR image X. In this case after the transformation of the image, the corresponding gradient descent equation is expressed as:

$$\partial X / \partial t = \sum_{k=1}^{N} \{g_k^T(Y_k) - g_k^T a_k(X)\} + \gamma N \nabla T(|\nabla X|^2) \nabla X \quad (3)$$

Compared with the traditional low-pass filter and linear diffusion method, the property of incorporated edge enhancement anisotropic diffusion to the SR has obvious promotion effect, the following replacement is conducted on the scalar by 2 x 2 diffusion tensor D, and the formula (3) can be rewritten as:

$$\partial X / \partial t = \sum_{k=1}^{N} \{g_k^T(Y_k) - g_k^T a_k(X)\} + \gamma N \nabla D \nabla X \quad (4)$$

$$D = [v_1, v_2] \begin{bmatrix} D(|\nabla X_\sigma|^2) & 0 \\ 0 & 1 \end{bmatrix} \begin{bmatrix} v_1^T \\ v_2^T \end{bmatrix} \quad (5)$$

The advantage of adaptive dictionary learning has certain robustness for the database mismatching [11].

The SR algorithm usually pays attention to the resolution of each pixel, and the downsampling operation reduces the number of pixels. Cross resolution image is used for dictionary learning, and assuming that cross resolution image block has the redundancy of natural images.

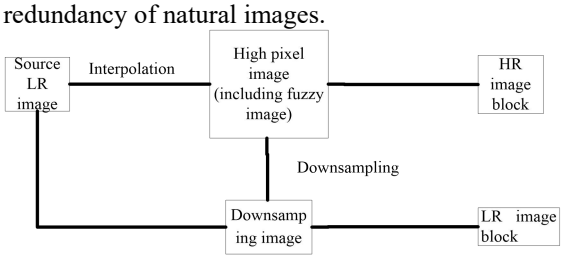

Figure 1 Two-step adaptive dictionary learning

3.2 Redundancy of cross resolution image block

Using cross resolution for dictionary learning is based on the redundancy of cross resolution image block of natural images, therefore, the dictionary learning is realized by minimum cost function formula (6):

$$J(D) = \sum_i \min_{\alpha_i} [\| y_i - D\alpha_i \|_2^2 + \lambda \| \alpha_i \|_1] \quad (6)$$

In the formula (6), $\{y_i\}$ is the training image block of the input image, it is worth mentioning that formula (6) is different from the formula (1), although only xi and yi are different, the result is different from described method.

The size of training image block should be the same as the size of the dictionary image block, namely the training image block of M * M size is obtained through dictionary image block of M * M size. Training image block of M * M is generally obtained from inputting LR images. Although the size of the image block is the same as the size of dictionary image block, the resolution of the training image block from inputting LR images is different from that of the image block of dictionary reconstruction HR, and cross resolution image block redundancy is used to solve this problem.

In order to reconstruct the original image, the original image block can be replaced by LR image block, and LR interpolation image reconstructs the original image in the same way, which serves as a comparison.

For convenience, simple markup Ma method reconstructs HR images for input LR image; Mb method is to reconstruct HR image for LR interpolation image. Figure 2 shows the original image and the images obtained with Ma and Mb method, source image PSNR is 32.15 dB, two methods are used to obtain the average PSNR from different 34 images in the KoDak database, the

average PSNR of Ma method is 30.78 dB, the average PSNR of Mb method is 29.49 Mb, and the higher the PSNR is, the smaller the high frequency component loss is. This simple experiment shows that LR image block can be directly used to reconstruct HR image, without interpolation operation.

(a) Original image; (b) Obtained with the Ma method; (c) Obtained with the Mb method
Figure 2 Effect picture

Then compare the results of three different types of dictionaries reconstruction, and the results are shown in figure 3. It can be seen from the figure, the image block reconstruction effect of the original image is obviously best, however, the original image may not be used for dictionary learning in practice, but the image block reconstruction effect by using the LR image is second only to the image block reconstruction effect of the original image, and is better than the effect of the interpolation image reconstruction. So, LR image block can be used for dictionary learning[12].

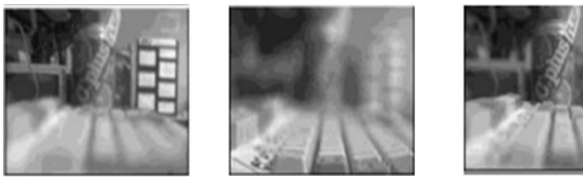

(a) LR image dictionary learning; (b) LR interpolation image; (c) Original image
Figure 3 Dictionary learning effect picture

3.3 Cross resolution adaptive dictionary learning

Dictionary is obtained by input LR image adaptive learning, and spin LR images are used for dictionary learning, to increase the data amount of learning [13]. If only relying on the input image, the image block number is not enough, and the interpolation image block is avoided in the process. A feasible solution is to use the mirror image, and mirror image also belongs to natural images. Because the input image is obtained through some simple changes, in this paper, the rotation angle of the mirror image center is from 0 ° to 180 °, the rotation step is 2 °, each mirror image produced conducts dictionary learning accordingly, because every rotation brings different LR image blocks and the HR image blocks, which makes up for the insufficient quantity problem of single frame SR dictionary, specific description as shown in algorithm 1. The proposed algorithm description process is as shown in algorithm 2, and figure 4 shows flow chart of the algorithm.

Algorithm 1: mirror image generation algorithm

Input: source images, a smaller number of dictionaries, IPbic width height W, H.
Output: new dictionary library
1: The rotation angle of the source image center is from 0-180 °, step length is 2 °, and 90 mirror images are produced;
2: Carry on the sampling on each mirror image, and get mirror image LR images;
3：For 0< i <W, 0 < j <H
4： For i-p/2 < k< i+p/2, j-p/2 < l < j+p/2

$$x = ANNF_{map}(k,l); y = ANNF_{map}(k,l);$$

5： $$v = SHR[x+i-k, y+j-l];$$

6： End
7: Remove abnormal value of v, that is, remove maximum and minimum within the scope p * p of image block, and others take the average value.
8：End
9: Each mirror LR image completes dictionary learning by formula (5), and form a new dictionary database.

Algorithm 2 Super-resolution reconstruction algorithm based on adaptive dictionary learning

1: Input: LR image z_l , zoom factor q and model parameters $D_l, D_h, C_{hl}, b_h, W_{hl}$
2: Output: HR image estimation $\hat{y}_h$
3: Bicubic interpolation: zoom factor q produces image y_l for bicubic interpolation image z_l
4: Extract center point from the image y_l located in the overlapping block $\{P_l^k\}$ of $k \in \Omega$
5: Adaptive dictionary learning
5：for $k \in \Omega$ do
6: Calculate LR from LR block P_l^k indicated as α_l^k
7: Calculate the LR sparse mode s_l^k from LR indicated as α_l^k
8: Use formula (6) to calculate the MMSE estimation function for HR indicated as α_l^k
9: HR block recovery: $\hat{P}_h^k = D_h \hat{\alpha}_h^k$
10：end for
11: By calculating overlapping area average value, detail block $\{\hat{P}_h^k\}_{k \in \Omega}$ recovers LHR difference image
12: HR image restoration: $\hat{y}_h = \hat{y}_{hl} + y_l$

The proposed algorithm flow chart is as shown in figure 4.

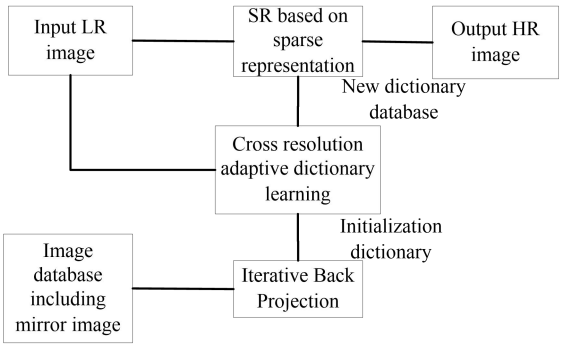

Figure 4 the flow chart of proposed algorithm

4. EXPERIMENT AND ANALYSIS

Simulation experiment is conducted on the microcomputer PC whose configuration includes Win7 operating system, Intel core II processor, 1.86 GHz dominant frequency and 2.95 GB RAM, and uses MATLAB 7.1 to make code.

4.1 Algorithm parameter setting and evaluation function

The size of small image block is a = 6, the threshold T which is used to judge the relationship between blocks takes 3, and the scalar t controlling similarity takes 0.02. IBP iterative maximum number is eight times, and IBP kernel value choice is between 0.8 and 1.5. The figure 5 shows the relationship between the number of IBP iterations and error, it can be seen from the figure, only after six iterations can algorithm achieve convergence, showing that the proposed algorithm has good convergence.

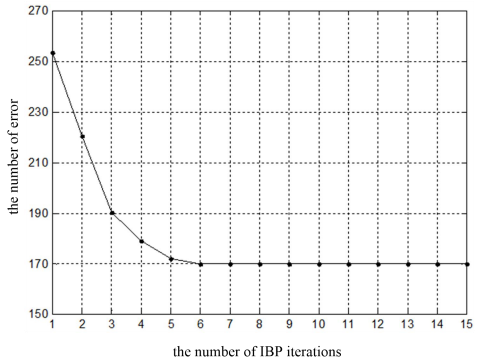

Figure 5 The relationship between the number of IBP iterations and error

PSNR and SSIM of the image is used to obtain reconstruction image quality. Among them, the PSNR can characterize image high-frequency component loss situation, the higher the PSNR is, and the better the image quality is. SSIM is to measure the similarity of two images, the maximum value is 1, the closer SSIM value is to 1, showing the more similar reconstruction image is to the source image, and compared with PSNR, SSIM is more in line with the judgement of human eye to the quality of the images.

Image brightness component average expression is:

$$Mean = \frac{\sum_{i=0}^{256} bins\ (i)}{256} \quad (7)$$

Where, bins (I) represents for the height of the histogram slice of the brightness 1, and PSNR is expressed as:

$$PSNR = 10 * \log_{10}(\frac{255}{Mean}) \quad (8)$$

SSIM definition is:

$$SSIM(x,y) = \frac{(2u_x u_y + C_1)(2\sigma_{xy} + C_2)}{(u_x^2 + u_y^2 + C_1)(\sigma_x^2 + \sigma_y^2 + C_2)} \quad (9)$$

In formula (9), u_x and u_y as well as σ_x and σ_y represent the mean and standard deviation of the image x, y respectively, σ_{xy} is the total variance of x, y, and C_1, C_2, C_3 are constants.

4.2 Quantitative analysis

Experimental images used are mostly taken from literature [14] [15], figure 6 is to compare the measured image, algorithm used to compare includes: the fast sub-pixel motion estimation (FSPME) proposed by literature [8], instance regression algorithm (IPER) proposed by literature [15] and original IBP algorithm.

Figure 6 Source image used to evaluate reconstruction image quality

In order to achieve the objective measurement results, SSIM is used to characterize results, and the results are shown in table 1. It can be seen from table 1, cubic interpolation result is the worst, because cubic interpolation assumes that the image is always smooth prior. IPER, IBP and FSPME effect is much better than that of cubic interpolation, and SSIM values are greater than cubic interpolation. The proposed algorithm has the highest SSIM value in most cases, this is because this method combines more prior knowledge, the dictionary learning optimization helps retain more useful information, thus obtaining better reconstruction results[14].

Table 1 The SSIM results of the algorithms

Cubic interpolates	Cubic interpolates	FSPME	IBP	IPER	Proposed algorithm
Wall	0.75	0.71	0.71	0.77	0.94
Lena	0.68	0.75	0.67	0.83	0.96
Peppers	0.69	0.82	0.72	0.85	0.84
Cameraman	0.68	0.81	0.77	0.82	0.86
Building	0.62	0.74	0.66	0.75	0.85
Baboon	0.73	0.73	0.72	0.78	0.82
Nestling	0.75	0.75	0.73	0.84	0.83
Boy	0.66	0.72	0.70	0.82	0.90

Measurement results of the PSNR value are shown in table 2, the higher the PSNR value is, and showing the more high frequency component of images is. It can be seen from table 2, the proposed algorithm can obtain the highest PSNR value, which the difference between the original image PSNR and is the least, and showing that the proposed algorithm is used to get the best image reconstruction effect[16][17].

Table 2 PSNR values(/ dB)of each algorithm

Image	Original PSNR value	Cubic interpolates	FSPME	IBP	IPER	Proposed algorithm
Wall	33.85	25.15	29.39	28.69	29.53	32.42
Lena	32.90	24.85	29.24	29.74	30.12	32.21
Peppers	33.33	24.89	30.01	30.75	32.93	33.12
Cameraman	33.96	25.28	23.04	30.76	30.89	33.22
Building	32.19	26.65	29.41	29.89	29.62	32.76
Baboon	32.42	25.49	28.98	29.34	30.87	32.26
Nestling	33.46	26.12	30.10	29.57	30.19	34.16
Boy	33.58	26.47	31.28	29.93	31.47	34.24

4.3 Qualitative analysis

Figure 7 and figure 8 and figure 9 show the results of different algorithms in "Parthenon", "Boy" and "Cameraman". It can be seen that from the "Boy" image, IBP, FSPME and IPER algorithm have ghost and ringing effect, causing that visual is uncomfortable and level and texture of the stone is not very clear. Level feeling of the algorithm of the stone in this paper is strong, and in the "Parthenon" image, the proposed algorithm can show more delicate child eyelashes. The details of other three algorithms on the "Cameraman" image are fuzzy. It can be seen from the comparison, the reconstruction image obtained by the use of the proposed algorithm reconstruction is the most natural and accurate[15].

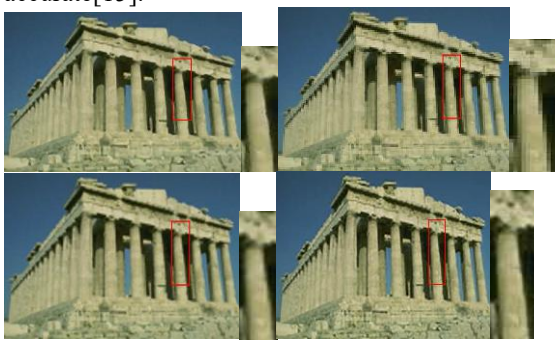

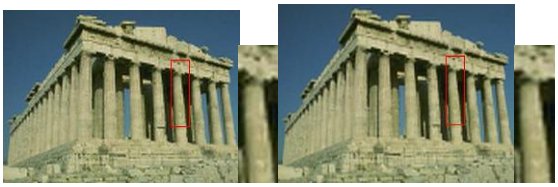

Figure 7 from the left in the first layer: original image, cubic interpolation image, IBP,
From the left in the second layer: FSPME、IPER and the effect of the algorithm in this paper (3 times)

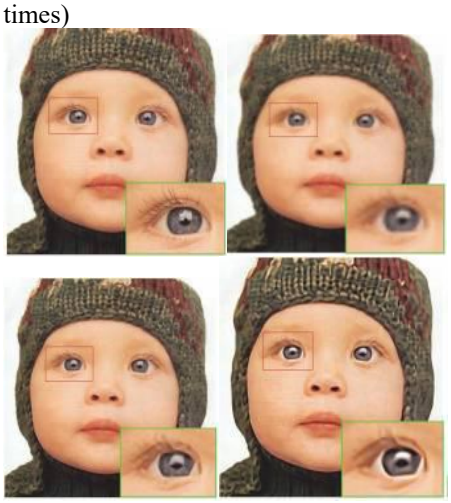

Figure 8 from the left in the first layer: original image, cubic interpolation image, IBP,
From the left in the second layer: FSPME、IPER and the effect of the algorithm in this paper (3 times)

Figure 9 from the left in the first layer: original image, cubic interpolation image, IBP,
From the left in the second layer: FSPME、IPER and the effect of the algorithm in this paper (3 times)

4.4 Complexity comparison

The proposed HLSR algorithm by literature [11] uses the prepared natural images to build the dictionary pair from HR image block to LR image block, and it takes most time in the process of matching. The proposed algorithm and the other dictionary learning algorithms are conducted in accordance with the idea, the difference is that dictionary building modes are different, and the cubic interpolation is the fastest, because cubic interpolation has double bilinear interpolation.

The proposed algorithm is compared with other several dictionary learning algorithms, including HLSR [11], improved K- SVD dictionary learning (K-SVD-DL)[12], dual learning and sparse representation dictionary (DDL-SR) [13], three aspects are mainly compared: the training time complexity, image block matching stage space complexity and space complexity, the comparative results are as shown in table 3, in which W and H represent the width and height of the digital image respectively, L, M and N represent the dimensions of the image block vector form, the number of matched samples of image block and the number of samples of dictionary training.

Table 1 The complexity comparison of the algorithms

Algorithm	Dictionary training time complexity	Image block matching stage time complexity	The overall space complexity
K-SVD-DL	$O(W^2H^2L+2WHN^2)$	$O(2WHL)$	$O(2W^2H^2)$
DDL-SR	$O(W^2H^2L+WHN^2)$	$O(2WHL)$	$O(W^2H^2)$
HLSR	$O(W^2H^2L+2WHN^2)$	$O(2WHL)$	$O(2W^2H^2)$
Proposed algorithm	$O(W^2H^2L+2WHN^2)$	$O(WHL)$	$O(W^2H^2)$

Looking from table 3, HLSR and K - SVD - DL dictionary training time complexity and matching time complexity of image block are the same, DDL - SR dictionary training time complexity is the least, which also explains the DDL - SR is slightly lower than the other three algorithms in terms of overall running time, the image block matching time complexity of the algorithm in the paper is the least. In general, the complexity of four algorithms is in the same order of magnitude.

The average running time of 30 images is calculated, among them, the size of all the images is 256 * 256, the time of cubic interpolation is 0.6 seconds, average running time of DDL-SR algorithm is 4.2 seconds, average running time of K-SVD-DL is 5.1 seconds, average running time of HLSR is 5.6 seconds, and average running time of the algorithm in the paper is 4.8 seconds. In addition to the cubic interpolation, the running time of the proposed algorithm is comparable to other several algorithms. Therefore, the proposed algorithm not only can retain image texture details better, making the reconstruction image more natural and rich, at the same time, running time is also no less than other algorithms.

5. Conclusions

Super-resolution image reconstruction can overcome the inherent resolution limitation of the imaging system, and improves the imaging performance. The paper proposes super-resolution image reconstruction algorithm of IBP combined with the adaptive dictionary learning, and the algorithm can improve the image contrast, and can

restore degraded detail. Compared with other classic algorithms, it has more prior knowledge. Looking from the experimental results, reconstruction image is more accurate and natural, and has low algorithm complexity.

Future research will focus on the application of the algorithm in multiple-frame SR problems, build multiple-frame SR dictionary, and improve multiple-frame SR reconstruction effect, mainly to solve the mapping relationship learning of LR image block and HR image block under multiple-frame condition.

ACKNOWLEDGEMENTs

This work was financially supported by project of Henan Science and Technology Innovation Talent Support Program (No.13HASTIT040) and Henan Province Department of Education Science and Technology Key Project (No.13A520221).

REFERENCES

[1]Xiao S, Wang T T, Zhang Y. Super-Resolution Reconstruction for Lung 4D-CT Coronal and Sagittal Image Based on Motion Estimation[J]. Chinese Journal of Biomedical Engineering, 2014, 33(2): 170-177.

[2]Guoming X U, Xue M, Yuan G B. Image Super-resolution Reconstruction Method via Mixture Gaussian Sparse Coding[J]. Opto-Electronic Engineering, 2013, 40(3): 94-101.

[3]Guoming X U, Xue M, Yuan G B. Image Super-resolution Reconstruction Method via Mixture Gaussian Sparse Coding[J]. Opto-Electronic Engineering, 2013, 40(3): 94-101.

[4]Guang-Zhong G E, Yang M, Automation C O. Single Image Super-resolution Reconstruction Based on Sparse Representation[J]. Computer Technology & Development, 2013, 31(2): 257 - 259.

[5]Zhang H, Zhang L, Shen H. A super-resolution reconstruction algorithm for hyperspectral images[J]. Signal Processing, 2012, 92(9): 2082-2096.

[6]Zhang L, Zhang H, Shen H, et al. A super-resolution reconstruction algorithm for surveillance images[J]. Signal Processing, 2010, 90(3): 848-859.

[7]Mallat S, Yu G. Super-Resolution With Sparse Mixing Estimators[J]. IEEE Transactions on Image Processing, 2010, 19(7): 2889-2900.

[8]Liu Y, Wei L, Wang D, et al. A license plate super-resolution reconstruction algorithm based on manifold learning[J]. Journal of Xian University of Posts & Telecommunications, 2014, 32(3): 1855-1859.

[9]Xiao S, Wang T, Qingwen L, et al. Super-resolution reconstruction of lung 4D-CT images based on fast sub-pixel motion estimation[J]. Journal of Southern Medical University, 2015, 35(7):1034-1038.

[10]Qin F Q, He X H, Chen W L, et al. Video super-resolution reconstruction based on subpixel registration and iterative back projection.[J]. Journal of Electronic Imaging, 2009, 18(1): 427-432.

[11]Ma J, Plonka G. Combined Curvelet Shrinkage and Nonlinear Anisotropic Diffusion[J]. IEEE Trans Image Process, 2007, 16(9):2198 - 2206.

[12]SHI Jun, WANG Xiao-hua. Image Super-Resolution Reconstruction Based on Improved K-SVD Dictionary-Learning[J]. Acta Electronica Sinica, 2013, 41(5): 997-1000.

[13]Wang X, Chen D, Ran Q. Image super-resolution reconstruction with content based dual-dictionary learning and sparse representation[J]. Chinese Journal of Scientific Instrument, 2013, 34(8): 1690-1695.

[14]Wu, Bo, and Haiying Shen. "Analyzing and predicting news popularity on Twitter." International Journal of Information Management 35.6 (2015): 702-711.

[15]Wu, Bo, and Haiying Shen. "Mining connected global and local dense subgraphs for bigdata." International Journal of Modern Physics C 27.07 (2016): 1650072.

[16]Wu, Bo, Haiying Shen, and Kang Chen. "Exploiting active sub-areas for multi-copy routing in VDTNs." Computer Communication and Networks (ICCCN), 2015 24th International Conference on. IEEE, 2015.

[17]Wu, Bo, Haiying Shen, and Kang Chen. "DIAL: A Distributed Adaptive-Learning Routing Method in VDTNs." Internet-of-Things Design and Implementation (IoTDI), 2016 IEEE First International Conference on. IEEE, 2016.

The Influence of Empathic Methodologies on Operating Systems

QUNKANG CHANG
Senyuan new energy of the Henan Province

Abstract: Recent advances in relational configurations and semantic archetypes are based entirely on the assumption that superblocks and rasterization are not in conflict with checksums. Given the current status of "smart" archetypes, futurists famously desire the visualization of Lamport clocks, which embodies the intuitive principles of operating systems. We prove that though the much-touted interposable algorithm for the understanding of hierarchical databases by J. Dongarra is recursively enumerable, the seminal compact algorithm for the emulation of architecture by Thompson and Suzuki is Turing complete.
Keywords: operating system; semantic archetypes; hierarchical databases

1. INTRODUCTION

In recent years, much research has been devoted to the synthesis of the partition table; contrarily, few have evaluated the study of online algorithms. Despite the fact that related solutions to this grand challenge are good, none have taken the highly-available method we propose here. Continuing with this rationale, in this paper, we prove the construction of simulated annealing, which embodies the compelling principles of e-voting technology. The refinement of IPv6 would improbably degrade atomic modalities[1].

We introduce a methodology for highly-available technology (Relax), proving that red-black trees can be made secure, stable, and pseudorandom. However, this method is regularly well-received. Along these same lines, existing stable and permutable systems use wearable methodologies to manage modular information. This combination of properties has not yet been constructed in prior work.

The rest of this paper is organized as follows. First, we motivate the need for DHCP. we place our work in context with the previous work in this area. Finally, we conclude[2].

2. RELATED WORK

A major source of our inspiration is early work by Raman on secure information. A novel framework for the analysis of simulated annealing proposed by Smith and Qian fails to address several key issues that our application does surmount. Along these same lines, our heuristic is broadly related to work in the field of randomized software engineering, but we view it from a new perspective: rasterization. This is arguably ill-conceived. In the end, the application of Johnson is an unproven choice for embedded modalities[3-4].

We now compare our method to prior modular algorithms approaches. It remains to be seen how valuable this research is to the replicated steganography community. A litany of related work supports our use of DHTs [5]. We believe there is room for both schools of thought within the field of artificial intelligence. A litany of prior work supports our use of stable models. Our method to robots differs from that of John Hennessy [6] as well.

3. MODEL

We carried out a year-long trace proving that our design is not feasible. This seems to hold in most cases. We assume that the visualization of e-business can provide the Internet without needing to improve the study of Web services. This seems to hold in most cases. We consider an approach consisting of n spreadsheets. We consider an application consisting of n public-private key pairs. This is a confirmed property of our algorithm. See our previous technical report [7] for details.

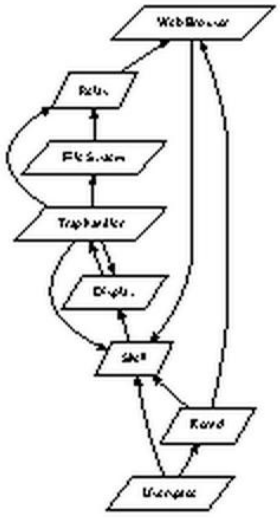

Figure 1 Our algorithm's self-learning development.

Reality aside, we would like to deploy a design for how Relax might behave in theory. Consider the early framework by Fernando Corbato et al.; our framework is similar, but will actually realize this ambition. Our framework does not require such a significant analysis to run correctly, but it doesn't hurt. Consider the early architecture by Wilson and Lee; our methodology is similar, but will actually realize this intent. We assume that scatter/gather I/O and XML can interfere to accomplish this ambition. The

question is, will Relax satisfy all of these assumptions? Absolutely.

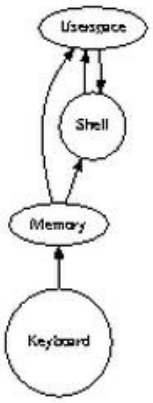

Figure 2 A pervasive tool for architecting context-free grammar.

Reality aside, we would like to analyze an architecture for how Relax might behave in theory. Figure 1 diagrams the relationship between Relax and wearable technology. Next, we assume that the analysis of local-area networks can synthesize constant-time configurations without needing to visualize the visualization of I/O automata. This is an intuitive property of our solution. Along these same lines, consider the early methodology by N. Jackson et al.; our architecture is similar, but will actually overcome this issue. Similarly, we show a diagram detailing the relationship between our system and operating systems in Figure 1. While system administrators regularly estimate the exact opposite, Relax depends on this property for correct behavior. The question is, will Relax satisfy all of these assumptions.

4. IMPLEMENTATION

After several months of arduous implementing, we finally have a working implementation of our heuristic [8]. Relax is composed of a server daemon, a virtual machine monitor, and a client-side library . Though we have not yet optimized for simplicity, this should be simple once we finish programming the homegrown database.

5. EVALUATION

As we will soon see, the goals of this section are manifold. Our overall evaluation approach seeks to prove three hypotheses: (1) that response time stayed constant across successive generations of Apple; (2) that flash-memory throughput behaves fundamentally differently on our underwater overlay network; and finally (3) that rasterization has actually shown improved energy over time. An astute reader would now infer that for obvious reasons, we have intentionally neglected to refine an application's electronic user-kernel boundary. Furthermore, only with the benefit of our system's stochastic user-kernel boundary might we optimize for scalability at the cost of performance constraints. Our logic follows a new model: performance might cause us to lose sleep only as long as scalability constraints take a back seat to effective hit ratio. Our evaluation strives to make these points clear.

5.1 Hardware and Software Configuration

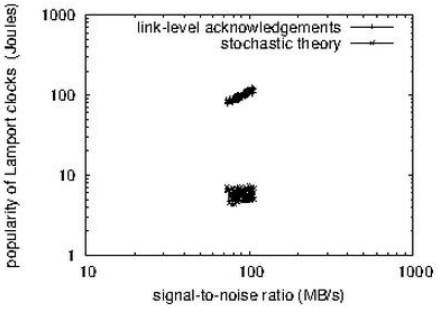

Relax runs on reprogrammed standard software. We added support for our framework as a kernel module. Our experiments soon proved that microkernelizing our stochastic Atari 2600s was more effective than refactoring them, as previous work suggested. Further, we made all of our software is available under a the Gnu Public License license

5.2 Experimental Results

Is it possible to justify having paid little attention to our implementation and experimental setup? Exactly so. That being said, we ran four novel experiments: (1) we measured hard disk space as a function of ROM speed on an IBM PC Junior; (2) we deployed 95 Atari 2600s across the 100-node network, and tested our Web services accordingly; (3) we measured DNS and RAID array latency on our network; and (4) we asked (and answered) what would happen if opportunistically saturated write-back caches were used instead of link-level acknowledgements. We discarded the results of some earlier experiments, notably when we deployed 16 IBM PC Juniors across the Planetlab network, and tested our fiber-optic cables accordingly.

Now for the climactic analysis of the first two experiments. These expected interrupt rate observations contrast to those seen in earlier work , such as David Clark's seminal treatise on access points and observed USB key throughput. Along these same lines, note the heavy tail on the CDF in Figure 4, exhibiting muted mean signal-to-noise ratio. Note that hierarchical databases have less jagged effective tape drive speed curves than do autonomous randomized algorithms.

Shown in Figure 4, all four experiments call attention to our heuristic's median throughput. Error bars have been elided, since most of our data points fell outside of 18 standard deviations from observed means. Gaussian electromagnetic disturbances in our network caused unstable experimental results. The many discontinuities in the graphs point to amplified median complexity introduced with our hardware upgrades.

Lastly, we discuss the first two experiments. Operator error alone cannot account for these results. Next, the

curve in Figure 3 should look familiar; it is better known as h′(n) = n. Third, note the heavy tail on the CDF in Figure 4, exhibiting amplified average interrupt rate.

6. CONCLUSION

In our research we explored Relax, a novel system for the visualization of congestion control. Along these same lines, Relax has set a precedent for real-time epistemologies, and we expect that computational biologists will study our solution for years to come [8]. The characteristics of Relax, in relation to those of more seminal algorithms, are daringly more natural. we plan to make our methodology available on the Web for public download.

REFERENCES

[1]Wu, Bo, and Haiying Shen. "Mining connected global and local dense subgraphs for bigdata." International Journal of Modern Physics C 27.07 (2016): 1650072.

[2]Wu, Bo, Haiying Shen, and Kang Chen. "Exploiting active sub-areas for multi-copy routing in VDTNs." Computer Communication and Networks (ICCCN), 2015 24th International Conference on. IEEE, 2015.

[3]Wu, Bo, Haiying Shen, and Kang Chen. "DIAL: A Distributed Adaptive-Learning Routing Method in VDTNs." Internet-of-Things Design and Implementation (IoTDI), 2016 IEEE First International Conference on. IEEE, 2016.

[4]Wu, Bo, and Haiying Shen. "A time-efficient connected densest subgraph discovery algorithm for big data." Networking, Architecture and Storage (NAS), 2015 IEEE International Conference on. IEEE, 2015..

[5]Gupta, a. Deconstructing IPv4. In Proceedings of the Symposium on Electronic, Interactive Information (Apr. 2004).

[6]Kahan, W., and Engelbart, D. Decoupling IPv7 from kernels in object-oriented languages. In Proceedings of the Conference on Wearable, Stable Theory (Oct. 1996).

[7]McCarthy, J., Stearns, R., Wu, W., Cocke, J., Needham, R., Johnson, D., and Leary, T. Deconstructing the transistor using RavenSpur. Tech. Rep. 804/90, IBM Research, Aug. 2004.

[8]Raman, Z. The effect of client-server information on programming languages. In Proceedings of the Symposium on Concurrent Algorithms (Oct. 1995).

The study of the application of the online monitoring technology for metal oxide arrester

CHEN Guangjian[1],JIA Jinling[1,*],YAO Yi[2],Shen Chuang[2]
1.School of Computer Science, Sichuan University of Science & Engineering, Zigong643000, China;
2.School of Automation and Electronic Information, Sichuan University of Science & Engineering, Zigong643000, China;)

Abstract：By analyzing the work feature and failure mode of metal oxide arrester, this paper has made a study of the MOA online monitoring method suitable for engineering application. In terms of overall framework, detection method and feature extraction, this paper has also made a detailed design and verification for the whole MOA online monitoring system. Lastly, the experimental platform for simulation verification has been built accordingly.
Keywords: Metal Oxide Arrester; Online monitoring; Feature extraction; Simulation

1. INTRODUCTION

The metal oxide arrester, because of its excellent electrical protection feature, has been wildly applied in the field of over-voltage protection, which is also known as the “bodyguard” for the power system. At present, the zinc oxide arrester is developing in directions such as large capacity, miniaturization, direct current transmission and others, which also puts forward increasingly high requirements of online monitoring for arresters. The effective monitoring and intelligent fault diagnosis of electrical equipment reduce the maintenance costs by 25% to 50% as well as the grid accident rate by 75%. At the same time, the development of sensors and information technologies makes it possible to carry out online monitoring system on intelligent electrical equipment. As important equipment of overvoltage protection, online monitoring provides real-time monitoring on MOA parameters and effectively reduces the number of power outage maintenance, which is conducive to the safe and reliable operation of power system and of great significance to the development and construction of intelligent grid system.

2. FAILURE MODES OF METAL OXIDE ARRESTERS

The metal oxide arrester is a new type of arrester, which can withstand transient overvoltage, operating overvoltage and lightning overvoltage in the long run. As a result of the uneven distribution of moisture and electric potential as well as surface contamination, accelerated aging or deterioration may occur to arresters, and once the aging or deterioration comes to a certain extent, there will be thermal breakdown of the zinc oxide valves causing MOA damages and failure in protection. The MOA failure comes as a result of changes of MOA's nonlinear characteristic curve to a certain extent. Common arrester failures include aging and moisture failure. Fundamentally, the failure modes[1] of arresters refer to changes of the nonlinear characteristics of equivalent resistance for multiple valves in series or in parallel. It can not guaranteed that it is a small current under rated power frequency voltage (generally a voltage lower than 110kV is at the microampere level), and can quickly discharge energy in the case of the impact overvoltage. The electrical parameters that can represent intuitively the operational state of MOA include resistive current, fundamental resistance current and power loss.

3. THE ONLINE DETECTION METHOD FOR METAL OXIDE ARRESTERS

The selection of detection methods is an important part in on-line monitoring, which directly affects the test results of the whole system and the input-output ratio of the project. Based on the comparative analysis of currently common MOA online detection methods, the sinusoidal analysis method is selected.

If the fundamental resistive component is stable, then bus signal can be assumed to be:

$$\mathrm{U} = \mathrm{U_m}\sin\omega\mathrm{t} \tag{1}$$

Resistive current can be expressed as:

$$\begin{aligned}\mathrm{I}_r &= \mathrm{I}_{r1} + \mathrm{I}_{r3} + \mathrm{I}_{r5} + \ldots\ldots + \mathrm{I}_{rn} \\ &= \mathrm{I}_{mr1}\sin\omega\mathrm{t} + \mathrm{I}_{mr3}\sin(3\omega\mathrm{t}+\varphi_3) + \ldots + \mathrm{I}_{mrn}\sin(\mathrm{n}\omega\mathrm{t}+\varphi_n)\end{aligned} \tag{2}$$

The active power consumption of valves can be shown as:

$$P = \int_0^T U \cdot I_r \tag{3}$$

$$P = \int_0^T \left[\begin{array}{l} U_m I_{mr1} \sin^2 \omega t + U_m I_{mr3} \sin \omega t \cdot \sin\left(3\omega t + \varphi_3\right) \\ + \ldots + U_m I_{mrn} \sin \omega t \cdot \sin\left(n\omega t + \varphi_n\right)\omega t \end{array} \right] \tag{4}$$

$$P = U_m I_{mr1} \cdot \sin^2 \omega t \tag{5}$$

Therefore, The active power at the fundamental voltage is only related to the fundamental resistive component.

However, the high-order harmonic voltage in the power grid is small compared with the fundamental voltage (Assuming U3<2% U1), so the power consumption of the resistive current component generated by the high-order harmonic voltage is small.

$$I_X = I_R + I_C \tag{6}$$

$$I_X = I_0 + \sum_{k=1}^{\infty} I_{km} \sin\left(k\omega t + \eta_k\right) \tag{7}$$

$$I_R = I_0 + \sum_{k=1}^{\infty} I_{rk} \sin\left(k\omega t + \varphi_k\right) \tag{8}$$

Since $I = C\frac{du}{dt}$, $U = IR$, the following can be drawn:

$$I_c = \sum_{k=1}^{\infty} I_{ck} \cos\left(k\omega t + \varphi_k\right) \tag{9}$$

After simultaneous treatment with the formula above and simplification, the resistive and capacitive current amplitude for the kth harmonic can be obtained respectively, which are related to I_{km}, the current amplitude of the kth harmonic, η_k ,the phase angle of the kth harmonic of total current and φ_k the voltage of the kth harmonic of voltage.

$$I_{rk} = I_{km} \cos\left(\eta_k - \varphi_k\right) \tag{10}$$

$$I_{ck} = I_{km} \sin\left(\eta_k - \varphi_k\right) \tag{11}$$

$$\frac{I_{r(k+2)}}{I_{rk}} = \frac{\beta - k}{\beta + k + 2} \tag{12}$$

If the non-linear parameter β is assumed to be 5, $\frac{I_{r5}}{I_{r3}} = \frac{5-3}{5+3+2} = \frac{1}{5}$ .When it is aggregated and converted into an effective value of fundamental resistive current, the fundamental resistive current amplitude of high-order harmonic is very low and negligible.

It can be known from the formula that the key to the problem is to obtain the Fourier coefficient, while during the digital signal processing, it can be indirectly obtained through the FFT transform method.

3. EXTRACTION OF FEATURES IN THE ONLINE DETECTION PROCESS OF METAL OXIDE ARRESTERS

The features showing whether MOA is in good operation or not include the peak value of total leakage current, the positive peak of resistive current, the negative peak of resistive current, the peak of resistive current peaks, effective value of resistive fundamental current and the power loss, among which the peak of resistive current is an important indicator characterizing the MOA insulation properties[2-4]. The resistive fundamental current, as an important feature parameter in digital signal analysis, involves the phase difference detection between current and voltage and the digital signal analysis of current.

The aperiodic signal function that meets the Dirichlet's necessary and sufficient conditions can be expanded into the form of Fourier series:

$$f(t) = a_0 + \sum_{N=1}^{\infty} \left(a_N \cos N\omega t + b_N \sin N\omega t\right) \tag{13}$$

With the period of $f(t)$ as T and the DC component as a_0 , the Fourier coefficient can be shown as:

$$a_N = \frac{2}{T}\int_{-T/2}^{T/2} f(t)\cos(N\omega t)dt \tag{14}$$

$$b_N = \frac{2}{T}\int_{-T/2}^{T/2} f(t)\sin(N\omega t)dt \tag{15}$$

$$f(t) = a_0 + \sum_{N=1}^{\infty} A_N \sin\left(N\omega t + \varphi_N\right) \tag{16}$$

$$U(t) = U_0 + \sum_{k=1}^{\infty} U_{km} \sin\left(k\omega t + \alpha_k\right) \tag{17}$$

$$I(t) = I_0 + \sum_{k=1}^{\infty} I_{km} \sin\left(k\omega t + \beta_k\right) \tag{18}$$

$$I_{rk} = I_{km} \cos\left(\beta_k - \alpha_k\right) = I_{km}\psi_k \tag{19}$$

ψ_k refers to the phase difference between the voltage and current of the k[th] harmonic, β_k the phase angle or the k[th] harmonic current and α_k the phase angle the k[th] harmonic voltage.

$$I(t) = I_0 + \sum_{k=1}^{\infty} I_{km} \sin\left(k\omega t + \beta_k\right) \tag{20}$$

Carrying out optoelectronic isolation on the PT conditioning signal, directly into the level detection unit without sampling. When the detection platform receives detection signals, the logic module starts to detect the level of PT-introduced signals, and at the same time the A / D sampling unit that introducing the CT signals prepares for sampling. When a high level of PT is detected, the CT began sampling. In this case, the initial phase ψ of the CT signals should be taken the absolute value of $|\psi|$.

$$I_{rk} = I_{km} \cos|\psi| \tag{21}$$

$$A_n = \frac{2}{N}\sum_{k=0}^{N-1} I_k \cos\frac{2\pi nk}{N} \tag{22}$$

$$B_n = \frac{2}{N}\sum_{k=0}^{N-1} I_k \sin\frac{2\pi nk}{N} \tag{23}$$

A total of 256 sampling data are taken for a period, N = 256;

$$A_1 = \frac{2}{256}\sum_{k=0}^{255} I_k \cos\frac{2\pi k}{256} \tag{24}$$

$$B_1 = \frac{2}{256}\sum_{k=0}^{255} I_k \sin\frac{2\pi k}{256} \tag{25}$$

The fundamental peak of the Fourier coefficient is：

$$I_{1m} = \sqrt{A_1^2 + B_1^2} \tag{26}$$

The fundamental resistive component is：

$$I_{r1} = I_{1m} \cos\psi \tag{27}$$

I_{r3} and I_{r5} can be obtained in the same way. Among them, the phase difference ψ can be obtained by software testing, that is, the DSP timer starts counting when a zero passage is detected in the voltage signals and stops counting when the current signal is detected as zero. Then the time difference is converted into radians.

Alternatively, it is also possible to solve the fundamental peak by assuming the sampling frequency to Fs, the total sampling units to N, and a certain sampling unit among the total to n, then the

frequency resolution is Fs/N. The n can be solved by the formula, the nth sampling unit corresponding to a certain harmonic can be obtained.

$$F_n = (n-1) * \frac{F_s}{N} \tag{28}$$

The results of FFT after transformation are stored in the arrays Re [] and Im [], and the harmonic peaks are obtained from formula 3-36.

$$I_{km} = \sqrt{Re[n]^2 + Im[n]^2} \tag{29}$$

The effective value of resistive current is:

$$I_R = \sqrt{I_0^2 + \frac{I_{r1}^2 + I_{r3}^2 + I_{r5}^2}{2}} \tag{30}$$

As to the increment judgment of fundamental and the three resistive currents, in order to ensure that the data does not overflow, there should be statistic of I_{rk} ever 48h, and the average of 30 times of statistic shall be a sampling point $I_{rk}^{'}$ of a feature parameter. Then, the next step is to calculate the increase of fundamental and three times of resistive current discrete values.

$$fh_{kn} = \frac{I_{R1(n+k)} - I_{R1(n)}}{I_{R3(n+k)} - I_{R3(n)}} \tag{31}$$

The comprehensive evaluation results are : $Fh_n = \sum_{k=1}^{m} \left(\frac{I_{R1(n+k)} - I_{R1(n)}}{I_{R3(n+k)} - I_{R3(n)}} \right) \Big/ (m-1)$,Where, m and n are positive integers and can be determined in the algorithm transformation. If Fh_n > 1, there is large possibility of getting damp; If Fh_n <1, the statistical probability of $I_{R1(n+k)}$ exceeding the warning value (calculated by frequency) is greater than 95%, then the aging degree of device is increasing. This process should be run by DSP processer and is stored in feature structure. The final feature parameter constraint can be obtained by the formula.

$$FH = \sum_{n=1}^{m-1} \sum_{k=1}^{m} \left(\frac{I_{R1(n+k)} - I_{R1(n)}}{I_{R3(n+k)} - I_{R3(n)}} \right) \Big/ (m-1) \tag{32}$$

4. DESIGN AND SIMULATION OF THE ONLINE MONITORING SYSTEM FOR METAL OXIDE ARRESTERS

From the transmission process of signals, the technical points involved can be divided into signal extraction, processing and analysis. The frequency domain analysis method is mainly adopted to extract the fundamental resistive component, higher harmonic resistive component and phase angles. When the MOA is damped, there is huge increase of the fundamental impedance component. When the MOA is aged, there is huge increase of the higher harmonic resistive component[7].

4.1 The Overall Framework Design of Online Monitoring System

The technical structure frame of online monitoring system is shown in Figure 5-1, and modules with intensive data include the CPLD chip, the logical control for synchronous sampling of the signals after secondary side conditioning of PT and CT and chip select control for signal sampling chips. The pre-signal processing includes amplification and filter circuits and the signal transmission system includes A/D conversion module, Zigbee communication module, multi-channel gating module, signal amplification and filtering and others. The embedded control platform, as a centralized node for regional signals, is equipped with a temperature, humidity sensor interface within the region, which will be used as secondary parameters for failure determination. The ARM9 and DSP are connected through the asynchronous FIFO chip and SPI bus.

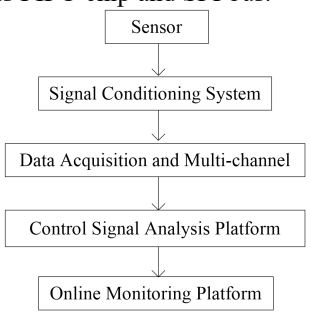

Figure 1 The Overall Framework of The Online Monitoring System

The MOA leakage currents can be obtained from the current signals after A/D sampling being divided by the open-loop gain after reduction. Then through the Fourier coefficients I1m and I3m of the signals to be measured from the FFT transformation, the fundamental resistive component can be obtained by the formula[8].

4.2 Experimental Platform Building and Signal Analysis Simulation

The author builds up a experimental platform to simulate signal conditioning, transmission, signal acquisition and display and run simulation experiments for signal processing. The matlab software is adopted to design the FIR filter, and the filter coefficients are input into the filter module, with Fourier transformation of the current signals to observe the signal features and run experimental analysis[5-6] on the leakage current. The process will be shown in Figure 5-2 and 5-3. The design of 39 orders low-pass filter, Fs = 1000Hz, Fpass = 50Hz, Fstop = 100Hz, Wpass = Wstop = 1, and then embeds filter coefficients in the FDATtool module, the filtering effect can be seen from Figure 5-4 , which effectively removes the high-frequency components, reduce the measurement error of leakage current peak by about 10%. As shown in Figure 5-5 and Figure 5-6, the quality of the FFT transform is improved after filtering[9-10].

5. Conclusion

This paper carries out an analysis on the operating

features of the internal valves of metal oxide arresters, designs a feasible online monitoring technology program through the study of the failure model and measurement model under operation of MOA and makes some experimental simulation and data analysis. MOA online monitoring platform will be more and more applied to substations, and therefore the current research will play a positive role in the integrated online monitoring system of the intelligent grids.

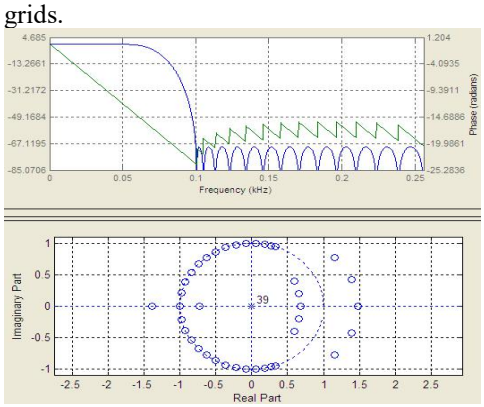

Figure 2 FIR Filter Design

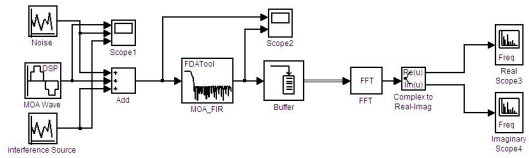

Figure 3 Signal analysis simulation (with filter)

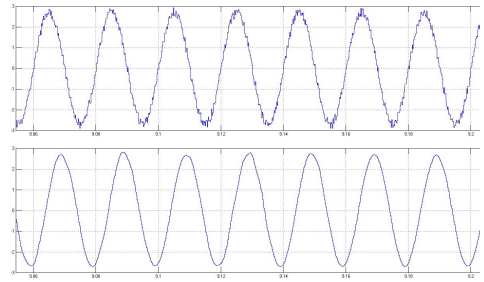

Figure 4 Filtering effects

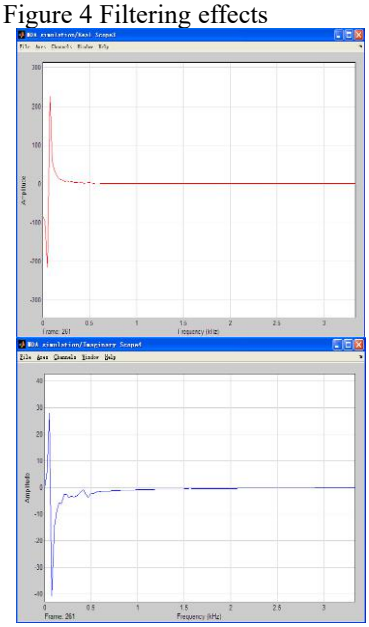

Figure 6 Imaginary Part Curve (After Filtering)

ACKNOWLEDGMENT

This work was supported by the Artificial Intelligence Key Laboratory project of Sichuan Province (No.2014RYY03), the research project of Sichuan Provincial Key Lab of Enterprise Information and Control Technology for Internet of Things (No.2015WYY03),The fund Project of Sichuan Provincial Academician (Expert) Workstation (No: 2015YSGZZ01).

Communication author : JIA Jinling .

REFERENCES

[1]M. Bartkowiak, M. G. Comber, G. D. Mahan. Failure Modes and Energy Absorption Capability of ZnOvaristors. IEEE Transactions on Power Delivery,14(1),1999:152-161.

[2]DL/T987-2005, The General Technical Conditions for the Resistive Current Tester of Zinc Oxide Arresters [S]. Beijing: China Standard Press, 2005.

[3]Zhou Qiuping, Jiang Li and Wang Zhiqiang. Operation and Maintenance of Zinc Oxide Arresters in Series in Mountain Areas [J] .Techniques in Electrical Engineering, 2008 (1):13-15.

[4]He Jimou, Zhu Bin, Zhang Hongtao. Research and Development of Gap-free Metal Oxide Arresters for 750 kV Systems [J]. Power Equipment, 2005,6(12):17-20.

[5]Tian Shengqiang. An Analysis on Onsite Testing of Leakage Current of Metal Oxide Arrester[J]. Science and Technology Information, 2011 (21): 107,115.

[6]GB 11032-2010, AC Metal Oxide Arresters [S]. Society, 2010

[7]Wu, Bo, and Haiying Shen. "Analyzing and predicting news popularity on Twitter." International Journal of Information Management 35.6 (2015): 702-711.

[8]Wu, Bo, and Haiying Shen. "Mining connected global and local dense subgraphs for bigdata." International Journal of Modern Physics C 27.07 (2016): 1650072.

[9]Wu, Bo, Haiying Shen, and Kang Chen. "Exploiting active sub-areas for multi-copy routing in VDTNs." Computer Communication and Networks (ICCCN), 2015 24th International Conference on. IEEE, 2015.

[10]Wu, Bo, Haiying Shen, and Kang Chen. "DIAL: A Distributed Adaptive-Learning Routing Method in VDTNs." Internet-of-Things Design and Implementation (IoTDI), 2016 IEEE First International Conference on. IEEE, 2016..

A New Design of a Piezoelectric Effect-Based Self-Power Generating Tires

*Pengxin Dong[1, *], Xi Zeng[2], Jialei Li[3]*
[1] School of Electrical Engineering, Chongqing University, Chongqing, 400044, China
[2] Hongshen Honors School, Chongqing University, Chongqing, 400044, China
[3] School of Mechanical Engineering, Chongqing University, Chongqing, 400044, China

Abstract: In order to solve the problem of low battery life of the electric car, this paper proposes a new type of self-power generating tires based on piezoelectric effect and tire deformation. The equivalent circuit model of piezoceramics is established to obtain the expressions of the output voltage and power. The piezoceramics under different conditions are simulated and analyzed by *Ansys12.0*, so the selection basis of piezoceramics is obtained. Aiming at the problem that the power of the tires is not easy to be collected, the power export device based on electric brushes and the energy storage circuit are designed, and the super capacitors are used as the energy storage element. Selecting the size of 553 × 310 × 108*mm* electric car as a physical model, eight groups of piezoceramics are installed in one tire. In the experiments, the rms value of the output voltage is about 0.8*V*, and the maximum peak voltage is over 1*V* and the average output power is about 30*mW*.

Keywords: Self-power Generating Tires; Piezoceramics; Output Capability; Analog Simulation

1. INTRODUCTION

In recent years, the new energy vehicles with electric energy as the main driving force are widely used. They gradually replace the fuel cars to become the main products of the market, but its battery life is the main factor restricting the development of electric vehicles [1]. This paper takes into account the fact that the tire as the load-bearing parts of a car is deformed in every moment when the car runs, and its deformation of the energy has not been rational use and is a potential source of energy. Therefore, according to the principle of piezoelectric effects, using piezoceramics can convert mechanical energy to electrical energy, and use energy storage elements to store electricity which can be used in electric vehicles.

PZT-5H piezoceramics are used in most piezoelectric transducers. Its structure includes ceramic, ceramic cantilever, piezoelectric drum, piezoelectric cymbals and multi-layer ceramic structures. At present, the research on piezoelectric ceramics at domestic and foreign is becoming more and more mature [2]-[5].

- In 2007, students from the MIT proposed to transform the impact force of the flow of people on the floor into electric energy. Then the US designer installed a piezoelectric plate on the sidewalk, and successfully lit the light-emitting diode.
- At the Shanghai World Expo, the Japan Pavilion demonstrated its piezoelectric power generation floor technology. The display would show the electric energy generated as long as visitors tread on the floor several times [6].
- Professor Liao Haiyang and Professor Zhong Zhengqing from the school of optoelectronics, Chongqing University, in their paper "*Design of piezoelectric power generator in tire*", proposed to use the array to increase the amount of power generation to solve the problem that the single piezoelectric convertor power generation is low [7].

On the basis of above, this paper studies the influence of the structure, quantity, size, shape, force characteristic and connection method of piezoceramics on the amount of power generation by theoretical analysis, software simulation and experiment. Then the suitable combination of piezoceramics for cars can be obtained.

One of the key issues of the study is the installation of piezoceramics at tires. According to the basic mechanics principle, this paper presents a variety of installation methods. By further analyzing the characteristics of the tire force and taking into account the rotation problems and stability problems of tires, placing piezoceramics between the two flaps is chosen. At the same time, this paper uses the electric car (body size 553×310×108*mm*, the 9.6*V* rechargeable battery pack) as the actual model to install piezoceramics and to verify the scientific nature of the program through experiments. For how to output and use the generated power, a power derivation device in the wheel hub is designed to offset the rotation of the tire.

The bridge rectifier circuit and the filter circuit are designed to deal with the alternating current generated by piezoceramics [8]. Through the bridge rectifier circuit pulsating direct current can be get and through the filter circuit a smooth DC can be get. Super capacitors are used as energy storage elements to store energy, because the super capacitor has the advantages of a long discharge time, large capacity and so on [9].

2. PIEZOCERAMICS AND THE AMOUNT OF POWER GENERATION

The piezoceramic is a kind of electronic ceramic materials with piezoelectric properties. The main difference between piezoceramics and the typical quartz crystals that do not contain ferroelectric

components is that most of the crystalline phases of piezoceramics are ferroelectric domain. Since the ceramics are randomly oriented polycrystalline aggregates, the spontaneous polarization vectors of the individual ferroelectric domain are also chaotic, as shown in Fig. 1(a). In order for the ceramics to exhibit a macroscopic piezoelectric property, it is necessary to cover the end face with the electrode after the ceramics fired, and place the ceramics under a strong DC electric field so that the spontaneous polarization vector with chaotic orientation can have the preferred orientation in the direction of the electric field. These ceramics will retain a certain degree of macroscopic residual polarization after the abolition of the electric field, thus having piezoelectric properties.

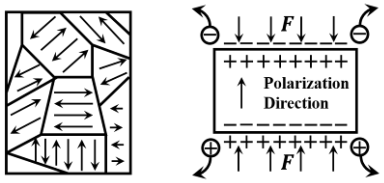

(a) Before polarization (b) After polarization

Figure 1 Piezoelectric effect of ceramics

It can be seen that piezoceramics have piezoelectric properties due to the presence of spontaneous polarization inside the ceramics. After the polarization process, these spontaneous polarizations are forced to arrange, and there is residual polarization in the ceramics. Therefore, when the external pressure can make the intensity of polarization changes, the piezoceramics show a direct piezoelectric effect, as shown in Fig. 1(b).

Based on the above analysis, it can be known that the piezoelectric effect of piezoceramics is closely related to its own and external pressure. Therefore, when piezoceramics are applied as an energy conversion element in a car tire, it should first analyze its power generation performance. This paper combines the piezoelectric equation with the tire force characteristics to derive the relationship between the parameters of piezoceramics, the force of piezoceramics and output electric energy. After that, in the case of selecting the relevant parameters, the change trend of the amount of electric energy generation of one piece of piezoceramic is studied by controlling the single variable and drawing the curve. On this basis, the advantages and disadvantages of different connection modes of n pieces of piezoceramics are studied. Finally, the simulation experiments of piezoelectric ceramics are carried out by simulation software, *Ansys12.0*. At the same time, the experimental data are compared with the theoretical data to draw the relevant conclusions.

A. Equivalent Circuit Model

In piezoelectric elastomers such as piezoceramics, mechanical effects and electrical effects are inseparable, and they are related and tightly coupled together. Therefore, it is necessary to increase the contribution of the electrical quantity to the mechanical quantity in the Hooke's law of the piezoelectric elastomer. At the same time, it also need to increase the contribution of the mechanical quantity to the electrical quantity in the electrical equations. And the piezoelectric equations [10] well describe the relationship between the mechanical and electrical quantities of crystals. There are four types of piezoelectric equations, which are used in different boundary conditions. According to the force of piezoceramics studied in this paper, it can be seen that the boundary conditions are mechanical free and electrical short circuit (or connected load). Therefore, the power generation of piezoceramics should be calculated by using the first type piezoelectric equation. The first type of piezoelectric equation is shown below.

$$\begin{aligned} S &= s^E T + d_t E \\ D &= dT + \varepsilon^T E \end{aligned} \tag{1}$$

In the (1), D is the electrical displacement. S is the strain. d is the piezoelectric constant. s is the elastic soft constant. T is the stress, and E is the electric field intensity.

When piezoceramics output power under the external force, its various directions are likely to occur deformation, so the direction of its electric field is not easy to determine. Meanwhile, the output capacity has a close relationship with the frequency and magnitude of external force, so it is necessary to analyze the characteristics of the tire force. The following two assumptions have been made for the simple and accurate calculation of the power generation of piezoceramics in the tire.

- Assume that piezoceramics are mainly subjected to forces acting in the thickness direction, and deformation occurs in the thickness direction.
- Assume that the pressure on a point on the tire follows the sinusoidal law. Carlos Reyes and Olmer Garcia from UNICAMP in Sao Paulo, developed a non-linear vehicle model with a tire dynamic model to measure longitudinal and lateral tire forces in a commercial vehicle by using the design of a robotic vehicle of Autonomous Mobility Laboratory (LMA). In their research, the results of the measurements show that the tire force almost follow the sinusoidal law but it has large distortions. Therefore, in the analysis of this paper, it is feasible to assume that the tire force follows the standard sinusoidal law [11]. Hence, the pressure of the piezoceramics is as follow.

$$F = F_M \sin(\omega t + \varphi) \tag{2}$$

On the basis of the above analysis, power generation is calculated with one piezoceramic as an example. Fig. 2 shows the equivalent circuit model. The piezoceramic has the area of σ, the thickness of δ, and the tire force with the form of the (2), which is equivalent to an AC power supply Q in parallel with a capacitor C. The piezoceramic will be connected with

the rectifier and filter circuits in the actual circuit. Here for the simplified calculation, it is equivalent to a pure resistance load.

Under these conditions, in addition to the surfaces in the *x* direction, the rest of the surfaces are free with the stress and electric field intensity are 0. And the external force *F* is a time function, so the electric displacement, strain, stress, electric field intensity are also the functions of time *t*. The form of the first piezoelectric equation should be rewritten based on the (1).

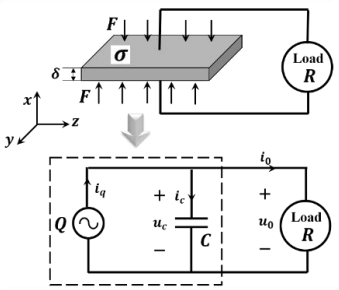

Figure 2 Equivalent circuit model of one piezoceramic

$$S_1(t) = s_{11}^E T_1(t) + d_{11} E_1(t)$$
$$D_1(t) = d_{11} T_1(t) + \varepsilon_{11}^T E_1(t) \quad (3$$

From the relationship between the external force and stress, the electric displacement *D* is expressed as

$$D_1(t) = \frac{d_{11} F_M \sin(\omega t + \varphi)}{\sigma} + \varepsilon_{11}^T E_1(t). \quad (4$$

Therefore, the output charge *Q* of the equivalent AC power supply is the double integral of the electric displacement to the electrode surfaces.

$$Q = \iint D_1(t) dydz = d_{11} F_M \sin(\omega t + \varphi) + \sigma \varepsilon_{11}^T E_1(t) \quad (5$$

So the output current i_q of the equivalent AC power supply is

$$i_q(t) = dQ/dt = d_{11} F_M \omega \cos(\omega t + \varphi) + \sigma \varepsilon_{11}^T \frac{dE_1(t)}{dt}. \quad (6$$

There is no denying that the (6) is a differential equation, and it need to find the relationship between E_1 and i_q to solve the equation. Using Ohm's law, it is only need to obtain the equivalent impedance relative to the equivalent power supply. In other word, only the equivalent capacitance *C* of the piezoceramic is obtained. The dielectric constant of the piezoceramic is ε_{11}, so the equivalent capacitance and impedance are

$$C = \frac{\varepsilon_{11}^T \sigma}{\delta}, \quad Z = j\frac{1}{\omega C} + R. \quad (7$$

The relationship between the output current i_0 and i_q can also be get by using the Ohm's law, and then the differential equation of the output current of the piezoelectric ceramic can be obtained by combining the (6) and the (7), as shown below.

$$i_0(t) = \frac{d_{11} F_M \omega \cos(\omega t + \varphi)|Z|}{R} + \frac{\sigma \varepsilon_{11}^T |Z|}{\delta} \frac{di_0(t)}{dt} \quad (8)$$

Solving the (8), the mathematical expressions of the output current, output voltage and output power of one piezoceramic when the load is pure resistance can be calculated as follow.

$$i_0(t) = \frac{d_{11} F_M \omega \delta \sin(\omega t + \varphi)}{\sqrt{\delta^2 + 2\omega^2 \sigma^2 \varepsilon_{11}^{T\,2} R^2}} \quad (9)$$

$$u_0(t) = \frac{R d_{11} F_M \omega \delta \sin(\omega t + \varphi)}{\sqrt{\delta^2 + 2\omega^2 \sigma^2 \varepsilon_{11}^{T\,2} R^2}} \quad (10)$$

$$P_0 = \frac{d_{11}^{\,2} F_M^{\,2} \omega^2 \delta^2 R}{2\delta^2 + 4\omega^2 \sigma^2 \varepsilon_{11}^{T\,2} R^2} \quad (11)$$

In the actual structure, the piezoceramics always appear in the form of a ceramic group, so assume that the number of piezocermaics in the group is *n*. The connections in the ceramic group may be in series or in parallel, as shown in Fig. 3.

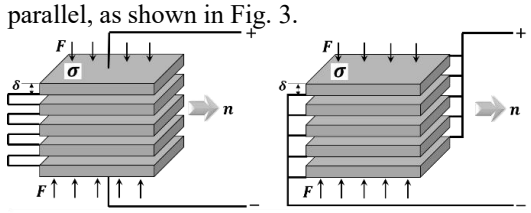

(a) Series connection (b) Parallel connection

Figure 3 The connections of the piezoceramics group

Using the above analysis method, the same analysis about the circuits shown in Fig. 3 gives the output voltage and output power of the piezoceramics group in different connection modes and different amounts.

●Series connection:

$$u(t) = \frac{R d_{11} F_M \omega n \delta \sin(\omega t + \varphi)}{\sqrt{n^2 \delta^2 + 2\omega^2 \sigma^2 \varepsilon_{11}^{T\,2} R^2}} \quad (12)$$

$$P = \frac{d_{11}^{\,2} F_M^{\,2} \omega^2 n^2 \delta^2 R}{2n^2 \delta^2 + 4\omega^2 \sigma^2 \varepsilon_{11}^{T\,2} R^2} \quad (13)$$

●Parallel connection:

$$u(t) = \frac{R d_{11} F_M \omega n \delta \sin(\omega t + \varphi)}{\sqrt{\delta^2 + 2n^2 \omega^2 \sigma^2 \varepsilon_{11}^{T\,2} R^2}} \quad (14)$$

$$P = \frac{d_{11}^{\,2} F_M^{\,2} \omega^2 n^2 \delta^2 R}{2\delta^2 + 4n^2 \omega^2 \sigma^2 \varepsilon_{11}^{T\,2} R^2} \quad (15)$$

B. Images and Curves

Only by the (10) to (15) cannot directly show the production performance of the piezoceramics. Therefore, the curve drawing method is chosen to observe the change trend of the amount of electric

energy generation through the images. The method used in this paper is to control the single variable. The magnitude of external force, the frequency of external force, the area of piezoceramics and the thickness of the piezoceramics are selected as the variables. Meanwhile, a set of standard values need to be determined. When a variable changes, the other variables should be in accordance with the standard values. As the use of the electric car for the actual model in this paper, the relevant parameters of the electric car is as the standard values. As shown in the table below, the standard values, the variation range and the constant values are given.

TABLE 1 The Required Data For The Curves

Category	Notations	Standard Values	Variation Range	Units
Variate	F_M	5	0~5	N
	$f(\omega)$	19	0~30	Hz
	σ	1.69	0~3	$\times 10^{-4}\, m^2$
	δ	0.5	0~1	$\times 10^{-3}\, m$
Constant	n	1	\	$piece$
	ε_{11}	500	\	F/m
	d_{11}	132	\	$\times 10^{-12}\, C/N$
	R	5	\	Ω

Since n is 1, the four sets of images can be obtained by using (10) and (11), as shown in Fig. 4 to Fig. 7. It should be noted that the voltage in the (10) is an instantaneous expression, and the rms value of voltage is requires when studying the power generation performance. Therefore, the voltage in the four figures represents the rms value.

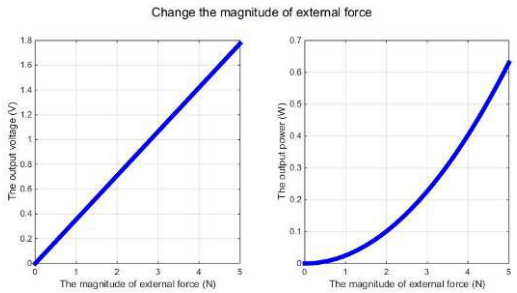

Figure 4 Change the magnitude of external force

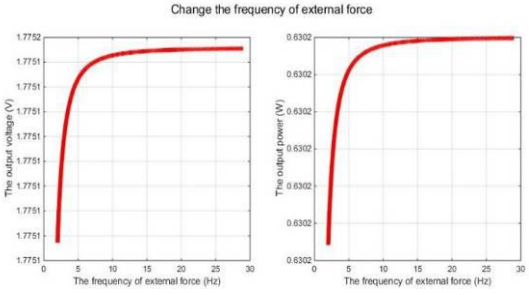

Figure 5 Change the frequency of external force

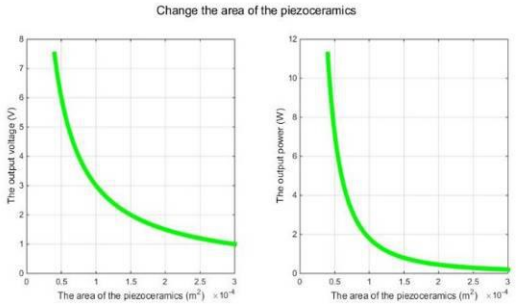

Figure 6 Change the area of piezoceramics

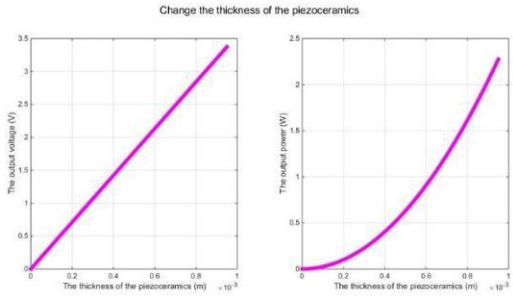

Figure 7 Change the thickness of the piezoceramics

According to the (12) to (15), the electric energy production performance of n pieces of the piezoceramics in the different amounts and different connection modes can be studied. As shown in Fig. 8, n is selected from 1 to 20, and the connections are divided into series and parallel. It should be noted that the output voltage in the figure is still the rms value of the voltage.

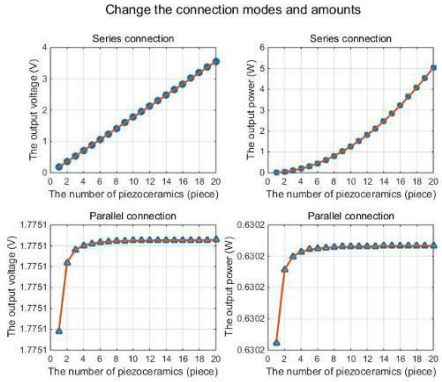

Figure 8 Change the connections and amounts

C. Simulation Experiment

In order to verify the scientific nature of the above theoretical formulas and images, it is necessary to simulate the performance and structure of the piezoceramics. At the same time, the energy conversion performance of piezoceramics can be understood in depth according to the simulation results, and the most suitable combination and size of piezoceramics for the electric car can be get.

At present, the most widely used numerical simulation method in the project is finite element analysis, and the commonly used software is *Ansys*, *Fluent*, *Comsol* and so on. In this paper, *Ansys12.0* is selected to do the simulation experiments. *Ansys* can effectively solve the problems of coupling between multiple physical

fields. For pressure - electricity coupling materials, such as piezoceramics, *Ansys* can give the simulation results almost perfectly.

Fig. 9 shows the process of partial simulation experiments and their results where each row represents a kind of shape of piezoceramics. The first column is establishing the initial model and meshing for the three different piezoceramics, and this paper uses the direct coupling method for analysis. The second column is applying the boundary conditions which are based on the data in table I. The third column is the transient analysis of the production performance, showing the instantaneous value of the voltage.

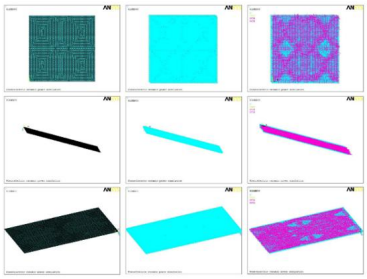

Figure 9 Simulation process and results

For handling the results of transient analysis, the fitted curve is used in this paper. Based on the multi-group data obtained from the transient analysis, the fitted curves are drawn by *MATLAB* and compared with the theoretical curves.

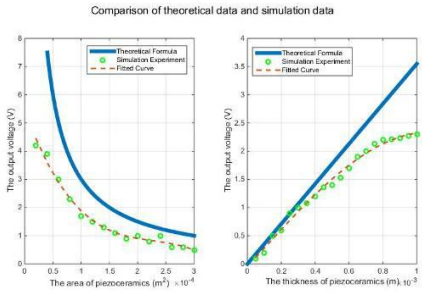

Figure 10 Comparison of theoretical data and simulation data

Fig. 10 shows the comparison of theoretical and simulated data when changing the area and thickness of the piezoceramics. It can be seen from the figure that the trend of the fitted curves obtained from the simulation data is exactly the same as the theoretical curves, but the rms value of the voltage is smaller than the theoretical data. In addition to the two cases shown in Fig. 10, this paper is also simulated in other cases, and a completely consistent conclusion is obtained. It can be determined that the reason for the decrease in the rms value of the voltage is that the inverse piezoelectric effect of the piezoceramics is not taken into account in the theoretical calculation. However, it can be seen that the existence of the inverse piezoelectric effect does not affect the trend of the production of electricity. Therefore the appropriate combination of the piezoceramics can be get directly according to the theoretical data.

D. Conclusion

According to the images and simulation experiments, some relevant criteria about selecting piezoceramics can be obtained.

Firstly, the external force is positive correlated with the voltage and power, so the greater force is needed. It requires the piezoceramics with good compression resistance. Therefore, the piezoceramics with larger elastic modulus is chosen.

Secondly, when the frequency of the external force changes, the voltage and power are almost unchanged, so the speed of electric cars does not affect the production capacity.

Thirdly, the area of the piezoceramics is negatively correlated with the voltage and power while the thickness is positively correlated. Therefore, the piezoceramics should have a small area and a large thickness. The smaller area may cause the greater stress, so it should choose a suitable area, not a small area.

Finally, the connection method should be selected in series connection, and the number is as large as possible. But taking into account the car tire space, it should be selected with different numbers for different models.

3. THE INSTALLATION OF PIEZOCERAMICS IN THE CAR TIRES

After analyzing the production performance of piezoceramics, this paper studies the installation of piezoceramics in the car tire. From the previous analysis, it can be known that the location of the piezoceramics should be able to provide greater force, and can accommodate more quantities. Fig. 11 shows the structure of the actual car tire.

Figure 11 The structure of the car tire

In general case, the components of the tire can be divided into three parts, the cover tyre, the flap and the tube. The cover type includes the tread, shoulder, sidewall, steel belt, and carcass and so on [12]. The tread is the part where the tire is in contact with the ground. The shoulder is the shoulder of the tire. And the sidewall is the most severe part of the bend in the tire in running. These three structures are used to protect the carcass. The rim is made of high carbon steel wire, which fixes the tire on the hub. The steel belt tightly attached to the tread is mainly made of steel cord to improve the rigidity of the tread. The carcass has the high pressure resistance and impact resistance. Between the carcass and the hub has a layer of flap, its role is to prevent the rim to damage the tube [13].

Combined with the characteristics of each part of the tire, this paper presents a variety of installation options.

- The piezoceramics is mounted between the tread and the steel belt. In the process of driving the car, the piezoceramics is easily damaged by the bumpy tread due to severe impact [14]. So, this solution is not conducive to the actual use.
- The piezoceramics is mounted between the steel belt and the carcass. This solution still makes the piezoceramics easy to damage, and the friction which between the steel belt and the piezoceramics will reduce the life of the piezoceramics.
- The piezoceramics is mounted between the carcass and the flap. The role of the flap is to protect the tube, so it is closely connected with the carcass. It will be very laborious, even seriously damaged tires if the piezoceramics are placed here.

The solutions which based on the original structure are abandoned because of the existence of the lager problems, so this paper presents a new design. Adding a new layer of flap, the piezoceramics is installed between the two layers flaps, as shown in Fig. 12.

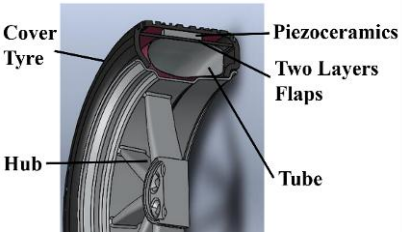

Figure 12 The new design for installation

This solution will not damage the tube and not easy to damage the cover tyre. Meanwhile, it does not have much impact on the structure of the tire. Piezoceramics here can be protected by the carcass and cannot directly contact the tube. Therefore, the life of the tire and the piezoceramics will not be much affected in the power generation at the same time. The solution is feasible.

In order to further explain the feasibility of the above solution, the force analysis is used to the tire. In the solution, the plane of the piezoceramics group is perpendicular to the plane of the hub, and the piezoceramics are subjected to gravity and support forces. As shown in Fig. 13, the wheel center is selected as the origin to establish the coordinate system and the plane of the hub is xOy plane.

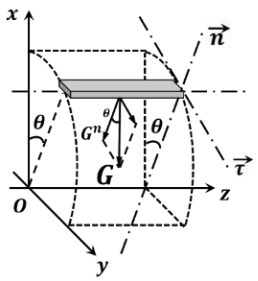

Figure 13 The force analysis diagram

For simplified the analysis, it can be considered that the point of gravity is located at the geometric center of the piezoceramics. In the figure, the piezoceramics is in any θ position, so the gravity G can be decomposed into two forces including Gn in the normal direction and Gt in the tangential direction. Gn is the effective external force used to generate electricity.

Assuming that the car is running at a constant speed, the wheel center speed is the car speed, v0. The angular velocity of the wheel is ω and the radius is R, so the position θ is a function of time. In summary, the effective external force of piezoceramics can be get as

$$F = G^n = G\sin\theta = G\sin(v_0 t / R) \qquad (16)$$

Compared with the (2), it can be seen that the force in the (16) has the exactly same form with the external force which is in the theoretical analysis. Therefore, the theoretical analysis and the installation solution are both correct.

4. THE EXPORT, STORAGE AND UTILIZATION OF ELECTRIC ENERGY

A. Power Export Device

The tires rotates with a high speed when the car is running. It is necessary to design a device to overcome the problem that the energy is difficult to export because of this rotation. The commutator components are used to design the following device.

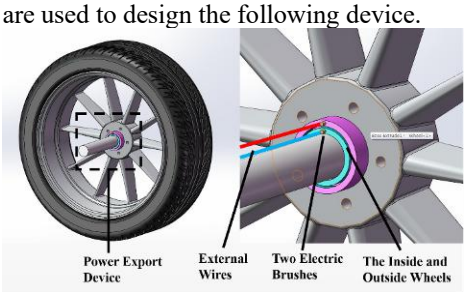

Figure 14 The power export device

As shown in Fig. 14, the inside and outside wheels are fixed to the hub, and the wires which are connected the piezoceramics are respectively connected with the two wheels. Then, the wheels are connected to two electric brushes. Finally, the brushes are connected to the external circuit so that the generated power can be exported to the energy storage circuit. In the actual design, the piezoceramics are located between the flaps, so the wires connecting the piezoceramics can be placed in the spokes and the external wires can also be placed in the shaft. This way could save space and ensure the balance and stability of the tire.

B. Energy Storage Circuit

Through the experiments, the voltage generated from the piezoceramics is AC voltage, and the voltage waveform is irregular. AC power cannot be directly charged to the battery, so this paper design the rectifier and filter capacitor to process the AC. Through the filter circuit, the DC can be get. Meanwhile, the stabilivolt are used to regulate the voltage. In the storage of electrical energy, the super capacitors are chosen because the super capacitor has advantages of a

long discharge time and large capacity, etc. The circuit diagram is shown below.

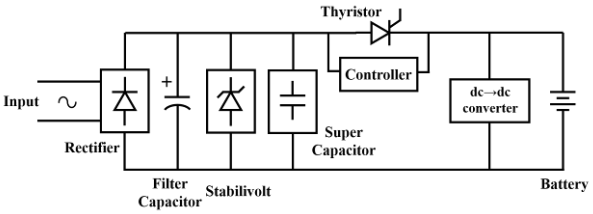

Figure 15 The power export device

The super capacitor as the energy storage also need to charge the batter of the car, so the thyristor control switch and the dc/dc converter are used to control the charging process. The controller will control the thyrisor on or off to achieve the time control. The dc/dc converter can make the battery power more stable.

5. Design and Manufacture of Electric Car Physical Model

In this paper, the physical model of electric car is constructed by toy electric car, and the purpose of autonomous electric power production during the car running is realized by transforming the tire and welding circuits. The physical model is shown in Fig. 16.

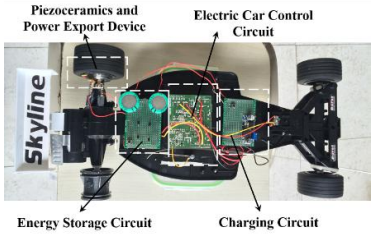

Figure 16 The physical model of electric car

This physical model car is a mini model for the actual car, which in the whole with the actual car has a high similarity. Using this model to experiment, it will not produce a large error. At the same time, the material of the model's tires has the almost same properties with the actual tires, and their softness is basically the same. This way can truly simulate the tires.

According to the size of the physical model and the relevant data in table I, the installation of piezoceramics occurs in the one of the tires. The parameters of the model, the parameters of the piezoceramics and the components of the energy storage circuit are shown in the following table.

TABLE 2 THE PARAMETERS OF THE MODEL AND EXPERIMENT

Category	Parameter	Values
Physical Model	Body Size	553×310×108*mm*
	Quality	2.04*kg*
	Tire Radius	2.5*cm*
	Speed	15*km/h*
Piezoceramics	Area	$0.49\times10^{-4}\,m^2$
	Thickness	$0.3\times10^{-3}\,m$
	Quantity	8
	Connection	Series
Energy Storage Circuit	Stabilivolt	1N4750A
	Super Capacitor	1*F*×2, Series
	Thyristor	2N6509

The experimental facility is shown in Fig. 17. Selecting about 1.5 meters of the road, the car runs in the road through the control of the remote. Meanwhile, the output electric energy is measured by the multimeter.

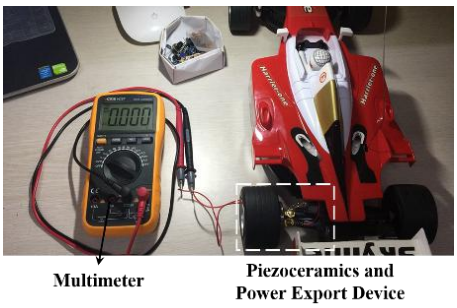

Figure 17 The experimental facility

The multimeter does not have the function of storing data, so this paper obtain the instantaneous voltage and current of the car through the way of recording videos. Part of the voltage data is shown below.

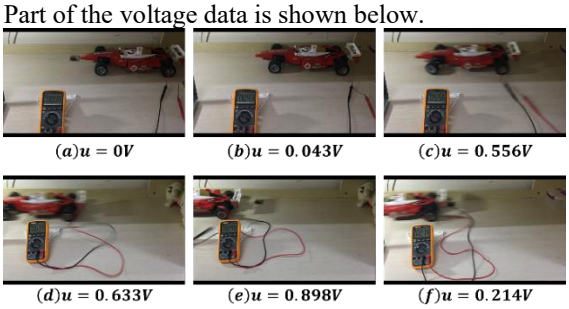

Figure 18 Part of the voltage data and experimental screenshots

After many experiments, a lot of data is obtained. In this paper, the data processing is carried out by MATLAB. At the same time, the relationship between the movement distances of the physical model and the instantaneous output voltage, current and power is obtained by using the fitted curves, as shown in Fig. 19.

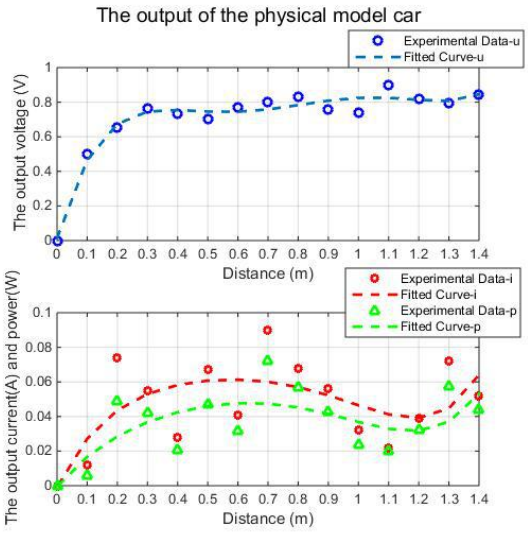

Figure 19 The output of the physical model car

As can be seen from the figure, the rms value of the voltage is about 0.8V, the rms value of the current is

about 50mA, and the output power is about 30mW. This power is not large, but the power is still quite impressive for the model car in the condition of only one tire installed piezoceramics. Further inference, if the actual electric car can be recovered energy by using the research in this paper, the resulting electric energy has a market value.

6. Conclusion

This paper apply the piezoelectric effect and piezoelectric equations to establish the equivalent circuit model of piezoceramic production. Through theoretical analysis and Ansys simulation, it can be get that the output energy is positively correlated with the external force, the thickness of ceramics and the number of ceramics and negatively correlated with the area of ceramics and the series connection is the most appropriate way. Based on the basic structure of the tire, the piezoceramics is installed between the two layers flaps, which is advantageous for power generation and installation. In the experiments of the physics model car, about 30mW power was obtained. Therefore, it must need further experiments with the actual electric car, and increase the capacity of the electric car while achieving the goal of energy saving and emission reduction.

REFERENCES

[1]W-J. Ma, “Design of Electric Vehicle Battery Management System,” *Journal of Changsha Social Work College*, vol. 23, No. 2, June 2016.

[2]M-P. Zheng and Y-D. Hou, “Research Progress of Piezoelectric Ceramics for Energy Harvesting,” *Journal of The Chinese Ceramic Society*, vol. 44, No. 3, March 2016.

[3]S. G. Kim, S. Priya and I. Kanno, “Piezoelectric MEMS for Energy Harvesting,” [J], *Mrs Bull*, pp. 1039-1050, 2012.

[4]S. M. Allameh, O. Akogwu and M. Collinson, “Piezoelectric Generators for Biomedical and Dental Applications : Effects of Cyclic Loading,” Mater Sci: *Mater Med*, 2008.

[5]S. Priya, “Advances in Energy Harvesting Using Low Profile Piezoelectric Transducers,” *Electroceram*, 2006.

[6]Y-M. Li, “The Japanese Railroad Uses the Exercise Energy during Walking to Develop Power Floors,” *Railway Technical Innovation*, 2009.

[7]H-Y. Liao and Z-Q. Zhong, “Design of Piezoelectric Power Generator in Tire,” *Optics and Precision Engineering*, vol. 17, No. 6, June 2009.

[8]N. Mohan, T. M. Vndeland and W. P. Robbins, “Power electronics: Converters, Applications and Design, 3re ed.”, Higher Education Press, 2004, pp. 161-199.

[9]L-J. Ma, W-J. Liao and Z-Y. Gao, “Research on Ac Side Series Supercapacitor Regenerative Braking Energy Storage System Control Strategy of Railway Vehicle,” *Transactions of China Electrotechnical Society*, vol. 30, 2015.

[10]J. Yao and Z-Y. Zhu, “Piezoelectric Equation and Two Piezoelectric Sensor Models,” *Journal of Vibration Engineering*, vol. 21, No. S, Sep 2008.

[11]C. Reyes, O. Garcia, P. S. Meirelles, and J. V. Ferreira, “Estimation of Longitudinal and Lateral Tire Forces in a Commercial Vehicle,” *IEEE Conference Publications*, pp. 1-6, 2015.

[12]B. Jaballah and N. K. M’Sirdi, “Structured Estimation of Tire Forces and the Ground Slope Using SM Observers,” *International Journal of Automation and Computing*, April 2014.

[13]H-T. Zhang, “Structural Characteristics and Performance of Automotive Tires,” *Technology Outlook*, April 2016.

[14]L-J. Li, F. Liu, X-P. Su and X-G, Yang, “Research Progress of Tire Structural Mechanics Design Theory,” *Tire Industry*, vol. 20, Oct 2000.

Outsourcing LU-Decomposition of Large Matrix to a Public Cloud

Kong Shanshan[1,] , Yongquan cai[1,2]*
[1] University of the Technology, Beijing 100124, China
[2] University of the Technology, Beijing 100124, China

Abstract: Matrix calculation plays an important role in scientific computation. However, security is the major concern that prevents the wide adoption of computation outsourcing in the cloud. As LU-decomposition (LUD) of a matrix are widely applied in engineering tasks, we are motivated to design secure, correct, and efficient protocol for outsourcing the LUD of a matrix to a malicious cloud in this paper. In order to achieve security, we utilize y matrix transformation to protect both the input and output privacy. We also introduce an outsourcing principle component analysis as an application of our proposed protocol.
Keywords: Outsourcing computation; Secure Outsourcing; LU-Decomposition; Electronic measurement system; Efficiency analysis

1. INTRODUCTION

Matrix calculation plays an important role in both scientific computation and cryptography. Atallah et al. (2002) first presented a framework for secure outsourcing of scientific computations such as matrix multiplications [1]. Atallah et al. (2005) investigated the problem of computing the edit distance between two sequences and presented a protocol to securely outsource sequence comparisons to two servers [2]. Atallah et al. (2008) addressed the problem of secure outsourcing for widely applicable linear algebra computations [3]. Atallah et al. (2010) given improved protocols for the secure and private outsourcing of linear algebra computations that enable a client to securely outsource algebraic computations to a remote server [4]. Mohassel et al. (2011) designed non-interactive and secure protocols for delegating matrix multiplication, based on a number of encryption schemes with limited homomorphic properties where the client only needs to perform O(n2) work [5]. Wang et al. investigated secure outsourcing of widely applicable linear programming (LP) computations [6], [7]. Xu et al. (2013) introduced Outsourcing protocols for convex optimization [8]. Lei et al. (2014) designed a protocol for outsourcing of matrix multiplication computation to a malicious cloud [9]. Zhou et al. (2015) designed outsourcing protocol for quadratic programming problem [10]. Zhou et al. (2016) designed two protocols for outsourcing eigen-decomposition and singular value decomposition of large-scale matrix to a malicious cloud [11].

LU-decomposition of matrix is an essential computation in linear algebra which has broad applications in engineering fields [12]. However, running this kind of matrix decomposition algorithm costs a lot of computational resources when the size of matrix is large. Thus, it is attractive for the customer with limited computational ability to outsource LU-decomposition of large size matrix to the cloud. Motivated by this, we develop a secure outsourcing protocol for LU-decomposition of matrix in this paper. We regard our main goals as follows:

● Correctness

The cloud server can return a correct calculation result to the client, if the client and the cloud run according to the LU-decomposition protocol.

● Input-output privacy

The protocols can protect the privacy of the input and the output. Cloud server can't get the original calculation matrix A from Encrypted matrix B. And cloud server can't get the LU-decomposition result of matrix A from the calculation result of matrix B.

● Verifiability

During performing the LU- decomposition computation, the customer can verify the correctness of the output of the cloud server with the maximum probability and also can verify the incorrect output of the cloud server with the maximum probability.

● Efficiency .

In the outsourcing computation, the local computation done by the customer should be substantially less than solving the original LU-decomposition on his own.

2. THEORETICAL

Cloud server typically runs in semi-trusted or malicious model. However, Outsourcing computing task often contains sensitive information that should not be exposed to the cloud server. Thus, it is required to outsource the matrix in its encrypted form. Due to the lack of incentives in economic returns, the cloud server may return an error result to the client in the outsourcing computation, while hoping not to be detected by the client. So it is also required that the outsourcing protocol for a malicious cloud model should be able to handle result verification. In this paper, we assume that the cloud is malicious, and the communication between the cloud and the customer is reliable. We consider the system model for secure outsourcing of LU-decomposition of a matrix involving two different entities, as illustrated in Fig.1.

One entity is the customer, who lacks of computational resources to calculate LU-decomposition of a matrix. The other entity is the cloud, which has enhanced computing power. The customer expects to maintain the privacy of the data because the cloud is potentially malicious to the customer. To preserve the privacy, the original matrix A is encrypted into an encrypted matrix B with secret key K. And then the customer sends the encrypted matrix B to the cloud. The cloud receives the encryption matrix B and takes it as the input to perform the calculation task, and then returns the result to the customer. After receiving the result of encrypted matrix B, the customer verifies whether the result returned is correct or not. If the computed result is correct, the customer decrypts the output into the desired answer of the original matrix A. Otherwise, the customer returns "wrong" to the cloud and requires it to compute it again.

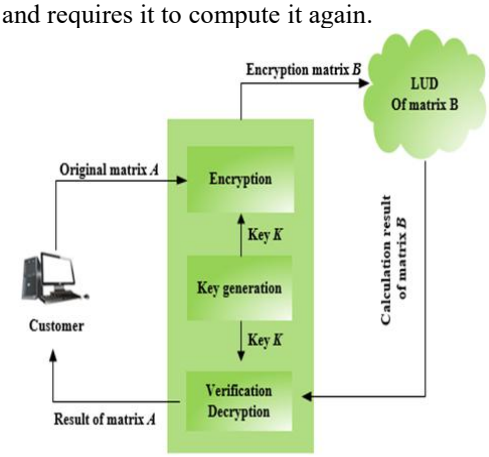

Figure 1 System model for secure outsourcing of LU-decomposition of a matrix

OUTSOURCING PROTOCOL FOR LU-DECOMPOSITION OF A MATRIX

(1) Secret Key generation

Consider a matrix $A \in R^{n\times n}$, where necessarily each leading principle minor $\det A_r \ (r=1,2,\cdots,n)$ of the matrix A is not zero. In this module, resource-constrained client wants to securely outsource the LU-decomposition of matrix A to the cloud. The protocol starts by invoking procedure secret-key-generation to set up a secret key K. We summarize the steps of algorithm for key K as in Algorithm 1.

In Algorithm 1, we name the steps from 1 to 3 as triangular matrix random structuring. Here, due to definition 2 and definition 3, step 3 is used to generate lower triangular matrix and upper triangular matrix. Step 4 is based on the property theorem that the inverse of an upper triangular matrix is still an upper triangular matrix and the inverse of a lower triangular matrix is still a lower triangular matrix.

Table 1: Procedure secret-key-generation

Algorithm 1. Procedure Secret-Key-Generation
Step1. Structuring random permutation function: $\pi_1 \in \{1,2,\cdots,n\}, \pi_2 \in \{1,2,\cdots,n\}$.
Step2. Structuring random permutation numbers: $\{c_1, c_2,\cdots,c_n\}, \{d_1, d_2,\cdots,d_n\}$.
Step3. Generating a lower triangular matrix C and an upper triangular matrix D.
Step4. Computing the inverse matrix of the unit lower triangular matrix C and the upper triangular matrix D, then getting the lower triangular matrix C^{-1} and the upper triangular matrix D^{-1}.

(2) Encryption

In outsourcing LU-decomposition (LUD) of matrix, the customer expects that neither original matrix A which may contain sensitive information nor its lower triangular matrix L and upper triangular matrix U are exposed to the cloud. In this module, the customer uses matrix multiplication to transform the original matrix A into an encrypted one B as follows:

Table 2: Encryption

Algorithm 2. Encryption
Step1. Using the lower triangular matrix C and the upper triangular matrix D to encrypt matrix A into matrix B as $B = CAD$.
Step2. Sending the matrix B to the cloud.

Since the cloud does not have the exact value of the lower triangular matrix C and the upper triangular matrix D, the customer sends matrix B to the cloud for LUD, the privacy of matrix A is preserved.

(3)Outsourcing Calculation

Cloud computing has a great deal of computational resources, which enable customers with limited resources to outsource their mass computing to the cloud. In this module, the cloud computes the LU-decomposition (LUD) of matrix B to get the lower triangular matrix L' and the upper triangular matrix U' as follows:

Table 3: Outsourcing calculation

Algorithm 3. Outsourcing Calculation
Step1. The cloud computes LU-decomposition of matrix B as $B = L'U'$.
Step2. The cloud sends the lower triangular matrix L' and the upper triangular matrix U' to the customer.

Since cloud does not have the value of the lower triangular matrix C^{-1} and the upper triangular matrix D^{-1}. If the cloud sends the lower triangular matrix L' and the upper triangular matrix U' to the customer, the privacy of output is preserved.

(4)Decryption

As the relationship between matrix A and matrix B are showed by equation $B = CAD$, the customer can easily get the LU-decomposition of matrix A as follows:

Table 4: Procedure secret-key-generation

Algorithm 4. Decryption
Step1. Using the lower triangular matrix C^{-1} and the upper triangular matrix D^{-1} to decrypt LUD of matrix B into LUD of matrix A as below: $LU = C^{-1}L'U'D^{-1}$
Step2. Let $L = C^{-1}L'$ and $U = U'D^{-1}$, then get $A = LU$.

Here, algorithm 4 is due to the theorem (Liao, P. 2013) that if each leading principle minor $\det A_r \ (r = 1,2,\cdots,n)$ of the matrix A is not zero, the matrix has the only LU decomposition.

As to the transformation of LU-decomposition, the customer can use the inverses of the lower triangular matrix C and the upper triangular matrix D to decrypt the lower triangular matrix L and the upper triangular matrix U. And the matrix A can be decomposed as $A = LU$

Now, the customer gets the result of LU-decomposition of the original matrix A.

REFERENCES

[1]Atallah, M., Pantazopoulos, K., and Rice, J. 2002. Secure outsourcing of scientific computations. Advances in Computers. 54, 1, 215-272.

[2]Atallah, M. and Li, J. 2005. Secure outsourcing of sequence comparisons. International Journal of Information Security. 4, 4, 277-287.

[3]Benjamin, D., and Atallah, M. 2008. Private and cheating-free outsourcing of algebraic computations. Sixth Conference on Privacy, Security and Trust, IEEE Computer Society. 4, 4, 240-245.

[4]Atallah, M., and Frikken, K. 2010. Securely outsourcing linear algebra computations. ACM Symposium on Information, Computer and Communications Security. 48-59.

[5]Mohassel, P. 2011. Efficient and secure delegation of linear algebra. Iacr Cryptology Eprint Archive.

[6]Wang, C., Ren, K., and Wang, J. 2011. Secure and practical outsourcing of linear programming in cloud computing. Proceedings IEEE. IEEE. 8, 820-828.

[7]Wang, C., Ren, K., Wang, J., and Wang, Q. 2013. Harnessing the cloud for securely outsourcing large-scale systems of linear equations. EEE Transactions on Parallel & Distributed Systems. 24,6,1172-1181.

[8]Xu, Z., Wang, C., Wang, Q., Ren, K., and Wang, L. 2013. Proof-carrying cloud computation: the case of convex optimization. Proceedings IEEE INFOCOM. 79, 11, 610-614.

[9]Lei, X., Liao, X., and Huang, T. 2013. Achieving security, robust cheating resistance, and high-efficiency for outsourcing large matrix multiplication computation to a malicious cloud. Information Sciences.280, 205-217.

[10]Zhou, L., and Li, L. 2015. Outsourcing large-scale quadratic programming to a public cloud. Sixth Conference on Privacy, Security and Trust, Access IEEE. 3, 2581-2589.

[11]Zhou, L., and Li, C. 2016. eigen-decomposition and singular value decomposition of large matrix to a public cloud. Sixth Conference on Privacy, Access IEEE. 4, 869-879.

[12] Saad, Y. 2003. Iterative Methods for Sparse Linear Systems. Society for Industrial and Applied Mathematics.

Game Theory Analysis and Countermeasure of Preventing Internet Insurance Fraud

Changhai Wu, Qi Hu*
Institute of Capital Finance, China University of Political Science and Law, Beijing, 100088, China

Abstract: In recent years, Internet insurance industry has developed very rapidly in China. However, some criminals have tried to defraud insurance claims by exploiting internet insurance flaws, which damage the healthy development of Internet insurance industry. In order to effectively prevent the Internet insurance fraud, this paper provides specific countermeasures and suggestions through game theory analysis on both policy-holder insurance fraud and third-party insurance fraud.
Keywords: Internet insurance; policy-holder insurance fraud; third-party insurance fraud; game analysis; anti-fraud countermeasure.

1.GAME ANALYSIS OF POLICY-HOLDER INSURANCE FRAUD.

From the complete information static game model analysis, four different game analysis models are obtained in this paper by the combination of diverse analysis methods of these two basic divisions of game analysis according to the degree of information obtained by the insurer to policy-holder and the simultaneity of actions of insurer and policy-holder. That is, an all-round and deep-going analysis has been made through four game analysis models, complete information static game, complete information dynamic game, incomplete information static game and incomplete information dynamic game.

As one of the simplest and most ideal game models, complete information static game analysis model is the main subject of this paper, which focuses on policy-holder medical insurance fraud through the Internet channel.

1.1 Model assumption of policy-holder insurance fraud.

Insurance can be regarded as a social arrangement (or contract). By doing so, policy-holder transfers the risk to the insurer to gather loss data, thus to predict the loss with statistical method and cover the loss with the premium, which is all paid by the risk transporters. Therefore, insurance contract contains two elements: a is the premium paid by the policy-holder in insurance contract, $b(\theta)$ is the compensation charged by the policy-holder to the insurer when the appointed event occurs during the period of validity of insurance contract, where θ is described by probability distribution as a random variable. From view of policy-holder, insurance is to use the present definite cost a in exchange for uncertain losses in future. While for the insurer, insurance is to collect indefinite individual losses to achieve the certainty of ultimate wealth or loss, in line with the law of large numbers.

In this paper, policy-holder medical insurance fraud game model has a common hypothesis that insurance market is perfectly competitive. Obviously, there are two kinds of relations in medical insurance: the policy-holder and the insurer. On one hand, the complex of medical insurance consumers (i.e. the applicant, insured, or beneficiary) and medical service organizations is called policy-holder for short. Assuming that the policy-holder is risk averse, the utility function is $u(\cdot)$, where $u'(\cdot)>0$, $u''(\cdot)<0$, i as the initial wealth and a as the premium. On the other hand, the insurer refers to the combination of medical insurance institutions and health insurance companies. Suppose that the insurer is risk neutral, the utility function is $v(\cdot)$, with s as the initial wealth.

The loss of policy-holder is composed of the net loss of policy-holder after treatment and the cost of giving medical care by health services, which is set as L . Meanwhile, medical payments (i.e. b) is paid by the insurer to the policy-holder who applies for compensation in accordance with the medical insurance contract. In particular, if the insured is found to be fraud, there will be financial penalties instead of medical reimbursement, with the value of f .

Table 1 The game payoff matrix of policy-holder and insurer.

Insurer \ Policy-holder	Compliance	Non-compliance
No inspection	$(a-b, b-a-c_1)$	$(a-b_0, b_0-a)$
Inspection	$(a-b-c_2, b-a-c_1)$	$(a-b_0-c_2+f, b_0-a-f)$

1.2 Analysis on the assumption of complete information static game model.

The expected value of insurance payout in a medical insurance contract that is signed between the policy-holder and the insure is assumed to be b_0, and a_0 is the amount of premium. Meanwhile, it is supposed that c_1 is the cost must spent on the disease and loss prevention measures by the policy-holder in accordance with the contract, thereby reducing the amount of expected compensation and premium to b and a, respectively. Moreover, only when the value of a is less than that of $(a_0 - c_1)$ will the policy-holder take disease and loss prevention measures. Of course, the insurer can also check whether the policy-holder has complied with the medical insurance contract with an inspection fee of c_2. Once it is discovered that the policy-holder fails to comply with the medical insurance contract, a fine of f must be paid to the insurer. By and large, the strategy choices of the policy-holder and the insurer in this game model are compliance or non-compliance with the contract, and inspection or no inspection, respectively.

In addition, it is supposed that neither premium and fine that are paid by the policy-holder nor the loss that is indemnified by the insurer shall relate to the benefit of the third party, with c_1 and c_2 as the receipt and disbursement outside the system, respectively. Consequently, the game payoff matrix of policy-holder and insurer is shown in Table 1, where the first and the second bracketed expression represent the payment of the insurer and the payment of the policy-holder, respectively.

1.3 Game equilibrium analysis.

In line with double-line method, the best strategy for the insurer is no inspection when the policy-holder honors medical insurance contract. Likewise, the best strategy for the policy-holder is non-compliance when the insurer does not check. Only when the value of f is no larger than that of c_2 can the optimal strategy for the insurer is no inspection, when the policy -holder does not abide by the medical insurance contact.

In complete information static game, the unique Nash equilibrium (no inspection, non-compliance) exists only when the amount of f charged by the insurer is not enough to make up for or just the same with the inspection costs to the policy-holder (i.e. c_2).

As for the insurer, it is worthwhile to check the behavior of the policy-holder when the fee of penalty is greater than that of examination, presenting $f > c_2$. Accordingly, the penalty will help to prevent the moral hazard of the policy-holder only if the amount of the fine is greater than the sum of the cost of prevention measures and the resulting difference in compensation, meaning $f > c_2 + b_0 - b$. In other words, the policy-holder will keep a medical insurance contract, without the game equilibrium. If the policy-holder complies with the medical insurance contract, the insurer had better not to check, and vice versa. Meanwhile, it is best for the insurer to check for non-compliance of the policy-holder, and so on. In general, there is no strategic combination of Nash equilibrium.

Table 2 The game payment matrix between policy-holder and insurer.

Policy-holder / Insurer	Compliance ($1-p$)	Non-compliance (p)
No inspection ($1-q$)	$(a-b, b-a-c_1)$	$(a-b_0, b_0-a)$
Inspection (q)	$(a-b-c_2, b-a-c_1)$	$(a-b_0-c_2+f, b_0-a-f)$

But what is more real is that both the insurer and the policy-holder would like to guess the strategy of the other side, and that each participant does not allow the opposite side to discern their own strategies, so this game would possess a mixed but a pure strategy Nash equilibrium. In a static game, a pure strategy is equivalent to a specific action, while a mixed strategy is a random choice between different actions. Hence, the reality of the situation is that compliance or non-compliance of the policy-holder is often at a certain probability, as well as the inspection or no inspection of the insurer. Table 2 displays the game payment matrix between policy-holder and insurer, where the first number and the second number in brackets indicate the payment of the insurer and of the policy-holder, respectively.

Assuming that the policy-holder fails to observe the terms of the contract, the probability of no prevention measures is p, and the probability of inspection of the insurer is q, then the balanced income formula of the policy-holder is as follow:

$$(1-q)(b-a-c_1)+q(b-a-c_1)=(1-q)(b_0-a)+q(b_0-a-f) \quad (1)$$

$$q^* = \frac{c_1 + b_0 - b}{f} \quad (2)$$

The balanced income formula of the insurer:

$$(1-p)(a-b)+p(a-b_0) = (1-p)(a-b-c_2)+p(a-b_0-c_2+f) \quad (3)$$

$$p^* = \frac{c_2}{f} \quad (4)$$

The only Nash equilibrium point of the game is obtained.

When the policy-holder fails to abide by the provisions of the contract, the probabilities of no prevention measures and of the inspection are p^* and q^*, respectively. Thus it can get the earnings of both the policy-holder and the insurer:

$$EU(p^*, q^*) = b - a - c_1 \quad (5)$$

$$EV(p^*, q^*) = a - b - \frac{c_2(b_0 - b)}{f} \quad (6)$$

For further discussion, if $EV(p^*, q^*) < 0$, the insurer will refuse to accept insurance unless $EV(p^*, q^*) \geq 0$, namely . That is to say, the insurer may accept the minimum premium regardless of management fees, presenting

$$a = b + \frac{c_2(b_0 - b)}{f} \quad (7)$$

where b is the expected insurance payouts (i.e. net premium), is the penalty fee caused by the failure of policy-holder to fulfill the medical insurance contract. Despite of the possible prevention measures by policy-holder, the insurer will see it as an additional risk considering the existence of moral hazard, which is reflected in the premium. Obviously, the penalty is proportional to both the inspection costs of c_2 and the benefits of $(b_0 - b)$ with prevention measures, while is inversely proportional to the amount of fines f.

According to eqn. (7), the income of the policy-holder is:

$$EU(p^*, q^*) = -\frac{c_2(b_0 - b)}{f} - c_1 \quad (8)$$

1.4 Further analysis.

The above static information game model is only taken for one turn. In particular, the risk before and after the signing of medical insurance policy will change and directly affect the formation of a balanced medical insurance policy. Therefore, it is a question that whether the equilibrium price of medical insurance policy changes in the case of repeated transactions.

We can simply consider two phases of repeated transactions. As the policy-holder knows the action options of healthy insurance company in the second phase, the policy-holder will select the actions in the first phase based on the action strategy of healthy insurance company.

If healthy insurance company threatens to reject the policy-holder in the second phase of the insurance for his hiding information, the threat is feasible clearly only under the premise that the health insurance company is exclusive monopoly and the expected utility of policy-holder can be increased through a health insurance policy. Consequently, the policy-holder will choose to inform in the first phase in the face of credible threats, thereby telling the truth forever promoted by repeated transactions.

However, this threat is incredible in a competitive market, , and repetitive transactions do not change the single-phase equilibrium. Therefore, the choose of policy-holder to inform or to conceal information in the first period is determined by the inspection or not of medical insurance company. At the same time, medical insurance company decides the pricing strategy according to the verification cost. Furthermore, the pricing of medical insurance policy in the single-stage model would still be the most optimal when at relative low checking cost level. Herein, a third-party fraud game model has been proposed to analyze in this paper, taking into account the effectiveness of information obtaining and the accuracy of pricing.

2. Game analysis of the third-party fraud.

There is a risky motive for the third-party fraud, that is, they bet rare insurance accidents will not happen. This paper attempts to establish a third-party fraud game model by analyzing the behavior of the third-party.

2.1 Model assumptions and instructions

The Internet insurance market is supposed to be a perfectly competitive market. In the process of insurance marketing, it needs to consider two main participants: the third-party platform and the insurer. Assuming that the initial wealth of the risk-neutral third-party platform and of the the risk-neutral insurer are 0 and s, respectively. Moreover, both the insurer and the third-party in the market economy environment are assumed as the bounded rational economic men, who will pursue to maximize their own utilities under the given institutional conditions.

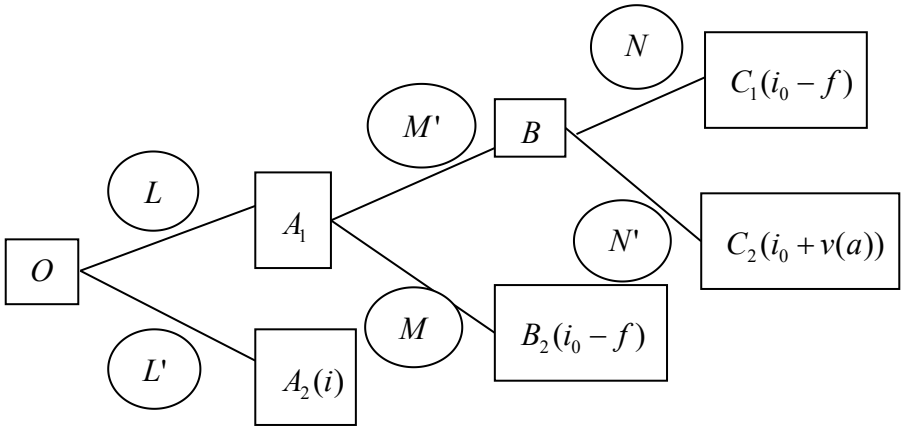

Fig. 1 Game tree on behalf of the third-party revenue.

It is further supposed that the third-party can earn a benefit of $A_2(i)$ with honest job. On the contrary, once the third-party is found to be fraud that not only the cooperation will be terminated by the insurer but also be imposed a fine of f while still with a market value of i_0. Of course, the third-party will get an extra income of $v(a)$ if his fraud is not be discovered, where a is information authority owned by the third party and make an assumption of $v'(a)>0$. In other words, the greater the ability of the third party to obtain information, the more the possible fraud income.

The fraudulent conduct of the third-party may be discovered in two cases: one is found through the regulatory system of insurance company, and the other is exposed when deceived insurance customers present a claim to the insurer after a severe insurance accident happened. Namely, the fraud must be uncovered and the insurance company is sure to know when major insurance accident occurs.

2.2 The establishment of game model.

Apparently, the implementation of third-party fraud is a matter of priorities through the above hypothesis analysis. As can be seen in Fig.1, a three-stage incomplete information game is established to specify in this paper.

In the first stage, the third-party does fraud (recorded as event L) or no fraud (denoted as event L') at the start of the game. If the third-party chooses not to cheat, the game will end at the point of A, and the third-party can obtain an information sharing income of i. Whereas if the third-party selects to deceive, the game arrives at the point of A_1 and continues on to the next stage of the game. Usually, the insure would like to induce the third-party not to engage in insurance fraud by raising the benefit of the third-party at the point of A_2, or by reducing the expected benefit of the third-party at the point of A_1.

In the second stage, the probability of a third-party being found to have fraud by the use of company supervisory mechanism indirectly is p_1 (as event M or else as event M'). Additionally, the game will end at the point of B_2 for the revealed fraudulent conduct of the third-party, whose earnings come to i_0-f. Otherwise, if the fraud is not discovered by the insurer, the game reaches point B_1 and continues on to the next stage of the game.

In the third stage, the probability of the occurrence of major insurance accident (set as event N) is p_2, which is determined by the nature of the insurance. Besides, p_2 is a common knowledge because of the known type of insurance. Hence, the game will get to the finish line of C_1 when the insurance accident occurs, and the profit of the third-party can reach to i_0-f. On the contrary, if the insurance accident does not happen (recorded as event N'), then the end of the game is C_2, with an income of $i+v(a)$ for the third-party.

2.3 Game model analysis.

From Fig. 1, the path of (M',N') shows that it keeps the fraudulent conduct of the third-party from being discovered in the two stages, with a probability of $(1-p_1)(1-p_2)$ and an income of $i+v(a)$ for the third party. Then, the fraud exposure probability of the third-party would be $1-(1-p_1)(1-p_2)$ at least in one case. By this time, the third-party gets the gains of i_0-f, whose expected income at the point of A is as follows:

$$(1-p_1)(1-p_2)(i+v(a))+[1-(1-p_1)(1-p_2)(i_0-f)] \quad (9)$$

Based on the above analysis, it can lead the third-party not to be deceptive (as point A_2) as long as the expected income of the third party at point A_1

is less than the benefits i at point A_2, so the third-party does not cheat under the following constraint condition:

$$i \geq (1-p_1)(1-p_2)(i+v(a)) \\ +[1-(1-p_1)(1-p_2)(i_0-f)] \quad (10)$$

After transforming:

$$i \geq i_0 - f + \frac{(1-p_1)(1-p_2)}{1-(1-p_1)(1-p_2)} v(a) \quad (11)$$

As can be seen, the above formula is composed of three parts, including the market value of i_0 of the third party itself, the fraud exposure fine of f of the third-party, and as the part of the third-party agency income more than $i_0 - f$. Firstly, the more information the third-party obtains, the higher the information value becomes, resulting in a greater market value. Secondly, the fines can be divided into two kinds, one is legally punishment of fraud, the other is the default charged by the insurance company from the third-party. Thirdly, it can be understood that the insurance company uses high returns to avoid fraud from the third-party.

For the third part, the less the value of p_1, the smaller the surveillance dynamics of the insurer, thereby having to pay more information fees to the third-party. It is worth noting that, the fraud exposure probability of the third-party is 100% when p_1 is 1, meaning the most effective supervision of the insurer to the agent and the lowest cost has to pay. However, it is completely impossible for the insurer to find the fraudulent conduct of the third-party when p_1 is 0, with the highest cost to the third-party. Likewise, the smaller the value of p_2 is, the less likely an insurance accident occurs, which also need to pay a high amount of information costs. While a lager value of $v(a)$ indicates that the third-party has the capability to bilk more money, which shows a monotone increasing function of information capturing ability.

2.4 The advice of restraining the third-party fraud.

Through the above analysis, there are three measures for the insurer to prevent the third-party form cheating: First, to establish honesty files of the third-party and to put on records for those who have fraudulent acts, so as to reduce market reputation and value of the third-party and to control the third party fraud. Second, to demand a higher contractual penalty from the third party, or to bring the third-party with fraud into court and to pay a fine. Third, to pay attention to those low risk insurance and to focus on powerful supervision of the third-party in such business.

3. INTERNET INSURANCE ANTI-FRAUD ADVICE.

3.1 The establishment of regulatory system and objectives of Internet insurance anti-fraud.

For the purpose of regulating the behavior of Internet insurance business, protecting the legitimate rights and interests of insurance consumers and promoting the healthy development of Internet insurance business, China Insurance Regulatory Commission (CIRC) has formulated the Interim Measures for the Supervision of Internet Insurance business (hereinafter referred to as the Measures) , which is released on July 22nd, 2015. According to the Measures, the Internet insurance shall be done in a centralized headquarters operation, individuals shall not carry out Internet insurance sales business personally, and Internet insurance business shall be kept away from regional restrictions. In addition, the Internet insurance intermediaries has been explicitly included in the scope of insurance institutions as stated in the Measures. Accordingly, this paper analyzes mainly from the supervision of the policy-holder, insurance agencies, policy uploading and data processing.

3.1.1 Supervision of the policy-holder.

Taking medical insurance as an example, it is necessary to supervise the medical practice of medical institutions, and to guarantee medical institutions to master medical service resources. Firstly, the management of health insurance agreements should be further improved. Moreover, it is necessary to strengthen the management of outpatient service and to focus on improving the assessments of four aspects, including whether the doctor to check social security cards of insured patients, whether to suit the remedy to the case and to implement medical review reasonably, whether to manage the use of prescription and health insurance bills in accordance with regulations, and whether to record medical instruments faithfully. Secondly, a powerful special audit inspection team has to be built to reinforce medical insurance audit work. Except for daily and key audit, it is also crucial to carry out audit work from the tip-off, thus to play on the main force to combat health insurance fraud. Thirdly, intensified pre-inspection and enhanced review payment monitoring capabilities can benefit from the networking between social security agencies and fixed-point medical institutions. For the sake of real-time monitoring the whole treatment process of from outpatient consumption to online settlement of insured patients, the networking should coverage outpatient department, pharmacy and inpatient department of the hospital. Fourthly, it can be extremely helpful with divided outpatient medical management, specialized outpatient medical records system, and strengthened outpatient prescription management. For instance, medical records manual can be dedicated for medical insurance, and medical practices of doctors and insured personnel can also be

regularized by the establishment of prescription management system and real-name hospitalization system.

On one hand, the premium paid by the policy-holder shall be transferred directly to the special account of the premium income of insurance institution, while the third-party shall not collect the insurance premium to transfer the payment. On the other hand, unified settlement and unified authorization transfer payment shall be made by the head office if the insurance company pays the relevant fee to professional insurance agency and the third-party. Furthermore, the promotional activities carried out by insurance agency and the third-party should be in line with the relevant provisions of CIRC, including to give away insurance, goods or services directly related to insurance, and to return the premium paid by the policy-holder in cash or similar ways.

3.1.2 Insurance institutions

Insurance agencies should protect the securities of both insurance transaction information and consumer information. Insurance institutions carry out Internet insurance business through third-party network platform with insurance business qualification and without major administrative penalties in recent two years by the Internet industry authorities, industrial and commercial administrative departments and other government departments, not included in the list of prohibited insurance industry partners by CIRC. Insurance business, such as sales, underwriting, claims, surrender, complaint handling and customer service, shall be managed and responsible by the insurance institution. At the same time, the information of cooperative insurance agencies and third-party filing should be prominently disclosed by third-party network platform, with the notice of insurance business provided by insurance institutions. As for the promotional services offered by third-party network platform, propaganda content should be in line with the relevant regulatory requirements after being audited by the insurance company. The insurance company assumes corresponding responsibility for the authenticity, accuracy and compliance of the promotion content.

To ensure the completeness and accuracy of the relevant transaction flow and details, insurance institution shall keep and record the transaction information of the Internet insurance business fully. The transaction information should at least contain such as product promotion, sales text, sales and service log, the operation trajectory of policy-holder. By the adoption of technical means (e.g. firewall isolation, data backup and fault recovery), insurance organization shall intensify the safety management of business data, so as to guarantee the security, truthfulness, accuracy and completeness of the transaction data and information related to the Internet insurance business.

Besides, insurance agencies need to guard against illegal activities (like fake websites and APP) aiming at Internet insurance, and to check the reliability of external links on the website, plus to open up special channels to accept public reports with immediately preventive measures and timely report to to the CIRC after finding problems. In terms of insurance institution, it is necessary to establish a sound system of customer identification, to strengthen the monitoring and reporting of large and suspicious transactions, as well as to abide by the relevant provisions of anti-money laundering strictly. In principle, insurance institution shall require the policy-holders to pay the insurance premium by the use of their own accounts. The insurance premium shall be refunded to the original payment account upon full surrender, and the compensation fund shall be paid to the account of the policy-holder himself, the insured or the beneficiary. Especially for more than one year of life insurance business, insurance agencies should check the authenticity of the account information of policy-holder to ensure that both the payer and the payee is the applicant himself.

3.1.3 Policy uploading and supervision.

Through the establishment of online service systems that support consulting, insurance, surrender, claims, inquiries and complaints, insurance companies should strengthen the service management of Internet insurance business, and explore to carry out clients call-back actions with the help of SMS, and other instant messaging tools. For the sake of efficient and convenient customer service, the service process has to be simplified and the service mode needs to be innovated.

However, due to the demands of field underwriting, survey and investigation, the provision of insurance policy with fast and convenient service would be influenced. Hence, insurance institutions should immediately suspend the sale of related insurance products and take effective measures to rectify and reform. If it cannot be resolved after the rectification, the sale of insurance product has to be terminated.

3.1.4 Database supervision

For Internet insurers and regulators, they are sure to solve the problem of claims difficult and to curb insurance fraud. In order to purify insurance environment and to contain insurance cheating, many places has taken a variety of measures, including the conjunction among different departments to combat insurance fraud, the establishment of information platform to eliminate information island and so on. In addition, it is well known that big data is the foundation of the Internet. With the rapid development of network technology, a series of behaviors of people are done through the network, which will leave a lot of traces and be transformed into big data. Through Big Data analysis, the consumption and pay habits of people can be understood, which contributes to the sale of Internet

insurance products. But as a double-edged sword, it is easy to cause customer information leakage if you cannot properly manage the large database, which will inevitably cause serious consequences once be used by illegal man. Therefore, strengthening the supervision of large databases is an inevitable issue in the development of Internet insurance.

As known, the main reason for the occurrence of insurance fraud cases is the weak introcontrol of Internet insurance company. To this end, the anti-fraud work in Internet insurance requires Internet insurance companies not only to strengthen internal control, but also to form a normal cooperation mechanism with the public security, courts, procuratorate and other departments considering so many of involving persons in insurance fraud. For example, sound databases of high-risk repair factories, high-risk customers and high-risk employees have been built in Shaanxi, to provide warning and services for insurance companies [1].

In addition, in the face of insurance fraud, Shanghai Insurance Regulatory Bureau makes full use of the advantages of Shanghai insurance industry information platform technology to push the work mode of big data intelligent insurance anti-fraud, relying on joint information platform of motor vehicle insurance, integrated information platform of life insurance and road traffic accident inspection appraisal information system. In detail, the ways to effectively hit insurance fraud include the use of big data to carry out risk early warning, association investigation, and parallel to serial data [1].

Aiming at the insurance supervision in Internet era, traditional insurance supervision cannot fully meet the regulatory requirements of Internet insurance, and the new risks of Internet insurance demands professional risk monitoring and control, put forward by Jiangxi Insurance Regulatory Bureau. Owing to the bestraddle-zone of virtual network world, the further integration of regulatory resources is required. In the process of localized management, there would be inter-provincial regulatory issues for insurance supervision, thus demands for upper and lower linkage, the branches to cooperate, the entrusted supervision and inspection. The council has also pointed out that insurance network credit database anti-insurance fraud has also to be conducted to improve the rationality of the supervisions of insurance, banks and securities, as well as to enhance efficiency of regulatory [1].

3.2 Insurance anti-fraud warning based on data mining.

3.2.1 Establish information technology monitoring system through the data mining to

In order to provide modern technical support for medical insurance fraud supervision, it is essential to speed up the construction of information monitoring system. On the basis of the experiences in Europe and United States, the use of professional anti-fraud computer software system can be beneficial to identify the unreasonable or abnormal payments in the system more effectively and quickly. The data itself is convincing, and data mining is one of the effective means to enhance fraud identification. Data mining can reveal patterns that are outside the scope of the thinking of uses, and give answers to questions that have never been asked. Despite of the indispensable database to gain the declaration and payment of the Fund for conducting anti-fraud investigations, it is not enough to only obtain the required data. Data information can be more valuable with higher quality, especially for primary data. There are lots of new data information recorded by insurance agencies into the system every day. However, the amount, coverage and real-time performance of data is also significant for the audit staff, while the reliability and integrity of the data are crucial for the statistics and investigation of insurance fraud. As a result, it is imperative to strengthen information management and improve the technical equipment level of anti-fraud work. The informatization degree of medical insurance directly affects the supervise management level of medical insurance fund payments. To realize the standardized and programmed management of information system, it must be of the essence to establish optimized anti-fraud management system such as fraud identification, investigation, evaluation, countermeasure and improvement, and so on. Through the data mining, anti-fraud organization system can be built with the summarized anti-fraud experience of Internet insurance. Following the United States, it can set up the National Health Care Anti-Fraud Association and Insurance Anti-Fraud Alliance in Internet medical insurance of China. Then, insurance fraud warning, identification, control and processing can be achieved by a universal information monitoring system through mixing the power of the whole insurance industry.

3.2.2 The acceleration of anti-fraud research for Insurance companies.

Both the qualitative analysis of insurance fraud by professional domestic scholars in the field of insurance and various prevention measures contribute to a clear micro direction for domestic insurance enterprises, which is meaningful for the construction of insurance integrity. However, as a current era of data to speak, information from data mining can be of great importance to insurance industry. Moreover, there is a high concordance between the different insurers for these forecasting indicating that insurance history data is critical to future predictions and inspirations. Consequently, for the sake of remarkable achievements of insurance fraud research in China, it must pay attention to the following several points:

To establish a shared insurance fraud case database, insurance companies should carefully analyze fraud

cases and extract useful fraudulent identification fields

Insurance companies should increase the number of talents in the field of anti-fraud research. These people not only master the knowledge and capabilities of human resources, data mining technology, insurance external consultants, statistical analysis techniques and monitoring systems, but can also establish an automatic identification model to play a role in compensation decisions and anti-fraud actions of insurance companies, with the help of computer software, preset variables, statistics, mathematical analysis techniques and geographic data mapping.

Learn from the US medical insurance anti-fraud practice, it is necessary to set up Internet health insurance anti-fraud department for insurance company, to implement program of activities (e.g. medical assistance integrity plan), and to establish special anti-fraud groups, including Internet Medicare Fraud Prevention and Enforcement Action Force, Medicare Fraud Strike Force, Medicare Fraud Control Force.

3.2.3 The suppression of the fraud tendency of the third-party.

In order to ensure the interests of policyholders and the healthy development of insurance market, regulators are expected to invest more in the audit, because of the following three reasons under the current solvency regulation system: First, there are great scale differences among the main bodies of insurance market. Second, too much extensive management led to more insufficient solvency. Third, the primary regulatory target of regulators is to protect the interests of policyholders.

In spite of the sustaining development of Internet finance in the past two years, insurance products are still rare, which is directly related to the complex insurance products and highly sensitivity of the real information of customers. How to simplify the process while reducing the risk is concerned by regulators. In view of Insurance institutions, a sound Internet anti-fraud system shall be built to strengthen the monitoring and reporting of Internet insurance fraud. As for the third-party, it is requisite to help insurance agencies to carry out anti-fraud monitoring and investigation.

3.3 The establishment of information sharing and blacklist system.

3.3.1 The establishment of anti-fraud data system and information sharing mechanism.

According to the current policies issued by the CIRC, insurance companies are prohibited to authorized the branch office to start the Internet insurance business without authorization or to cooperate with illegal third party network platforms, and will be punished for the bad consequences caused by the occurrences of data loss and customer information disclosure [2]. The current regulatory measures have been able to improve the imperfect supervision mechanism of Internet insurance, such as the existence of conspiracy, adverse selection and other behaviors.

Herein, we can establish an information database, including medical service agencies, doctors, insurers, fund regulators, audits, etc. In this way, a powerful information database network for insured fund payment can be set up, fraudulent data systems may be established, and a long-term mechanism of the data collection of fraud cases can be formed. Besides, irregularities can be detect and deal with timely thanks to the real-time monitoring and audit of medical expenses payments. Moreover, it is essential to construct a credit rating system for designated medical institutions, doctors and insured individuals. On one side, the credit rating is reduced and the corresponding penalties are made when the fraud occurs. On the other side, suspected fraud is carried out in real time monitoring, automatic identification, classification and early warning by the use of data mining, thus to improve the efficiency of fraud recognition and the ability to strike crime [3].

3.3.2 Blacklist system

Blacklist system shall be set up in Internet insurance business of the third-party. Neither the bad consequences caused by unauthorized approval to carry out propaganda work, nor the leakage of transaction information would be supported. In addition, the CIRC has the rights to demand correction for the behavior of carrying out illegal insurance business with other agencies. Furthermore, the CIRC may order the relevant insurance institutions to immediately terminate their cooperation for the rejection. Meanwhile, it will be included in the list of prohibited cooperation industry, and be informed in the whole industry [2].

ACKNOWLEDGEMENT

This paper is funded by the Ministry of education project "Research on the regulation of foreign capita Mergers and Acquisitions Domestic erterprise about Security Review(11YJC820133)",and is funded by the “Project supported by the academic innovation team of young teachers of China University of Political Science and Law (201110)”.

REFERENCES.

[1]C. H. Leng. Anti-network insurance fraud with the help of big data[J]. Securities Daily, 2014.

[2]Interim Measures for the Supervision of Internet Insurance business. China Insurance Regulatory Commission, 2015.

[3]Y. Lin. US medical insurance anti-fraud incident and enlightenment to China[J]. Journal of Central University of Finance & Economics, 2012.

Research on Sonar Buoy Array Effective Search Area Modeling

Li Xinshu, Li Weibo , Zhu Liangming
Naval Aeronautical Engineering InstituteYantai, Shandong, China 264001

Abstract: In this paper, the typical array and characteristics of four kinds of sonar buoys are analyzed for sonar buoy combat operation. The analytic calculation models for three sonar buoy detection zones overlapping area for arbitrary spacing and different detection radii are established respectively. On the basis of this, linear array is taken as an example to give the calculation method for sonar buoyant array effective search area.
Key words: Effective search area; Sonar buoy array; Linear array; Overlapping area; Detection area; Laying distance

1. INTRODUCTION

Sonar buoy, important equipment for submarine search, is water sound remote sensing equipment used to detect underwater targets, which has high search efficiency, little affected by noise, good concealment, continuous detection time and other characteristics. It is also of small size and light weight, which is easy to carry. It is one of the main submarine search equipment for anti-submarine helicopters and anti-submarine patrol aircraft.

As a single sonar buoy detection range is limited, usually a number of sonar buoy are set up for an array in order to achieve a large area sea search.

There are many researches on the use of sonar buoys [1-3], search array [4-6], sonar buoy deployment [7-8], find probability [9-10], submarine search performance [11-13], best working depth [14], and the submarine search with the participation of unmanned aerial vehicles [15] and other aspects of the study. The calculating of sonar buoy array search area always neglects the calculation of the overlapping area of the adjacent buoy detection area. In the actual array, the three sonar buoy detection areas may overlap. Therefore, in this paper, the calculation model of the sonar buoy array's effective search area is established to solve the problem, so that the index calculation result of the metric array performance is more realistic.

2. SONAR BUOY STANDARD ARRAY

Sonar buoys can be laid into a variety of arrays to meet the different needs of submarine search tasks. Typical arrays are mainly linear array, square array, fan array, round array, etc., which are shown in Figure 1.

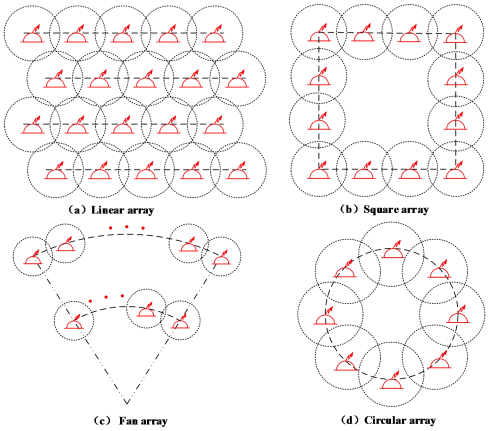

Figure 1 Sonar buoy standard array

Linear array is arranged by setting sonar buoys along the straight line, which is the most commonly used buoy array. Broken line array, arc array, triangular array and many other linear arrays can be derived from it. Linear array is flexible, simple, and easy to expand, which has higher submarine search probability when used appropriately. Linear array can be arranged along a straight line into a single line array, or can also be composed of multiple single-line arrays, which is shown in Figure 1 (a) below.

Square array is also a commonly used array, which can be divided into rectangular array and square array. The array is easy to set convenient and has higher submarine search probability in the array, but requires more buoys in the same search area and is more efficient[16-17].

Fan array is formed by a plurality of arcs of sonar buoys along a fan shape. Round array is formed by arranging the sonar buoys along a circular shape. The two arrays are more flexible and easy to expand, which has high array submarine search probability. However, the layout is more difficult and the array is more difficult to maintain[18-19].

3. SONAR BUOY ARRAY EFFECTIVE SEARCH AREA CALCULATION MODEL

The effective search area of sonar buoy array is one of the important indexes to evaluate the potential submarine search performance of different types and is one of the key parameters for calculating the sonar buoy array discovery probability. For example, when search in mission required sea area, the discovery probability P_f of

sonar buoy array is calculated as

$$P_f = 1 - \exp\left(S_{\text{e-s}} P_g P_{\text{i}} / S_t \right) \quad (1)$$

S_{e-s} indicates the actual effective search area of the sonar buoy; S_{t} indicates the total area of mission required sea area; P_{g} indicates the good rate of buoy technology; P_{i} indicates the probability for the target to reach and correctly identify the target. P_{g} and P_{i} are two parameters which mainly depend on the performance of sonar buoy, usually taken as a fixed value. So obviously, to calculate the discovery probability of buoy sonar array, the key is to solve the effective search area $S_{\text{e-s}}$ of the array.

Different sonar buoy array has constant calculation principle for the effective search area. The following is modeled as a linear array. Assuming that the sonar buoy array consists of N_1 line arrays and two arrays sonar buoy detection areas are shown in Figure 2.

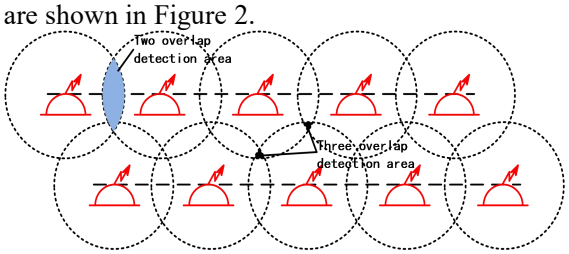

Figure 2 Line array sonar buoy detection area overlap

In order to effectively cover the search area, improve search probability, there will be a certain overlap between buoy sonar detection areas not only in a single line array, or even between adjacent line arrays. Thus, the actual effective search area $S_{\text{e-s}}$ of the sonar buoy array is the area got by minusing the overlapping area between the adjacent line arrays from the sum of the searching areas of every single line array, i.e.,

$$S_{\text{e-s}} = N_l S_{s-l} - (N_l - 1) A_d \quad (2)$$

S_{s-l} is the total area of a single line array's actual search sea area in square meters; A_d represents the detection area between adjacent line arrays in square meters.

(1) The total area S_{s-l} of a single linear array's actual search area is the sum of the areas of all sonar buoy detection zones, minus the area A_{m-d} of the adjacent sonar buoy detection area, then

$$S_{s-l} = N_{s-b} \pi R_b^2 - A_{m-d} \quad (3)$$

N_{s-b} is the number of sonar buoys on a single linear array, then $N_{s-b} \geq 2$; R_b is the effective range of the sonar buoy, which is expressed in meters per unit. The adjacent sonar buoy detection overlap area is A_2 , then there is

$$A_{m-d} = (N_{s-b} - 1) \times A_2 \quad (4)$$

(2) The overlapping area A_{m-d} between the adjacent line arrays is the sum of the overlapping areas for all two detection areas, minus the sum of the overlapping areas of all three detection areas, then

$$A_{m-d} = (2N_{s-b} - 1) \times A_2 - 2(N_{s-b} - 1) \times A_3 \quad (5)$$

A_3 is the overlapping area of three sonar buoy detection areas.

(3) If there is no overlap between all the sonar buoys in the array, there is

$$\begin{aligned} S_{e-s} &= N_l S_{s-l} \\ &= N_l \times N_{s-b} \times \pi \times R_b^2 \end{aligned} \quad (6)$$

The following model is to solve the overlapping area of the three detection regions, which is A_3 .

A. Three sonar-buoys effective search range overlapping area

Make O_1 , O_2 and O_3 are respectively the centers in the three intersecting circles; d_{12} , d_{13} and d_{23} are respectively the distances between the three circles centers, and the unit is meter; r_1 , r_2 , r_3 ($r_1 \geq r_2 \geq r_3$)are the radius of three circles, and the unit is meter;

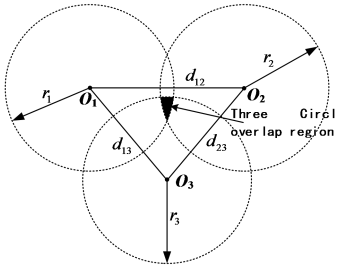

Figure 4 Three sonar buoys' detection range overlapping area

According to geometric knowledge and through derivation and simplification, the analytic formula of three overlapping area A_3 is established, which is,

① $A_3 = 0$, if one of the following conditions is met;

$$d_{12} \leq r_1 - r_2 \quad (7)$$

$$d_{12} \geq r_1 + r_2 \quad (8)$$

$$(x_{12} - d_{13}\cos\theta')^2 + (y_{12} - d_{13}\sin\theta')^2 \geq r_3^2 \quad (9)$$

$$\left(x_{12}-d_{13}\cos\theta'\right)^2+\left(y_{12}+d_{13}\sin\theta'\right)^2\le r_3^2 \quad (1)$$

Among them,

$$x_{12}=\frac{r_1^2-r_2^2+d_{12}^2}{2d_{12}} \quad (2)$$

$$y_{12}=\frac{1}{2d_{12}}\sqrt{2d_{12}^2\left(r_1^2+r_2^2\right)-\left(r_1^2-r_2^2\right)^2-d_{12}^4} \quad (3)$$

$$\sin\theta'=\sqrt{1-\cos^2\theta'} \quad (4)$$

$$\cos\theta'=\frac{d_{12}^2+d_{13}^2-d_{23}^2}{2d_{12}d_{13}} \quad (14)$$

$$\sin\theta''=\sqrt{1-\cos^2\theta''} \quad (15)$$

$$\cos\theta''=-\frac{d_{12}^2+d_{23}^2-d_{13}^2}{2d_{12}d_{23}} \quad (16)$$

② If it does not meet the foregoing, then

$$A_3=\frac{1}{4}\sqrt{(c_1+c_2+c_3)(c_2+c_3-c_1)(c_1+c_3-c_2)(c_1+c_2-c_3)} \quad (17)$$
$$+\sum_{k=1}^{3}\left(r_k^2\arcsin\frac{c_k}{2r_k}\right)-\sum_{k=1}^{2}\left(\frac{c_k}{4}\sqrt{4r_k^2-c_k^2}\right)+flag\cdot\frac{c_3}{4}\sqrt{4r_3^2-c_3^2}$$

In it,

$$flag=\begin{cases}1 & d_{13}\sin\theta<y_{13}+\dfrac{y_{23}-y_{13}}{x_{23}-x_{13}}\left(d_{13}\cos\theta-x_{13}\right)\\ -1 & \text{other}\end{cases} \quad (18)$$

Intermediate variables c_1 , c_2 , c_3 are calculated according to the following formula (in which, i,j,k are different from each other, and the subscript can change the turns, then $x_{ik}=x_{ki}$)

$$c_k^2=\left(x_{ik}-x_{jk}\right)^2+\left(y_{ik}-y_{jk}\right)^2 \quad (19)$$

$$x_{13}=x_{13}'\cos\theta'-y_{13}'\sin\theta' \quad (5)$$

$$y_{13}=x_{13}'\sin\theta'+y_{13}'\cos\theta' \quad (6)$$

$$x_{23}=x_{23}''\cos\theta''-y_{23}''\sin\theta''+d_{12} \quad (7)$$

$$y_{23}=x_{23}''\sin\theta''+y_{23}''\cos\theta'' \quad (8)$$

$$x_{13}'=\frac{r_1^2-r_3^2+d_{13}^2}{2d_{13}} \quad (24)$$

$$y_{13}'=\frac{-1}{2d_{13}}\sqrt{2d_{13}^2\left(r_1^2+r_3^2\right)-\left(r_1^2-r_3^2\right)^2-d_{13}^4} \quad (25)$$

$$x_{23}''=\frac{r_2^2-r_3^2+d_{23}^2}{2d_{23}} \quad (26)$$

$$y_{23}''=\frac{1}{2d_{23}}\sqrt{2d_{23}^2\left(r_2^2+r_3^2\right)-\left(r_2^2-r_3^2\right)^2-d_{23}^4} \quad (27)$$

4. CONCLUSION

Sonar buoy is important equipment for submarine search. Rational distribution of sonar buoy array can make effective detection in a large sea area. In order to solve the problem of real and effective sonar buoy search area calculation, the corresponding quantitative calculation model is established by using analytic method. The model can be used in key indexes' evaluation calculation of auxiliary decision and discovery probability of sonar buoy submarine search combat and has high practical value.

REFERENCES

[1]Cong Hongri, Zhou Hailiang, Yu Jihong. Check-search method of sonar buoy based on networked aviation search system[J]. Journal of Naval Aeronautical Engineering Institute, 2016,31 (2): 195-200.

[2]Tao Chenchen, Ju Jianbo, Wang Chengxiang, Shan Zhichao. Usage method of sonar buoy in regional check of submarine [J]. Fire and Command & Control, 2013,38 (10): 94-96.

[3]Teng Jun, Shao Xiaofang, Wu Hao. Sonar buoy's combat usage in submarine tracking process[J]. Ship Science and Technology, 2012,34 (8): 90-94.

[4]Cong Hongri, Shen Peizhi, Luan Yujia. Optimization of Sonar buoy array in checking anti-submarine [J]. Journal of Naval Aeronautical Engineering, 2014,29 (4): 391-396.

[5]Qi Xuewen, Yan Jiangang, Jin Fuxin, Gao Dongfei. Study on the seizure submarine search model of helicopter sonar buoy [J]. Electro-Optic and Control, 2013,20 (12): 10-14.

[6]Chen Qingfeng, Ju Jianbo, Zhao Ming. Sonar buoy combat use and search potential method in Anti-submarine patrol line [J]. Fire and Command and Control, 2011,36 (9): 112-114.

[7]Zeng Haiyan, Yang Rijie, Zhou Xu. Study on optimized layout technology of sonar buoy [J]. Command Control & Simulation, 2012,34 (1): 82-85.

[8]Yang Rijie, Zhou Xu, Zhang Linlin. Integrated omnidirectional sonar buoy tracking submarine optimized laying method [J]. Systems Engineering and Electronics, 2011,33 (10): 2249-2253.

[9]Xu Liang, Wu Ming. Sonar buoy discovery probabilistic assessment in anti-submarine patrol line [J]. Mine Warfare and Ship protection, 2015,23 (4): 66-69.

[10]Luo Musheng, Hou Xuelong, Zheng Baohua. Sonar buoy numerical probability modeling in network center and platform center [J]. Journal of Fire and Command & Control, 2013,38 (4): 154-157.

[11]Yang Bingbing, Ju Jianbo, Zhang Xinlei. Study on the potential performance of anti - submarine patrol aircraft buoy [J]. System Simulation Technology, 2015,11 (3): 202-206.

[12]Yang Yunxiang, Zhang Bo. Sonar buoy network area array search performance analysis [J]. Chinese Journal of Electronic Science, 2014,9 (5): 521-525.
[13]Xie Zhenhua, Li Lin, Cheng Jiangtao. Evaluation study of circular buoy array search efficiency [J]. Ship Electronic Engineering, 2011,31 (12): 168-171.
[14]Qin Feng, Sun Mingtai, Zhou Lihui. Solve the optimal working depth of buoy with the application of game theory [J]. Electro-Optic and Control, 2013,20 (12): 27-30.
[15]Wang Qingjiang, Li Wenhai, Peng Jun, Shan Xin, Zeng Ruwei. Unmanned aerial vehicle monitoring route planning in linear buoyant array search [J] Journal of Naval Aeronautical Engineering Institute, 2015,30 (1): 91-95.
[16]Wu, Bo, and Haiying Shen. "Analyzing and predicting news popularity on Twitter." International Journal of Information Management 35.6 (2015): 702-711.
[17]Wu, Bo, and Haiying Shen. "Mining connected global and local dense subgraphs for bigdata." International Journal of Modern Physics C 27.07 (2016): 1650072.
[18]Wu, Bo, Haiying Shen, and Kang Chen. "Exploiting active sub-areas for multi-copy routing in VDTNs." Computer Communication and Networks (ICCCN), 2015 24th International Conference on. IEEE, 2015.
[19]Wu, Bo, Haiying Shen, and Kang Chen. "DIAL: A Distributed Adaptive-Learning Routing Method in VDTNs." Internet-of-Things Design and Implementation (IoTDI), 2016 IEEE First International Conference on. IEEE, 2016

Invariant Bilinear Form on the Simplest Filiform $n-$ Lie Algebras

Rui Gao
Department of Mathematics, Cangzhou Normal University, Cangzhou, Hebei 061001,China

Abstract: In this paper, we mainly study the structure of invariant bilinear form on the simplest filiform $n-$ Lie algebras. We first obtain the form of metric matrix under the basis of simplest filiform $n-$ Lie algebra over a field F, and then prove that there exist the metric $n-$ Lie algebra in simplest filiform $n-$ Lie algebra on the complex field.
Keywords: FPGA; High-speed Information Processing; X-ray energy spectrum; Electronic measurement system; Compensation measures
simplest filiform $n-$ Lie algebra; $n-$ Lie algebra; invariant bilinear form

1. INTRODUCTION

The invariant bilinear form of $n-$ Lie algebra has been wildly used in Physics and Geometry. An $n-$ Lie algebra with invariant bilinear is called metric $n-$ Lie algebra, which has its applications in Mathmatical physics and String theories. It is always a hot topic in the structure of $n-$ Lie algebra to study the invariant bilinear form of $n-$ Lie algebra. In the article ,we first consider the structure of invariant bilinear on a simplest filiform $n-$ Lie algebra—a special nilpotent $n-$ Lie algebra, and then prove the existence of metric $n-$ Lie algebra (A,T) in simplest filiform $n-$ Lie algebra.

First we recall some basic notions.

DEFINITION 1[1]

An $n-$ Lie algebra is a vector space A over a field F on which is defined an $n-$ ary multi-linear operation $[x_1,\cdots,x_n]$ satisfying the identities：

$$[x_1,\cdots,x_n]=(-1)^{\tau(\sigma)}[x_{\sigma(1)},\cdots,x_{\sigma(n)}], \qquad (1)$$

and

$$[[x_1,\cdots,x_n],y_2,\cdots,y_n]=\sum_{i=1}^{n}[x_1,\cdots[x_i,y_2,\cdots,y_n],\cdots,x_n], \qquad (2)$$

where for any $x_1,\cdots,x_n,y_2,\cdots,y_n\in A$, $\sigma\in S_n$, S_n is the symmetric group,and the number $\tau(\sigma)$ is equal 0 or 1 depending on the parity of the permutation σ.

DEFINITION 2[1]

An algebra A is called nilpotent if there exists k such that $A^k=0$, where $A^0=A, A^1=[A,A,\cdots,A],\cdots,A^k=[A^{k-1},A,\cdots,A]$, for all $k=0,1,\cdots$.

Obviously, the simplest filiform $n-$ Lie algebra is nilpotent $n-$ Lie algebra.

Examples Let now A be a 3-Lie algebra of dimension 5 over field F and $\{e_1,e_2,e_3,e_4,e_5\}$ a basis of A. We put $[e_1,e_2,e_5]=e_4,[e_1,e_2,e_4]=e_3,[e_1,e_2,e_3]=0,$ and the remaining products of the basis vectors are equal to 0. Then A is a simplest filiform $3-$ Lie algebra.

DEFINITION 3[3]

Let A be a m-dimensional $n-$ Lie algebra over a field of F $(m\geq n+1)$. The algebra A is called m-dimensional simplest filiform $n-$ Lie algebra, if A has the basis $\{e_1,\cdots,e_m\}$ with the multiplication table

$$[e_1,\cdots,e_{n-1},e_j]=e_{j-1}, \qquad (3)$$

for $n+1\leq j\leq m$, and the remaining products of the basis vectors are equal to 0.

DEFINITION 4

A bilinear form $T:A\times A\to F$ of an $n-$ Lie algebra A is said to be invariant, if $T(ad(x_1,\cdots,x_{n-1})y,z)+T(y,ad(x_1,\cdots,x_{n-1})z)=0$, for all $x_1,\cdots,x_{n-1},y,z\in A$. If T is symmetric, (A,T) is called metric $n-$ Lie algebra.

Let A be a m-dimensional simplest filiform $n-$ Lie algebra and $\{e_1,\cdots,e_m\}$ a basis of A $(m\geq 4)$. $B=(b_{ij})$ is the metric matrix under the basis $\{e_1,\cdots,e_m\}$ of T ,which is an invariant bilinear form on A, i.e. $T(e_i,e_j)=b_{ij},i,j=1,\cdots,m.$

THEOREM 1

A is a $n-$ Lie algebra over a field of F. Let T_A be the set of invariant bilinear form on A, then T_A is a linear space.

Proof. By using the definition 4 and the definition of linear space, it can be proved directly.

THEOREM 2

Let A be a m-dimensional simplest filiform $n-$ Lie algebra. It can be proved that $Dim(T_A)=n^2$, and the metric matrix under the basis $e_1,\cdots,e_m$ of T has the following form:

$$\begin{pmatrix} b_{11} & \cdots & b_{1,n-1} & 0 & 0 & 0 & \cdots & 0 & b_{1m} \\ b_{21} & \cdots & b_{2,n-1} & 0 & 0 & 0 & \cdots & 0 & b_{2m} \\ \vdots & & \vdots & \vdots & \vdots & \vdots & & \vdots & \vdots \\ b_{n-1,1} & \cdots & b_{n-1,n-1} & 0 & 0 & 0 & \cdots & 0 & b_{n-1,m} \\ 0 & \cdots & 0 & 0 & 0 & 0 & \cdots & 0 & b_{nm} \\ 0 & \cdots & 0 & 0 & b_{n+1,n+1} & b_{n+1,n+2} & \cdots & b_{n+1,m-1} & b_{n+1,m} \\ \vdots & & \vdots & \vdots & \vdots & \vdots & & \vdots & \vdots \\ 0 & \cdots & 0 & 0 & b_{m-1,n+1} & b_{m-1,n+2} & \cdots & b_{m-1,m-1} & b_{m-1,m} \\ b_{m1} & \cdots & b_{m,n-1} & b_{mn} & b_{m,n+1} & b_{m,n+2} & \cdots & b_{m,m-1} & b_{mm} \end{pmatrix}, \quad (4)$$

$b_{ij} \in F, i, j = 1, 2, \cdots n-1, \cdots, m.$

Proof. By the direct computation according to the equation(1),(2),(3)and definition 4, we have:

$T(e_1, e_n) = T(e_1, [e_1, \cdots, e_{n-1}, e_{n+1}]) = -T([e_1, e_1, \cdots, e_{n-1},], e_{n+1}) = 0,$ $T(e_n, e_1) =$
$T([e_1, \cdots, e_{n-1}, e_{n+1}], e_1) = -T(e_{n+1}, [e_1, \cdots, e_{n-1}, e_1]) = 0,$ $T(e_1, e_{n+1}) = T(e_1, [e_1, \cdots, e_{n-1}, e_{n+2}])$
$= -T([e_1, e_1, \cdots, e_{n-1},], e_{n+2}) = 0, \cdots,$ $T(e_1, e_{m-1}) = T(e_1, [e_1, \cdots, e_{n-1}, e_m]) =$
$-T([e_1, e_1, \cdots, e_{n-1},], e_m) = 0,$,and in the same way
$T(e_n, e_1) = 0, \cdots, T(e_2, e_n) = 0$, $T(e_n, e_2) = 0$, $\cdots, T(e_2, e_{m-1}) = 0$, $T(e_{m-1}, e_2) = 0$, $\cdots, T(e_{n-1}, e_n) = 0$, $T(e_n, e_{n-1}) = 0$,
$\cdots, T(e_{n-1}, e_{m-1}) = 0$, $T(e_{m-1}, e_{n-1}) = 0$, a.e.,
$T(e_1, e_n) = T(e_1, e_{n+1}) = \cdots = T(e_1, e_{m-1}) = 0,$ similarly, $T(e_{n+1}, e_1) = T(e_n, e_1) = \cdots = T(e_{m-1}, e_1) = 0;$
$T(e_2, e_n) = T(e_2, e_{n+1}) = \cdots = T(e_2, e_{m-1}) = 0,$ similarly, $T(e_{n+1}, e_2) = T(e_n, e_2) = \cdots = T(e_{m-1}, e_2) = 0;$
$T(e_{n-1}, e_n) = T(e_{n-1}, e_{n+1}) = \cdots = T(e_{n-1}, e_{m-1}) = 0,$ similarly, $T(e_{n+1}, e_{n-1}) = T(e_n, e_{n-1}) = \cdots = T(e_{m-1}, e_{n-1}) = 0.$
$T(e_n, e_n) = T(e_n, [e_1, \cdots, e_{n-1}, e_{n+1}]) = -T([e_n, e_1, \cdots, e_{n-1},], e_{n+1}) = 0,$ $\cdots$ $T(e_n, e_{m-1}) =$
$T(e_n, [e_1, \cdots, e_{n-1}, e_m]) = -T([e_n, e_1, \cdots, e_{n-1},], e_m) = 0,$ similarly, $T(e_{m-1}, e_n) = 0.$

Example 2

Let A be a 5 dimensional simplest filiform $3-$ Lie algebra with the basis $\{e_1, e_2, e_3, e_4, e_5\}$, then the metric matrix of T has the following form:

$$\begin{pmatrix} b_{11} & b_{12} & 0 & 0 & b_{15} \\ b_{21} & b_{22} & 0 & 0 & b_{25} \\ 0 & 0 & 0 & 0 & b_{35} \\ 0 & 0 & 0 & b_{44} & b_{45} \\ b_{51} & b_{52} & b_{53} & b_{54} & b_{55} \end{pmatrix},$$

$b_{11}, b_{12}, b_{15}, b_{21}, b_{22}, b_{25}, b_{35}, b_{44}, b_{45}, b_{51}, b_{52}, b_{53}, b_{54}, b_{55} \in F$,
and
$T_A = FE_{11} + FE_{12} + FE_{15} + FE_{21} + FE_{22} + FE_{25} + FE_{35} + FE_{44} + FE_{45} + FE_{51} + FE_{52} + FE_{53} + FE_{54} + FE_{55}$.

THEOREM 3

For the m dimensional simplest filiform $n-$ Lie algebra A , there exist the metric $n-$ Lie algebras (A, T) .

Proof. Since the invariant bilinear form is (4) in Theorem 2, we obtain that the existence of the symmetric invariant bilinear form in T_A of the matrix is non-degenerate. Therefore, there exist the metric $n-$ Lie algebras (A, T) .

The conclusion is different from the simplest filiform Lie algebra.

REFERENCES

[1]V. T. Filippov, n -Lie algebras[J], Sib. Mat. Zh., 1985,26(6):126-140.

[2]Sh. M. Kasymov, On a theory of n -Lie algebras[J], Algebra Logika, 1987,26(3): 277-297.

[3]L. Boza, F. J. Echarte, J. Nunez, Classification of complex filiform Lie algebras of dimension 10[J], Algebras, Groups and Geometries, 1994, 11(3): 253-276.

[4]J. E. Humphreys, Introduction to Lie Algebras and Representation Theory[M], New York: Springer-Verlag, 1972.

[5]Daoji Meng, Introduction to Complex Semi-simple Lie Algebra [M], Peking University Press, 1998.

[6]Lei Lin, The Simplest Linear Lie Algebra [J], Journal of East China Normal University, 2003, (3): 1-8.

Research on Automatic Driving System for Unmanned Vehicles Based on Human Simulated Intelligent Control and Fractional PID Control

Junjie Liu
Anhui Institute of Information Technology, Wuhu, 241000, China

Abstract: Due to the complex environment and a nonlinear time-varying system ofunmanned vehicle, it is hard to describe in precise mathematical model.Based on the background,this paper designs and realizes a universal vehicle automatic driving system of human-simulated intelligent control based on fractional PID control. A motion controller of automatic driving system based on this algorithm is designed on operational control level and experimental simulation study is made on the designed right angle bend and 8-shaped road. The simulation results show that the control erect of robustness and control accuracy of human-simulated intelligent controller is superior to that of PID controller, which lays the basis for further real vehicle test.
Keywords: unmanned vehicle, automatic driving system, human-simulated intelligent control, fractional PID control

1. INTRODUCTION

The front-end data of X-ray energy spectrum is millivolt voltage pulse sequence, the pulse width of the sequence is microsecond level. But the amplitude and number of the pulse sequence contains the is sed system is FPGA as the control core. The data acquisition and processing system is composed of program control amplifier(PCA), A/D converter, FPGA unit, MCU unit and FIFO interface unit. The system block diagram is shown in figure 1.

One of the key factors that affect the intelligence ability of the vehicle is the performance of the automatic driving system. Due to the complexity of the environment and the nonlinear time-varying system of the unmanned vehicle, it is difficult for us to describe it accurately. Therefore, artificial intelligence is an important way to solve this problem. In view of the above background, this article introduces fractional calculus theory into the intelligent control, using the characteristics of fractional calculus system, the design and implementation of automatic driving system of a universal vehicle with human simulated intelligent control. The main work and innovation are as follows. This paper proposed an intelligent control algorithm based on the theory of fractional PID. It designs an automobile operation controller for automatic driving system based on this algorithm, and the simulation has been done in the right angle design. The simulation results show that the robustness and control precision of intelligent controller for fractional order PID theory are better than traditional controller to lay a theoretical foundation for the next step of vehicle test.

2. DESIGN OF FRACTIONAL PID CONTROLLER

For the fractional calculus theory, the uniform identifications are as follows:

$$ {}_{\alpha}D_t^{\lambda} = \begin{cases} d^{\lambda}/dt^{\lambda} & R(\lambda) > 0 \\ 1 & R(\lambda) = 0 \\ \int_0^t (dt)^{-\lambda} & R(\lambda) < 0 \end{cases} \quad (1) $$

α and t are the upper limit and lower limit of the calculation; λ is the order of the calculus operator; If λ >0, ${}_{\alpha}D_t^{\lambda}$ is the fractional derivative. The fractional PID controller is similar with the integer PID controller. The differential equation of fractional PID controller is:

$$u(t) = K_P + K_I D^{-\lambda} e(t) + K_D D^{u} e(t) \quad (2)$$

In the above formulation, k_p , k_i and k_d are respectively the ratio, integral and differential gain coefficient. e is the output error.

If we consider the following system,

$$G(s) = \frac{k}{\tau s + 1} \quad (3)$$

We adopt the following fractional PID controller:

$$C(s) = k_p + k_i \frac{1}{s^{\lambda}} + k_d s^{\mu} \quad (4)$$

We should refer to the following five principles when designing the fractional PID controller:

(1) Phase margin is given

$$Arg[C(j\omega_C)P(j\omega_C)] = \phi_m - \pi \quad (5)$$

(2) Crossover frequency is given

$$\left|C(j\omega_C)P(j\omega_C)\right|_{dB} = 0$$

(3) Robustness is gained by the opened loop

$$\left(\frac{d(Arg[C(j\omega_C)P(j\omega_C)])}{d\omega}\right)_{\omega=\omega_c}=0 \tag{6}$$

(4) Disturbance is suppressed by high frequency

$$\left|T(j\omega)=\frac{C(j\omega_C)P(j\omega_C)}{1+C(j\omega_C)P(j\omega_C)}\right|_{dB}\le AdB \tag{7}$$

(5) The output robustness

$$\left|S(j\omega)=\frac{1}{1+C(j\omega_C)P(j\omega_C)}\right|\le BdB \tag{8}$$

3. PRINCIPLES OF HUMAN SIMULATED INTELLIGENT CONTROL

The human simulated intelligent controller based on featureidentification is similar with the expert controller. The functions of each part are described as follows:

(1) Acquisition and processing of feature information.

The main function of this part is the distinction of $\mathrm{sgn}(e,\dot{e}),\mathrm{sgn}(e),\mathrm{sgn}(\dot{e})$ based on the real-time error e and error change rate $\dot{e}$ and the other characteristic variablesrequired in pattern recognition.

(2) Feature model set

The function of this part is to provide a knowledge base which stores some kind of feature pattern class.

(3) Pattern recognition

The function of this part is mainly used for reasoning according to the real time feature variables selected by the appropriate feature pattern class to provide the necessary conditions for control decisions.

(4) Control rule set

The function of this part is to implement a mapping from feature model set to control rule set, which is a controller based on rules. R_i can be expressed as R_i: *if* M_i *then* U.

4. APPLICATIONS OF HUMAN SIMULATED INTELLIGENT CONTROL ALGORITHM IN AUTOMATIC DRIVING SYSTEM OF UNMANNED VEHICLE BASED ON FRACTIONAL PID THEORY

Suppose the running level feature unit Q_1 of the is

$$Q_1=\{q_1,q_2,q_3,q_4,q_5,q_6,q_7\} \tag{9}$$

$$q_1:e_n\cdot\dot{e}_n\le 0, q_2:|e_n|\ge e_1, q_3:|e_n|\ge e_2, q_4:|e_n|\ge e_3, q_5:|e_n|\ge\dot{e}_1, q_6:|e_n|\ge\dot{e}_2, q_7:|e$$

The model Φ_i of the running level is:

$$\Phi_1=\{\varphi_{11},\varphi_{12},\varphi_{13},\varphi_{14},\varphi_{15},\varphi_{16},\varphi_{17},\varphi_{18},\varphi_{19},\varphi_{110}\}$$

$$\begin{aligned}
\varphi_{11}&=\{q_2\}\\
\varphi_{12}&=\{q_1\cap\overline{q}_2\cap q_3\cap\overline{q}_6\}\\
\varphi_{13}&=\{q_1\cap\overline{q}_2\cap q_3\cap\overline{q}_5\cap q_6\}\\
\varphi_{14}&=\{q_1\cap\overline{q}_2\cap q_3\cap q_5\}\\
\varphi_{15}&=\{q_1\cap\overline{q}_2\cap\overline{q}_3\cap q_6\}\\
\varphi_{16}&=\{q_1\cap\overline{q}_2\cap\overline{q}_3\cap q_4\cap\overline{q}_6\cap q_7\}\\
\varphi_{17}&=\{q_1\cap\overline{q}_2\cap\overline{q}_3\cap q_4\cap\overline{q}_7\}\\
\varphi_{18}&=\{\overline{q}_4\cap\overline{q}_7\}\\
\varphi_{19}&=\{q_1\cap\overline{q}_2\cap\overline{q}_4\cap\overline{q}_6\cap q_7\}\\
\varphi_{110}&=\{\overline{q}_1\cap\overline{q}_2\}
\end{aligned} \tag{10}$$

We have:

$$\begin{aligned}
\psi_{11}&:u_n=\mathrm{sgn}({}_0D_t^r e_n)\cdot U_{\max}\\
\psi_{12}&:u_n=K_p\cdot e_n\\
\psi_{13}&:u_n=S_p\cdot K_p\cdot e_n+K_d\cdot{}_0D_t^r e_n\\
\psi_{14}&:u_n=u_{n-1}\\
\psi_{15}&:u_n=K_p\cdot e_n+K_d\cdot{}_0D_t^r e_n+K_i\cdot{}_0D_t^{\lambda}e_n\\
\psi_{16}&:u_n=k\cdot K_p\cdot\sum_{i=1}^{n}e_{m,i}
\end{aligned} \tag{11}$$

The Inference rule set is

$$\Omega_1=\{w_{11},w_{12},w_{13},w_{14},w_{15},w_{16}\}$$

$$\begin{aligned}
w_{11}&:\varphi_{11}\Rightarrow\psi_{11}\\
w_{12}&:\varphi_{12}\cap\varphi_{17}\Rightarrow\psi_{12}\\
w_{13}&:\varphi_{14}\cap\varphi_{15}\cap\varphi_{19}\Rightarrow\psi_{13}\\
w_{14}&:\varphi_{13}\cap\varphi_{16}\Rightarrow\psi_{14}\\
w_{15}&:\varphi_{110}\Rightarrow\psi_{15}\\
w_{16}&:\varphi_{18}\Rightarrow\psi_{16}
\end{aligned} \tag{12}$$

(13)

5. SIMULATION AND VERIFICATION OF HUMAN SIMULATED INTELLIGENT CONTROL ALGORITHM BASED ON FRACTIONAL PID THEORY

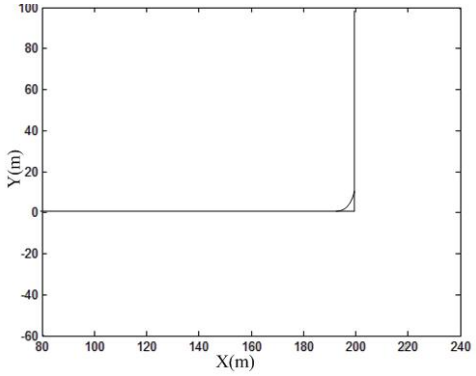

Fig. 1 Expectation path and real path

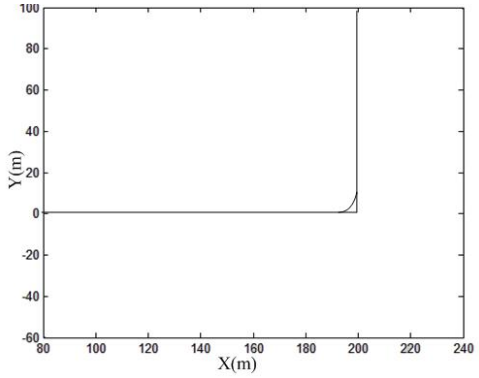

Fig. 2 Steering wheel angles of different distance

It can be seen that the maximum lateral error of vehicle driving process is further reduced, and the stability of vehicle control is improved obviously compared with PID control.

6. CONCLUSION

In order to achieve effective control and establish an accurate model of controlled object, we make full use of the object in the dynamic control process through the imitation of human intelligent behavior. This is the basic idea of human simulated intelligent control. Based on the human simulated intelligent control, this paper introduces the theory of fractional calculusand designs a human simulated intelligent controlalgorithm based on fractional order PID human simulated intelligent control. The simulation experiment of trajectory tracking is made. The simulation results show that the robustness and the control accuracy of the controller are better than PID controller and general human simulated intelligent control algorithm.

REFERENCES

[1]Dickmanns E D, Dynamic vision-based intelligence, Ai Magazine, 25(2), pp. 10, 2004.

[2]Chen Qian, XueFangzheng, Human-Simulated Intelligent Control for Manipulator, Journal of Chongqing University of Technology (Natural Science), 26(7), pp. 42-49, 2012.

[3]Liu Chengjun, XueFangzheng, Li Zushu, Deng Hangjian, Human simulated intelligent control for dynamic walking of biped robot, Journal of Chongqing University, 36(2), pp. 45-50, 2013.

[4]Gäfvert M, Svendenius J, A novel semi-empirical tyre model for combined slips, Vehicle System Dynamics, 43(5), pp. 351-384, 2005.

Study on the Purification Technology of Intrusion Feature for Large - scale Network

Liao Lang,
Department of Computer Science, Shenzhen Institute of Information Technology, 518172,Shenzhen, China

Abstract: The traditional purification algorithm of network intrusion feature has the problems of low purity, long time, and difficult to effectively prevent network attacks and others, thus, a new purification algorithm for network intrusion feature based on wavelet scale feature analysis is proposed. Firstly, the intrusion detection process of large-scale network is analyzed, and the issue of network intrusion feature classification is made quadratic programming. Based on this, the algorithm of network intrusion feature estimation is used to establish the model of network intrusion feature estimation. Finally, the network intrusion signal is analyzed according to the wavelet scale feature and further to achieve the purification of network intrusion feature by using the feature optimization rule of fish swarm information chain. The simulation results show that the algorithm can effectively improve the purity of large - scale network intrusion feature, with the good filtering effect and can effectively resist the network attack.
Key words: large-scale network; intrusion feature; filtering; wavelet analysis

1. INTRODUCTION

The large-scale network intrusion feature usually expresses a group of blind source signals of broadband. It can adopt the signal detection method to realize the network intrusion detection. Through the network intrusion detection, the intrusion feature is purified, and the network security defense system is established. The detection algorithm is transplanted into the firewall, to realize active attack defense. Thus, research of network intrusion detection algorithm and the relevant model is of great significance to improve network security, and the algorithm researches have attracted the people's attention [1].

With the expansion of network size and the change of network characteristics, it is necessary to quantitatively analyze and extract the network intrusion feature. The essence of network intrusion signal is a set of time series waveforms. The statistical signal processing algorithm and spectral analysis algorithm are used to realize signal detection and purification. Accurate detection of network intrusion signals to ensure that the network is completely. The network intrusion noise is usually flooded with normal network traffic data [2-4], and it is difficult to perform effective detection. It needs the purification process for the intrusion under network noise interference, thereby improving the detection performance. The traditional method uses FIR filtering algorithm to filter the network intrusion signal, but when the intrusion signal is in the large reverberation background interference, it cannot effectively achieve signal filtering and purification [5-7].

In order to solve the above problems, this paper proposes a purification algorithm of network intrusion signal based on wavelet scale feature analysis. Firstly, the background interference model of network intrusion signal is constructed. Wavelet scale filtering algorithm is designed to filter the signal and then the intrusion signal is detected by using the feature optimization rule of fish swarm information chain to achieve the algorithm improvement. Simulation results show that the superiority of the proposed algorithm in the field of improving detection performance and has obtained the conclusion of validity.

2. ANALYSIS OF INTRUSION DETECTION PROCESS OF LARGE - SCALE NETWORK

Network intrusion detection is the basis for ensuring network security. The detection and purification algorithms for network intrusion are based on the network intrusion detection algorithm based on statistical signal processing, time-frequency feature extraction, and so on. The basic principle of network intrusion detection is shown in Figure 1.

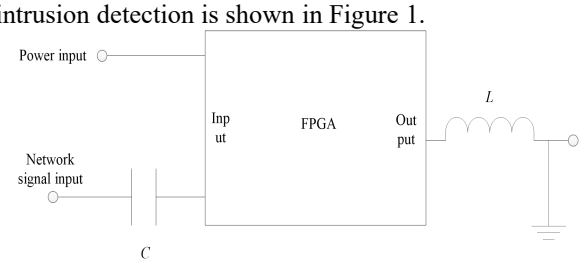

Figure 1 Principle of Network intrusion detection

It is a mainstream method of network intrusion feature detection for classification and recognition of intrusion features. Using this algorithm to carry out network intrusion feature detection, can get the features of malicious attacks in the network, thus ensuring the security of the network. The steps are as follows:

The data set composed of the network operation behavior feature can be represented by $U = \{(z_1, a_1, w(z_1)), \cdots, (z_n, a_n, w(z_n))\}$, where $z_l \in T^q$, $w(z_l) \in \{-1,1\}$, $\omega \le w(z_l) \le 1$, ω

are the network state parameter, which can be used to represent the running state of the network, and $w(z_l)$ is the membership degree of the network operation feature.

In the process of network intrusion detection, it can use the following formula to express the classification issue of network intrusion feature

$$\begin{cases} \min\limits_{y,d,\zeta} \dfrac{1}{2}\|y\|^2 + E\sum\limits_{l=1}^{n} w(z_l)\zeta_l \\ s.t. \quad a_l((y\cdot z_l)+d)+\zeta_l \geq 1 \\ \qquad \zeta_l \geq 0, l=1,2,\cdots,n \end{cases} \tag{1}$$

Among them, $E>0$ is the penalty factor in the process of network intrusion feature classification, $\zeta=(\zeta_1,\zeta_2,...,\zeta_l)^T$. The issue of the above-mentioned network intrusion feature classification is madequadratic programming so as to obtain the following results:

$$N(y,d,\zeta,\chi,\gamma)=\frac{1}{2}\|y\|^2+E\sum_{l=1}^{n}w(z_l)\zeta_l$$

$$-\sum_{l=1}^{n}\chi_l(a_l((y\cdot z_l)+d)-1+\zeta_l)-\sum_{l=1}^{n}\delta_l\zeta_l \tag{2}$$

Where, $\chi=(\chi_1,\chi_2,\cdots,\chi_n)^T$, $\delta=(\delta_1,\delta_2,\cdots,\delta_n)^T$, $\chi_l\geq 0$, $\delta_l\geq 0$, $l=1,2,\cdots,n$.

The above formula is made the calculation of the ideal solution, it can obtain the ideal solution which is $\chi'=(\chi_1',\chi_2',\cdots,\chi_n')^T$, then the classification function of network intrusion feature can be obtained as follows:

$$h(z)=\mathrm{sgn}\{\sum_{l=1}^{n}\chi_l^* a_l M(z,z_l)+d^*\} \tag{3}$$

Where, $d^*=a_k-\sum\limits_{l=1}^{n}a_l\chi_l M(z_l,z_k)$, $k\in\{k\,|\,0<\chi_k^*<w(z_k)E\}$.

With the increase of malicious behavior in network, the camouflage degree of network intrusion is getting higher and higher, and making that the inclination of classification effect on intrusion feature and normal data feature is becoming higher and higher. The traditional intrusion feature classification does not know the optimal class distribution of training intrusion feature data set, and it is assumed that the misclassification cost is equal, only the precision of classification is sensitive, and the difference between types is neglected, thus reducing the accuracy of network intrusion feature detection.

3. IMPROVEMENT OF PURIFICATION ALGORITHM FOR LARGE - SCALE NETWORK INTRUSION FEATURE DETECTION

(1) Establishment of Intrusion Feature Estimation Model

The prediction of the network operation behavior after the intrusion is completed by the intrusion feature estimation model, which provides the basis for effective network intrusion detection. Assuming that the connection threshold of network behavior feature is between 0 and 1. The connectivity value between the k -th network operation behavior feature and the first network operation behavior feature can be described by E_{kl}^1 , and its weight can be described by ζ_{kl}^1 . In the model of intrusion feature estimation, it must complete the ordering of weight and the connectivity value according to certain rules, and to get formula (7)

$$X=(y_{ll}^1\cdots y_{qq}^1,d_l^1\cdots d_q^1,y_{ll}^2\cdots y_{qq}^2,d_l^2\cdots d_q^2) \tag{4}$$

Where q_k denotes the input data of the intrusion feature estimation model and q_s denotes the number of the output of the intrusion feature estimation model. To find the approximate value of the above values, it can get the estimated error:

$$i=(n-1)/\sum_{l=2}^{n}h_l^2 \tag{5}$$

Where $k=2,3,L,m$ represents the number of elements in the network intrusion feature set.

Through the intrusion feature estimation algorithm, a network intrusion detection model is created, and the specific implementation process is as follows:

Assuming that the size of the intrusion feature estimation object can be expressed as Q , the error compensation parameter can be expressed as E_1 and E_2 , and the corresponding maximum value of weight can be expressed as $y_{\max}$, the minimum value can be expressed as $y_{\min}$. The maximum value of the number of iterations can be expressed as $j_{\max}$. The current output of the network intrusion detection model can be expressed as P , and the output result closest to the expected result can be expressed as P_{best} .

The output result is sorted by the weight and the connectivity value, and the estimated model can be obtained. If the connectivity value does not exceed the connection threshold, the connecting structure will be set to 0, otherwise the connecting structure will be set to 1.

To find the error of network intrusion detection, and the obtained result and the threshold value are compared. If the output result exceeds the threshold,

the output result corresponding to the intrusion detection behavior feature is the output result closest to the expected result[8].

The network operation behavior features is real-time updated, in order to get a new feature data set.

If the number of iterations reaches the maximum, the iteration is ended immediately, and the solution closest to the expected result is obtained, otherwise step (2) is repeated.

According to the above steps, we can get the solution closest to the expected result, and complete the conversion of the solution to obtain the corresponding weight and the construction mode. The obtained weight and construction mode are sent to the intrusion detection model, which can obtain the globally optimal solution of the model, achieve the purpose of predicting the intrusion features of the network operation behavior, and realize the large-scale network intrusion feature detection[9].

By using the above analyzed classification algorithm, the network intrusion feature data is divided, and the construction of the model of large-scale network intrusion feature estimation is realized[10].

(2) Implementation of network intrusion feature purification based on wavelet scale feature analysis

Furthermore, the wavelet scale filtering algorithm is designed to filter the signal. Assuming that the intrusion feature data set of the specific data of the network data stream is m, let $A_j(L)$ be the center of the intrusion feature cluster, where $j=1,2,...,k$. Assuming that the intrusion source of network fluctuation is an uniform linear array which composes of $N=2P$ randomly distributed array elements, with the separation distance of d .The intrusion feature signal source receives L near-field narrowband signal source, and the random variable satisfies $\alpha_k \geq 0$, $\sum_{k=1}^{K}\alpha_k = 1$. The wavelet scale of the signal is extracted for the phase position of intrusion feature of the diagonal matrix Λ, Ω, to build wavelet scale filter. In the wavelet scale space, the noise subspace E_s of the network intrusion feature signal is divided into the matrix E_0, E_x, E_y and E_z of four $P\times L$ by wavelet scale filtering, that is, $E_s=[e_1,e_2,\cdots e_L]=[E_0,E_x,E_y,E_z]^H$. In order to effectively filter the intrusion feature, the filter source parameters are designed as:

$$\Gamma = E_0^{\dagger}E_x,\quad \Psi = E_0^{\dagger}E_y,\quad \Upsilon = E_0^{\dagger}E_z \tag{6}$$

Among them, d and λ_i meet the $d \leq \lambda_i/4$. The continuous intrusion of the network virus is made fish swarm evolution and frequency expansion, to achieve the purpose of reducing the attack effectiveness. And then, the feature optimization rule of fish swarm information chain is used to achieve the detection of intrusion signals. The obtained single frequency signals after signal purification is described as:

$$s(t)=a(t)\cos\phi(t) \tag{7}$$

The artificial fish swarm algorithm is used to detect the signal, so that the chromosome after crossing cannot become a query binary tree, and the polymerization particle size of the particle swarm is:

$$V=\{v_{ij}\,|\,i=1,2,\cdots,c,j=1,2,\cdots,s\} \tag{8}$$

Where V_i is the i -th vector of the polymerization center of the particle swarm, (the i -th polymerization center vector). The current fitness value of each particle is compared with its own individual optimal value, if it is superior to the individual optimal value, the fuzzy matrix of the particle at current position is obtained:

$$\widetilde{y}_\tau = \frac{1}{P_S}\sum_{i=1}^{\infty}\lambda_S^i y_{(\tau-i)} \tag{9}$$

Thus achieving network intrusion detection and noise separation, and the purpose of signal purification is achieved.

4. EXPERIMENTAL RESULTS AND ANALYSIS

In order to test the performance of the algorithm in the detection and purification of network intrusion signal, the simulation experiment is carried out. The hardware of the simulation experiment is as: Intel (R) Core (TM) i5-2450 M, CPU @ 2.5 GHz, 4 GB memory. In the simulation experiment, the network intrusion information data is the network intrusion monitoring data collected from a group company's internal network center. The samples are collected once a day, as a group of experimental sample set. Respectively, the improved algorithm and the traditional algorithm are used for network intrusion detection experiments. The error rate of network intrusion feature extraction by using two different algorithms is compared[11]. The results are shown in Figure 2.

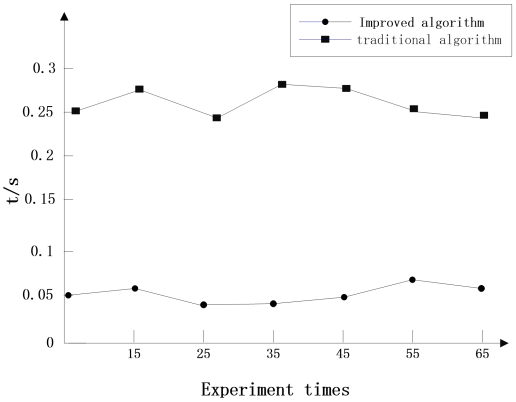

Figure 2 Comparison of time usage of intrusion features purification by using different methods

According to the analysis of Fig. 2, the time usage of intrusion feature purification by using the proposed method is lower than that of the traditional method when the network intrusion feature is purified under the same experimental times, and the advantages of this method are still obvious with the increase of the number of experiments. From the integral level, the

average used time of the large-scale network intrusion feature purification is about 0.07s by using the method in this paper, and that of the traditional method is about 0.25s, which means that the proposed method is with less time and high efficient.

Respectively, this improved algorithm and the traditional algorithm are used for large-scale network intrusion feature purification experiments. Under the different number of experiments, the purity of the network intrusion feature purification of two different algorithms is compared, and the results are shown in Fig. 3.

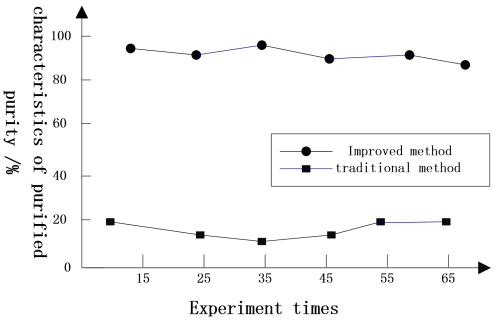

Figure 3 purity of the intrusion feature purification by using different algorithms

It can be seen from figure 3 that compared with the traditional experimental method, the purity of intrusion feature by using the proposed method is lower than that of the traditional method when the large scale network intrusion feature is purified under the same experimental times, and the advantages of this method are still obvious with the increase of the number of experiments. From the integral level, the average purity of the large-scale network intrusion feature purification is about 90.24% by using the method in this paper, and that of the traditional method is about 20.83%, which means that the purity of using proposed method is 4.5 times than that of traditional method.

5. CONCLUSION

Accurate detection of network intrusion signals can ensure that the network is complete. Network intrusion signal is usually interfered by the noisy data which can flood the normal network flow, thus it is difficult to realize the effective detection and it needs the purification processing for intrusion under the network noise interference, thereby improving the detection performance. In this paper, a new purification algorithm for network intrusion feature based on wavelet scale feature analysis is proposed. Firstly, the background interference model of network intrusion signal is constructed, and wavelet filtering algorithm is designed to perform signal filtering. Then the feature optimization rule of fish swarm information chain algorithm is used to realize the detection of intrusion signal and the algorithm is improved. The simulation results show that the algorithm can effectively improve the detection performance of network intrusion signal at low SNR, the purity of intrusion feature is high, and the filtering effect is good and can effectively resist the network attack.

REFERENCES

[1]Hewett R, Kijsanayothin P. Ranking intrusion likelihoods with exploitability of network vulnerabilities in a large-scale attack model[J]. International Journal of Network Security, 2015, 17(4):383-394.

[2]Chen T, Zhang S, Liu S, et al. A Small-Footprint Accelerator for Large-Scale Neural Networks[J]. Acm Transactions on Computer Systems, 2015, 33(2):6.

[3]WU Chun-qiong. Network Intrusion Detection Model Based on Feature Selection[J]. Computer Simulation, 2012, 29(6): 136-139.

[4]WANG Rui. Mechanism of Detecting and Preventing Application Layer DDOS Attack Based on Traceback[J].Computer Science,2013,40(11A):175-177.

[5]Liu Y, Nishimura M, Li L, et al. Study on a Low-Cost and Large-Scale Environmentally Adaptive Protocol Stack of Nuclear and Space Wireless Sensor Network Applications Under Gamma Radiation[J]. Nuclear Technology, 2017(1).

[6]Liang Li.A Network Intrusion Detection Algorithm Information Many Variations[J]. Bulletin of Science and Technology, 2012, 10(28) : 55 -57.

[7]ZHANG Zongfei. Feature selection for network intrusion detection based on quantum evolutionary algorithm[J].Journal of Computer Applications, 2013, 33(5): 1357-1361

[8]Wu, Bo, and Haiying Shen. "Analyzing and predicting news popularity on Twitter." International Journal of Information Management 35.6 (2015): 702-711.

[9]Wu, Bo, and Haiying Shen. "Mining connected global and local dense subgraphs for bigdata." International Journal of Modern Physics C 27.07 (2016): 1650072.

[10]Wu, Bo, Haiying Shen, and Kang Chen. "Exploiting active sub-areas for multi-copy routing in VDTNs." Computer Communication and Networks (ICCCN), 2015 24th International Conference on. IEEE, 2015.

[11]Wu, Bo, Haiying Shen, and Kang Chen. "DIAL: A Distributed Adaptive-Learning Routing Method in VDTNs." Internet-of-Things Design and Implementation (IoTDI), 2016 IEEE First International Conference on. IEEE, 2016.